UNIVERSITÀ' DEGLI STUDI DI VERONA

DEPARTMENT OF
Neuroscience, Biomedicine, and Movement

GRADUATE SCHOOL OF
Life and Health Sciences

DOCTORAL PROGRAM IN
Neuroscience, Psychology and Psychiatry

WITH THE FINANCIAL CONTRIBUTION OF
Ministerial scholarship D.M. 198/2003

Cycle: **XXIX cycle**

TITLE OF THE DOCTORAL THESIS

Brain microvessels and neuronal excitability: who is exciting who?

S.S.D. **BIO/16 HUMAN ANATOMY**
(Please complete this space with the S.S.D. of your thesis – mandatory information)*

Coordinator: **Prof. Leonardo Chelazzi**

Tutor: **Prof. Paolo Francesco Fabene**

Doctoral Student: **Dott.ssa Beatrice Mihaela Radu**

* For the list of S.S.D. please refer to the Ministerial Decree of 4th October 2000, Attachment A "*Elenco dei Settori Scientifico – Disciplinari"* available at: http://www.miur.it/atti/2000/alladm001004_01.htm

“Nella vita non bisogna mai rassegnarsi, arrendersi alla mediocrità, bensì uscire da quella zona grigia in cui tutto è abitudine e rassegnazione passiva, bisogna coltivare il coraggio di ribellarsi.”

RITA LEVI-MONTALCINI

Acknowledgements

Firstly, I would like to express my sincere gratitude to my advisor Prof. Paolo Francesco Fabene for the continuous support of my Ph.D thesis, for his patience, motivation, and for being one of my best friends. I could not have imagined having a better advisor and mentor for my Ph.D study. Thanks Paolo for everything.

Additionally, I would like to address a special acknowledgement to Prof. Giuseppe Bertini, who patiently helped me drafting all the manuscripts in the last years, and always challenged me to become a better scientist. Probably I will never forget how to pronounce "acetylcholine".

Besides my advisor, I would like to thank the members of the Doctoral School in Neuroscience, Psychology and Psychiatry: Prof. Leonardo Chelazzi, Prof. Giuseppe Busetto, Prof. Cristiano Chiamulera, and Prof. Francesco Fumagalli, for their insightful comments and encouragement, but also for the hard question which incented me to widen my research from various perspectives. Additionally, I would like to express my thanks to Prof. Marcel Ameloot from the University of Hasselt, Belgium and to Prof. Gilles Van Luijtelaar from the Radboud University, Netherlands, for reviewing this thesis and for the useful suggestions that definitely helped me to improve the thesis.

My sincere thanks also goes to all the internal and external collaborators Prof. Gabriela Constantin, Prof. Michael Assfalg, Prof. Alejandro Giorgetti, Prof. Petr Kacer, Prof. Sergio Fucile, Dr. Eda Suku who contributed to this complex research project; without their precious support would have been impossible to conduct this research.

I thank my fellow labmates for the stimulating discussions, for the help in performing experiments, and for all the fun we have had in the last three years. My thoughts I going to you Beatrice, Federico, Emanuele, Inna, Grisha, Cristina, Michele, Valeria, Andrea. A special thanks for Marzia and Flavia, who supported me as researchers and friends, and to all the other members of the department who warmly encouraged and supported me.

Last but not the least, I would like to thank my family: my parents, my husband and my wonderful daughter for their patience and continuous support throughout this thesis and for forgiving me for all the time that I have neglected them.

Table of contents

Chapter 1. Introduction

1.1. Neurovascular unit components

The term 'neurovascular unit' (NVU, **Figure 1.1**) refers to the ensemble of structures linking the brain parenchyma to its blood vessels and to their coordinated functional response (Abbott et al., 2006). The NVU is based on the anatomical and functional relationships of neurons and glia with blood vessel endothelial cells and pericytes, through the intervening extracellular matrix. Functional interactions within the NVU are fundamental in the migration and differentiation of neural precursors (Balenci et al., 2007; Wittko et al., 2009), and play crucial roles in both acute and chronic brain pathology. After acute brain injury, the NVU reacts with a coordinated response aimed at minimizing neuronal damage, while promoting tissue repair and reorganization.

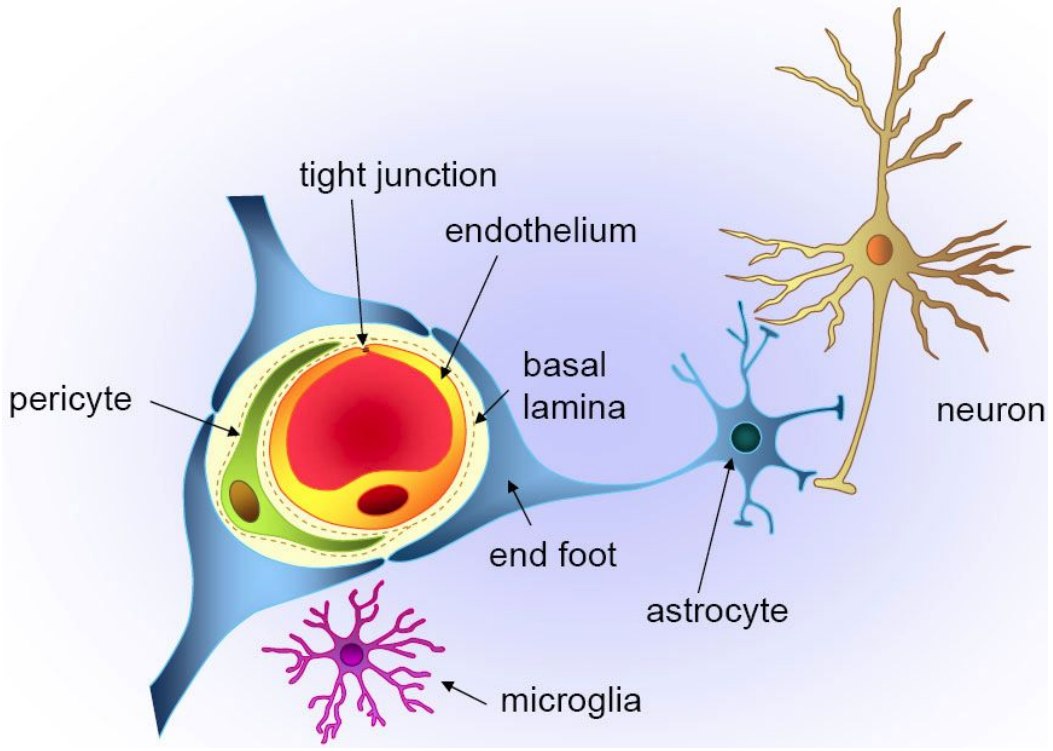

Figure 1.1. Neurovascular unit structure (according to Abbott and Yusof, 2010)

Parts of this chapter have been published in the paper: Bertini G, Bramanti P, Constantin G, Pellitteri M, **Radu BM**, Radu M, Fabene PF. (2013) New players in the neurovascular unit: insights from experimental and clinical epilepsy. Neurochem Int. 63(7):652-9.

NVU activity is modulated by molecules traditionally implicated in inflammatory activity, which seem to have adapted, in the brain, to serve a variety of physiological roles, quite distinct from the immune response. Recent evidence suggests an unexpected role of soluble factors (i.e., glutamate, ATP and D-serine) released by glial cells in synaptic plasticity underlying memory formation (Stellwagen and Malenka, 2006), or to long term potentiation (LTP) in the hippocampus (Halassa and Haydon, 2010; Henneberger et al., 2010).

The alternation of sleep and wakefulness, as well as the behavioral and cognitive correlates of each state can be modulated by the immune system. For example, some cytokines are involved in sleep regulation under physiological conditions, while others can modulate sleep by interacting with neurotransmitter, peptide, and/or hormone systems to initiate a cascade of responses that subsequently alter sleep–wake behavior (Krueger et al., 1998a; Krueger et al., 1998b; Opp, 2005). Thus, state-dependent behavior offers unique paradigms for the study of such factors.

1.1.1. Neurons

Neuronal activity is the primary source of functional communication in the nervous system. Among the major players in cortical neurovascular coupling were identified: (a) projection neurons sending fibers to the neocortex from subcortical centers (Cauli et al., 2004, Elhusseiny and Hamel 2000, Zhang et al. 1995), (b) local excitatory and inhibitory neurons (Cauli and Hamel, 2010, Lecrux et al., 2011), and (c) astrocytes (Attwell et al., 2010, Howarth 2014, Zonta et al., 2003), which contribute by means of the released vasoactive substances.

Independently of etiology and progress, brain pathology inevitably leads to perturbation of electrical and ligand-dependent responsiveness of neurons. In turn, altered neuronal functioning is responsible for the clinical symptoms characteristic of each disease. While it is understandable that research efforts have historically been devoted almost uniquely to the role of neurons in brain function and disease, such extreme focus may have neglected the important contribution of other brain components. It is out of the purpose of this thesis to describe this topic.

1.1.2. The blood–brain barrier

The blood-brain barrier (BBB) is the regulating interface between circulating blood and brain parenchyma. Endothelial cells of brain capillaries, unlike those of the peripheral circulation, are characterized by the absence of cell membrane fenestrations, the presence of tight junctions, having a high number of cytosolic mitochondria, and minimal pinocytotic activity (Hawkins and Davis, 2005). As an exception, the so-called circumventricular organs (CVOs) do possess fenestrated vasculature. In particular, secretory CVOs (median eminence and neurohypophysis) present a higher vascular permeability for low-molecular-mass tracers

compared to sensory CVOs (organum vasculosum of lamina terminalis, subfornical organ, and area postrema) (Morita and Miyata, 2012).

Anatomical and physiological considerations help understanding the importance of cerebrovascular function in neuronal activity (Winkler et al., 2011). It has been estimated that the total cerebral vascular length is approximately 600–700 km (Zlokovic, 2005) in adult humans and, in rodents, the distance from each neuronal cell body to a neighboring capillaries is ~15 μm (Tsai, 2009). Proper neuronal function necessitates a highly regulated extracellular environment, where the concentrations of sodium, potassium, and calcium ions need to be maintained within very narrow ranges. In this respect, the active interface between the CNS and the peripheral circulatory system, the blood–brain barrier (BBB), is of fundamental importance. The BBB functions as a dynamic regulator of ion balance, a facilitator of nutrient transport, and a barrier to potentially harmful molecules (Hawkins and Davis, 2005). Thanks to the BBB, the cerebrovasculature is not simply a passive conduit, but rather a highly dynamic multicellular structure capable of integrating and responding to both systemic and neural cues (Winkler et al., 2011).

1.1.3. Glial cells

Glial cells, long thought to act as a mere 'support' network, have gained increasing attention in the last decade as crucial protagonists in a variety of neural functions, including information processing. In particular, it has been demonstrated that astrocytes control synaptogenesis (Christopherson et al., 2005), modulate synaptic strength (Zhang et al., 2003), cradle and shepherd newborn dentate granule cells of the hippocampus to their final destination (Shapiro et al., 2005). Furthermore, it has recently been established that astrocytes in the visual cortex, like neurons, respond to visual stimuli with a high degree of selectivity (Schummers et al., 2008). Microglia, on the other hand, scan the environment (Nimmerjahn et al., 2005), phagocytose debris, and present antigens to lymphocytes. Thus, despite the classical concept of 'immune-privilege' in the brain, mechanisms of innate immune response do occur in the central nervous system (CNS) (Nguyen et al. 2002), and microglia are recognized as key players in such response, exerting also neuroprotective functions (Streit, 2002).

1.1.4. Pericytes

Pericytes modulate BBB integrity (Thanabalasundaram et al., 2011; Vandenhaute et al., 2011; Winkler et al., 2011; Zlokovic, 2008) and the contractile proteins (e.g., alpha-SM actin) expressed in pericytes contribute to the regulation of capillary blood flow (Bandopadhyay et al., 2001). Pericytes surrounding endothelial cells (connected via integrin molecules, connexin 43, and N-cadherins) are located in the perivascular space of the BBB. In general, pericytes contribute to BBB anatomy and physiology, providing vascular stability

and modulating vessel diameter and blood flow (Marchi and Lerner-Natoli, 2013). It has also been demonstrated that pericyte deficiency leads to a leaky BBB (Armulik et al., 2010; Armulik et al., 2011).

1.1.5. The humoral network: cytokines

Various cell types in the CNS, especially astrocytes and microglia, secrete cytokines, small (810 kD) proteins produced by a variety of hematopoietic and non-hematopoietic cell types. While cytokines have been traditionally identified as systemic mediators of both innate and acquired immune responses, increasing evidence indicates that these molecules play key roles in the modulation of intercellular signaling within the CNS (Pickering and O'Connor, 2007; Viviani et al., 2007). Numerous cytokines can have both pro-inflammatory and anti-inflammatory roles, depending on target cells and their specific responsiveness to the cytokine (Sriram and O'Callaghan, 2007).

Interestingly, though, the roles played by pro-inflammatory cytokines, such as interleukin (IL)-1β and tumor necrosis factor (TNF)-α appear markedly distinct in the brain from what has been observed systemically. In particular, the presence of these cytokines is not necessarily related to ongoing inflammatory processes (Galea et al., 2007). Rather, cytokines in the brain seem to subserve highly regulated communication pathways between cells of the NVU, contributing to the maintenance of the brain's structural and functional integrity, modulating the delicate balance between substrate delivery through blood flow, neuronal excitability, and energy demands imposed by neural activity itself (Abbott et al., 2006; Willis et al., 2008).

1.1.6. Differences of NVU in the cerebral microvasculature

Cerebral microvasculature is formed by brain arterioles, venules (0 - 100 μm in diameter) and capillaries (<10 μm diameter). It is very important to emphasize that it was evidenced a different control of the cerebrovascular function at the level of arterioles and capillaries (Andreone et al., 2015), and there are differences in NVU for arterioles and capillaries (**Figure 1.2**).

Cerebral endothelial cells are heterogenous over the microvasculature (Wilhelm et al., 2016). Arterial and venous endothelial cells present differences in the signalling molecules profile, i.e. ephrinB2 and EphB4, members of the Notch signaling, Hedgehog morphogens and VEGF-A (Swift and Weinstein, 2009), that play essential roles in the regulation of BBB functions and in the endothelial cell fate during development (Swift and Weinstein, 2009, Wilhelm et al., 2016). There is a heterogeneity of the genes profiles in brain microvessels: (i) solute transport are preferentially expressed in cerebral capillaries, (ii) inflammation-associated genes have a high expression in venules, and (iii) P-glycoprotein transporter has a low expression in venules and a high expression in capillaries and arterioles (Macdonald et al., 2010).

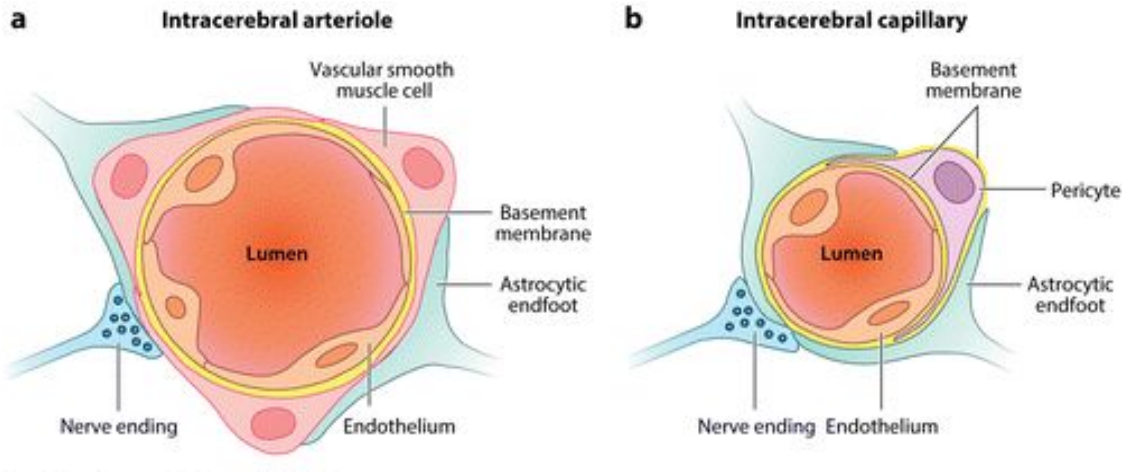

Figure 1.2. Differences between the neurovascular unit for intracerebral arterioles and intracerebral capillaries (according to Andreone et al., 2015)

The neuronal control exerted on the arteriole diameter (i.e. vasodilation or vasoconstriction), reflects the NVU integration of the signals controlling the contractile properties of vascular smooth muscle cells (Hamel 2006, Hillman 2014). CNS capillaries were described to lack vascular smooth muscle cells, with approximately 80% of their abluminal surface being covered by pericytes (Armulik et al., 2005, Peppiatt et al., 2006). Pericytes were characterized as contractile cells, contributing to the regulation of capillary diameter in response to neural activity (Hamilton et al., 2010, Itoh and Suzuki, 2012, Peppiatt et al., 2006), without contributing significantly to global cerebral blood flow regulation (Fernandez-Klett et al., 2010). However, a recent study demonstrated that pericytes increase blood flow in the somatosensory cortex through the vasodilation initiated at the capillary level (Hall et al., 2014).

1.2. Interactions between neurovascular unit components

1.2.1. Microglia–astrocytes–neurons interactions

In the healthy brain, resting microglia are constantly scanning their environment with long cellular processes that undergo continuous cycles of withdrawal and de novo formation at a speed of 1.47 μm/s (Davalos et al., 2005; Nimmerjahn et al., 2005). Microglial processes establish brief (5 min), direct contacts with neuronal synapses at a frequency of about once per hour (Wake et al., 2009), suggesting an involvement of microglia in monitoring/restoring synaptic activity (Wake et al., 2009; Ji et al., 2013). It has recently been shown that microglia actively engulf synaptic material and play a major role in synaptic pruning during postnatal development in mice (Paolicelli et al., 2011).

Both in physiological and pathological conditions, as a result of changes in osmolarity or neuronal activity, astrocytes increase or decrease in volume (Hansson et al., 1994;

Allansson et al., 1999). Neuronal activity leads to a rise in extracellular K^+ around astrocytic processes, which in turn leads to K^+ entry and astrocytic membrane depolarization (Kofuji and Newman, 2004). Moreover, astrocytes respond to neuronal activity with an elevation of their internal Ca^{2+} concentration, as shown by in vitro electrophysiological and calcium imaging studies. Calcium increases trigger the release of chemical transmitters from the astrocyte itself which, in turn, causes feedback regulation of neuronal activity and synaptic strength (Araque et al., 1999). It should be noted, on the other hand, that in vivo two-photon microscopy indicates the absence of spontaneous Ca^{2+} transients in microglia under physiological conditions (Eichhoff et al., 2011).

A permanent cross-talk exists between microglia and astrocytes. Studies on co-cultures of astrocytes and microglia under physiological conditions and in the presence of the inflammatory cytokine interferon-γ have evidenced an ATP-mediated calcium signaling mechanism of interaction (Verderio and Matteoli, 2001). On the other hand, brain endothelium has inductive influence on astrocytes (Estrada et al., 1990; Spoerri et al., 1997; Wagner and Gardner, 2000).

An increasing body of evidence points out the role of neuronal cyto-active mediators such as tissue-type plasminogen activator (tPA), which can directly affect astrocytes and lead to the development and progression of neurodegenerative diseases, as well as the modulation of neural function (Kim et al., 2011; Kwon et al., 2011). tPA has been recently proposed as an important element in the cross talk between neurons and astrocytes and it could be considered a gliotransmitter (Cassè et al., 2012).

1.2.2. Glia–endothelium interactions

The endfeet of astrocytes form a lacework of fine lamellae attached to the endothelium (Kacem et al., 1998). Glial–endothelial interactions occur either on a short time scale (seconds to minutes) involving receptor-mediated signaling and intracellular calcium fluctuations (Braet et al., 2001, Braet et al., 2004; Paemeleire, 2002) or on a long time scale, involving alterations in gene expression encoding for BBB tight junction proteins, transporters and enzymes (Dehouck et al., 1990; Schinkel, 1999; Brix et al., 2012). Among the CNS cells, astrocytes are considered responsible for inducing endothelial cells to form the tight junctions characteristic of the BBB (Janzer and Raff, 1987). Primary cultures or immortalized cell lines of brain endothelial cells present a reduction of barrier characteristics (down-regulation of tight junction proteins, of enzyme and transport systems) that is partly recovered when co-cultured with astrocytes (Rist et al., 1997; Sobue et al., 1999; Helms et al., 2012).

Astrocytes send inductive signals to the endothelium (Abbott, 2002). In co-culture systems it was proven that induction depends on the correct polarity between endothelium and glia (Abbott, 2002), and it has been speculated that astrocytes release key molecules responsible for their inductive signals, such as TGF-β, GDNF, bFGF, IL-6, hydrocortisone and angiopoietin 1 (Hoheisel et al., 1998; Tran et al., 1999; Utsumi et al., 2000; Lee et al.,

2003). *In vivo* imaging studies have been also performed to identify the effects exerted by astrocytes versus endothelial cells. For example, after systemic 3-chloropropanediol administration, male Fisher F344 rats showed astrocytic loss in selected brainstem loci, loss of endothelial tight junction protein expression, and loss of BBB integrity (Willis et al., 2004; Willis, 2012). The affected areas were repopulated 8–28 days later (Willis et al., 2004). Moreover, under hypoxic stress conditions, increased glial fibrillary acidic protein (GFAP)-expression associated with changes in tight junction protein expression and loss of BBB integrity (Willis, 2012) were demonstrated. Two-photon microscopy on brain mice evidenced that damage to a single cortical neuron can induce Ca^{2+} elevation in surrounding microglia (<50 μm cell body-to-cell body distance) (Eichhoff et al., 2011).

1.2.3. Pericyte-endothelium interactions

In vitro pericyte/endothelial cell interactions have been studied in various co-culture models, both in the presence and absence of glial cells (Vandenhaute et al., 2011; Al Ahmad et al., 2011). Pericytes in co-culture with glial and endothelial cells stabilize the formation of capillary-like structures (Ramsauer et al., 2002), and can induce occludin expression in endothelial cells (Hori et al., 2004). Both astrocytes and pericytes significantly suppress endothelial proliferation (Al Ahmad et al., 2011). Pericytes induce proper localization of barrier proteins, lumen polarization, and functional activity of ABC-transporters similar to astrocytes, but the presence of both cells is required to maintain optimal barrier characteristics (Al Ahmad et al., 2011). Pericyte/endothelial cell interaction increases matrix metalloproteinase 9 (MMP-9) activity (Zozulya et al., 2008).

1.2.4. Cross-talk between cerebral endothelium and brain parenchyma

There are several pieces of evidence for the crosstalk between cerebral vascular endothelium and brain parenchyma, mainly formed by neurons and glial cells.

Among the factors contributing to the interaction between cerebral endothelium and neurons, vascular endothelial growth factor (VEGF) and brain-derived neurotrophic factor (BDNF) seem to be key players (Vezzani, 2005, Li et al., 2009). VEGF was demonstrated to play an important role in angiogenesis, neurodegeneration, blood-brain barrier permeability and astroglial proliferation (Krum et al., 2002; Croll et al., 2004a; Croll et al., 2004b; Storkebaum et al., 2004). VEGF is not specific for endothelial cells, by neuroglia or neurons might also expressed it (Vezzani, 2005). VEGF expression in the rat hippocampal neurons enhances neurogenesis, being associated with improved cognition, but independent of endothelial cell proliferation (Cao et al., 2004). Considering its physiological roles, VEGF represents an attractive target to modulate brain function at the neurovascular interface in neurological diseases (Lange et al., 2016). VEGF and BDNF have been also shown to play an important role in the reciprocal modulation of neural stem cells and brain-derived endothelial cells in the induction and the maintenance of the neurovascular niche (Li et al., 2009).

Another modality of communication between cerebral endothelium and neurons is by means of the small vesicles (i.e. secretory exosomes and microvesicles) released in the bloodstream that are abundant in microRNAs and mRNAs (Smalheiser, 2009).

Several studies have also indicated the crosstalk between cerebral endothelium and oligodendrocytes (Pham et al., 2012, Miyamoto et al., 2014), and several factors have been demonstrated to contribute to this trophic coupling, e.g. brain-derived neurotrophic factor, fibroblast growth factor-2, transforming growth factor-beta, adrenomedullin, vascular endothelial growth factor, matrix metalloproteinases, etc. (Miyamoto et al., 2014). This crosstalk was suggested to contribute to vascular remodeling after white matter injury (Pham et al., 2012).

1.3. Neurovascular unit: new insights from ictogenesis

The conventional notion that neurons are exclusively responsible for brain signaling is increasingly challenged by the idea that brain function in fact depends on a complex interplay between neurons, glial cells, vascular endothelium, and immune-related blood cells, as part of NVU. The progressive establishment of the NVU as a key concept in brain function and disease triggered the inevitable shift from a purely 'neurocentric' perspective to a more integrated approach.

Seizures are correlated with the abnormal excessive or synchronous neuronal activity in the brain, but epilepsy could not be reduced only to this phenomenon. In the last decade, cytokines and vascular alterations have been discussed in relation to the pathogenesis of epilepsy, suggesting a potential role for inflammation mechanisms in seizure induction. Moreover, blood cellular, molecular, and dynamic parameters (e.g. shear stress, pH, temperature, platelet counts, etc.) seem to play relevant roles in modulating neuronal excitability.

1.3.1. Contribution of 'classical' NVU components to seizures

After decades of preclinical and clinical epilepsy research aimed at elucidating the neuronal alterations responsible for seizuring activity, the role of other brain components, such as endothelial cells and leukocytes has emerged in recent years (Fabene et al., 2010; Fabene et al., 2013).

BBB leakage has been implicated both in the induction of seizures and in the progression to chronic epilepsy (Seiffert et al., 2004; Ivens et al., 2007; Marchi et al., 2007; van Vliet et al., 2007). In addition, BBB opening leads by itself to neuronal hypersynchronization and epileptiform activity mediated by exposure of NVU players, in particular astrocytes and neuronal cells, to blood albumin or potassium ions, respectively (Seiffert et al., 2004; Ivens et al., 2007; Marchi et al., 2007). Moreover, it has been shown that BBB disruption by intra-arterial injection of mannitol in human patients suffering from

cerebral lymphoma induces focal motor seizures (Marchi et al., 2007). Seo et al. (2012) recently surveyed the potential role of MMPs in BBB dysfunction. MMPs have thus been reported to contribute to BBB disruption and permeability, interfering with cell-cell signaling in NVU, particularly mediating occludin degradation (Liu et al., 2012). MMPs and associated NVU mechanisms have been proposed as potential targets in a broader range of CNS disorders (Seo et al., 2012).

Recent evidence indicate that astrocytes also contribute to neurologic disorders such as epilepsy as equal partners to neurons, and may represent a promising new target for the development of antiepileptic drugs (Kovács et al., 2012). In fact, activated astrocytes are a common hallmark in patients with mesial temporal lobe epilepsy (TLE) and Ammon's horn sclerosis. Status epilepticus is associated with increased permeability of the BBB, which allows the ionic composition of serum to modulate neuronal excitability; astrocytic uptake of albumin induces transforming growth factor β (TGF-β)-mediated signaling cascades, leading to changes in astrocytic properties, resulting in disturbances in spatial K^+ buffering, thereby rendering the NVU more prone to seizures (Kovács et al., 2012).

Additionally, pericytes have been indicated as potential players in NVU remodeling in the epileptic brain (Marchi and Lerner-Natoli, 2013).

1.3.2. Contribution of leukocytes to seizures

Recent evidence demonstrates that leukocytes play an active role in promoting the physiological neurogenesis that occurs in the adult mammalian brain. In particular, rodents housed in an enriched environment showed increased neurogenesis that depended on the recruitment of circulating T-cells and on the activation of resident microglia (Ziv et al., 2006). The same T-cells contributed to spatial learning, suggesting a complex interplay between circulating blood cells, non-neuronal brain cells, and neuronal plasticity. The involvement of leukocytes in NVU modulation has also been studied in pathological conditions such as experimental and clinical epilepsy. In particular, several studies have shown that pro-epileptogenic drugs can activate brain endothelium and induce up-regulation of adhesion molecules, potentially allowing leukocyte adhesion and transmigration. Specifically, in vivo administration of the pro-convulsant agent kainic acid has been reported to up-regulate integrin ligands such as intercellular adhesion molecule 1 (ICAM-1) and vascular cell adhesion molecule 1 (VCAM-1) on the surface of brain endothelial cells (Bell and Perry, 1995). These results were also recently confirmed and extended by in vivo staining data showing increased expression of P-selectin as well as ICAM-1 and VCAM-1 after kainic acid-induced status epilepticus (Fabene et al., 2013). It was previously demonstrated that leukocyte trafficking mechanisms induce BBB damage leading to seizure generation in animal models of epilepsy (Fabene et al., 2008). The role of immune cells in epilepsy was further supported by the study of Kim and collaborators, demonstrating that leukocyte migration through the brain endothelium breaks down the BBB and causes severe seizures in an animal model of meningitis (Kim et al., 2009).

Moreover, we reported that spontaneous recurrent seizures lead to chronic expression of VCAM-1, the ligand for α4β1 integrin, potentially contributing to BBB permeability, neuroinflammation, and brain damage that could explain, at least in part, the evolution to chronic disease with spontaneous seizure generation (Fabene et al., 2008). It is interesting to note that the Th1 (but not Th2) lymphocytic phenotype were preferentially recruited in inflamed brain venules after seizures, suggesting that these adaptive immune cells, known to play a key role in the induction of autoimmunity and inflammation, may also contribute to the progression of epilepsy (Fabene et al., 2008). In support to our data, in vitro studies have shown that epileptiform activity induced by bicuculline can rapidly up-regulate the expression of adhesion molecules on brain endothelium in an experimental model of isolated guinea pig brain (Librizzi et al., 2007), suggesting that each seizure may induce pro-inflammatory mediators able to activate brain endothelium, which in turn may favor the generation of more seizures.

Vascular alterations and lymphocyte accumulation in the brain parenchyma were also documented in epileptic patients, independent of disease etiology (Hildebrandt et al., 2008; Fabene et al., 2008). Altogether, data obtained in experimental models of epilepsy and results obtained from humans strongly suggest a key role for leukocytes and vascular inflammation mechanisms in the induction of seizures (**Figure 1.2**). Furthermore, the dissociation between anatomical lesions and occurrence/severity of the epileptic condition (Navarro Mora et al., 2009) suggests that future research efforts should move beyond the long-standing focus on neuronal damage and loss, and extend to the mechanisms that modulate NVU excitability.

It is important to point out that treatment of mice with an anti-α4-integrin mAb after the onset of status epilepticus inhibited leukocyte recruitment in pilocarpine-induced epilepsy, and led to a drastic reduction in seizure frequency, thus suggesting that α4 integrins play a role in epileptogenesis (Fabene et al., 2008). In addition, preventive therapy with anti-α4 integrin inhibited the induction of the acute phase and completely blocked spontaneous recurrent seizures and development of epilepsy, suggesting that blockade of α4 integrins have preventive as well as therapeutic effect in the pilocarpine-induced experimental model of epilepsy (Fabene et al., 2008). Taken together, these results strongly suggest that leukocyte trafficking contribute to NVU dysfunction and seizure generation.

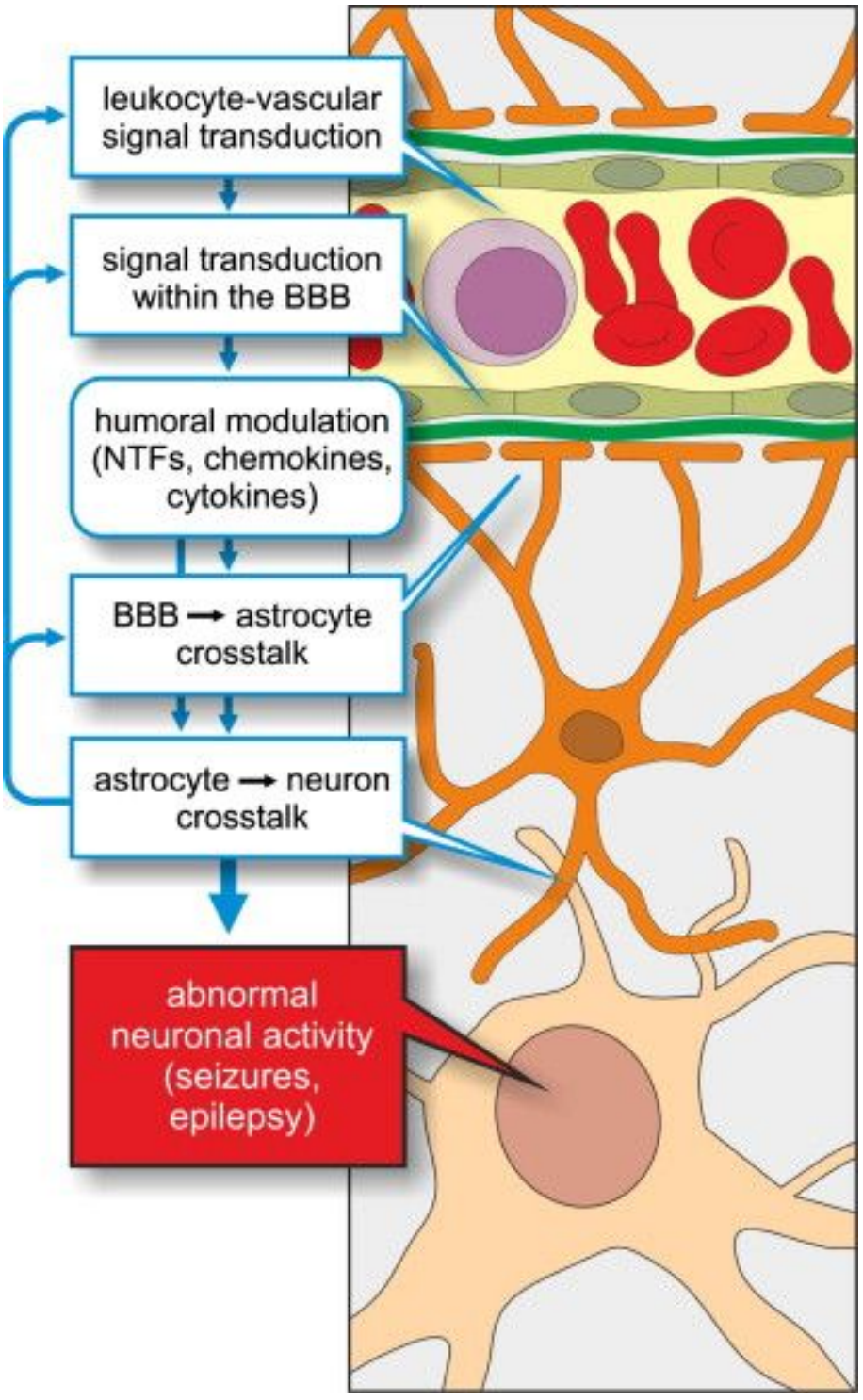

Figure 1.2. A schematic view of the different cellular and molecular interactions at NVU leading to seizure. (Bertini et al. 2013)

1.3.3. Contribution of chemokines to seizures

Chemokines (chemoattractant cytokines, characterized by the ability to induce chemotaxis in nearby responsive cells) are usually secreted by immune cells after pathogen detection, and they have also been proposed as a new class of neuromodulators (Rostene et al., 2007; Cardona et al., 2008). Chemokines and chemokine receptors modulate leukocyte-vascular adhesion during seizure induction. CNS vascular activation parallelled by upregulation of adhesion molecules and involvement of chemokines and chemokine receptors can be provoked by chemo-convulsant agents or by inflammatory pathologies. Activation of brain endothelium leads to leukocyte adhesion, which compromises the endothelial barrier function resulting in leakage of plasma constituents into the brain parenchyma (Fabene et al., 2008; Fabene et al., 2010; Fabene et al., 2013).

It was reviewed recently the clinical and experimental evidence of the active role of chemokines in modulating NVU activity in pathological conditions, such as epilepsy (Fabene et al., 2010). Altered gene expression for chemokines CCL2, CCL3, CCL4 in hippocampi surgically removed from TLE patients has been reported (Lee et al., 2007). CCL2 and CCL3 proteins can attract polymorphonuclear leukocytes, monocytes, memory T cells, and dendritic cells in the hippocampus of TLE patients. In support of these results, neutrophils and activated T cells with Th1 phenotype have been shown to interact with brain endothelium and migrate perivascularly or into the brain parenchyma after pilocarpine-induced status epilepticus in mice (Fabene et al., 2008). Data obtained in TLE patients also showed expression of VCAM-1, suggesting that vascular adhesion molecules and chemokines may together control leukocyte trafficking during epilepsy (Fabene et al., 2010). Astrocytes, perivascular microglia, and infiltrating leukocytes have been identified as major cellular sites of CCL3 and CCL2 production in the brain (Karpus and Ransohoff, 1998) and their receptors CCR1 and CCR2 are expressed on the abluminal surface of human brain endothelial cells (Andjelkovic and Pachter, 2000) and may direct leukocyte trafficking inside brain parenchyma during inflammatory responses (Fabene et al., 2008; Hildebrandt et al., 2008; see **Figure 1.2**).

Expression of CXCR4 may also be related to NVU activity alterations associated with pro-epileptogenic conditions. In fact, increases of CXCR4 expression have been reported in the hippocampus of TLE patients, mainly in microglia and in a small population of astrocytes (Lee et al., 2007). Increased expression of CXCR4 could allow for enhanced CXCL12 binding, thereby inducing microglia to release TNFα, which potentiates prostaglandin-dependent Ca^{2+} activation and glutamate release (Lee et al., 2007), eventually leading to NVU altered activity.

In agreement with human data, CCR2 and CCL2 have been shown to increase in the hippocampus following pilocarpine-induced seizures in rats (Foresti et al., 2009). After status epilepticus, hypertrophic astrocytes exhibited CCR2-labeling, whereas microglial cells were more closely apposed to the CCR2-labeled cells in status epilepticus rats (Foresti et al., 2009), confirming the involvement of non-neuronal cells in the pathology. In addition, CCL2

was induced in reactive glial cells, as well as in blood vessel, at late time-points after pilocarpine-induced status epilepticus in mice, which is potentially related to changes in permeability of the BBB during epileptogenesis (Xu et al., 2009). CCL2 upregulation has also been shown following kainate-induced seizures in the rat hippocampus, correlating to the temporal profile of BBB permeability and immune cell recruitment at the injury site (Manley et al., 2007). Other chemokine receptors, such as CCR7, CCR8, CCR9 and CCR10 have been reported to be down-regulated during pilocarpine-induced status epilepticus (Liu et al., 2012).

1.3.4. Contribution of the extracellular matrix to seizures

As a major component of the neurovascular unit, the extracellular matrix (ECM) is deeply involved in BBB functionality not only as a support scaffold, but also with specific roles in modulating BBB permeability (Hawkins and Davis, 2005). The endothelial baso-lateral membrane, pericytes, and astrocytic endfeet are in close proximity to the basal lamina. This matrix is a dynamic structure that evolves as a function of the physiological state of the system and of the complex interactions between cells. ECM constituents such as laminin, heparan sulfate proteoglycans, fibronectin, and collagens reside predominantly in basement membranes surrounding brain capillary endothelial cells (Colognato and Yurchenco, 2000).

The connection between the cells and the basement membrane is primarily established by the integrins and dystroglycan, which form the matrix adhesion receptors (del Zoppo and Milner, 2006). The integrins and dystroglycan are αβ heterodimeric structures that link the cytoskeleton to the specific binding sites on the lamina. The role of integrins controlling BBB properties is unique and markedly different from other type of blood vessels. Glia-derived ECM decreases the permeability of vascular brain endothelial monolayer whereas aortic endothelial cell-derived ECM has an opposite effect (Hartmann et al., 2007). The roles of integrins have been extensively studied in knockout mouse models in which certain α or β subunit-encoding genes have been deleted, with dramatic effects on CNS development from neonate status to adulthood. Deletion of αv or β8 subunits results in leaky vasculature, thereby inducing cerebral hemorrhage and premature death in affected mice (McCarty et al., 2002). Some results suggest that αvβ8 integrins expressed by astrocytes control the activation of TGF-β stabilizing the endothelium (Cambier et al., 2005). Integrin expression is also related to the developmental stage of the brain. The expression of β1-integrin has been associated with angiogenesis in the developing mouse CNS (Milner and Campbell, 2002). Once the development of blood vessels completes, ECM-related protein expression changes: (i) β1-integrin is up-regulated, (ii) in the first postnatal day, β1-integrin is expressed together with α4- and α5-integrin, switching to α1- and α6-integrin expression in adulthood, and (iii) fibronectin is down-regulated while laminin is up-regulated. Considered together, these observations suggest a switch from fibronectin-mediated signaling pathway in the early phases of microvascular vessels development to a laminin-mediated one in the adult CNS, in support of a profound involvement of ECM in modulating NVU functionality.

MMPs form a large family of structurally related zinc-dependent, secreted or membrane-bound proteinases, and are considered major executors of ECM remodeling throughout the body (Sternlicht and Werb, 2001). MMPs are enzymes that are able to influence neuronal function through extracellular proteolysis in various normal and pathological conditions. Animal studies suggested that MMP-9 plays an important role in epileptogenesis (Mizoguchi et al., 2011; Takács et al., 2010; Wilczynski et al., 2008). A recent study on human epileptogenesis indicates that up-regulation of MMP-9 is prominent and consistent in focal cortical dysplasia (FCD) tissue derived from epilepsy surgery, regardless of the patient's age (Konopka et al., 2012; see **Figure 1.2**).

1.3.5. Contribution of the hemodynamic parameters to seizures

Relatively little attention has been paid to the contribution of cerebral hemodynamic and metabolism to neurological diseases. However hemodynamic (e.g., blood pressure, systemic vascular resistance, etc.) or oxygenation changes (partial pressure of arterial oxygen, partial pressure of arterial CO_2, pH, saturation, etc.) occurring for instance in traumatic brain injury, stroke, and epilepsy, result in NVU alterations, related to several pathophysiological mechanisms of injury (Bor-Seng-Shu et al., 2012). It has been suggested that uncoupling of cerebral blood flow from metabolism can trigger secondary brain lesions, particularly in the early phases of the primary incident, with consequent worsening of the patient's outcome (Bor-Seng-Shu et al., 2012).

Hemodynamic regulation is influenced by blood gas content, blood viscosity, body temperature, cardiac output, altitude, cerebrovascular autoregulation, and neurovascular coupling, mediated by chemical agents such as nitric oxide (NO), carbon monoxide (CO), eicosanoid products, oxygen-derived free radicals, endothelins, K^+, H^+, and adenosine (Bor-Seng-Shu et al., 2012). Nitric oxide acts as a diffusible cell-to-cell messenger, conveying information associated with its concentration dynamics, both the synthesis via glutamate stimulus and inactivation pathways determine the profile of NO concentration change (Laranjinha et al., 2012).

1.3.6. Contribution of the cross-talk between endothelium and brain parenchyma to seizures

The cross-talk between cerebral endothelium and CNS neurons was suggested to play an important role in ictogenesis. In pilocarpine-induced seizure models, was reported that seizures dramatically increased VEGF both in neurons and in glia (Croll et al., 2004a). Consequently, VEGF binding to VEGFR1 on local microvasculature might contribute to the increase in vascular permeability and BBB leakage during seizures (Croll et al., 2004a). In VEGF-mediated rat brain inflammation, was described the upregulation of intercellular adhesion molecule (ICAM)-1 and the chemokine macrophage inflammatory protein (MIP)-1α, as well as a preferential extravasation of monocytes (Croll et al. 2004b). In the same model, VEGF was indicated to cause a dramatic BBB breakdown, which is

characterized by decreased investment of the vasculature with astroglial endfeet (Croll et al. 2004b). Additionally, in a pilocarpine-induced model, VEGF was demonstrated to be up-regulated after status epilepticus, to ensure protection against seizure-induced neuronal loss in hippocampus (Nicoletti et al., 2008), and to preserve learning and memory after status epilepticus (Nicoletti et al., 2010). In a model of epileptiform activity induced with kainate in organotypic rat hippocampal cultures, were demonstrated the overexpression of VEGF and VEGF receptor-2 associated with vascular remodeling and zonula occludens 1 downregulation (Morin-Brureau et al., 2011).

The crosstalk between cerebral endothelium and oligodendrocytes was also suggested to contribute to vascular remodeling after white matter injury (Pham et al., 2012).

1.4. Open questions

Integrating the above described information several open questions have emerged:

(1) what is the exact sequence of events in ictogenesis, and the alteration in neuronal excitability is a primary or secondary event with respect to the blood brain barrier permeabilization?

(2) is brain endothelium the site of action of different stimuli from the bloodstream that can trigger the cascade of events leading to seizure-like events?

(3) if one of the NVU partners is altered then by crosstalk the other NVU components activate and finally the ictogenesis occurs?

(4) are the alterations/impairments in leukocyte-endothelium adhesion and in neutrophils recruitment contributing to the neuroinflammation in brain parenchyma?

(5) is the cross-talk between cerebral endothelium and brain parenchyma modified in epilepsy, and to what extend different signaling molecules (e.g. chemokines) are contributing to the mismatched transmission between the NVU partners?

We will try to tackle these questions, at least in part, in the next chapters of the thesis by using *in vitro* and *in vivo* models.

Chapter 2. Aim of the study

Taking into account the multiple interactions between neurovascular unit components that were described in the Introduction chapter, e.g. microglia–astrocytes–neurons interactions, glia–endothelium interactions, pericyte-endothelium interactions, cross-talk between cerebral endothelium and brain parenchyma, we focused our attention on brain endothelium as the first barrier encountered before ”accessing” the brain parenchyma.

The working hypothesis of our study is that **any stimulus from the bloodstream that acts at the level of the endothelium of brain capillaries, and activates the endothelium, is consequently activating the neurovascular unit as a whole by means of the intercellular crosstalk**. Considering this working hypothesis, a stimulus that activates the brain microvascular endothelium (e.g. triggering calcium waves, stimulating cytokines release, acting on tight junction proteins, stimulating the blood brain barrier leakage etc.) might cause neuronal depolarization followed by neuronal hyperexcitability (e.g. seizure-like events).

Microvasculature alterations play an important role in epilepsy. To date, recent studies demonstrated that abnormal capillary vasodynamics, especially cerebral oxygen changes in and around microvasculature, contributes to ictal neurodegeneration in epilepsy (Leal-Campanario et al., 2017, Zhang et al. 2017). Specific cerebrovascular segments have been proposed to be differentially implicated in the pathophysiology of epilepsy, and, moreover, differences in cerebrovasculature between white and grey matter have been also considered (Librizzi et al., 2017). In this context, it is important to evaluate the effects of different stimuli acting on the brain endothelium, as part of the neurovascular unit, and their possible contribution to the abnormal neuronal activity.

The main objectives of the thesis were:

O1. To evaluate the effect of Qtracker®800 vascular labels on brain microvascular endothelial cells

O2. To perform an extended functional description of the muscarinic receptors in brain microvascular endothelial cells

O3. To evaluate the effect of pilocarpine on brain microvascular endothelial cells

O1. To evaluate the effect of Qtracker®800 vascular labels on brain microvascular endothelial cells

Previous studies from Fabene’s group (Salvetti 2014, *Doctoral thesis*; Fabene et al., 2015) demonstrated that Qtracker®800: (i) accumulate in tissues and cross the blood brain barrier, remaining in the organs, including the brain for at least 3 weeks, (ii) induce

alterations in proinflammatory cytokines levels in the liver and hippocampus, (iii) determine alterations in behaviour and in the electroencephalographic rhythms, (iv) exacerbate the effect of unrelated inflammatory conditions and pro-convulsive agents in the brain. These studies concluded that conventional *in vivo* tests used as first screening tools in toxicology, may not be enough to highlight the nanoparticle-induced functional alterations involving the brain.

Qtracker®800 are commonly used for *in vivo* deep tissue vasculature imaging, but our previous data have determined us to question if this nanoparticles are only ”inert dyes” for imaging vasculature or there are also interacting with the vasculature. Considering their prolonged presence in the animal body upon injection (up to 3 weeks, which is far beyond the imaging window), it is important to understand if these nanoparticles are able to exert a direct action on brain endothelium and if this action would contribute to the alterations in neuronal excitability.

We have first characterized the nanoparticles by employing dynamic light scattering and electron microscopy methods. Then, we evaluated the functional interaction between Qtracker®800 and brain microvascular endothelial cells (in primary and immortalized cell cultures) by means of ratiometric calcium imaging and cell viability analysis. In order to avoid experimental biases, the effect of Qtracker®800 was also tested on human umbilical vein endothelial cells in primary culture from different donors. The complete description of the technical aspects, the results, and the conclusions of this study are further detailed in **Chapter 3**.

O2. To perform an extended functional description of the muscarinic receptors in brain microvascular endothelial cells

Our goal is to evaluate the effect of pilocarpine on brain microvascular endothelial cells, and in this context, after the screening of the literature become obvious that a complete description of the functional expression of muscarinic receptors in mouse brain endothelium was missing. It is already known that pilocarpine is partial agonist of the muscarinic receptors and a chemo-convulsant used in the epilepsy-induced models (Schaafsma et al., 2006; Marchi et al., 2007; Thomas et al., 2009; Nezu et al., 2015). Given the potential importance of this receptor family as non-neuronal drug targets (Zhang et al., 2014), and the increasing use of mAChR knockout mice as models for common neurological disorders (Zhang, 2006; Langmead et al., 2008; Wess et al., 2003) a detailed characterization of muscarinic receptors expression and functionality in the mouse brain microvasculature is a high priority and become one of the goals of this thesis.

We first evaluated the gene and protein expression, respectively, for the muscarinic receptors in brain microvascular endothelial cells (in primary and immortalized cell cultures)

by means of reverse transcription polymerase chain reaction, immunofluorescence and MALDI-TOF mass spectrometry. Then, the functional expression of these receptors was tested by ratiometric calcium microfluorimetry technique. Finally, the pharmacological characterization of these receptors was performed by ratiometric microfluorimetry imaging technique and results were compared with the molecular docking data.

The complete description of the technical aspects, the results, and the conclusions of this study are further detailed in **Chapter 4**.

O3. To evaluate the effect of pilocarpine on brain microvascular endothelial cells

After bringing more light into the functional characterization of muscarinic receptors in brain microvascular endothelial cells (*O2.*), the next step was to focus our attention on deciphering the complex mechanisms by which pilocarpine is able to permeabilize the blood brain barrier. The starting point of this study was based on previous data the literature indicating that pilocarpine administration caused seizures and lethality in wild-type and M_2-M_5 *knockout mice*, but had no effect in the M_1 *knockout mice* (Hamilton et al., 1997) or had reduced effect in the mice knockout for M_1 in the parvalbumin-positive inhibitory neurons (Yi et al., 2015). Previous studies have focused their attention on the effects of M_1 receptor knockout at the neuronal level, and our working hypothesis was that M_1 receptor knockout in brain endothelium also plays a critical role in ictogenesis.

We first quantified the levels of cytokines released upon pilocarpine treatment in an *in vivo* mouse model (pilocarpine-induced epilepsy model) and an *in vitro* cell culture model (brain microvascular endothelial cells exposed to pilocarpine) using MAGPIX technology.

Using the *in vitro* model of hippocampal slices exposed to pilocarpine, we evaluated by patch-clamp technique the capacity of pilocarpine to produce seizure-like events or to induce amplitude and frequency changes of spontaneous postsynaptic potentials.

Using the *in vitro* model of brain microvascular endothelial cells exposed to pilocarpine we evaluated the adhesion molecules expression by immunofluorescence and flow cytometry, and we correlated our results with previous data in brain capillaries after *status epilepticus* (Fabene et al. 2008). The gene and protein expression, respectively, for the muscarinic receptors and tight junctions proteins in brain microvascular endothelial cells upon pilocarpine treatment were quantified by means of reverse transcription polymerase chain reaction and immunofluorescence. We also quantified the gene and protein expression, respectively, for the tight junctions proteins in brain microvascular endothelial cells upon pilocarpine treatment, and we tried to correlate these data with changes in permeability of the

blood brain barrier model using spectrophotometric quantification of the FITC-dextran diffusion through the endothelial monolayer.

Using the same *in vitro* model of brain microvascular endothelial cells exposed to pilocarpine, we tested the capacity of pilocarpine to trigger intracellular calcium release by ratiometric microfluorimetry imaging technique. The competition of pilocarpine and acetylcholine on the binding site of the muscarinic receptors was evaluated ratiometric microfluorimetry imaging technique and results were compared with the molecular docking data.

The complete description of the technical aspects, the results, and the conclusions of this study are further detailed in **Chapter 5**.

Chapter 3. Are they in or out? The elusive interaction between Qtracker® 800 vascular labels and brain endothelial cells

3.1. Summary

Aim: Qtracker®800 Vascular labels (Qtracker®800) are promising biomedical tools for high-resolution vasculature imaging; their effects on mouse and human endothelia, however, are still unknown. **Materials & methods:** Qtracker®800 were injected in Balb/c mice, and brain endothelium uptake was investigated by transmission electron microscopy (TEM) 3-hrs post-injection. We then investigated, *in vitro*, the effects of Qtracker®800 exposure on mouse and human endothelial cells by calcium imaging. **Results:** TEM images showed nanoparticle accumulation in mouse brain endothelia. A subset of mouse and human endothelial cells generated intracellular calcium transients in response to Qtracker®800. **Conclusion:** Qtracker®800 nanoparticles elicit endothelial functional responses, which prompts biomedical safety evaluations and may bias the interpretation of experimental studies involving vascular imaging.

Keywords: nanoparticles; calcium imaging; cytosolic calcium transients; nanoparticle uptake; mouse brain endothelium; human umbilical vein endothelial cells; transmission electron microscopy.

3.2. State-of-art

Cerebral vasculature imaging is required in the diagnosis of cerebrovascular pathology and healthcare stakeholders are increasingly interested in safer, cheaper, and higher-resolution clinical imaging solutions. In the last decade, the field of nanotechnology has exploded, and new nanomedicine and nano-neuromedicine approaches have been proposed as alternative or complementary solutions to already existing vasculature imaging tools (e.g., MRI- and/or CT-based angiography).

The data presented in this chapter have been published as: **Radu BM**, Radu M, Tognoli C, Benati D, Merigo F, Assfalg M, Solani E, Stranieri C, Ceccon A, Fratta Pasini AM, Cominacini L, Bramanti P, Osculati F, Bertini G, Fabene PF. (2015) Are they in or out? The elusive interaction between Qtracker® 800 vascular labels and brain endothelial cells. *Nanomedicine (Lond)*. 10(22):3329-42.

Several metallic and organic nanomaterials have been approved by the Food and Drug Administration (FDA) are at different clinical trial stages of clinical trials as diagnostic tools; semiconductor nanomaterials (e.g. quantum dots) are, on the other hand, generally considered for research use only (Kim et al., 2010; Clift and Stone, 2012). Recently, a new generation of fluorescent silica nanoparticles called Cornell dots (C-dots), with efficient urinary excretion (Burns et al., 2009) and effective cancer-targeting properties (Benezra et al., 2011; Bradbury et al., 2013), received FDA approval for clinical use. This FDA approval opens a new era for nanomedicine, and deeper understanding of cell-specific action of semiconductor-based nanoparticles is urgently needed.

Rapid nanotechnology advances in preclinical brain vasculature imaging (Ding et al., 2013; Jaruszewski et al., 2014; Li et al., 2014; Keunen et al., 2014; Radu and Radu, 2015) have substantially increased our ability to unveil vascular contributions to the pathogenesis of brain ischemia, brain tumor formation, Alzheimer disease, and epilepsy (Fabene et al., 2008; Burrel et al., 2013; Hyun et al., 2013).

Quantum-dot nanoparticles (QDs) gained popularity over the last decade (Zhu et al., 2013), due to their superior optical properties with respect to conventional organic dyes (Medintz et al., 2005; Michalet et al., 2005; Stylianou and Skourides, 2009). In particular, Qtracker® vascular labels (Qtracker®565, Qtracker®605, Qtracker®655, Qtracker®705 and Qtracker®800, named according to their emission wavelength) have been designed for *in vivo* deep-tissue imaging of blood vessel distribution and morphological properties in small animals (http://www.thermofisher.com/order/catalog/product/Q21071MP). The high-wavelength Qtracker®800 allows the deepest imaging of tissue vasculature of the series. Preclinical *in-vivo* imaging studies of the vessels using Qtracker®800 have already been carried out to highlight mouse tumor vascularization (Mayes et al., 2008) and bone marrow vasculature (Lo Celso et al., 2011).

Biocompatibility is a key requirement for QD-based *in-vivo* vascular imaging. The "ideal" QDs should be "inert" with respect to the microenvironment (e.g. circulating and endothelial cells). In practice, this desired property is usually sought by coating the QDs with a thin polymer layer, one of the most used being polyethylene glycol (PEG), without any functional group. This layer reduces the non-specific interaction of coated QDs with the surrounding molecular species, including those present on the cell plasma membrane (Bentzen et al., 2005; http://www.thermofisher.com/order/catalog/product/Q21071MP]. Indeed, PEG coating of QDs drastically minimizes non-specific interactions and decreases cellular uptake rate, as proved in three tumor cell lines (Kelf et al., 2010; http://www.thermofisher.com/order/catalog/product/Q21071MP).

A very recent report, however, demonstrated the uptake of PEG-coated silica nanoparticles in brain endothelial cells (Liu et al., 2014). Since these coated nanoparticles are between 25 nm and 100 nm (i.e. almost 5-10 times the core diameter of QDs) and given the authors' claim that nanoparticle transport across the blood-brain barrier is size-dependent, we

wondered whether PEG-coated QDs might show significant interactions with endothelial cells. To our knowledge, there are no published reports describing such direct interaction.

Based on these premises, we investigated: a) whether *in vivo* Qtracker®800 are uptaken by endothelial cells, and b) the functional consequences of endothelial exposure to Qtracker®800, studied *in vitro*. First, the hydrodynamic diameter of Qtracker®800 was estimated by dynamic light scattering (DLS) and the core size was calculated from electron microscopy images in order to characterize the nanoparticles. Next, in a set of *in vivo* experiments, Qtracker®800 uptake in mouse brain endothelia was investigated by electron microscopy. As previously described, many aspects of vascular endothelium physiology are regulated by calcium signaling pathways, since most of the stimuli relaxing or contracting brain capillaries act directly on the endothelial cells, producing changes in intracellular free calcium concentration (Itoh and Suzuki, 2012; Moccia et al., 2014; Taylor and Francis, 2014). Based on the above, we also investigated *in vitro* the ability of a Qtracker®800 flux to induce fluctuations of free cytosolic calcium concentration and/or changes in mouse brain endothelial cell viability. We have also extended our *in vitro* study to another type of endothelial cells (human umbilical vein endothelial cells) in order to discriminate between a specific effect on mouse brain endothelial cells and an ubiquitous effect.

3.3. Materials and methods

3.3.1. Chemicals

Qtracker®800 (Q21071MP, lot #1216103, Life technologies, USA) were dissolved in 0.9% saline solution for the *in-vivo* studies, and in Ringer HEPES-buffered solution (NaCl, 140 mM; KCl, 5.6 mM; $MgCl_2$, 2 mM; $CaCl_2$, 2 mM; glucose, 10 mM; HEPES 10 mM; pH 7.4 with NaOH) or phosphate-buffered solution (5 mM; pH 7.4) for the *in-vitro* experiments. Fura-2 acetoxymethyl ester (Fura-2 AM) and pluronic acid F-127 (Life technologies, USA) were dissolved in Ringer solution. All other reagents were purchased from Sigma-Aldrich (St Louis, MO, USA).

3.3.2. Hydrodynamic size measurements by Dynamic light scattering

Dynamic light scattering was performed on Qtracker®800 using a Zetasizer Nano ZS instrument (Malvern Instruments Ltd, USA) operating with a 633 nm He-Ne laser light source and a fixed detector angle of 173°, as previously described (Ceccon et al., 2013). Qtracker®800, 2-µM stock solution in 50 mM borate buffer, pH 8.3 (Life Technologies, USA) was diluted down to 50 nM to the range of 40-80 nM either in Ringer solution or in saline solution (See *Chemicals*). Lower particle concentrations resulted in poor signal/noise and

large fit errors (using either single or multiple exponential models). Hydrodynamic diameter values were determined by averaging the intensity-weighted size distributions obtained from 20 successive DLS runs of 10 s each. Measurements were repeated 3 times and results are reported as mean ± SD. The distribution widths were quantified by the Polydispersity Index (PdI). DLS measurements were carried out at 25°C before and after filtration (through acetate-cellulose Costar Spin-X Centrifuge Tube Filters, 0.22 μm pore size, Cole Parmer, USA) or centrifugation (18000 xg for 15 min) of Qtracker®800 solutions. No filtration or centrifugation were used on the Qtracker®800 solutions employed for the *in viv*o and *in vitro* experiments.

3.3.3. Zeta potential measurements

Measurements were performed with a Zetasizer Nano ZS instrument (Malvern Instruments Ltd, USA). Qtracker®800 particles were dispersed at a final concentration of 75 nM in phosphate buffer, pH 7.4, and transferred to a disposable zeta cell. Measurements were carried out at 25 °C after 120 s equilibration time, performing 7 runs comprising 12 sub-runs each. The applied voltage was 100 V and the measured conductibility was 4.540 ± 0.334 mS cm^{-1}. All measurements passed technical quality criteria based on inspection of phase and frequency plots, and were reproducible after sample spinning at 18000 xg for 15 min. Zeta potential was evaluated from electrophoretic mobility applying the Henry equation.

3.3.4. Animals and QD injection

Male Balb/c mice acquired from Harlan-Nossan (Udine, Italy) were adapted to the laboratory and maintained on a 12-hour inverted light/dark cycle, at 23 ± 1°C, with access to food and water *ad libitum*. Experiments started when animals were 6 weeks old and weighed 25 ± 5 g.

Experiments were approved by the University of Verona ethical committee. Animals (n = 10) were divided in 2 equal groups, one received injection of saline solution and the other of Qtracker®800, and both groups were sacrificed 3 hrs after injection.

Qtracker®800 solutions (or saline) were administered through a single injection (0.4 μM, 10 μL/g for each mouse) into the tail vein. Mice were then deeply anesthetized (zolazepam and tiletamine, i.p. 20 mg/kg), and perfused transcardially with PBS followed by phosphate-buffered 4% paraformaldehyde. Cortical brain samples were collected to evaluate Qtracker®800 presence in the endothelium, based on transmission electron microscopy and immunohistochemistry analysis.

According to the recommendation of the producer, the optimal time-interval for *in vivo* vasculature imaging with Qtracker®800 is 3 hrs post-injection

(http://www.thermofisher.com/order/catalog/product/Q21071MP). Therefore, the 3-hr time point is essential in understanding Qtracker®800 distribution into the cerebral bloodstream and if this time interval is sufficient for the nanoparticles to interact with the mouse brain vascular endothelium.

3.3.5. Transmission electron microscopy (TEM)

Brain tissue samples were fixed in 2% glutaraldehyde in Sorensen buffer pH 7.4 for 2 hrs, postfixed in 1% osmium tetroxide in aqueous solution (2 hrs), dehydrated in graded concentrations of acetone, and embedded in Epon-Araldite mixture (Electron microscopy Sciences, Fort Washington, PA, USA). Ultrathin tissue sections (70 nm) were placed on Cu/Rh grids with Ultracut E (Reichert, Wien, Austria) and were observed using a Morgagni 268D microscope (Philips, The Netherlands).

For imaging the Qtracker 800 in solution, a droplet of nanoparticle solution was put on the grid (FCF-150-Cu, Electron Microscopy Science, PA, USA) and, after drying, the grid was imaged without any other processing.

3.3.6. Human umbilical vein endothelial cell cultures

Human umbilical vein endothelial cells (HUVECs) from seven healthy donors were individually harvested as previously described (Fratta Pasini et al., 2012) and used between passages 2 and 5. The medium was refreshed every 2 days. At the beginning of each experiment, cells were harvested by trypsinization, using 0.05% trypsin (Sigma-Aldrich, St. Louis, Mo, USA) and 0.537 mM ethylenediaminetetraacetic acid (EDTA) in phosphate-buffered saline without calcium and magnesium (Seromed, Berlin, Germany). Cells were plated at a density of $2*10^4$ cells/cm^2 onto 24-mm cover glasses for intracellular calcium imaging measurements.

3.3.7. Mouse brain endothelial cell cultures

Primary cultures of brain microvascular endothelial cells (BMVECs from Balb/c mice, passage 3-6; #PB-BALB-5023, PELOBiotech, Germany) were cultivated according to the producer's protocol. bEnd.3 (passage 22-30; #ATCC® CRL-2299™, USA), a Balb/c mouse cell line, was grown in Dulbecco's modified Eagle's medium (DMEM) with Glutamax-I, 10% fetal bovine serum (Gibco), 100 U/ml penicillin, 100 µg/ml streptomycin, 5% CO_2 (37°C). Cells were plated at a density of $2*10^4$ cells/cm^2 onto 24-mm cover glasses for intracellular calcium imaging measurements or 96-well plates for viability assays.

3.3.8. In-vitro Qtracker®800 studies

In order to apply Qtracker®800 *in vitro* in concentrations comparable to those used for the *in vivo* studies, we first estimated that the above described injections yielded blood concentrations around 44 nM, based on a mouse whole blood volume of ~ 2 mL (Endo et al., 2014). Taking into account this approximate value and the range of concentrations previously reported for *in vitro* studies using Qtracker® 655 (Zhang and Monteiro-Riviere, 2009), we used between 10 and 40 nM Qtracker®800 in our *in vitro* experiments. To shed light on the Qtracker®800 direct action against brain microvascular endothelial cells, we performed calcium imaging and cell viability measurements on bEnd.3 cells and BMVECs.

3.3.9. Intracellular calcium imaging on endothelial cells

Fura-2 AM-based, Ca^{2+} imaging experiments on endothelial cells were performed as previously described (Radu et al., 2012). Images were captured using a cooled CCD camera (Clara, Andor, Northern Ireland) in a set-up including a monochromator Polychrome V (Till Photonics, Germany) coupled to an inverted microscope (Diaphot 200, Nikon, Japan), and were acquired on a computer using an image acquisition software (Live Acquisition, Till Photonics, Germany). Solutions were delivered on top of the endothelial cells through a 100 µm quartz perfusion head using an 8-channel valve pressurized perfusion system (ALA Scientific Instruments, USA). Cells were incubated with Fura-2 AM (2.5 µM) and pluronic acid (F-127, 0.01%) for 45 min. After 15 min, the necessary time for Fura-2AM deesterification, the cells were imaged. Before starting the nanoparticle flux, the cell monolayer was perfused with Ringer HEPES-buffered for 5 minutes. Cytosolic Ca^{2+} transients were elicited by the administration of 20 nM Qtracker®800 for 5 min followed, after a Ringer HEPES-buffered wash-out period of 10 min, by the application of either ATP (30 µM, 20 s) for BMVECs and bEnd.3 cells, or histamine (10 µM, 20 s) for HUVECs. ATP and histamine are topical vasoactive substances that regulate brain capillary blood flow and vascular permeability (Akdis and Simons, 2006; Itoh and Suzuki, 2012), and were therefore used as positive controls for evoking intracellular calcium transients in endothelial cells. Cells that did not show a response to the positive control were excluded from subsequent analyses.

3.3.10. Endothelial cell viability by Trypan blue assay

Trypan blue assay was performed on bEnd.3 and BMVECs in control conditions and after 24 hrs treatment with Qtracker®800 (10, 20 and 40 nM). Cells were detached by trypsin, trypan blue was added (0.2 %) and viable cells were counted (at least 150 cells). The viability

was calculated relative to controls. Measurements were done in three replicates. Cells exposed to 3 mM H_2O_2 (1h) were used as positive control.

3.3.11. Data analysis

Data analysis was performed using OriginPro 8 (OriginLab Corporation, USA), Offline Acquisition software (Till Photonics, Germany) and Matlab (Mathworks, Natick, MA).

Intracellular calcium changes were estimated from the ratio $R = I_{340nm}/I_{380nm}$ (I_{340} and I_{380} are the intensities measured at the emission wavelength of 510 nm when Fura-2 was excited at 340 nm and 380 nm, respectively). The ratio R was calculated in regions of interest (ROIs) covering each cell in the microscope field, after background subtraction.

R values were corrected by subtracting baseline signals averaged over the 5 minutes of perfusion prior to the application of nanoparticles. The resulting ΔR values were used for subsequent analyses. Only responses with an amplitude higher than 3 times the standard deviation of the background noise (measured before QD administration) were considered.

In view of the lack of standard quantitative methods to describe calcium transients in the literature (Taylor and Francis, 2014), we defined a set of parameters characterising the signal envelope (**Figure 3.1**). The onset and offset of the response were marked by the signal raising above and descending below a 5% threshold of the peak amplitude (ΔR_{max}). Response latency was the time from beginning of nanoparticle perfusion to response onset. Total response duration was the interval between response onset and offset. In order to differentiate between fast transients with sustained late responses and signals reaching a peak later in time, we computed a response asymmetry ratio (b/a), where a is the time from response onset to peak, and b is the time from response peak to offset. Total response area was the integral over response duration. Finally, we computed the maximum slope of the ascending transient (V_{max}). Pairwise correlations (along with Pearson and Spearman coefficients) among these parameters were computed with custom Matlab scripts. One-way ANOVAs followed by Fisher LSD *post-hoc* tests were used to assess BMVEC and bEnd.3 endothelial cell viability, comparing cells treated with different concentrations of Qtracker®800 to untreated controls.

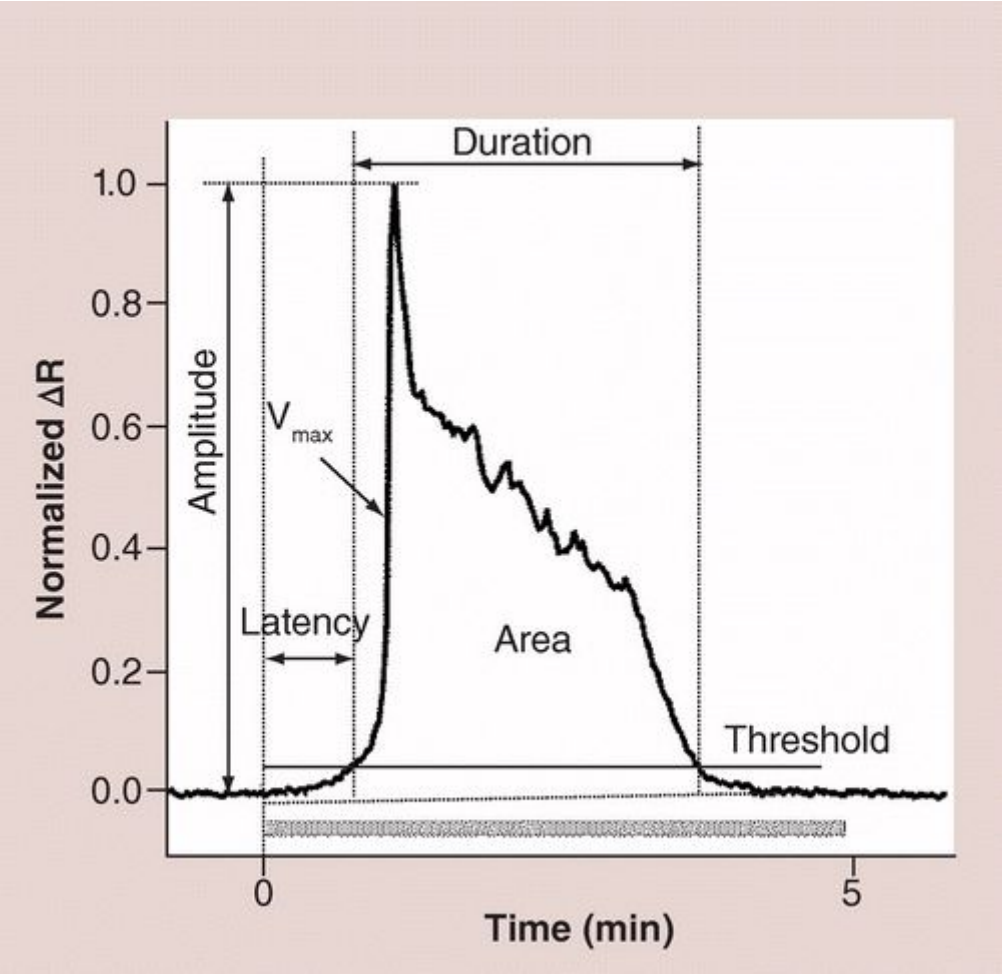

Figure 3.1. Relevant parameters in a calcium transient trace.

3.4. Results

3.4.1. Characterization of nanoparticles (size, hydrodynamic diameter, and zeta-potential)

We measured the hydrodynamic diameter of Qtracker®800 by means of the DLS technique. DLS measurements were performed on QDs dissolved in saline solution or in Ringer HEPES-buffered solution.

For both saline and HEPES-buffered Ringer solutions, we found in the intensity distribution plots a major peak centered near the expected size of Qtracker®800 (**Figure 3.2. A, B**), as well as a minor peak corresponding to larger components (e.g. aggregates of nanoparticles). The DLS graphs in **Figure 3.2** refer to 50 nM Qtracker®800, but note that the distribution did not significantly change for the analysed range of nanoparticle concentrations (40-80 nM). A global polydispersity index (PdI) of ~0.35 was determined for both solutions. The major, lower-diameter peak can be attributed to isolated Qtracker®800 particles. Given the wider scattering of larger particles, the relative populations of the species corresponding

to the two peaks can be better appreciated after conversion of the data into a number distribution (dotted lines) which results in a single peak and confirms the prevalence of well-dispersed Qtracker®800 particles.

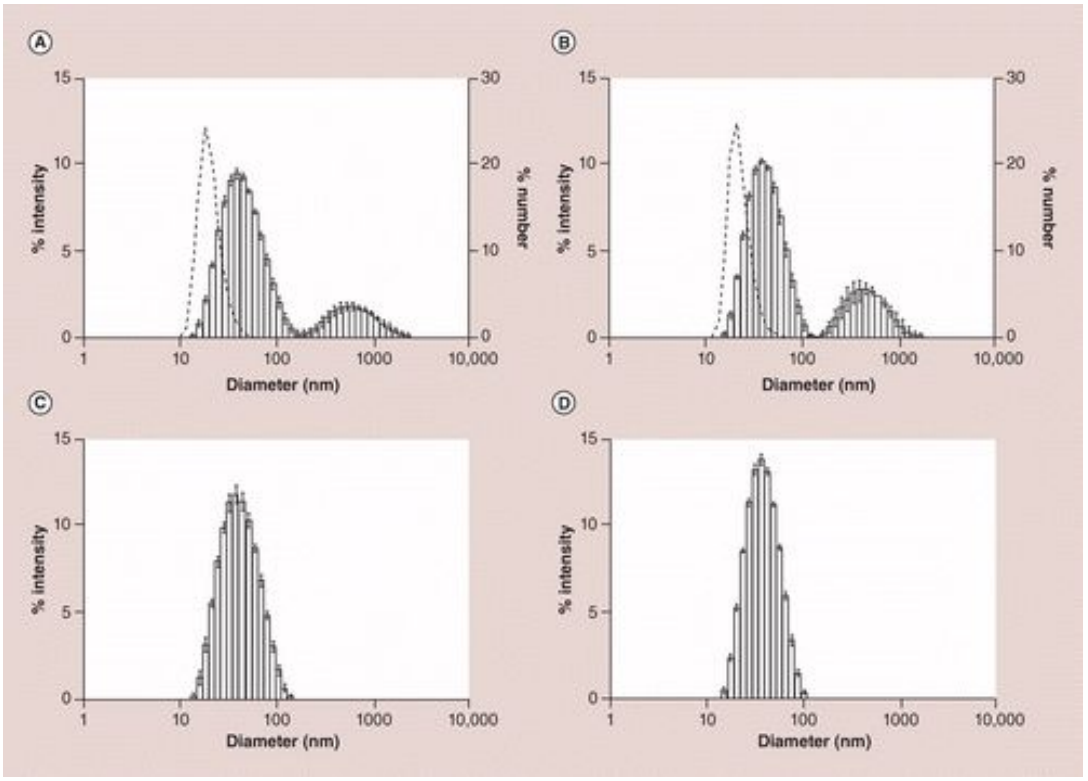

Figure 3.2. Distribution of Qtracker®800 particle sizes measured by dynamic light scattering. (A) Qtracker®800 in Ringer HEPES-buffer solution; **(B)** Qtracker®800 in saline solution; **(C)** same as **(A)** after centrifugation; **(D)** same as **(B)** after centrifugation. Histograms are size distribution by intensity plots (left y-axes). Error bars show the SD of three replicate measurements. Dotted curves in **(A & B)** correspond to number distribution plots (right y-axes) obtained by conversion from the underlying intensity distributions.

An attempt to remove the larger-size contaminant by filtration was unsuccessful. On the other hand, centrifugation followed by DLS measurements on the supernatant resulted in very clean samples displaying a single peak in size distribution plots (**Figure 3.2. C, D**). The monomodal distribution observed for these two preparations allowed us to perform a rigorous cumulant analysis and evaluate the harmonic intensity-averaged particle diameter (Z-average). The Z-average of Qtracker®800 was 36.56 ± 0.13 nm in Ringer HEPES-buffer (PdI = 0.180) and 35.80 ± 0.34 nm in saline solution (PdI = 0.151). The zeta potential value was -0.0124 ± 0.206 mV, indicating that Qtracker®800 particles are essentially neutral at pH 7.4. Qtracker®800 were also characterized by TEM (**Figure 3.3. A**) and their cores, as visualized in suspension, were irregular in shape and their longest axis measured on average 8.27 ± 1.27 nm (SD).

3.4.2. Qtracker®800 accumulation in mouse brain microvascular endothelium

We then proceeded to evaluate the interaction of Qtracker®800 with the brain vascular endothelium in Balb/c mice upon nanoparticle injection. TEM analysis of mouse cortical brain sections indicated the presence of Qtracker®800 in the brain vascular endothelium 3 hrs after the i.v. injection, the time window recommended by the nanoparticle producer for vasculature imaging studies (**Figure 3.3. B and C**). Nanoparticles can be detected in the cytoplasm, both concentrated within vesicle-like structures, and free in the cytosol. An in-depth histological characterization (sampling different brain regions and cellular compartments, different time-points, or even different organs) of the subcellular distribution of Qtracker®800 nanoparticles distribution is beyond the scope of the present study.

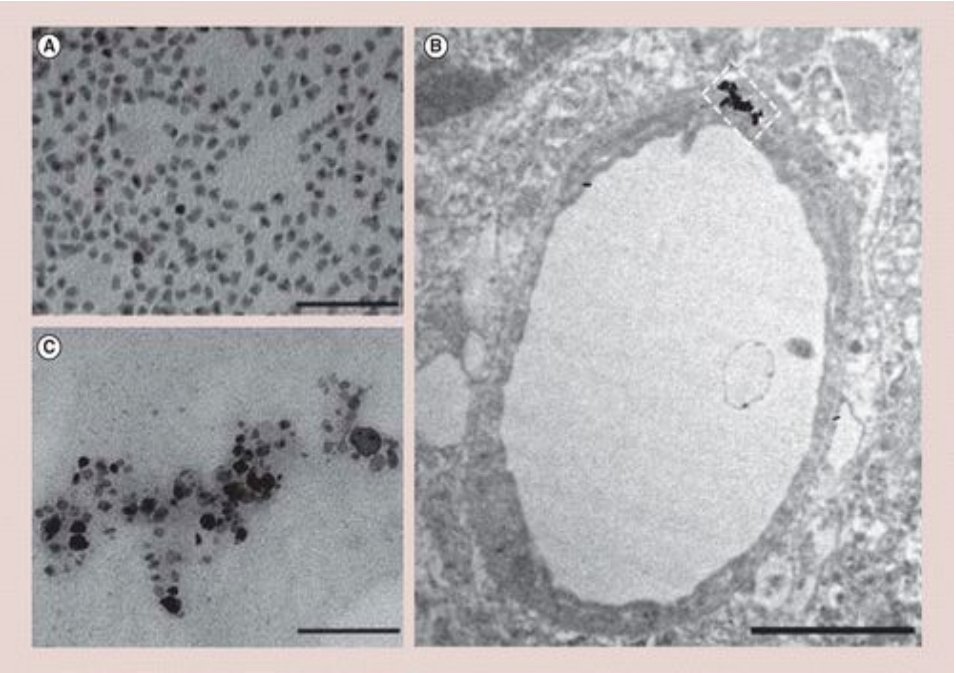

Figure 3.3. Transmission electron microscopy images on Qtracker®800 and their accumulation in Balb/c mouse brain endothelium. (A) Qtracker®800 in suspension; scale bar: 100 nm. **(B)** Qtracker®800 *in vivo* accumulation in brain vascular endothelium, 3 h after intravenous injection; scale bar: 1 μm. **(C)** Detailed image of nanoparticle accumulation in the endothelium; scale bar: 100 nm.

3.4.3. Qtracker®800 treatment does not lead to major cell death in vitro

Given the *in vivo* accumulation of Qtracker®800 in mouse brain endothelium demonstrated by TEM data, we have further verified, by *in vitro* tests, if nanoparticle administration modified endothelial cell viability. Viability slightly decreased as a function of nanoparticle concentration (BMVECs: $F(3,8) = 5.25$, $p < 0.05$; bEnd.3s: $F(3,8) = 5.37$, $p < 0.05$). Fisher *post-hoc* tests confirmed that the reduction was statistically significant only for the highest nanoparticle concentration, when viability dropped to about 93% (**Figure 3.4)**.

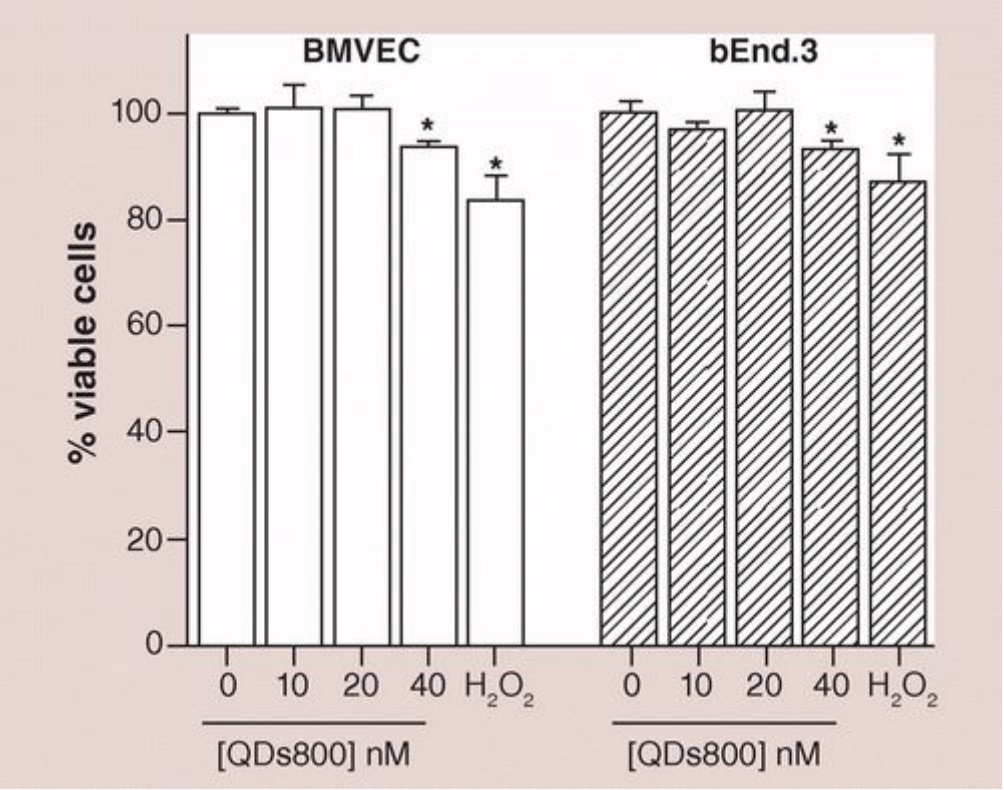

Figure 3.4. Viability of brain microvascular endothelial cells upon 24 h *in vitro* exposure to Qtracker®800. Percentage of viable cells (means ± standard deviation) obtained by Trypan blue assay on brain microvascular endothelial cells and bEnd.3 cells exposed for 24 h to 0, 10, 20 and 40 nM Qtracker®800 and 3 mM H_2O_2 (positive control). Statistically significant differences ($p < 0.05$) from the control (0 nM) conditions are indicated by an asterisk (*). bEnd.3: Brain endothelial cell line derived from mice cerebral cortex; BMVEC: Brain microvascular endothelial cells from Balb/c mice in primary culture; QD: Quantum dot.

3.4.4. Qtracker®800 generate intracellular calcium transients in mouse brain endothelial cells and human umbilical vein endothelial cells

As *in vitro* endothelial cell viability tests revealed only small effects on cell survival of Qtracker®800 in the concentration ranges relevant for *in vivo* imaging studies (see Materials & methods, "*in-vitro* Qtracker®800 studies" section), we explored the possibility of more subtle, functional nanoparticle-induced alterations of endothelial cells, by studying intracellular calcium fluctuations.

Acute (5 min) exposure to 20 nM Qtracker®800 generated cytosolic calcium transients in BMVECs (**Figure 3.5.A**), bEnd.3 cells (**Figure 3.5.B**), and HUVECs (**Figure 3.5.C, D**). Based on the inclusion criteria described above, we found that 13.7% (52/380 cells) of BMVECs and 13.9% (57/410 cells) of bEnd.3 cells were responsive to Qtracker®800. Out of a total 1796 studied HUVECs, 189 (or 10.5%) responded to Qtracker®800. Interestingly, the fraction of responsive cells varied significantly between the seven donors (**Figure 3.5.D**),

suggesting the possibility that subjects may be either sensitive (20% or more of responsive cells) or non-sensitive (5% or less) to nanoparticles.

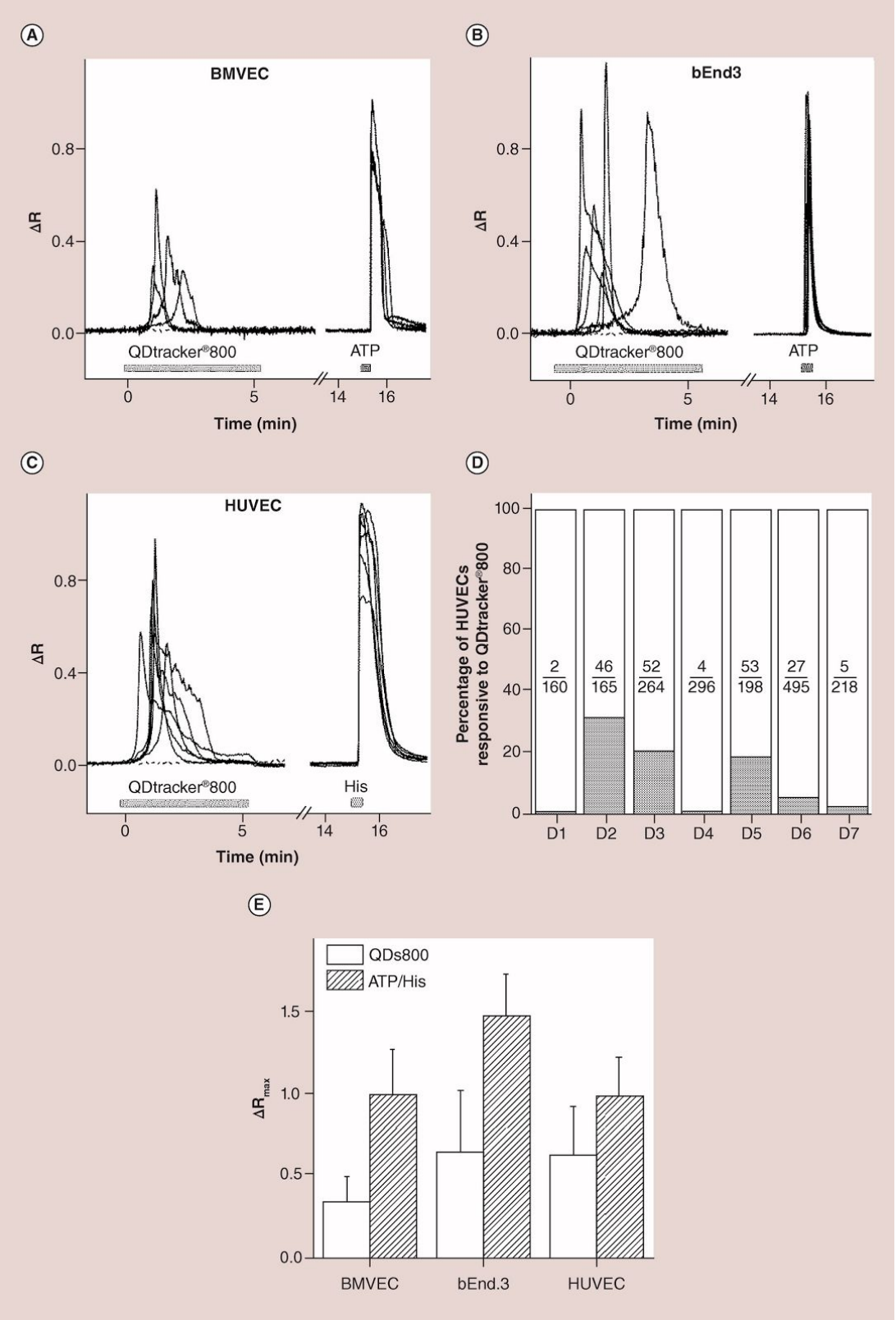

Figure 3.5. Qtracker®800 evoked $(Ca^{2+})_i$ transients in mouse and human endothelial cells. Representative traces of ΔR over time for **(A)** brain microvascular endothelial cells; **(B)** bEnd3, and **(C)** HUVECs. An

endogenous control response was evoked by ATP (30 μM) in **A & B**, and by histamine (10 μM) in **(C)**. **(D)** HUVECs' sensitivity to Qtracker®800 exposure, where responsive cells are considered those able to generate intracellular calcium transients upon brief exposure (5 min) to Qtracker®800. Percentage of responsive (gray) and nonresponsive (white) endothelial cells from different donors. The number of Qtracker®800-responsive cells are plotted against the total number of tested cells in separate columns for each donor (D1–D7). The percentages of responsive cells for each donor are: D1: 1.25%; D2: 27.87%; D3: 19.69%; D4: 1.35%; D5: 26.76%; D6: 5.45%; D7: 2.29%. **(E)** ΔR_{max} for BMVEC, bEnd.3 and HUVEC in response to Qtracker®800 and to ATP or His, respectively**.** bEnd.3: Brain endothelial cell line derived from mice cerebral cortex; BMVEC: Brain microvascular endothelial cells from Balb/c mice in primary culture; D: Donor; His: Histamine; HUVEC: Human umbilical vein endothelial cell; QD: Quantum dot.

ΔR_{max} values induced by Qtracker®800 perfusion were on average a sizeable fraction of those induced in the positive control conditions. Namely, average ΔR_{max} values for BMVEC and bEnd.3 cells were about ⅓ and ½, respectively, of those produced by ATP administration; HUVEC cells had an average ΔR_{max} of about ⅔ of that induced by histamine administration.

The quantitative analysis of calcium imaging recordings revealed a diversity of calcium transient profiles generated during the acute exposure of endothelial cells to the nanoparticle flux. The majority of observed calcium transients had a sharp onset, followed by a longer sustained response and decay (high asymmetry ratios). This pattern was substantially more marked in HUVECs than in mouse cells (**Figure 3.5.A-C** and **Figure 3.6**).

In spite of certain commonalities, responses differed in several respects among cell types (**Figure 3.6.A**). HUVEC transients showed the highest mean amplitude, area and duration (**Figure 3.6.A**) i.e. they produced the strongest responses to nanoparticle administration. HUVEC transients were also highly asymmetrical (approx. 3 times more than the mouse endothelial transients). Interestingly, the ΔR_{max} and V_{max} distributions were remarkably similar. Indeed, a strong and highly significant correlation between the two parameters was observed (**Figure 3.6.B**, upper panels. See also **Figures 3.7-3.9**, and **Tables 3.1-3.3** for a complete presentation of the correlations and distribution histograms). This suggests that a very rapid increase in the ascending phase of the transient tends to produce high peak amplitudes. Even more important is the fact that the slope of the linear regression was very similar between cell types. This suggests a common mechanism of calcium transient triggering, irrespective of endothelial types.

On the other hand, response latencies were similar across endothelial cell types, again suggesting a common triggering mechanism. Additionally, an interesting pattern was observed when plotting response latencies against V_{max} (**Figure 3.6.B**, lower panels). The charts suggest that cells with relatively short latencies are characterized by a wide range of response transient velocities, while longer latencies were associated with relatively slower transients. In other words, delayed transients tended to be restricted to less steep ascending transients (smaller V_{max}) and consequently smaller amplitude.

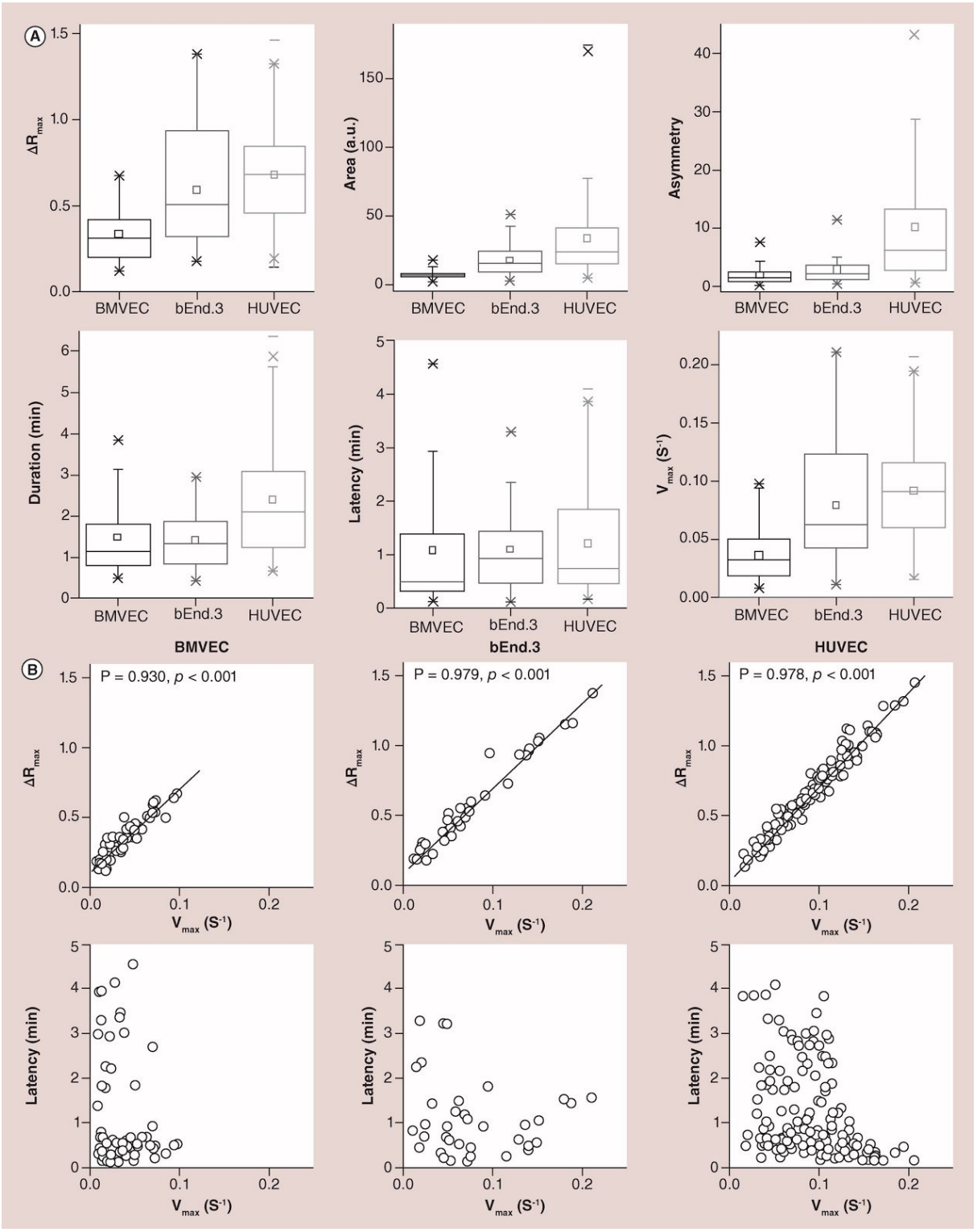

Figure 3.6. Analysis of the parameters in Qtracker®800-induced calcium transients. (A) Distributions of each of the six calcium transient parameters (y-axis label) defined in the 'Materials & methods' section. The boxplots show the median, 25th and 75th percentiles. In addition, the mean (□), 1% and 99% percentiles (×), and the minimum and maximum data points (-) are reported. **(B)** Correlations between selected parameter pairs for each cell type (the linear fit with Pearson coefficient – P, and the confidence level – p – are presented for the upper panels). See Figures 2.7-2.9 for the complete pairwise correlation matrices. BMVEC: Brain microvascular

endothelial cells from Balb/c mice in primary culture; HUVEC: Human umbilical vein endothelial cell; V_{max}: Maximum slope of the ascending calcium transient.

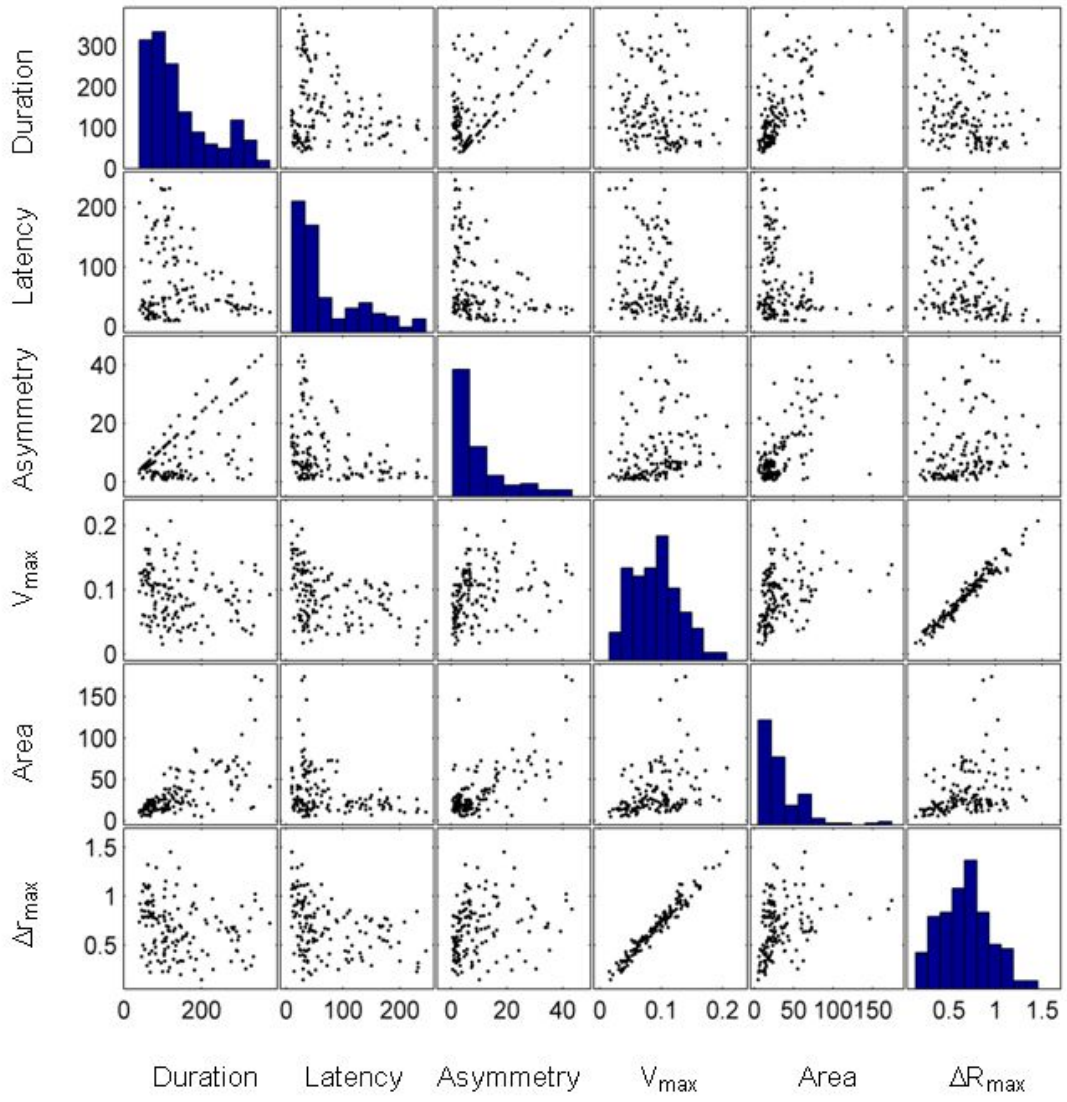

Figure 3.7. Correlations of calcium transients' parameters (defined in **Figure 3.1**) induced by Qtracker®800 in HUVECs.

Table 3.1. Pearson and Spearman correlation coefficients and their probabilities computed for the calcium transients' parameters (see plots in **Figure 3.7**) induced by Qtracker®800 in HUVECs

Pearson coefficient *p value*	**Duration**	**Latency**	**Asymmetry**	**V_{max}**	**Area**	**ΔR_{max}**
Duration		-0.2251 *0.0061*	0.6336 *0.0000*	-0.1761 *0.0329*	0.6956 *0.0000*	-0.1836 *0.0260*
Latency	-0.2251 *0.0061*		-0.3408 *0.0000*	-0.3437 *0.0000*	-0.2836 *0.0005*	-0.3187 *0.0001*
Asymmetry	0.6336 *0.0000*	-0.3408 *0.0000*		0.2465 *0.0026*	0.6436 *0.0000*	0.2034 *0.0135*
V_{max}	-0.1761 *0.0329*	-0.3437 *0.0000*	0.2465 *0.0026*		0.3297 *0.0000*	**0.9784** *0.0000*
Area	0.6956 *0.0000*	-0.2836 *0.0005*	0.6436 *0.0000*	0.3297 *0.0000*		0.3272 *0.0001*
ΔR_{max}	-0.1836 *0.0260*	-0.3187 *0.0001*	0.2034 *0.0135*	**0.9784** *0.0000*	0.3272 *0.0001*	

Spearman coefficient *p value*	**Duration**	**Latency**	**Asymmetry**	**V_{max}**	**Area**	**ΔR_{max}**
Duration		-0.0375 *0.6517*	0.3743 *0.0000*	-0.2396 *0.0035*	0.6727 *0.0000*	-0.2421 *0.0031*
Latency	-0.0375 *0.6517*		-0.3733 *0.0000*	-0.3954 *0.0000*	-0.2319 *0.0047*	-0.3778 *0.0000*
Asymmetry	0.3743 *0.0000*	-0.3733 *0.0000*		0.3822 *0.0000*	0.5402 *0.0000*	0.3129 *0.0001*
V_{max}	-0.2396 *0.0035*	-0.3954 *0.0000*	0.3822 *0.0000*		0.4035 *0.0000*	**0.9784** *0.0000*
Area	0.6727 *0.0000*	-0.2319 *0.0047*	0.5402 *0.0000*	0.4035 *0.0000*		0.3995 *0.0000*
ΔR_{max}	-0.2421 *0.0031*	-0.3778 *0.0000*	0.3129 *0.0001*	**0.9784** *0.0000*	0.3995 *0.0000*	

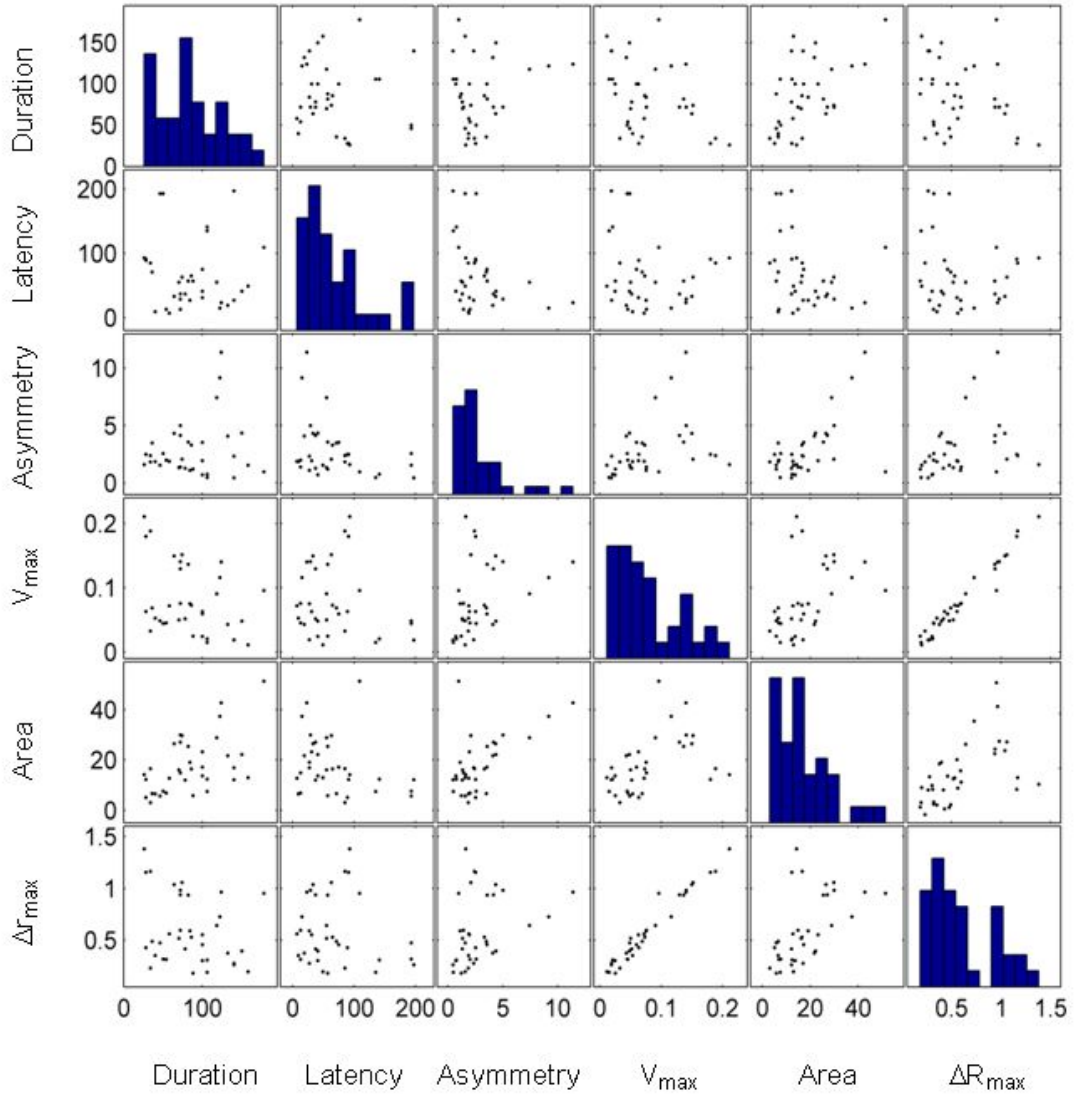

Figure 3.8. Correlations of calcium transients parameters induced by Qtracker®800 in bEnd.3 cells

Table 3.2 Pearson and Spearman correlation coefficients and their probabilities computed for the calcium transients' parameters (see plots in **Figure 3.8**) induced by Qtracker®800 in bEnd.3 cells

Pearson coefficient *p value*	**Duration**	**Latency**	**Asymmetry**	**V_{max}**	**Area**	**ΔR_{max}**
Duration		-0.0698 *0.6859*	0.1822 *0.2875*	-0.3599 *0.0311*	0.5398 *0.0007*	-0.2557 *0.1322*
Latency	-0.0698 *0.6859*		-0.3468 *0.0383*	-0.1596 *0.3524*	-0.2881 *0.0884*	-0.1299 *0.4500*
Asymmetry	0.1822 *0.2875*	-0.3408 *0.0000*		0.3871 *0.0197*	0.5879 *0.0002*	0.3363 *0.0449*
V_{max}	-0.3599 *0.0311*	-0.1596 *0.3524*	0.3871 *0.0197*		0.4687 *0.0039*	**0.9791** *0.0000*
Area	0.5398 *0.0007*	-0.2881 *0.0884*	0.5879 *0.0002*	0.4687 *0.0039*		0.5653 *0.0003*
ΔR_{max}	-0.2557 *0.1322*	-0.1299 *0.4500*	0.3363 *0.0449*	**0.9791** *0.0000*	0.5653 *0.0003*	

Spearman coefficient *p value*	**Duration**	**Latency**	**Asymmetry**	**V_{max}**	**Area**	**ΔR_{max}**
Duration		-0.1305 *0.4481*	-0.0482 *0.7803*	-0.3855 *0.0202*	0.4807 *0.0030*	-0.2978 *0.0777*
Latency	-0.1305 *0.4481*		-0.3064 *0.0692*	-0.1231 *0.4744*	-0.3246 *0.0534*	-0.0994 *0.5641*
Asymmetry	-0.0482 *0.7803*	-0.3408 *0.0000*		0.5005 *0.0019*	0.4991 *0.0019*	0.4609 *0.0047*
V_{max}	-0.3855 *0.0202*	-0.1231 *0.4744*	0.5005 *0.0019*		0.5439 *0.0006*	**0.9737** *0.0000*
Area	0.4807 *0.0030*	-0.3246 *0.0534*	0.4991 *0.0019*	0.5439 *0.0006*		0.6242 *0.0000*
ΔR_{max}	-0.2978 *0.0777*	-0.0994 *0.5641*	0.4609 *0.0047*	**0.9737** *0.0000*	0.6242 *0.0000*	

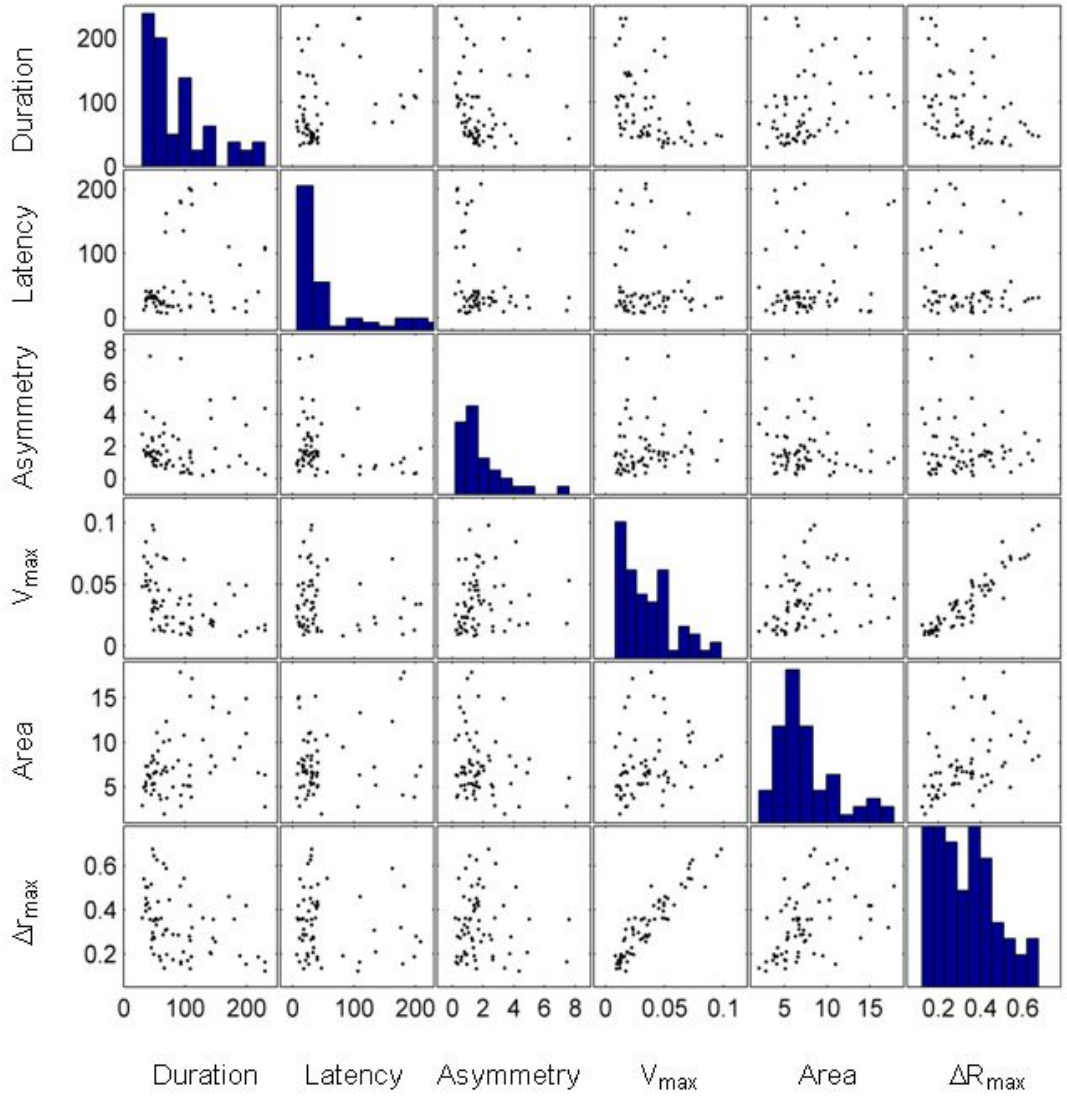

Figure 3.9. Correlations of calcium transients' parameters induced by Qtracker®800 in BMVECs

Table 3.3. Pearson and Spearman correlation coefficients and their probabilities computed for the calcium transients' parameters (see plots in **Figure 3.9**) induced by Qtracker®800 in BMVECs

Pearson coefficient *p value*	**Duration**	**Latency**	**Asymmetry**	**V_{max}**	**Area**	**ΔR_{max}**
Duration		0.0808 *0.5224*	-0.0185 *0.8839*	-0.4359 *0.0003*	0.3176 *0.0099*	-0.4006 *0.0009*
Latency	0.0808 *0.5224*		-0.2643 *0.0334*	-0.1886 *0.1325*	-0.0437 *0.7298*	-0.1709 *0.1735*
Asymmetry	-0.0185 *0.8839*	-0.2643 *0.0334*		0.1084 *0.3900*	-0.2235 *0.0735*	-0.0631 *0.6173*
V_{max}	-0.4359 *0.0003*	-0.1886 *0.1325*	0.1084 *0.3900*		0.2253 *0.0712*	**0.9301** *0.0000*
Area	0.3176 *0.0099*	-0.0437 *0.7298*	-0.2235 *0.0735*	0.2253 *0.0712*		0.4539 *0.0001*
ΔR_{max}	-0.4006 *0.0009*	-0.1709 *0.1735*	-0.0631 *0.6173*	**0.9301** *0.0000*	0.4539 *0.0001*	

Spearman coefficient *p value*	**Duration**	**Latency**	**Asymmetry**	**V_{max}**	**Area**	**ΔR_{max}**
Duration		0.0504 *0.6900*	-0.2599 *0.0365*	-0.5478 *0.0000*	0.3400 *0.0056*	-0.4610 *0.0001*
Latency	0.0504 *0.6900*		-0.2652 *0.0327*	-0.1249 *0.3215*	-0.1348 *0.2843*	-0.1091 *0.3869*
Asymmetry	-0.2599 *0.0365*	-0.2652 *0.0327*		0.2446 *0.0496*	-0.1519 *0.2271*	0.0585 *0.6436*
V_{max}	-0.5478 *0.0000*	-0.1249 *0.3215*	0.2446 *0.0496*		0.3545 *0.0038*	**0.9219** *0.0000*
Area	0.3400 *0.0056*	-0.1348 *0.2843*	-0.1519 *0.2271*	0.3545 *0.0038*		0.5419 *0.0000*
ΔR_{max}	-0.4610 *0.0001*	-0.1091 *0.3869*	0.0585 *0.6436*	**0.9219** *0.0000*	0.5419 *0.0000*	

3.5. Discussion

In this study, we report for the first time a functional interaction of Qtracker®800 with the brain vascular endothelium. In particular, we found that: a) QDs may be uptaken *in vivo* by brain endothelial cells; b) the interaction between QDs and endothelial cells results in the activation of free cytosolic calcium signaling in primary and immortalized brain endothelial cells, as well as in human umbilical vein endothelial cells; c) such activation does not appear to be related to cytotoxicity, resulting instead in interferences with normal calcium-mediated signal transduction pathways ; d) HUVEC data indicate a high inter-individual variability of QDs-cell interaction susceptibility.

3.5.1. Non-targeted PEGylated near-infrared emitting Qtracker®800 accumulate in brain vascular endothelium

Previous studies demonstrated the uptake by endothelial cells of different functionalized and/or targeted PEGylated quantum dots (Koole et al., 2008; Pollinger et al., 2013; Chen et al., 2013), but not of non-targeted Qtracker® Vascular labels. The latter nanoparticles can be uptaken in different cell types (Maysinger et al., 2007; Ryman-Rasmussen et al., 2007; Zhang and Monteiro-Riviere, 2009; Xiao et al., 2010), but to our knowledge no reports are available for endothelial cells. Furthermore, uptake of Qtracker®800 has not been reported for any cell type.

Endocytosis, which is thought to be the main pathway for nanoparticle internalization (Damalakiene et al., 2013; Kou et al., 2013), depends on nanoparticle size (Shang et al., 2014). Specifically, endocytosis-mediated uptake of nanoparticles was found to be more efficient for hydrodynamic diameter values around 50 nm (Osaki et al., 2004). In this respect, although the optical qualities of Qtracker 800 make it suitable for deep vasculature imaging, their high hydrodynamic diameter (~ 35-36 nm based on our data) compared to the other dyes of the Qtracker vascular label series (the second largest being the 26.6 nm Qtracker 705; Ho et al., 2011), makes them potentially more prone to endocytic internalization.

In *in vivo* or cell-culture experiments, the issue of nanoparticle fate is further complicated by the very complex media (blood, cell-culture medium) with which they interact. Very recent reports show the strong dependence of nanoparticle aggregation, particularly quantum dots, with respect to medium composition and coating structure (Moquin et al., 2015; Balog et al., 2015). Even in a simpler solution, bovine serum albumine in PBS, the hydrodynamic diameter of Qtracker®800, as measured by DLS, increased with albumin concentrations, becoming more than double at protein concentrations equivalent to those present in the mouse blood serum (Rampazzo el al., 2012). Blood fibrinogen was also proven to strongly bind Qtracker®800 (Pozzi-Mucelli et al., 2009). In this context, it is very

difficult to further speculate about the mechanism by which Qtracker®800 particles are uptaken into the cells.

A vascular label such as the Qtracker® nanoparticles is expected to be inert with respect to the physiology of the target system. Our study, however, shows that non-targeted, near-infrared emitting Qtracker®800 are captured by the brain vascular endothelium in the first 3 hours upon vein injection, which raises important concerns, including the possibility that such uptake (and interaction more in general) may lead to alteration of endothelial cell functionality.

3.5.2. Qtracker®800 alters 'normal' calcium signalling in brain endothelial cells

It was previously shown that acute exposure (5 to 30 min) to non-PEGylated or functionalized QDs elicits *in vitro* cytosolic calcium increases in different excitable and non-excitable cells (Tang et al., 2008; Tang et al., 2008; Clift et al., 2010; Miragoli et al., 2013). Our study points out that nanoparticle PEG-ylation, at least in the case of Qtracker®800, does not prevent functional consequences on the vascular endothelium, as revealed by the occurrence of calcium transients during the 5-min exposure.

The vascular endothelium has mechanosensitive properties, as part of the adaptation to the permanent shear stress exerted by the bloodstream. Endothelial cells may react to mechanical stimuli through a variety of mechanisms, such as transient receptor potential channels, ATP-operated cation channels, GTP-binding protein coupled receptors, and adhesion molecules (Ando and Yamamoto, 2013). In turn, a variety of downstream intracellular signalling pathways are activated, the majority involving either calcium release from internal stores, the intake of extracellular calcium, or both (Tran et al., 2000, Ando and Yamamoto, 2013). The strong positive correlation between calcium release amplitude (ΔR_{max}) and steepness (V_{max}) shown in the present study has similarities with the previously reported amplitude-dependent calcium release in response to local mechanical stimuli (Yamamoto et al., 2000) and might imply that Qtracker®800 act as a mechanical trigger for the calcium-induced transients.

The wide range of calcium event latencies we have observed, and the fact that only a subset of cells were activated, lead to the following speculation. Some cells are triggered by a probabilistic, direct interaction with the nanoparticles (possibly of mechanical nature) while neighboring cells are indirectly recruited in a wave of calcium events through intercellular communication mechanisms, as previously described in other endothelial cell types (Long et al., 2012). In this view, while fast and steep transients could be the result of direct nanoparticle-to-cell interactions, slower and shallower transients could be related to indirect activations.

3.5.3. Qtracker®800 might activate different components of the neurovascular unit

It has already been stated that brain microvascular endothelium is a major component of the neurovascular unit, playing essential roles in physiological and pathological neuronal-activation states (Fabene et al., 2008, Bertini et al., 2013, Radu et al., 2013). The spatio-temporal Ca^{2+} dynamics contribute to many physiological properties of the vascular intima (Taylor and Francis, 2014); asynchronous and synchronous Ca^{2+} waves control vascular tone (Mufti et al., 2010). Local changes at the level of vascular endothelium (e.g. leukocyte-endothelial adhesion, leukocyte rolling) can translate into alterations of neuronal excitability (Fabene et al., 2008). In this general context, the Qtracker®800-induced intracellular endothelial Ca^{2+} transient activation shown by our results deserves attention in nanomedicine, and might imply not only localised endothelial Ca^{2+} events but also the initiation of a complex signalling pathway involving multiple components of the neurovascular unit. Previous studies have highlighted the action of nanoparticles on different components of the neurovascular unit, by demonstrating that Qtracker®705: 1) accumulate *in vitro* in primary cortical cultures; 2) activates astrocytes after microinjection in brain cortex (Maysinger et al., 2007). Furthermore, large silica (NH_2) PEGylated nanoparticles *in vitro* are uptaken into bEnd.3 cells and, *in vivo*, are transported across the blood-brain barrier in Balb/c mice (Liu et al., 2014).

Based on our data, we wonder whether Qtracker®800-induced alteration of 'normal' calcium signaling in endothelial cells may bias the interpretation of results in studies of brain vascular function where nanoparticles are used as labels.

3.5.4. How suitable are Qtracker®800 for translational studies?

Our results indicate that the nanoparticle-induced endothelial activation is not specific to mouse brain vessels, but it extends at least to a different species (human) and a different endothelial cell localisation (umbilical vein). A further generalisation of the observation will require *ad-hoc* studies on endothelial cells derived from other species and organs.

A key result in our study is the striking difference in HUVEC sensitivity to Qtracker®800 from one donor to another (almost an all-or-none effect). Our data agree with previously reported donor-dependent variability of HUVECs exposed to laminar shear stress (Feairheller et al., 2011), and might have implications for the use of near-infrared-emitting quantum dots in clinical vascular imaging applications.

Whether a similar donor-dependent variability of responses in HUVECs exists also in rodents is not easy to establish, since *in-vitro* studies make use of sample pooling between several subjects (approximately ten mice for a single culture; Ruck et al., 2014). But this is a relevant issue, because if on one hand the mean number of activated cells in mice and in

humans are comparable (13.7% vs. 10.5%) establishing potential effects based on such averages might underestimate the effects on the individuals more prone to QD-induced activations.

3.6. Conclusions & Future perspective

Our study partly fills the knowledge gap regarding the interaction of near-infrared-emitting Qtracker®800 nanoparticles with biological systems, in particular the brain vascular endothelium. Both *in vitro* and *in vivo* data indicate the accumulation of QDs in the vascular endothelium as well as functional effects revealed by intracellular calcium changes in a subset of cells. In addition, we observed substantial inter-individual differences in HUVEC activation. Altogether, the findings raise two types of concern: 1) in studies of vascular function in living animals, the use of QD-based labeling might bias the results in difficult-to-detect ways; 2) in view of possible clinical applications, the between-subject variability in susceptibility may complicate safety assessments.

Undoubtedly, brain vasculature imaging techniques can greatly benefit from the use of nanoparticle labels. On the other hand, as we have shown, such labels may be internalized by and functionally interact with blood vessel endothelia, which raises obvious safety concerns. It is quite possible that the effects uncovered represent the tip of an iceberg, and that further studies are necessary to better characterize the full extent and consequences of the activations. Ideally, the development of novel labels should be focused on reducing or eliminating their interactions with biological tissues. Considering the vast potential of these nanoparticles for brain vasculature imaging, we hope that further chemical engineering will optimize their biostability, biocompatibility, and efficient clearance profile.

3.7. Executive summary

Aim

- To assess the possible interaction of Qtracker®800 Vascular labels (Qtracker®800), a powerful nanotechnology tool for biomedical vasculature imaging, with mouse and human endothelium.

Results

- Transmission electron microscopy showed Qtracker®800 accumulation in mouse brain microvascular endothelium 3 h after their administration.

- Mouse brain endothelial cells, both in primary and immortalized cultures, are Qtracker®800-sensitive; 14% of cells generate intracellular calcium transients during acute 5-min exposures.
- Human umbilical vein endothelial cells in primary culture derived from different donors present substantial variability in transient calcium responses (0 ÷ 30%) when acutely exposed to Qtracker®800.
- The chronic *in vitro* exposure to Qtracker®800 for 24 h did not reveal major changes in endothelial cell viability.

Conclusion & future perspective

- We demonstrated a direct action of Qtracker®800 on the vascular endothelium in the first 3 h after administration, thus overlapping the time window recommended for vasculature imaging studies with these fluorescent nanoparticles.
- Keeping in mind the enormous potential of Qtracker®800 deep-tissue penetration in biomedical applications, better manufacturing solutions to diminish/eliminate endothelium actions should be found.

Chapter 4. Functional expression of murine muscarinic acetylcholine receptors in CNS microvascular endothelium

4.1. Summary

Clinical and experimental studies indicate that muscarinic acetylcholine receptors are potential pharmacological targets for the treatment of neurological diseases. Although these receptors have been described in human, bovine and rat cerebral microvascular tissue, a subtype functional characterization in mouse brain endothelium is lacking. Here, we show that all muscarinic acetylcholine receptors (M_1-M_5) are expressed in mouse brain microvascular endothelial cells. The mRNA expression of M_2, M_3, and M_5 correlates with their respective protein abundance, but a mismatch exists for M_1 and M_4 mRNA versus protein levels. Acetylcholine activates calcium transients in brain endothelium via muscarinic, but not nicotinic, receptors. Moreover, although M_1 and M_3 are the most abundant receptors, only a small fraction of M_1 is present in the plasma membrane and functions in ACh-induced Ca^{2+} signaling. Bioinformatic analyses performed on eukaryotic muscarinic receptors demonstrate a high degree of conservation of the orthosteric binding site and a great variability of the allosteric site. In line with previous studies, this result indicates muscarinic acetylcholine receptors as potential pharmacological targets in future translational studies. We argue that research on drug development should especially focus on the allosteric binding sites of the M_1 and M_3 receptors.

4.2. State-of-art

While it is widely known that acetylcholine (ACh) is released by axonal terminals of cholinergic neurons, cholinergic receptors are not found solely on target neurons. Rather, these receptor subtypes are also expressed by multiple non-neuronal cell types, both in the CNS (central nervous system) and peripherally, including endothelial, epithelial, mesothelial and immune cells (Eglen, 2006). This is not surprising, since cholinergic regulatory mechanisms have been described even in organisms lacking nervous systems, including plants, algae, and bacteria (Wessler and Kirkpatrick, 2012).

The data presented in this chapter have been published as: **Beatrice Mihaela Radu**, Antonio Marco Maria Osculati, Eda Suku, Adela Banciu, Grygoriy Tsenov, Flavia Merigo, Marzia Di Chio, Daniel Dumitru Banciu, Cristina Tognoli, Petr Kačer, Alejandro Giorgetti, Mihai Radu, Giuseppe Bertini, Paolo Francesco Fabene (2017) All muscarinic acetylcholine receptors (M_1-M_5) are expressed in murine brain microvascular endothelium. *Scientific Reports. 7(1):5083. doi: 10.1038/s41598-017-05384-z.*

Of particular interest is the role of muscarinic cholinergic receptors (mAChR) in modulating brain circulation, as it is known that ACh plays an important regulatory role at the level of brain arterioles, capillaries and venules (Sato et al., 2004). For example, anatomical evidence from rats shows that a significant portion of the projections from basal forebrain neurons to fronto-parietal cortical microvessels are cholinergic (Vaucher and Hamel, 1995). Additionally, it has been shown that intrinsic ACh neurons innervate intracortical cerebral blood vessels in rats (Chedotal et al., 1994). More recently, it has been reported that the somatosensory cortex microvasculature is innervated by cholinergic neurons (Kuznetsova and Schliebs, 2013). The functional effects, such as vasodilation, of ACh and equivalent agonists (e.g., carbachol) have been demonstrated on both the luminal and parenchymal sides of brain vasculature in humans and hamsters (Tsukahara et al., 1989; Rivers and Duling, 1992). However, the mechanisms by which ACh may act on the endothelium of brain microvasculature (independent of whether direct vascular innervation can be established), are not yet fully understood.

The exchange of signals between the blood stream and the brain parenchyma is facilitated by the close proximity of neurons or glial cells to the capillary anastomoses; in the mouse cortex, the average distance among the nearest blood capillary and neurons is 15 microns (Tsai et al., 2009). ACh has been shown to regulate peripheral vascular homeostasis, especially via actions on the endothelium (Cooke, 2000), for instance by stimulating epoxyeicosatrienoic acids production (Campbell and Fleming, 2010). Indeed, cholinergic mechanisms in the mouse endothelium have been described in a variety of fresh tissue preparations of the macro- and microcirculation (Peyter et al., 2008; Bagher et al., 2011; Gericke et al., 2011a; Gericke et al., 2011b). ACh has also been detected and quantified in the bloodstream, where it may interact with the luminal side of the endothelium (Kawashima et al., 1998). Notably, however, endothelial cells present a high degree of heterogeneity in the expression of surface markers, carrier proteins, and intracellular enzymes, across and within tissues (Cines et al., 1998).

The localization and functional activity of muscarinic and/or nicotinic ACh receptors in brain microvascular endothelia have been described humans, rats, and bovines (Elhusseiny et al., 1999; Luiten et al., 1996; Badaut et al., 1997; Traish et al., 1994; Tracey and Peach, 1992) but not in mice. Given the potential importance of this receptor family as non-neuronal drug targets (Zhang et al., 2014), and the increasing use of mAChR knockout mice as models for common neurological disorders (Zhang, 2006; Langmead et al., 2008; Wess et al., 2003), a detailed characterization of mAChRs expression and functionality in the mouse brain microvasculature is a high priority.

The mAChRs are a sub-class of the G-protein-coupled receptors (GPCRs) family, comprising 5 subtypes (M_1-M_5). M_1, M_3, and M_5 are coupled with the G_q protein and, via phospholipase C signaling pathway, generate cytosolic calcium transients; M_2 and M_4, on the other hand, couple with the G_i protein inhibiting the adenylyl cyclase (Langmead et al., 2008;

Wess et al., 2003). While obtaining mAChRs subtype-selective ligands is a primary goal in drug development (Langmead et al., 2008; Conn et al., 2009), previous attempts have failed due to the highly conserved structure of the orthosteric binding site across the muscarinic receptor family members (Felder et al., 2000; Wess, 2005). On the other hand, the allosteric binding site seems to hold promise as a specific pharmacological target (Conn et al. 2009). Yet, despite considerable recent progress in crystallography and molecular modeling of mAChRs (as well as the successful crystallization of human M_1, M_2, M_4, and rat M_3 receptors Haga et al., 2012; Kruse et al., 2012), no 3D structure predictions based on homology modeling studies have been carried out for mouse muscarinic receptors.

Indeed, previous studies of mAChRs expression in different species reported rather contradictory results, possibly due to the different cell sources and/or techniques used. Initially, using a radioligand binding assay, the presence of M_1 and M_3 was demonstrated in membrane samples from human and bovine microvessels (Linville and Hamel, 1995). However, subsequent ultrastructural investigations in rat capillaries showed a lack of mAChRs at this level; the few samples in which mAChR expression was detected on the perivascular astroglia and have been attributed to the endfeet of cholinergic neurons innervating the capillary basement membrane (Luiten et al., 1996; Badaut et al., 1997). In contrast, mAChRs have been reported in human endothelial cells from brain microvessels and capillaries (Elhusseiny et al., 1999). In particular, the M_2 and M_5 receptors (and occasionally M_1) have been identified in cells cultivated from intracortical biopsies obtained from patients with temporal lobe epilepsy. In addition, M_3 and M_2 receptors have been found in post-mortem fetal cerebral cortex samples (10-18 weeks of gestation). However, the peculiarity of these samples limits the generalization of the results.

Here, we report direct evidence that all 5 mAChRs subtypes are expressed in mouse brain microvascular endothelial cells using a combination of quantitative analyses of mRNA and protein levels. The M_1 and M_3 subtypes, in particular, show functional and pharmacological properties consistent with previous reports in the same tissue types from other species. While we confirm the abundant presence of M_3 in mouse brain endothelial cells, similar to findings in other species, we report for the first time the expression, but low functional relevance, of M_1 in these cells. We analyzed the conservation of the orthosteric and allosteric binding site among receptor subtypes along all annotated (as from GPCRdb, Lu and Hulme, 1999) eukaryotic species. Our data confirm the idea that, while the orthosteric cavity is highly conserved, the allosteric site is highly variable and thus represents a potential pharmacological target for drug design. Our findings support further translational and experimental cerebrovascular studies in mice.

4.3. Materials and Methods

All experimental protocols were approved by the University of Verona ethical committee. The methods were carried out in accordance with the relevant guidelines and regulations.

4.3.1. Brain endothelial cell cultures

To avoid biases due to contamination from astrocytes and/or terminals (Elhusseiny et al., 1999), we studied mAChRs in primary cultures of endothelial cells separated from brain microvascular tissue or in an endothelial cell line. Balb/c mouse primary brain endothelial microvascular cells BMVECs (#PB-BALB-5023, PELOBiotech, Germany; passages 3–6) and cells from the Balb/c mouse cell line bEnd.3 (#ATCC® CRL-2299™, ATCC, USA; passages 20–30) were cultivated as previously described (Radu et al., 2015). Both endothelial cell types were tested for mycoplasma contamination twice per year using the Hoechst (#B2883, Sigma) DNA staining protocol. Cells were plated at a density of 2 x 10^4 cells/cm^2 onto 24-mm cover glasses for the intracellular calcium imaging and immunofluorescence protocols, or into 25 cm^2 flasks and further harvested for qRT-PCR and protein quantification assays.

4.3.2. Gene expression via qRT-PCR

To quantify the expression levels of *Chrm1-5* (M_1-M_5 receptor-encoding genes) in mouse brain microvascular endothelial cells, total RNA was extracted using the GenElute Mammalian Total RNA MiniPrep Kit (RTN70, Sigma) according to manufacturer's instructions. RNA concentrations were determined via spectrophotometric measurements of absorption at 260 and 280 nm (Beckman Coulter DU 730).

DNase I treatment was used to remove contaminating genomic DNA. In agreement with manufacturer guidelines (Sigma), in our experiments the A_{260}:A_{280} ratio was 2.03 ± 0.06 (bEnd.3) and 1.93 ± 0.03 (BMVEC). Reverse transcription was performed using the High-Capacity cDNA Archive Kit (Applied Biosystems, USA). *Actb* and *Gapdh* were used as housekeeping genes. The following mouse Taqman primers (Life Technologies, USA) were used in accordance with manufacturer guidelines: *Chrm1* (Mm00432509_s1), *Chrm2* (Mm01701855_s1), *Chrm3* (Mm01338409_m1), *Chrm4* (Mm00432514_s1), *Chrm5* (Mm01701883_s1), *Gapdh* (Mm999999_g1), and *Actb* (Mm00607939_s1). Further information on primer selection for *Chrm1* and *Chrm2* is provided in **Figure 4.1**. The relative abundance of *Chrm1-5* transcripts was assessed via qRT-PCR using the TaqMan methodology and the ABI Prism 7300 Sequence Detection System (Applied Biosystems, USA). Reactions were carried out in triplicate for 50 cycles.

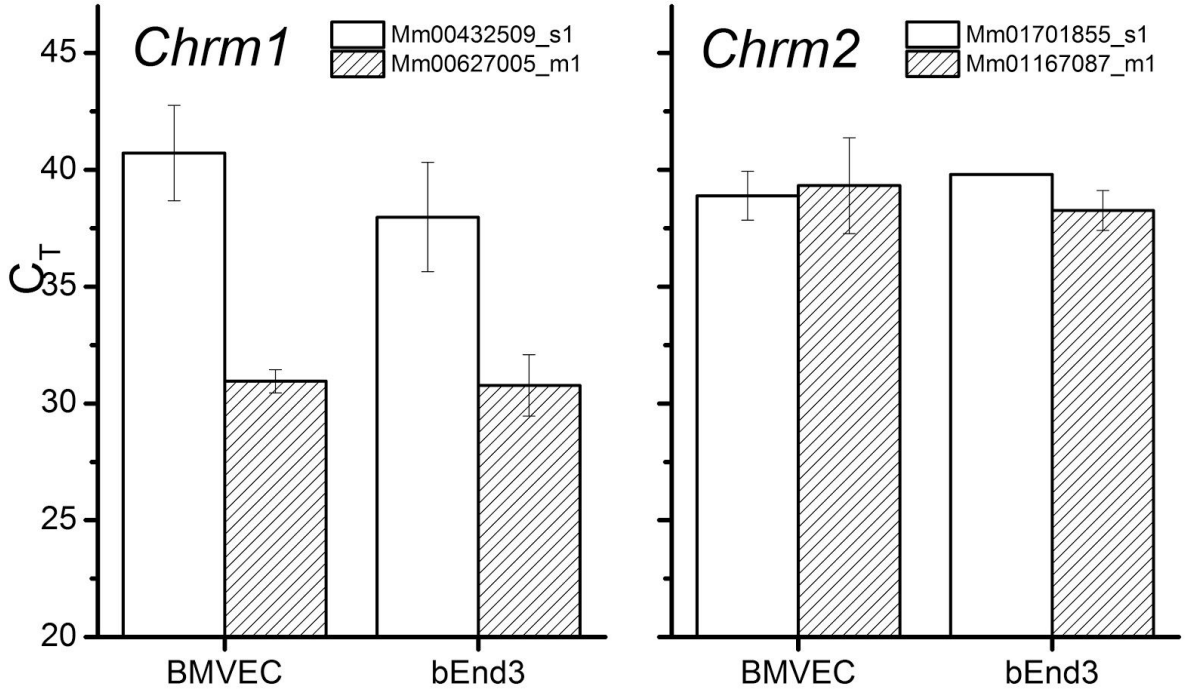

Figure 4.1. Primer screening for optimal quantification of *Chrm1* and *Chrm2* mRNA levels. Comparative threshold cycle (C_T) values (mean ± SD, N = 5) are plotted for each tested primer. Even if *Chrm2* primer Mm01701855_s1 (gray shading) reached the threshold at almost the same cycle number as its "white" counterpart, reproducibility was better since the latter resulted in amplification in only 3 out of 9 repetitions. In the end, the "grey" primers were used in generating the data presented in the manuscript (Figure 4.2, see also Methods section).

4.3.3. Assessment of muscarinic receptor localization via immunofluorescence and confocal microscopy

The cellular localization of the M_1-M_5 receptors was evaluated via immunofluorescence. Brain endothelial cells were treated with a blocking and permeabilization solution (0.3% Triton 100, 1% bovine serum albumin, 2% normal goat serum) for 30 min and were incubated overnight at room temperature with the primary antibody. They were then incubated for 1 h with the secondary antibody followed by an incubation with TO-PRO®-3 (1:3000, Life Technologies) for 10 min for nuclear staining, and were finally mounted with a fluorescent mounting medium. The following polyclonal rabbit primary antibodies from Alomone, Israel were used: anti-M_1 (1:100, #AMR-001), anti-M_2 (1:100, #AMR-002), anti-M_3 (1:100, #AMR-006), anti-M_4 (1:100, #AMR-004), and anti-M_5 (1:100, #AMR-005). The primary antibody was omitted in negative-control samples. Goat anti-rabbit Alexa 488 (1:1000, Life Technologies) was used as the secondary antibody. Normal goat serum and fluorescent mounting medium were purchased from Dako, Milan, Italy.

Specimens were examined using a confocal fluorescence microscope (LSM 710, Carl Zeiss, Germany) equipped with a 63x oil objective. The following acquisition parameters were used: pinhole corresponding to 1 Airy Unit for each laser, 62 μm for the 488 nm laser and 66 μm for the 633 nm laser, digital gain of 1.00, and intensity of 5% for each laser. The acquisition parameter settings were kept fixed for each channel across different image acquisition sessions. Image acquisition was carried out using Zeiss LSM Image Browser software (Carl Zeiss, Germany). A visual evaluation of fluorescence intensity distribution in the nucleus, cytoplasm, and plasmalemma was used to characterize the cellular localization of the receptors. The green channel intensity was scored as follows: - (not observable), + (low), ++ (medium) and +++ (high). For each receptor were scored 40 cells. Because of the intrinsic difficulty in clearly isolating membrane labeling, we regard this evaluation as strictly qualitative.

4.3.4. Protein extraction protocol

We employed a protein immunomagnetic affinity capture technique for the mass spectrometry-based quantification of M_1-M_5 receptors from BMVEC and bEnd.3 cell samples. Cells were harvested in microvials and immediately placed on ice. They were then homogenized with a series of 10 ultrasonic pulses (Sonopuls HD 2070, Bandelin, Germany), 1 sec each at 50% of the maximum frequency in 10 mM PBS (pH 7.4, Sigma) supplemented with the Protease Inhibitor Cocktail for use with mammalian cell and tissue extracts (#P8340, Sigma), according to the manufacturer's instructions. Homogenates were subsequently centrifuged at 1000x*g* for 10 min at 4°C to remove cellular debris. Cell lysates were collected, mixed with Laemmli loading buffer (#161-0737, Bio-Rad, Hercules, CA, USA) and heated at 70 °C for 20 min.

Using 4-15% Criterion™ TGX Stain-Free™ Protein Gels (#567-8084, Bio-Rad), we separated 15 μg of the lysate for each cell sample. The total protein profiles of the samples were then visualized using a Bio-Rad ChemiDoc MP imager within a few minutes after the completion of electrophoresis to check for protein sample and separation quality (**Figure 4.2A**). After visualization and image acquisition, UV activation of the bands was performed using the ChemiDoc MP system. Gels were split into individual lines, each containing separated proteins (from 10 to 250 kDa). Individual lines were then placed in vials containing 10 mL of distilled water. Next, the water solution and lines of gel were homogenized and consequently sonicated in an ultrasonic bath (Sonorex, Germany) for 20 min at 4 °C. Samples were then centrifuged at 6500 x*g* (room temperature) and supernatants, filtered on a 0.2 mm PTFE microfilter were collected. A small volume of the supernatant was used to determine the total amount of proteins by the Bradford method (**Figure 4.2B**). Next, 1 mL of supernatant (i.e. 10% of the total) was incubated with antibody-coated magnetic particles that were prepared as described below.

We bound undiluted anti-$M_{1\text{-}5}$ antibodies (1 μL, Alomone) to functionalized magnetic particles (Dynabeads® M-280, Tosyl-activated superparamagnetic polystyrene) for

immunoaffinity capture. Protein standards for the M_1-M_5 receptors were provided by Alomone, Israel and were used as calibration controls in the matrix-assisted laser desorption ionization time-of-flight (MALDI-TOF) mass spectrometry analysis.

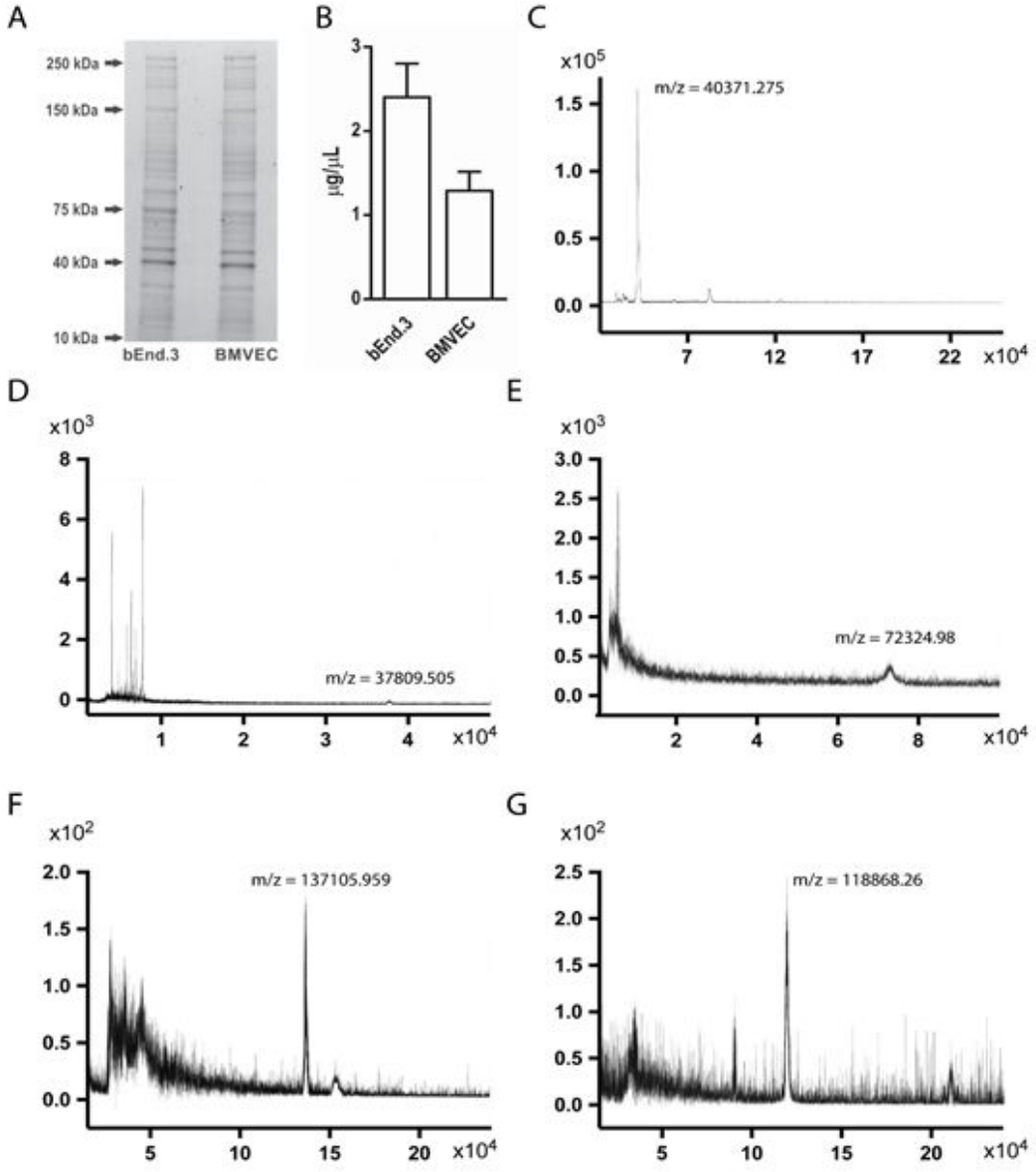

Figure 4.2. Representative examples of stain-free gel and mass spectra. A. Gel electrophoresis of the total proteins extracted from BMVEC and bEnd.3 samples run on 4-15% Criterion™ TGX Stain-Free™ Protein Gels. The visualization of stain-free gels after gel electrophoresis shows well-separated proteins in the range of ~12 to ~200 kDa for both brain endothelial cell extracts. **B.** Total protein content (mean ± SD, N=5) quantified via the Bradford method. Protein levels were significantly higher in bEnd.3 compared to BMVEC samples (unpaired t-test, t = 8.384, df = 18, $p < .0001$). **C-G.** MALDI-TOF mass spectra of M1-5 receptors in BMVEC samples (identical MS spectra were obtained for bEnd.3 cells). Receptors were identified based on the molecular or fragment peaks in the spectra corresponding to the most abundant, singly charged protein ions. On axis Y - intensity in atomic units, on X - m/z values.

4.3.5. Immunomagnetic isolation followed by MALDI-TOF MS analysis

We followed our previously published protocol (Hasuo et al., 1996) with the antibodies detailed below. Candidate muscarinic receptors were isolated by using polyclonal affinity-purified antibodies purchased from Alomone Labs (as described above). The MALDI matrix 1,2-dimethoxy-4-hydroxycinnamic (sinapinic acid) and other chemicals were purchased from Sigma-Aldrich (St. Louis, MO, USA) and chemical solvents were purchased from Merck (Darmstadt, Germany).

The following buffers were used during the isolation procedure:

- Buffer A: 0.1 M sodium-phosphate buffer pH 7.4
- Buffer B: Phosphate-buffered saline (PBS) pH 7.4 with 0.1% (w/v) bovine serum albumin (BSA)
- Buffer C: 0.2 M Tris pH 8.5 with 0.1% (w/v) BSA;
- Buffer D: 100 mM glycine (pH 2.5)

Dynabeads M-280, tosyl-activated superparamagnetic polystyrene beads coated with polyurethane, were washed twice in Buffer A to remove sodium azide (NaN_3) using magnetic particle concentrator following the manufacturer's protocol (Thermo Fisher Scientific, Waltham, MA, USA). The above-listed antibodies (1 μL each) were dissolved in 100 μL of Buffer A and added to 100 μL suspension of Dynabeads, mixed for 1 min, followed by 24-hour incubation at 37 ^{o}C with mixing. Then, the supernatant was removed and the particles were washed twice with Buffer B (500 μL) at 4 ^{o}C. Free tosyl groups on the beads were blocked with Buffer C (500 μL; 4 h, 37 ^{o}C), followed by washing with Buffer B (500 μL; 5 min, 4 ^{o}C). Each individual preparation of the antibody-coated magnetic beads was resuspended in 1 mL of supernatant and incubated with shaking for 1 h at 37 ^{o}C. The supernatants were then removed and the beads were washed five times with Buffer B (500 μL; 4 ^{o}C, 5 min, vortexing). The captured antigens were eluted with Buffer D (50 μL; 4 ^{o}C, 1 min, vortexing) and the beads were magnetically separated. The eluates were desalted using C18 ZipTip (EMD Millipore, Billerica, MA, USA) before analysis by matrix-assisted laser desorption ionization-time-of-flight mass spectrometry (MALDI-TOF MS).

4.3.6. MALDI-TOF MS analysis

MALDI-TOF MS data were acquired on Autoflex mass spectrometer (Bruker Daltonics, Germany) with MALDI sample target (600 µm Chip™; Bruker Daltonics). Ionization was achieved by irradiation with a nitrogen laser (337 nm) operating at 4 Hz. Ions were accelerated at 20 kV with 250 ns of pulsed ion extraction delay. Freshly prepared 1,2-dimethoxy-4-hydroxycinnamic acid was used as matrix (10 mg/mL) in 50% acetonitrile 0.1% (v/v) of trifluoroacetic acid. The instrument's parameters and laser energy were kept constant during a series of experiments performed on the same day for the comparison of intensity values (cps).

First, we obtained MS spectra of standard receptor proteins (data not shown). The areas under the peak of interest were used to construct calibration curves, allowing later on the quantification of receptors in our samples. The protonated molecular ion peak (MH+) for each protein was detectable to a sub-pmol level with a signal-to-noise ratio > 50. This detection limit was comparable with immunochemical assays.

The MS spectra obtained with our samples showed the MH+ peaks at the expected m/z values, matching those observed with the standard proteins. The areas under the peak were then normalized against those interpolated from the calibration curves. The MALDI-TOF MS is a semiquantitative method; however, using rigorous sample preparation and data acquisition method, the intensity of the MH+ peak(s) increased linearly with increasing quantities of each protein from nanomolar to picomolar ranges. Therefore, in this concentration range, the evaluations of protein biomarkers can be considered quantitative (Hasuo et al., 1996).

4.3.7. Intracellular calcium imaging measurements

Fura-2 AM-based Ca^{2+} imaging experiments were performed on brain microvascular endothelial cells as previously described (Radu et al., 2015). Measurements were performed using a cooled CCD camera (Clara, Andor, Northern Ireland) and a Polychrome V monochromator (Till Photonics, Germany) coupled to a SliceScope (Scientifica, UK) upright fluorescence microscope with a 40x-water immersion objective (Olympus, Japan). Data acquisition was performed using Live Acquisition imaging software (Till Photonics, Germany), and calcium changes were determined based on the intensity ratio ($R = I_{340nm}/I_{380nm}$). Ratios were calculated for each cell in the microscope field and were based on individually defined regions of interest after background subtraction. Calcium imaging data were analyzed using Offline Analysis software (Till Photonics, Germany) and are plotted as the mean fluorescence ratio amplitude ($\Delta R = R - R_0$, where R_0 represents the calcium signals recorded in unstimulated cells) ± SEM.

Solutions were delivered to brain endothelial cells through a 100 µm quartz perfusion head using an 8-channel valve pressurized system (ALA Scientific Instruments, USA). The Ringer's solution contained (in mM) 140 NaCl, 5.6 KCl, 2 $MgCl_2$, 2 $CaCl_2$, 10 glucose, 10 HEPES (pH 7.4, adjusted with NaOH). Fura-2 acetoxymethyl ester (Fura-2 AM) and pluronic acid were purchased from Life Technologies, USA, and all common salts were from Sigma-Aldrich, Milan, Italy. Cytosolic Ca^{2+} transients resulting from the activation of muscarinic acetylcholine receptors were elicited by a 20-s pulse of 1 µM acetylcholine chloride (ACh, Sigma) application. The reproducibility of the effect of ACh was tested via a double-pulse protocol, with a 10-minute between-pulse Ringer's washout period. In some experiments, we replaced the first pulse of ACh with a pulse of either (±)-muscarine chloride hydrate (#M104, Sigma) or (−)-nicotine hydrogen tartrate salt (#SML1236, Sigma) at previously described concentrations (100 µM and 300 µM, respectively) (Moccia et al., 2004; Hasuo et al., 1996), followed by the second pulse (1 µM ACh) after a 10-min recovery period.

Dose-response curves for the mAChR antagonists were obtained by preceding the second ACh pulse with a 2-min application of the antagonist. The following antagonists were used: J104129 fumarate (M_3 antagonist, Tocris Bioscience, USA), VU 0255035 (selective M_1 antagonist, Tocris Biosciences), 4-DAMP (1,1-dimethyl-4-diphenylacetyl piperidinium iodide; M_3 antagonist, Sigma), and telenzepine dihydrochloride hydrate (M_1 antagonist, Sigma). We also tested the effect of AC-42 (#SML0787, Sigma), a selective allosteric M_1 agonist, with the EC_{50} = 29 nM (based on a Receptor Selection and Amplification Assays) for M_1 and without any effect on M_2-M_5 (Spalding et al., 1992) AC-42 was applied at its maximal activation concentration, based on the previously determined EC_{50} value of 0.2 µM evaluated by a calcium mobilization assay (Jacobson et al., 2010). Moreover, we have tested the effect of the muscarinic toxin MT-7 (Smartox Biotechnology, France) at its saturation concentration, as previously described (Adem and Karlsson, 1997), considering its high affinity for the M_1 receptor, i.e. k_i = 0.2 nM for M_1 and k_i > 2000 nM for M_2-M_5 (Adem and Karlsson, 1997).

4.3.8. Homology modeling and molecular docking

The eucaryotic sequences were downloaded from the Pfam database (10.1093/nar/gkv1344) and the conservation of the residues were calculated as a percentage (X/P)*100, where X is the residue and P the length of the multiple sequence alignment. Since mouse M_1-M_5 lack structural information, homology modeling was carried out to predict their 3D structures. The sequences were retrieved from the Uniprot database, and the models were generated through the GOMoDo web-server (Sandal et al., 2013). To enforce the conserved structural fingerprints of class A (rhodopsin-like) GPCRs (Venkatakrishnan et al., 2013), all sequence alignments between targets and templates (illustrated in detail in **Table 4.1**) were verified manually. The 3D structures obtained in the homology modeling step were used to perform virtual docking studies using the HADDOCK docking program (De Vries et al., 2010) through the GOMoDo web-server. We used the GPCRdb generic number position (Isberg et al., 2016), which generalizes the classical Ballesteros-Weinstein numbering. Residues in positions 3.32, 3.33, 3.36, 3.37, 4.57, 5.39, 5.42, 6.48, 6.51, 7.39, and 7.43 were considered as 'Active Residues' to guide the docking. These residues have already been characterized as being involved in agonist/antagonist binding (Goodwin et al., 2007; Lu and Hulme, 1999). The structures of the four antagonists were downloaded from the ZINC database (Irwin et al., 2012), and were parametrized with ACPYPE (Sousa da Silva and Vranken, 2012). The docking protocol included three stages: (a) a rigid-body energy minimization, (b) a semi-flexible refinement in torsion angle space, and (c) a final refinement in an explicit solvent. We chose 1000 structures for the first step and 200 structures for the second and third docking steps, using default parameters. We selected the best structure for each docking as the one corresponding to the most populated cluster with the lowest energy value. Figures were generated with Chimera (Pettersen et al., 2004).

Table 4.1. Mouse muscarinic receptor *in silico* docking. Summary of the residues involved in the most important interactions with each of four antagonists, arranged by bond type.

Antagonist	M_1	M_2	M_3	M_4	M_5	Interaction
4-DAMP	$D^{3.32}$	$D^{3.32}$	$D^{3.32}$	$D^{3.32}$	$D^{3.32}$	salt bridge
	$Y^{3.33}$ $S^{3.36}$ $Y^{6.51}$	$Y^{3.33}$			$Y^{6.51}$	h-bond
	$V^{3.40}$ $W^{4.50}$ $F^{5.40}$ $T^{5.42}$ $F^{5.47}$ $W^{6.48}$	$W^{4.50}$ $F^{5.40}$ $T^{5.43}$ $Y^{6.51}$ $W^{6.48}$	$Y^{3.33}$ $F^{5.40}$ $T^{5.42}$ $V^{6.55}$	$F^{5.40}$ $T^{5.42}$ $W^{7.34}$	$W^{7.36}$ $F^{5.40}$	hydrophobic
			$Y^{6.51}$	F^{185}		pi-stacking
Telenzepine	$D^{3.32}$	$D^{3.32}$	$D^{3.32}$	$D^{3.32}$	$D^{3.32}$	salt bridge
	$Y^{6.51}$ $N^{6.52}$	$Y^{3.33}$	$Y^{6.51}$ $Y^{7.39}$	$Y^{6.51}$ $Y^{7.43}$ $N^{6.52}$	$Y^{3.33}$ $S^{.57}$	h-bond
	$W^{4.50}$ $Y^{7.39}$	F^{101}	F^{224} L^{224} $T^{5.40}$	F^{188} L^{226} $T^{5.40}$	L^{226} $T^{5.40}$ $W^{6.48}$	hydrophobic
	$Y^{3.33}$					pi-stacking
VU 0255035	$D^{3.32}$					salt bridge
	$S^{3.36}$ $Y^{7.39}$		$Y^{7.39}$	$Y^{6.51}$ $Y^{7.43}$		h-bond
	$W^{4.50}$ $Y^{6.48}$ ECL3 $W^{7.34}$	$W^{4.50}$ $T^{5.41}$ ELC3 $Y^{7.39}$ $Y^{7.43}$	$T^{5.40}$ ECL3 $T^{5.43}$ $W^{7.34}$	ECL2 $T^{5.40}$ $T^{5.43}$	$W^{7.34}$ $T^{5.40}$ $T^{5.43}$ ECL2 $W^{4.57}$	hydrophobic
	$W^{7.35}$	$Y^{3.33}$	$W^{6.48}$	$Y^{3.33}$		pi-stacking
J104129 fumarate	$D^{3.32}$		$D^{3.32}$		$D^{3.32}$	salt bridge
	$Y^{3.33}$ $Y^{6.51}$	$Y^{7.38}$	$Y^{3.33}$ $Y^{6.51}$		$Y^{3.33}$ $Y^{6.51}$	h-bond
	$W^{4.50}$ $T^{5.41}$ $Y^{7.39}$ $W^{7.35}$ $W^{6.48}$	$Y^{3.33}$ $T^{5.41}$ $W^{4.57}$ $Y^{7.39}$	$W^{4.50}$ $Y^{5.41}$ $Y^{6.51}$ $Y^{7.39}$	$I^{2.52}$ $L^{3.31}$ $V^{3.34}$ $W^{4.50}$ $W^{4.54}$	$W^{4.50}$ $T^{5.40}$ $T^{5.43}$ $Y^{7.39}$	hydrophobic
			$Y^{7.39}$			pi-stacking

4.3.9. Data analysis

Quantitative RT-PCR data were obtained by normalizing *Chrm1-Chrm5* mRNA levels to those of *Gapdh* and *Actb* using the 2(-Delta C(T)) method, as previously described (Livak and Schmittgen, 2001). The results were expressed as $\log_{10}$-fold changes due to their extended scale distribution and were plotted as the mean ± SD.

The Hill formalism (Collison et al., 2000) was used to fit both the ACh concentration–response and the inhibition curves determined via calcium imaging recordings from BMVECs and bEnd.3 cells. For the concentration-response curves, the following equation was used:

$$R/R_{max} = C^{\alpha}/(C^{\alpha} + EC_{50}^{\alpha}) \qquad (\mathbf{4.1})$$

C corresponds to the agonist concentration, ΔR_{max} is the amplitude ratio for the maximal response to 10 µM ACh, EC_{50} is the concentration of agonist required to elicit a half-maximal response, and α is the Hill coefficient describing cooperativity and mAChR receptor occupancy (Collison et al., 2000). Inhibition curves resulting from the calcium imaging data analysis were fitted with the following equation:

$$R/R_{max} = 1 + (X-1)C^{\alpha}/(C^{\alpha} + IC_{50}^{\alpha}) \qquad (\mathbf{4.2})$$

IC_{50} is the antagonist concentration required to reduce the agonist response by 50%, C is the agonist concentration (1 µM), α is the Hill coefficient. In equation (1) and (2) a Hill coefficient value of 1 indicates that only one molecule of agonist/antagonist is activating/inhibiting one receptor). X = 0 for telenzepine, J104129 fumarate and 4-DAMP, and X = the fitting parameter for VU 0255035.

The apparent dissociation constant was calculated using the Cheng–Prusoff equation, as follows:

$$K_a = IC_{50} / (1 + C/EC_{50}) \qquad (\mathbf{4.3})$$

Protein abundance was determined in the MALDI/TOF MS analysis, as described previously (Schlosser et al., 2007). Briefly, the area under the curve of the most abundant mass band (peak) for each protein standard or sample was calculated in series of ten repetitions, and the computed average was used to determine the concentration of each muscarinic receptor protein. The mass band (peak) identification and quantification of each muscarinic receptor protein in our samples was determined in relation to the protein standard peak. Next, protein contents for each muscarinic receptor were normalized to the total amount of proteins in the sample.

Statistical analyses comparing the expression of the 5 receptor subtypes were carried out as follows. Differences in mRNA expression based on RT-PCR data were analyzed with one-way ANOVA (according to Yuan et al., 2006) followed by post-hoc Bonferroni tests. Protein quantification based on MALDI-TOF data were analyzed with one-way ANOVA

followed by post-hoc Holm-Sidak 2 test. Analysis and data plotting were performed using OriginPro 8 (OriginLab Corporation, USA) and GraphPad Prism version 7.00 (GraphPad Software, La Jolla California USA).

4.4. Results

4.4.1. All muscarinic acetylcholine receptor subtypes are expressed by mouse brain microvascular endothelial cells

We first sought to identify and quantify mRNA expression of mAChRs M_1-M_5 in two types of mouse brain microvascular endothelial cells. Quantitative real-time PCR (qRT-PCR) analyses using both β-actin (*Actb*) and glyceraldehyde 3-phosphate dehydrogenase (*Gapdh*) as reference genes indicated that both brain microvascular endothelial cells (BMVECs) and brain endothelial cells (bEnd.3) express mRNA transcripts for *Chrm1-5*, which encode mAChRs M_1 - M_5. The ranking of mRNA levels in BMVECs and bEnd.3 cells was as follows: *Chrm3* > *Chrm4* □ *Chrm1* □ *Chrm5* > *Chrm2* (**Figure 4.3.A-D**).

These rankings were consistently observed when data were normalized against either reference gene, despite the different functional roles of the latter. The most abundant muscarinic receptor gene, *Chrm3*, was approximately 10^5 times more abundant than *Chrm2,* and about 200 times, 500 times and 3000 times more than *Chrm4, Chrm1 and Chrm5*, respectively.

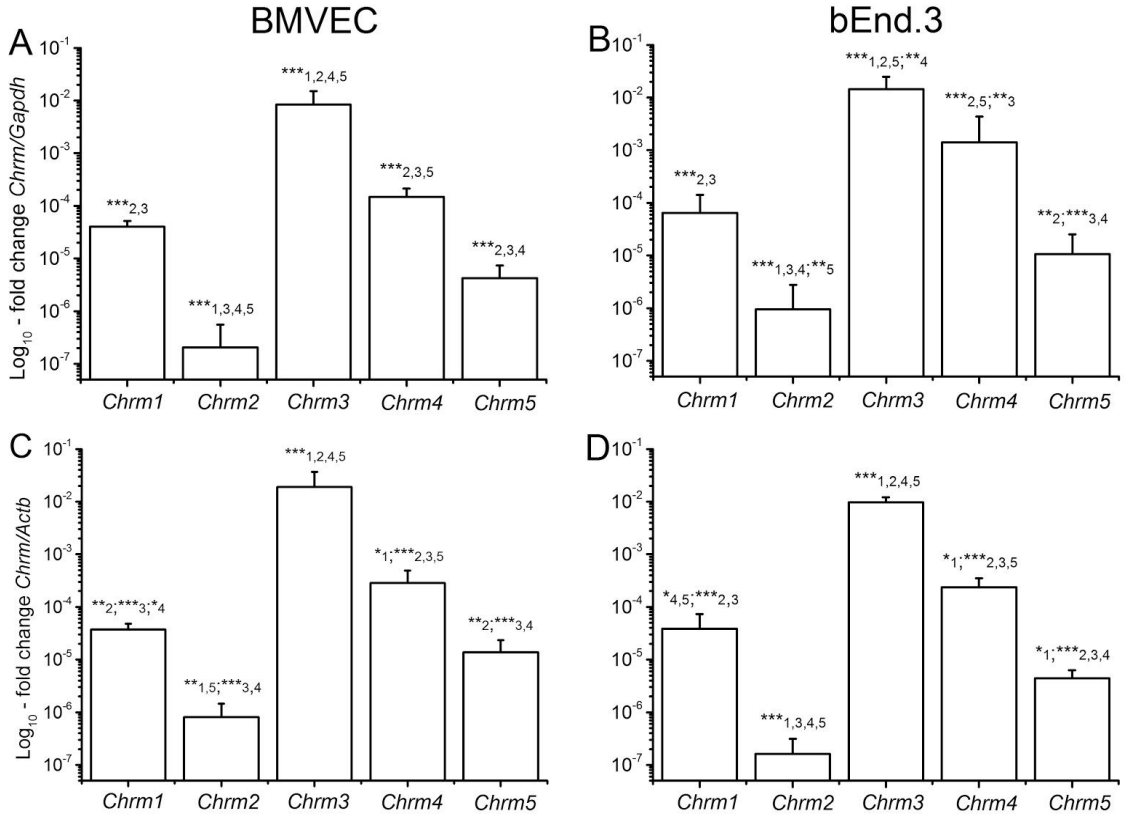

Figure 4.3. mRNA levels for *Chrm1* - *Chrm5*, respectively encoding the M_1-M_5 receptors, quantified via qRT-PCR in BMVECs (**A, C**) and bEnd.3 cells (**B, D**). Data are normalized against two different reference genes, *Gapdh* (A, B) and *Actb* (C, D), and are plotted as mean ± SD (N = 5), from three different cell batches. One-way ANOVA analysis indicated: (A) $F(32) = 80$, $p < 0.001$; (B) $F(25) = 56$, $p < 0.001$; (C) $F(25) = 58$, $p < 0.001$; (D) $F(14) = 121$, $p < 0.001$. Statistical pairwise significance is indicated with asterisks (* $0.01 < p < 0.05$; ** $0.001 < p < 0.01$; *** $p < 0.001$) followed by the compared variant.

We next confirmed the presence of all muscarinic receptor subtypes and their subcellular distribution in both BMVECs and bEnd.3 cells via immunofluorescence staining (**Figure 4.4**). A qualitative analysis did not reveal substantial differences in receptor expression between the two cell types; however, each subtype showed a specific subcellular localization pattern (**Table in Figure 4.4**). In particular, most subtypes (M_1-M_4) are strongly present in the cytoplasm (mainly in the perinuclear region), while M_5 was much more concentrated in the plasmalemma. Interestingly, an important fraction of M_1 was localized in the nucleus, and was almost absent from the plasma membrane. M_3 was abundant in the cytosol, but its presence partly extended to the plasma membrane.

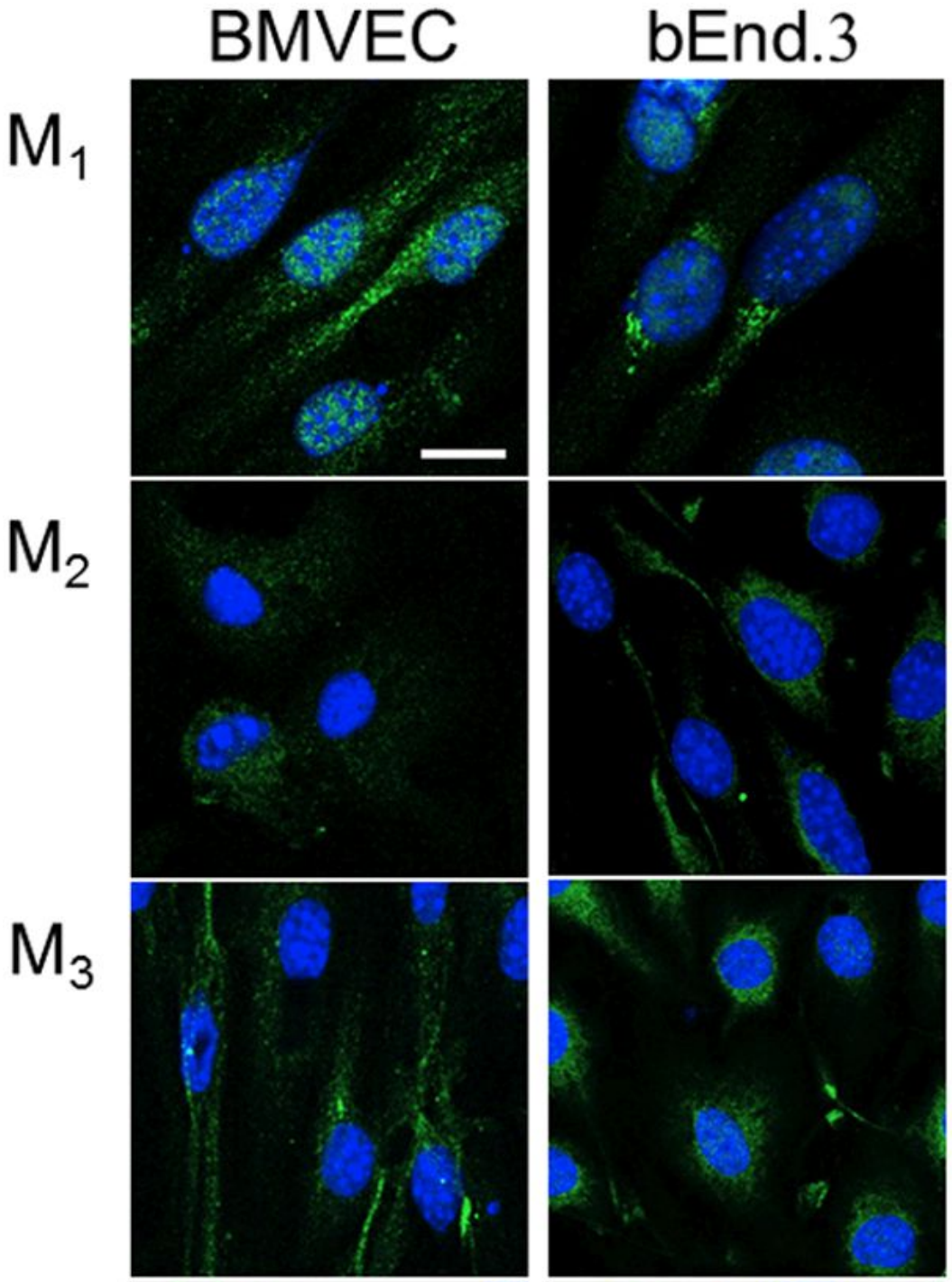

Figure 4.4. (*see the second part of the figure on the next page*)

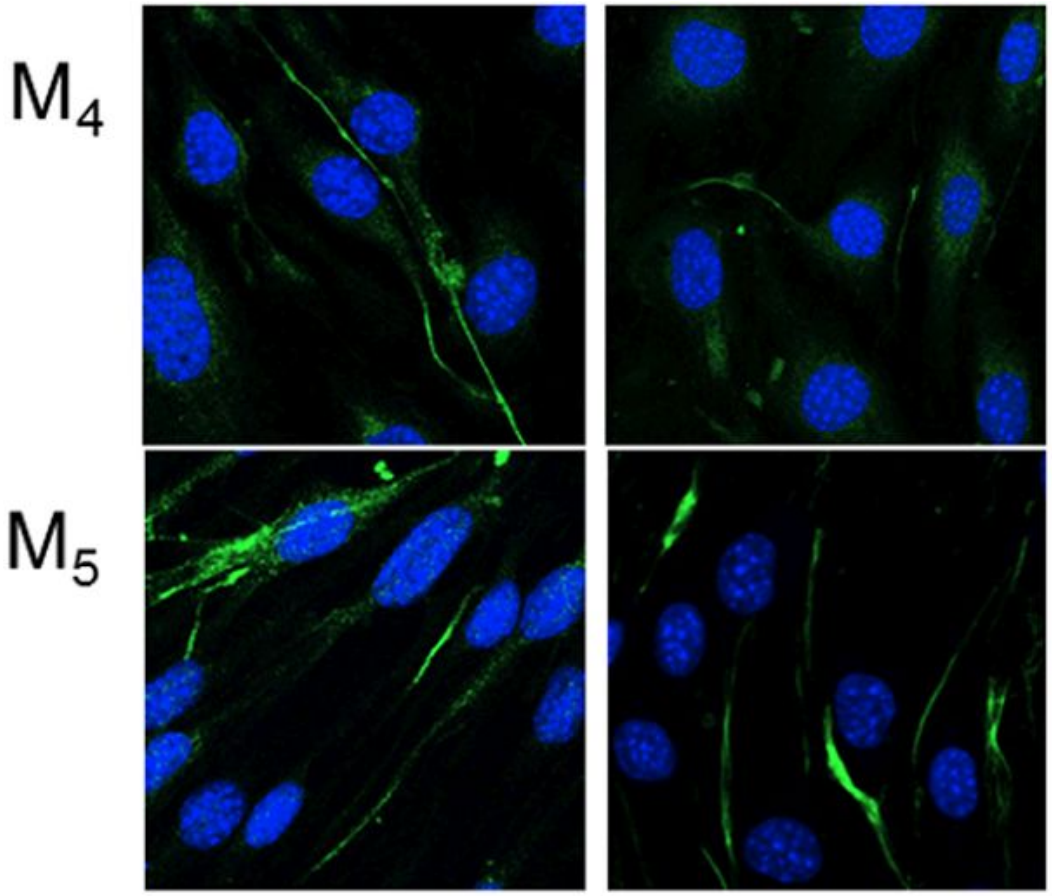

mAChR	BMVEC			bEnd.3		
	PM	Cyt	N	PM	Cyt	N
M_1	+	+++	++	−	+++	++
M_2	−	+++	−	+	+++	−
M_3	+	+++	+	+	+++	+
M_4	++	+++	+	+	+++	+
M_5	+++	+	+	+++	+	+

Figure 4.4. Detection of M_1-M_5 receptors by means of immunofluorescence in BMVECs and bEnd.3 cells. The labeling obtained with anti-$M_{1\text{-}5}$ antibodies (green) is here merged with TO-PRO®-3 nuclear staining (blue); scale bar: 10 µm. The table shows qualitative estimates of protein abundance in the plasma membrane (PM), cytoplasm (Cyt), and nucleus (N). The evaluation was based on visual assessment of green fluorescence intensity on 40 cells per antibody, scored from not observable (-) to very intense (+++).

4.4.2. M_1, M_3, and M_4 are the most abundant receptors in brain microvascular endothelial cells

With the transcriptomic expression and subcellular distribution of mAChRs established, we next confirmed and quantified mAChR protein expression in mouse brain microvascular endothelial cells (BMVECs and bEnd.3 cells). Using the matrix-assisted laser desorption ionization time-of-flight (MALDI-TOF) mass spectrometry, we examined the amount of all muscarinic receptor proteins in brain microvascular endothelial cells (**Figure 4.2C-G**). Ratios of each mAChR ($x10^{-6}$) normalized to the total amount of protein were calculated. One-way ANOVA analyses showed significant differences between subtypes for BMVEC cells ($F(64) = 62.03$, $p < .0001$) and b.End3 cells ($F(34) = 222.8$, $p < .0001$). Followed Holm-Sidak *post-hoc* tests indicated much higher levels of M_1, M_3 and M_4 compared to M_2 and M_5 subtypes in both BMVECs (**Figure 4.5A**) and b.End3 cells (**Figure 4.5B**). Moreover, M_1 expression was significantly higher than M_3 and M_4 in BMVECs significantly higher expression than M_4 in bEnd.3 cells.

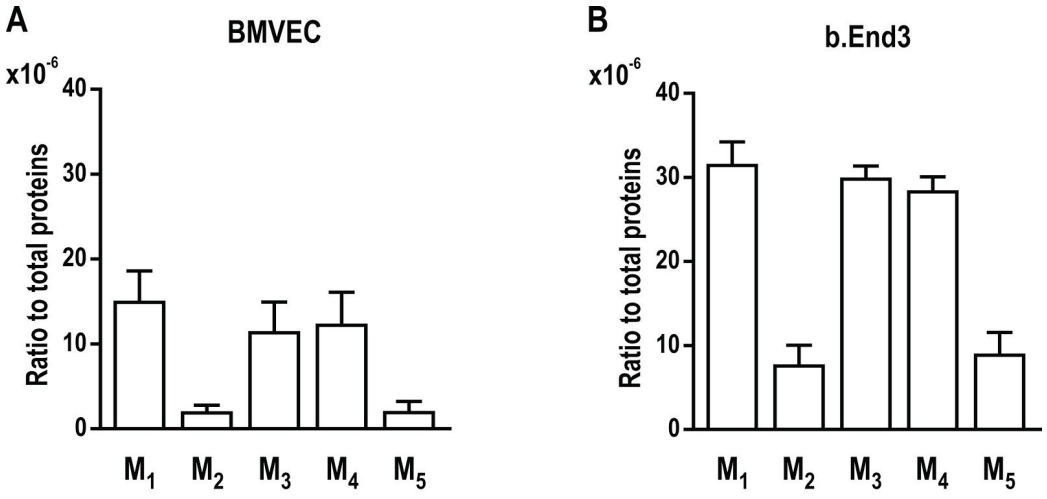

	BMVEC				b.End3			
subtype	M_2	M_3	M_4	M_5	M_2	M_3	M_4	M_5
M_1	11.87**	3.28*	2.48*	11.82**	21.15**	n.s.	2.78*	20.02**
M_2		8.59**	9.39**	n.s.		19.71**	18.37**	n.s.
M_3			n.s.	8.53**			n.s.	18.57**
M_4				9.33**				17.23**

Figure 4.5. Relative protein abundance of M_1-M_5 receptors in brain microvascular endothelial cells (mean ± SD, N = 5). One-way ANOVA analyses showed significant differences between subtypes for both cell types: (**A**) $F(64) = 62.03$, $p < .0001$; (**B**) $F(34) = 222.8$, $p < .0001$. The **Table** shows the results (t values) of pairwise Holm-Sidak *post-hoc* tests (* $p < .05$; ** $p < .0001$) .

We also found that, for each mAChR subtype, expression in bEnd.3 cells was almost double that in BMVECs, and very similar results were obtained by means of the Bradford method (unpaired t-test, t = 8.384, df = 18, $p < .0001$, **Fig. 4.5 B**) thereby excluding potential biases due to overall differences in protein expression. Similar discrepancies in mAChR expression between primary and immortalized endothelial cells have been reported between freshly isolated and cultured bovine aortic endothelial cells (Tracey and Peach, 1992).

Protein quantitation data indicates that the M_1 and M_4 subtypes are present in both cell types in amounts comparable to M_3, in spite of significantly lower mRNA levels. A mismatch between mRNA and protein levels is not surprising *per se*, as such correlation in complex biological samples has been reported to be poor (Maier et al., 2009). Different normalization factors between methods can play a role as well. Total protein loading control was reported to be more reliable than the housekeeping proteins loading controls (Colella et al., 2012). We also examined the levels of β-actin and α-tubulin to see if they can be used as a reliable loading control under our experimental conditions. We found that the protein expression level for β-actin is ~ 3.8 times higher in BMVEC than in bEnd.3 cells, the level of α-tubulin is ~ 5.6 times higher (*data not shown*). Therefore, the total amount of protein in our samples was used as the normalization factor.

4.4.3. Cholinergic activation of calcium signaling pathways in brain microvascular endothelial cells depends on muscarinic, but not on nicotinic receptors

The finding of muscarinic receptor transcripts and proteins, together with their subcellular localization in brain microvascular endothelial cells, prompted the characterization of their functional properties, which we pursued by means of calcium imaging recordings. As already mentioned, M_1, M_3 and M_5 have been shown to trigger calcium transients in the cytosol in response to the binding of specific muscarinic agonists (Langmead et al., 2008). The typical response to ACh for both BMVECs and bEnd.3 cells began with a sharp peak, followed by a smaller but sustained response (see **Figures 4.6 - 4.8,** for representative examples), particularly after higher ACh concentrations (1 µM and 10 µM; **Figure 4.6**). This is consistent with the slow but sustained influx through store-operated calcium channels located in the plasma membrane that follows the peak in muscarinic-mediated vascular endothelial Ca^{2+} signaling (Moccia et al., 2012).

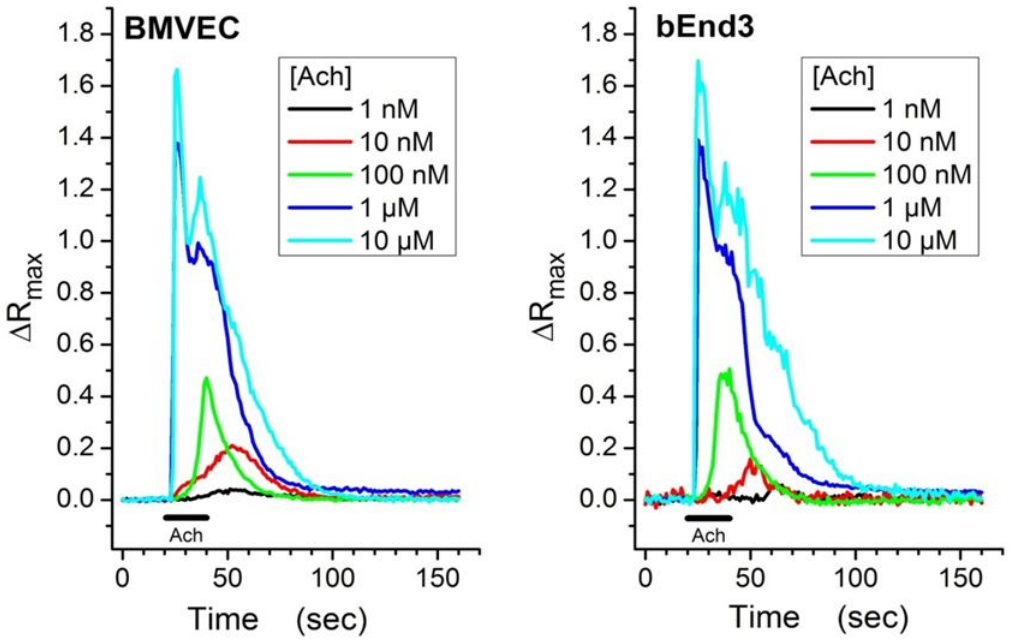

Figure 4.6. Representative traces of mean fluorescence ratio (ΔR) changes induced by acetylcholine in BMVECs (*left*) and bEnd.3 cells (*right*) during calcium imaging recordings.

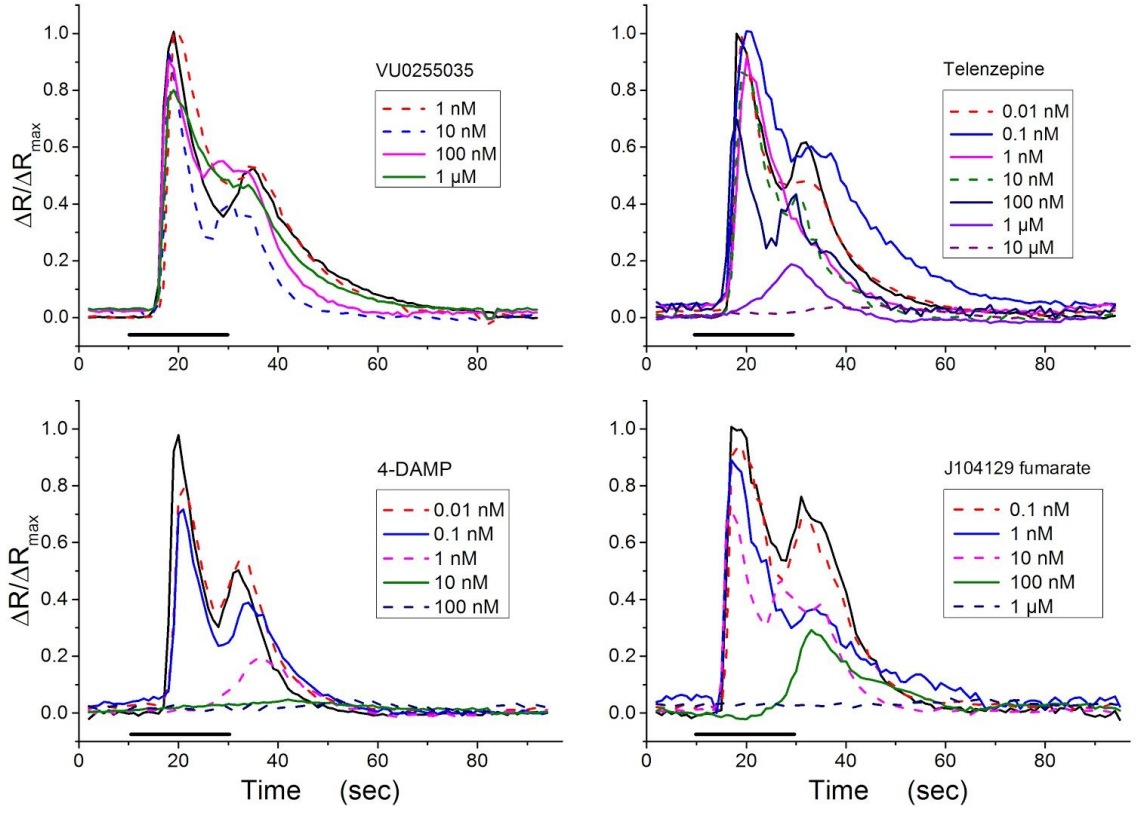

Figure 4.7. The effect of four mAChR antagonists on the ACh (1 μM)-induced calcium signal in bEnd.3 cells. Representative traces of relative fluorescence ratio ($\Delta R/\Delta R_{max}$) changes are plotted. The double-pulse protocol was used, and antagonists were applied 2 min prior to the second ACh pulse (only the second pulse is represented in the graph, and the black bar marks the ACh application period).

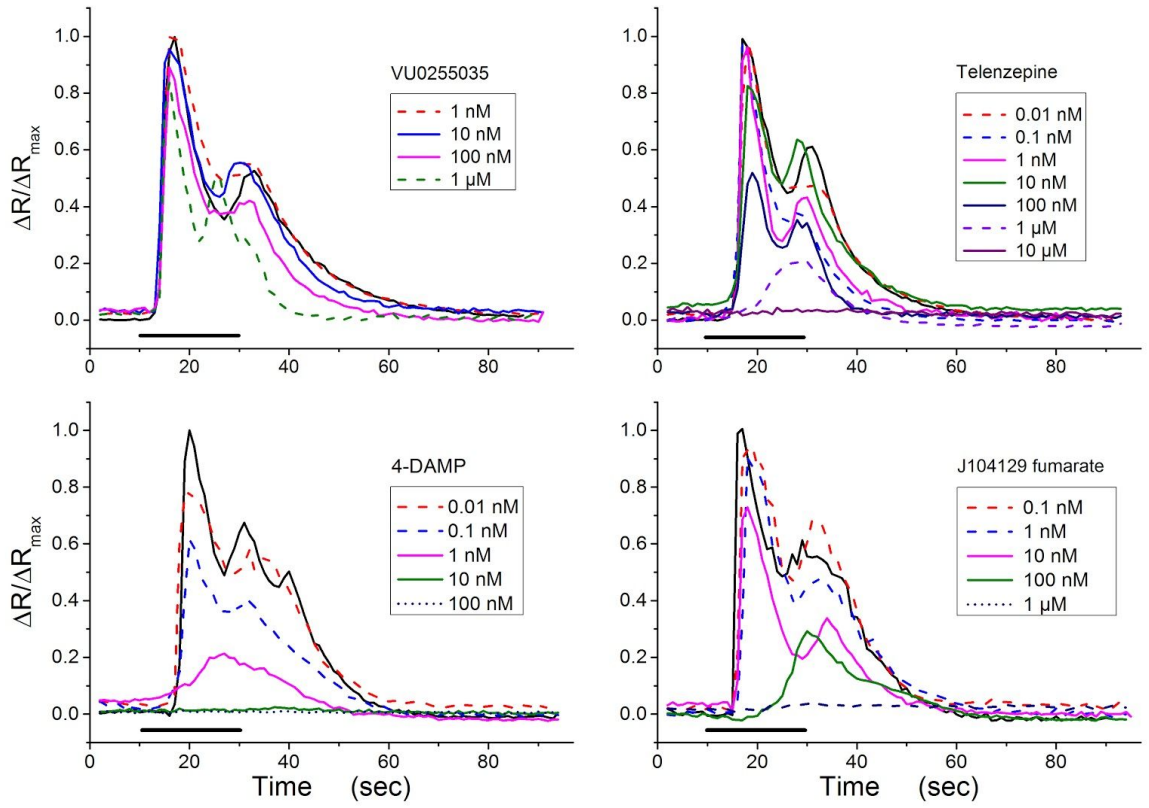

Figure 4.8. The effect of four mAChR antagonists on the ACh (1 μM)-induced calcium signal in BMVEC cells. Representative traces of relative fluorescence ratio ($\Delta R/\Delta R_{max}$) changes are plotted. The double-pulse protocol was used, and antagonists were applied 2 min prior to the second ACh pulse (only the second pulse is represented in the graph, and the black bar marks the ACh application period).

Since ACh is an agonist for both nicotinic and muscarinic receptors, we examined the contribution of each receptor type to the overall ACh-induced Ca^{2+} signal. To accomplish this, we used a double-pulse protocol, starting with the application of the specific agonist (either nicotine or muscarine) followed by a 10-minute washout period, and subsequent application of ACh as a positive control (**Figure 4.9**). The 10-minute delay was confirmed to be sufficiently long in control experiments where ACh was applied both before and after the washout, triggering responses of similar amplitude in both trials (**Figure 4.9 A, B**). Muscarine administration (100 μM) induced an intracellular calcium signal amplitude similar to the one triggered by 10 μM ACh (**Figure 4.9 C, D**), while nicotine (300 μM) did not produce any response (**Figure 4.9 E, F**). These results demonstrate that nicotinic receptors did not contribute to ACh-dependent calcium mobilization in our preparation and that the elicited signal depended entirely on GPCR muscarinic receptors.

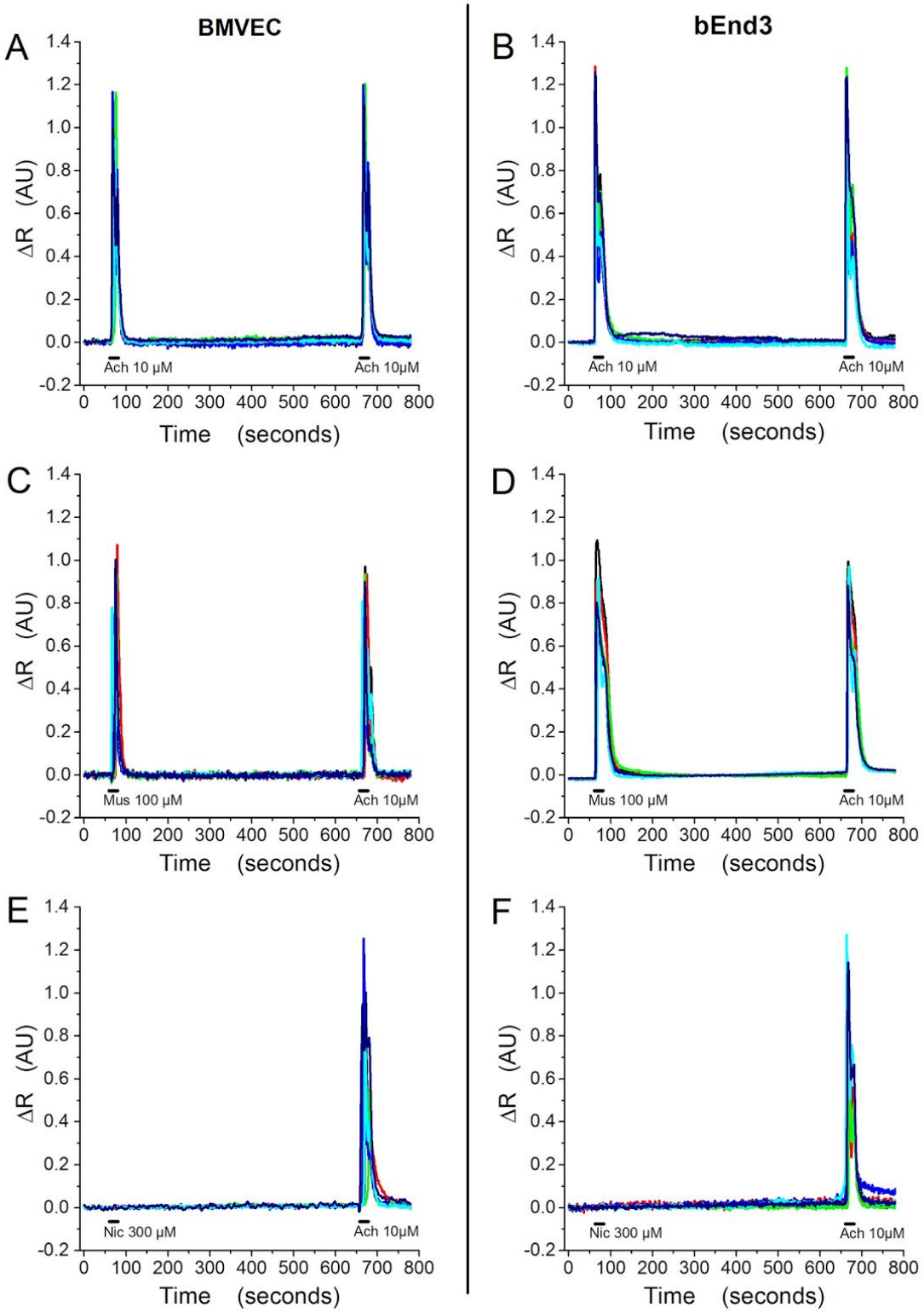

Figure 4.9. Representative traces (each trace was recorded for an individual cell) of mean fluorescence ratio (ΔR) changes induced by acetylcholine (10 μM) (**A, B***)*, muscarine (100 μM) (**C, D***)*, and nicotine (300 μM) (**E, F***)* in BMVECs (**A, C, E**) and bEnd.3 cells (**B, D, F**).

We further characterized muscarinic receptor functionality by investigating the concentration-response curve for ACh concentrations in the range of 1 nM to 10 µM. Increased ACh concentrations produced higher-amplitude calcium peaks (representative traces are shown in **Figure 4.6**). The best-fit curve for the data by the Hill equation (eq (1), details in Methods section) was obtained with $\alpha = 1$. The fit concentration-response curve yielded EC_{50} values of 0.216 ± 0.016 µM (mean ± S.E.M) for BMVECs and 0.290 ± 0.035 µM for bEnd.3 cells (**Figure 4.10**). Our data are in the same range as the EC_{50} values at 0.4 µM previously calculated for ACh-induced calcium signals in the HLE-B3 human lens epithelial cell line (Collison et al., 2000). Interestingly, no direct correlation was observed between the abundance of M_1-M_5 receptor proteins (**Figure 4.5**) and the EC_{50} curve left-shift (**Figure 4.10**) or the maximal mean fluorescence ratio induced by ACh (**Figure 4.6**). Moreover, our results indicate that primary BMVEC cells are more sensitive to agonist exposure compared to the immortalized counterparts, their EC_{50} curve being left-shifted. These data are in accordance with the distinct Ach-induced calcium response of muscarinic receptors in primary cultivated vs. immortalized human lens epithelial cells (Collison et al., 2000).

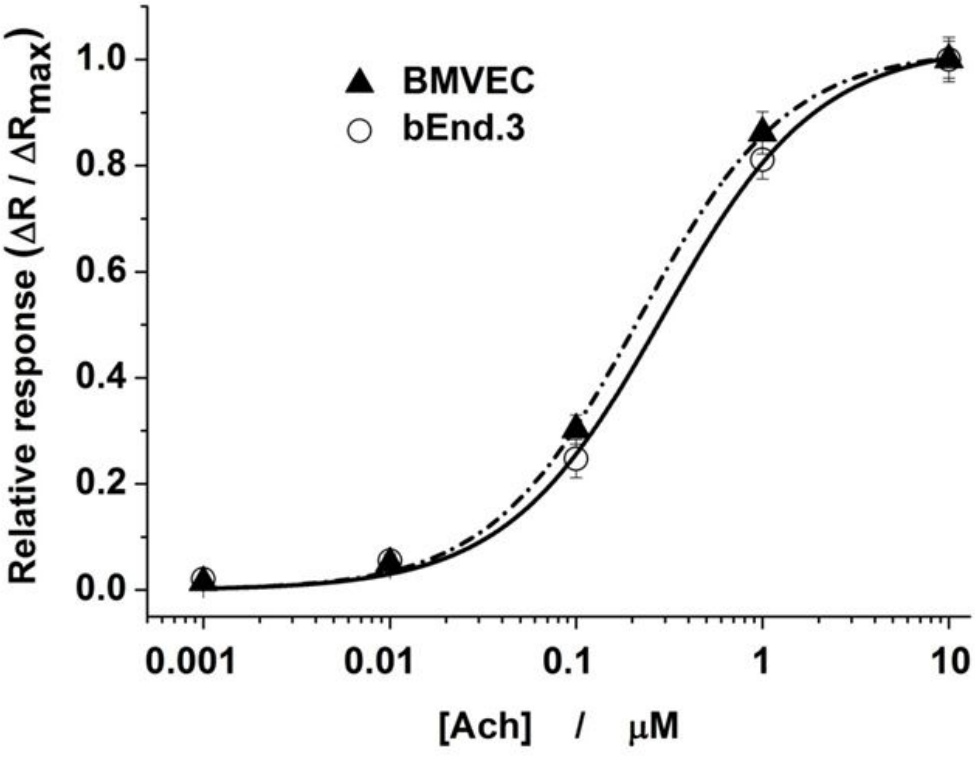

Figure 4.10. Concentration-response curves for ACh-induced increases in the normalized fluorescence ratio ($\Delta R/\Delta R_{max}$) in BMVECs and bEnd.3 cells. Curves were fitted with eq. (1). Acetylcholine was used at concentrations ranging from 0.001 - 10 µM. Data are plotted as the mean ± SEM, N = 30 independent cells, from three different cell batches.

4.4.4. Selective blocking of M_3 receptors (but not M_1) reduces ACh-induced calcium signals

The differential functional contribution of muscarinic receptor subtypes expressed by BMVECs and bEnd.3 cells was next investigated by calcium imaging, adding muscarinic orthosteric antagonists to the medium two minutes before ACh application. The results (**Figure 4.11**) indicate that the M_1 receptor antagonist VU 0255035 was ineffective in blocking ACh-induced calcium signals, while 3 other antagonists (M_3 receptor antagonists J104129 fumarate and 4-DAMP, and M_1 receptor antagonist telenzepine dihydrochloride hydrate) completely inhibited the signals triggered in response to 1 μM ACh (representative traces are presented in **Figure 4.7** for bEnd.3 cells and in **Figure 4.8** for BMVECs). The significant difference between the poor inhibition induced by the VU 0255035 and complete inhibition produced by telenzepine, both of them being accepted as M_1 antagonists, can be explained by the difference in their affinity to M_3 (8-fold less than for M_1 in the case of telenzepine and 58-fold less for VU 0255035). Thus, at high concentrations, the former also inhibited M_3 while the latter did not.

Inhibition curves for the 3 effective antagonists, when fit to a sigmoidal function (eq (2)), yielded a Hill coefficient near 1 and absolute IC_{50} values in the range of 1 nM to 200 nM (**Figure 4.11** and **Table 4.2**). The maximal inhibition produced by VU 0255035 in the tested range of concentrations, as determined by the fit to eq (2), was found to be less than 20%, and the relative IC_{50} was in the range of 75 nM to 150 nM. These data indicate that despite comparable protein expression levels for M_1 and M_3, the number of functional M_1 receptors in the plasma membrane is much less compared to M_3 receptors. Unfortunately, the lack of commercially available M_5-specific antagonists limited our pharmacological characterization. The functional expression of mAChRs in BMVECs and bEnd.3 cells was also evaluated by applying agonists/antagonists targeting the allosteric site of the receptors. We found that the selective allosteric M_1 antagonist MT-7 (20 nM, Fruchart-Gaillard et al., 2008) did not exert any inhibitory effect on the ACh-induced calcium signal in either type of brain microvascular endothelial cells (**Figure 4.12A**). In line with these findings, the selective allosteric M_1 agonist (Jacobson et al., 2010) AC-42 (10 μM), did not elicit any calcium signals (**Figure 4.12 B).** Taken together, these results lead to the conclusion that only low levels of the functional form of the M_1 receptors are present on the plasma membrane.

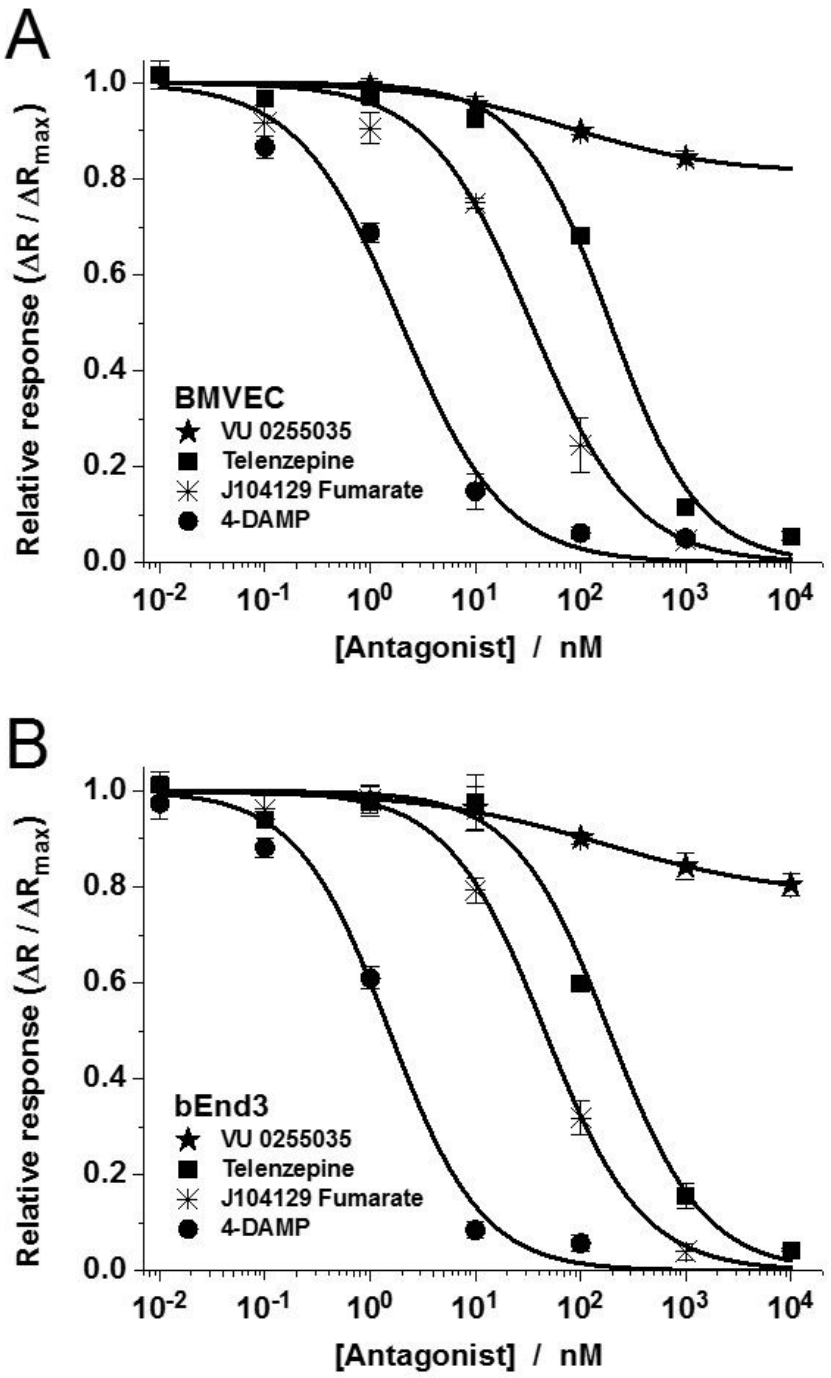

Figure 4.11. Inhibition curves of the response to acetylcholine (1 μM) in BMVECs (**A**) and bEnd.3 cells (**B**) in the presence of mAChR antagonists telenzepine, VU 0255035, J104129 fumarate, and 4-DAMP. Results are expressed as average fractions (±SEM on N = 40 independent cells) of the maximal fluorescence ratio (recorded at 10 μM ACh) produced by the lowest concentration in the tested range. Ratios ($\Delta R/\Delta R_{max}$) are plotted as a function of antagonist concentration. Curves were fitted with eq. (2), and IC_{50} values are presented in Table 1.

Table 4.2. Effects of 4 different muscarinic antagonists on the response of BMVECs and bEnd.3 cells to 1 μM ACh. Absolute IC_{50} values and affinity constants K_a were calculated based on eq. (2) and (3), respectively, from the data presented in Fig. 5. For comparison, previously reported affinity constants for M_1 and M_3 receptors (K_i), determined on individual clones expressed in testing cell lines, are also shown. *For VU 0255035, the absolute value of IC_{50} could not be established, due to this antagonist's very low efficacy in blocking the calcium signal; **K_i values were determined via a radioligand binding assay (Michel et al., 1989; Sheffler et al., 2009), but the authors note that the K_i values obtained via a calcium mobilization assay could be at least two times higher than those determined in the radioligand binding assay.

	BMVEC		**bEnd.3**		**Published reports**	
mAChR antagonist	**IC_{50} (nM)**	**K_a (nM)**	**IC_{50} (nM)**	**K_a (nM)**		**K_i (nM)**
Telenzepine	191.29 ± 28.51	33.98	162.08 ± 21.86	36.43	M_1 M_3	2.5 (Tanda et al. 2007) 20.7 (Tanda et al. 2007)
VU 0255035*	> 10^4	>1770	> 10^4	>2250	M_1 M_3	14.9 (Michel et al., 1989; Sheffler et al., 2009) 877** (Michel et al., 1989; Sheffler et al., 2009)
J104129 fumarate	33.81 ± 3.80	6.00	43.31 ± 3.62	9.74	M_1 M_3	19 (Mitsuya et al. 2000) 4.2 (Mitsuya et al. 2000)
4-DAMP	1.96 ± 0.48	0.42	1.39 ± 0.25	0.31	M_1 M_3	1 (Dorje et al., 1991; Lazareno et al., 1990) 0.6 (Dorje et al., 1991; Lazareno et al., 1990)

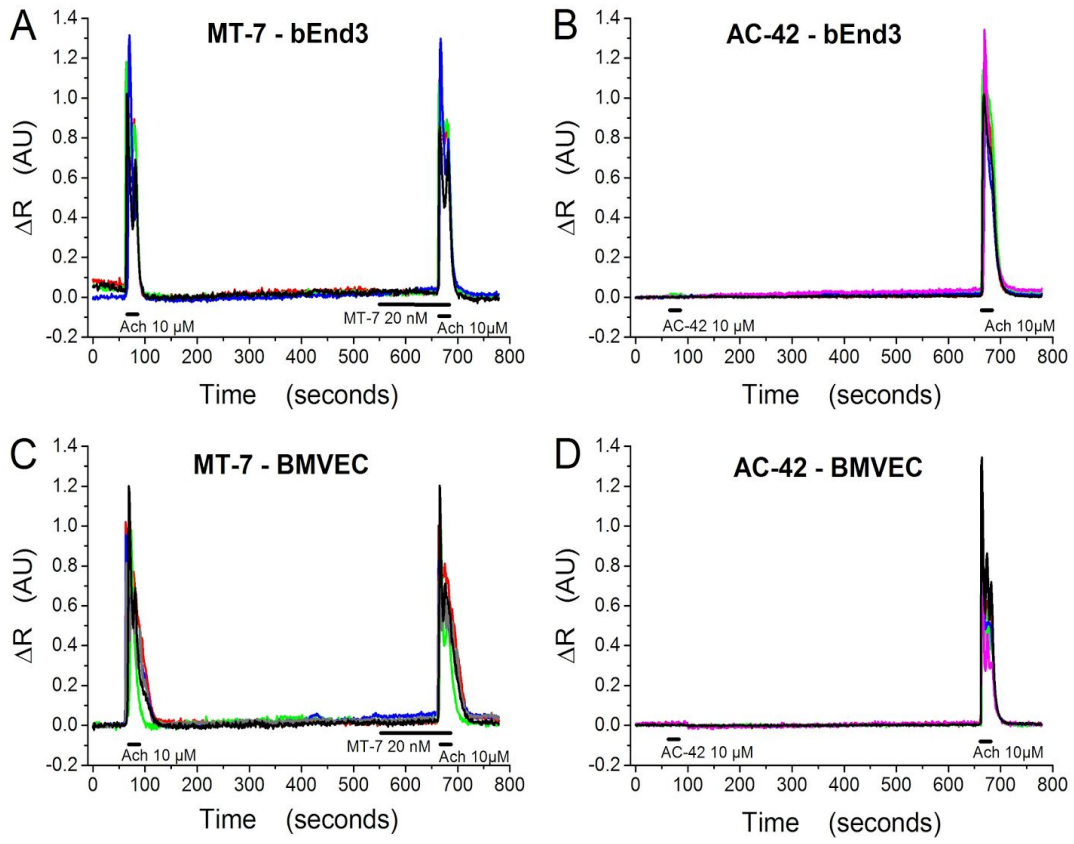

Figure 4.12. Representative traces of mean fluorescence ratio (ΔR) changes induced by MT-7 (20 nM), a potent M_1 antagonist (**A, C**), and AC-42 (10 μM), an M_1 specific agonist (**B, D**) in bEnd.3 cells (*A, B*), and BMVECs *(C, D)*.

4.4.5. The variability of mouse muscarinic receptors lies in the allosteric binding site

We next complemented our functional analyses with a bioinformatics approach, analyzing residues' conservation of both allosteric and orthosteric binding sites. The multiple sequence alignment of muscarinic receptors, along eukaryotic species, reflects the fully conservation of the residues present in the orthosteric site (Wess, 2005; Goodwin et al., 2007) (**Figure 4.13**). Conversely, the residues present in the allosteric binding site (Kruse et al., 2012) emerges as highly variable (**Figure 4.13 A, B**). This suggests a clear selectivity role of the allosteric cavity in ligand binding and activation mechanism. We performed docking experiments on M_1-M_5 modeled mouse muscarinic receptors with the four antagonists (**Figures 4.14 - 4.17**): Telenzepine, J104129 fumarate, VU 0255035 and 4-DAMP. Within the limitations of the method, it can be observed that, while three of these antagonists (Telenzepine, J104129 fumarate, 4-DAMP) interact with residues located in the orthosteric binding site, VU 0255035, due to its larger size, interacts also with residues positioned in the allosteric binding site (**Figure 4.13 A, Table 4.3**). Hence differences in affinities could be

explained by the observation that VU 0255035 network of interactions involves a less conserved region (**Figure 4.15**).

A

Generic residues numbering (Class A)	Conservation residues percentage		
2.60	F=32%	Y=68%	
2.62	T=56%	L=24%	V,A=10% each
3.22	T,P=21% each	S,A=16% each	D,W,Y=1% each
3.32	D=100%		
3.33	y=100%		
3.39	S=100%		
ECL2	P=59%	L,E=16% each	M,H=1% each
ECL2	P=35%	D,A=24% each	S,L,K=1% each
ECL2	G=62%	E=24%	N=8%
ECL2	E=67%	Q=24%	T,A=1%each
5.36	E=40%	N=40%	Q=16%
5.37	P=70%	A=30%	
6.44	F=100%		
6.48	W=100%		
6.51	Y=100%		
6.52	N=98%	Y=2%	
ECL3	D=40%	A,K=18% each	Q=10%
ECL3	S=29%	L,P, D=18% each	C,N=1% each
7.31	N,K,E=23%	E,V=15%	
7.32	T=72%	F,V,R,A,E=3% each	
7.38	Y=100%		
7.42	Y=100%		

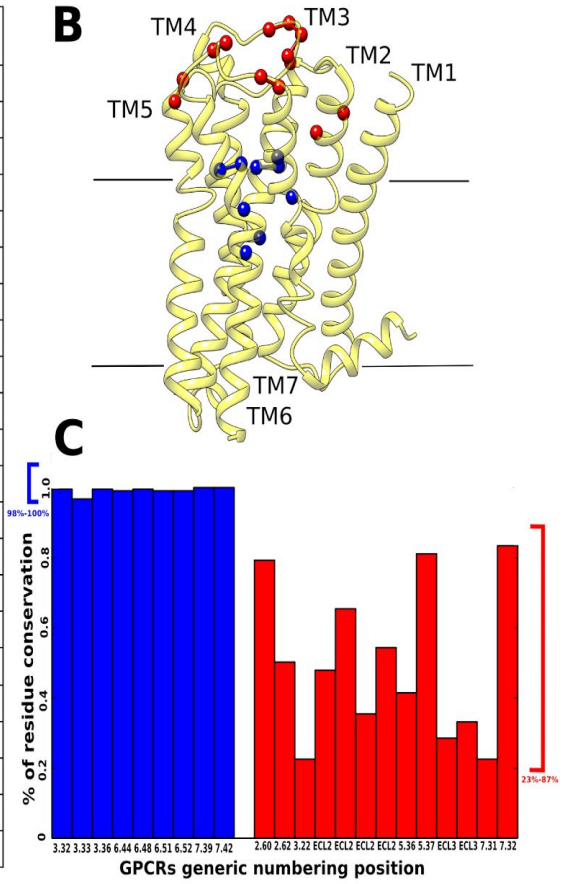

Figure 4.13: Conservation of orthosteric and allosteric site residues among annotated eukaryotic muscarinic receptors. (**A**) Conservation values of residues located in allosteric (red) and orthosteric (blue) binding sites. (**B**) Orthosteric and allosteric binding-site residues mapped on the M_3 solved structure (PDB code: 4MQS). The residues are indicated as colored balls, following the same color code as in (A). (**C**) Plot of residues' conservation values; residues of the orthosteric binding site (blue) and residues in the allosteric binding site (red).

Table 4.3. Muscarinic receptors homology modeling templates for mouse M_1-M_5. Each entry in black represents the template PDB code and the sequence identity (S.I.), for the receptors for which 3D structures were obtained through homology modeling.

	M_1	**M_2**	**M_3**	**M_4**	**M_5**
Template	4DAJ	3UON	4U16	3UON	4DAJ
S.I.	77.27%	97.24%	97.10%	83.50%	78.79%

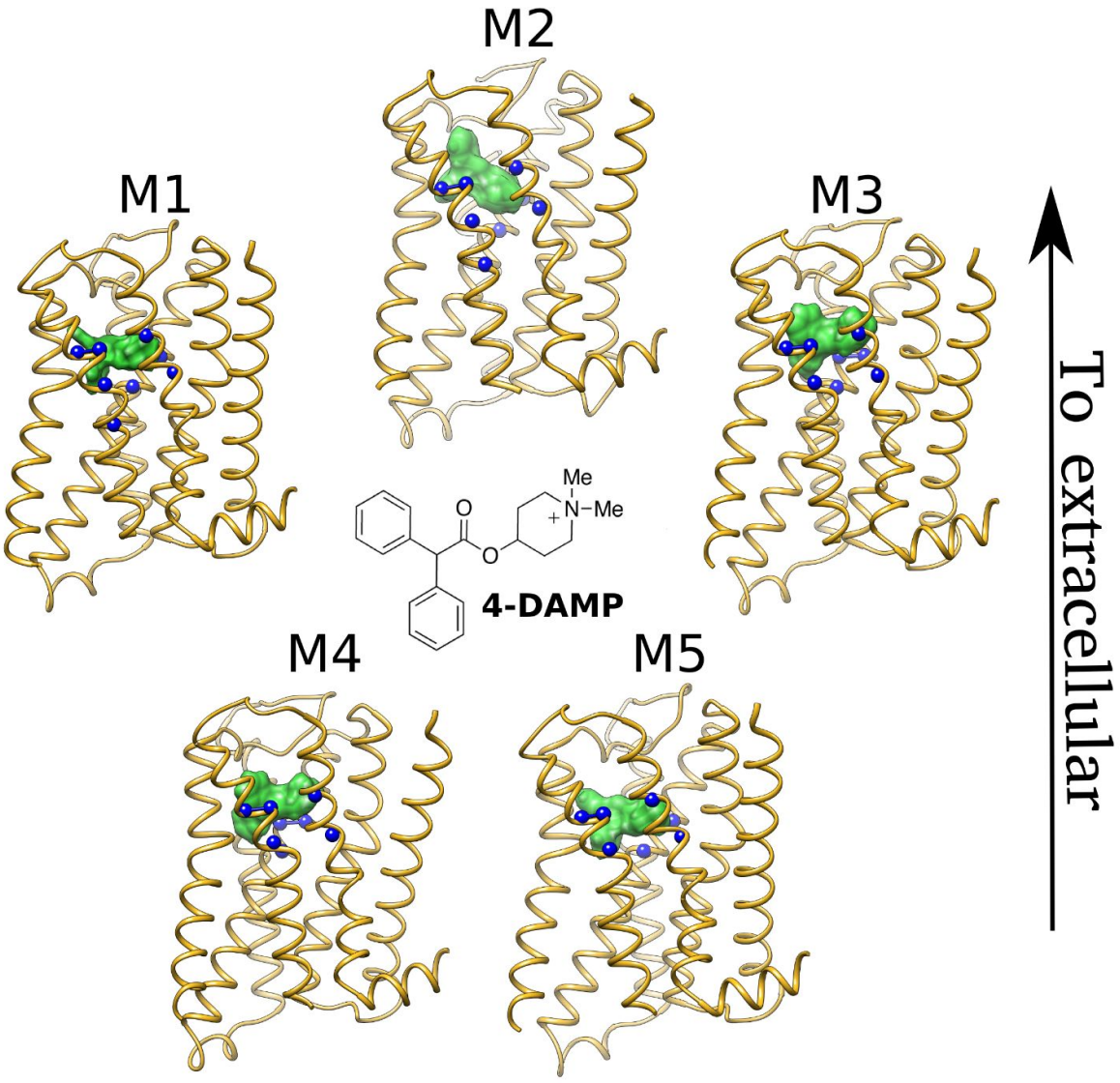

Figure 4.14. 4-DAMP docking at the binding sites of the M_1-M_5 mouse receptors. The chemical structure of the antagonist, is shown in a 2D representation at the center of the figure, receptors are shown in a ribbon representation, ca of residues located in the orthosteric cavity are shown in blue.

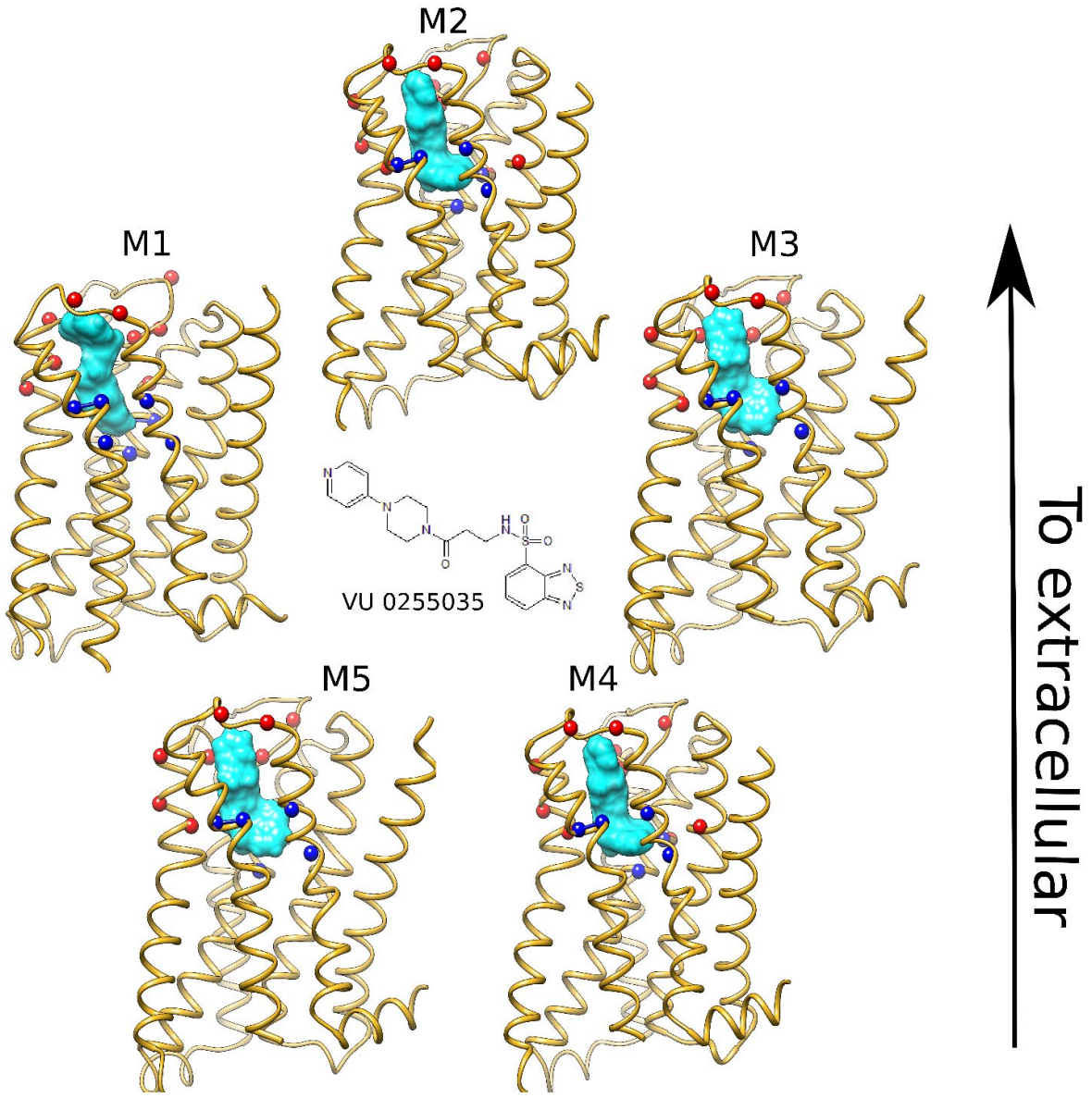

Figure 4.15. VU 0255035 docking at the binding sites of the M_1-M_5 mouse receptors. The chemical structure of the antagonist, is shown in a 2D representation at the center of the figure, receptors are shown in a ribbon representation, ca of residues located in the orthosteric cavity are shown in blue and ca of residues located in the allosteric cavity are shown in red.

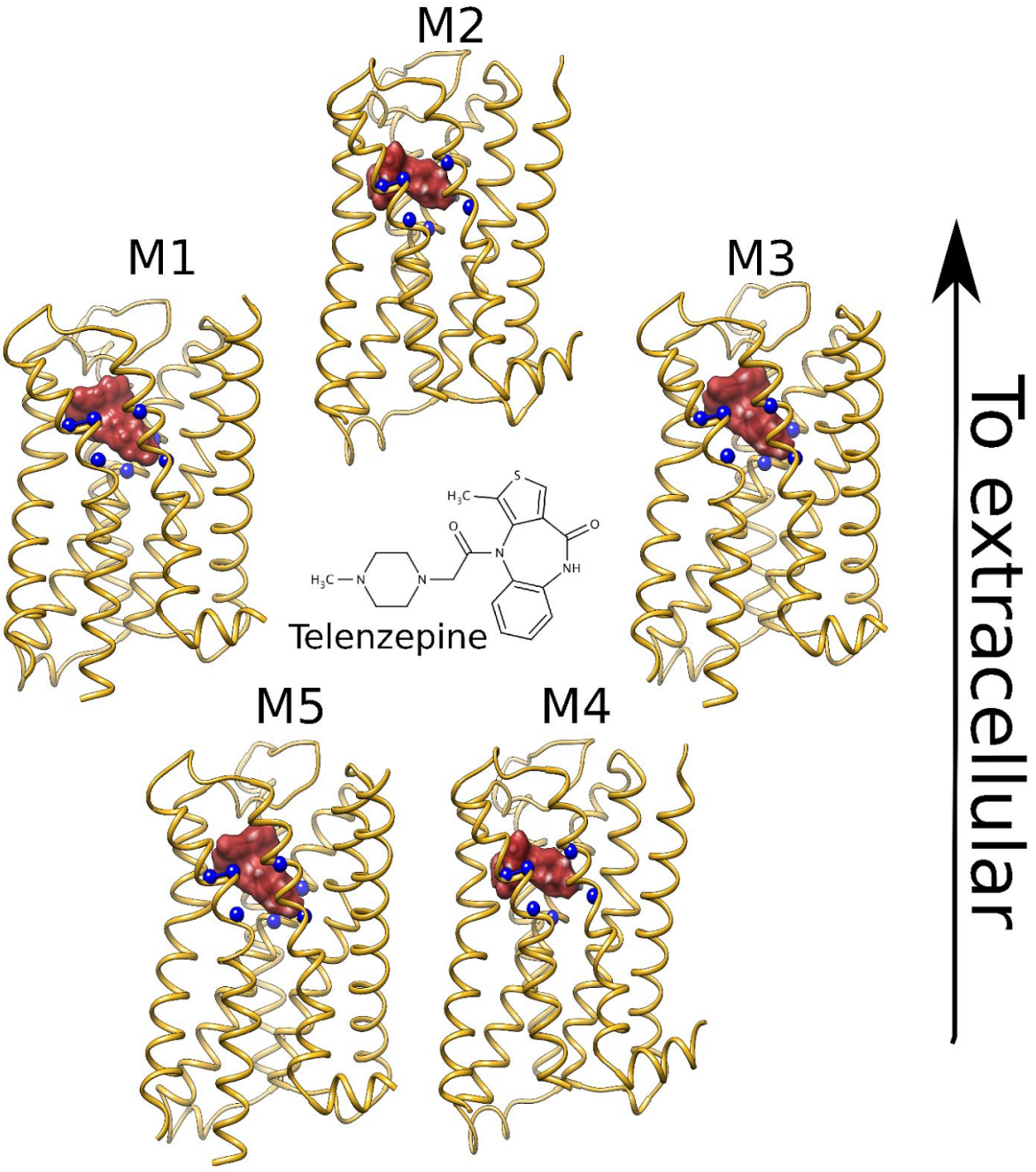

Figure 4.16. Telenzepine docking at the binding sites of the M_1-M_5 mouse receptors. The chemical structure of the antagonist, is shown in a 2D representation at the center of the figure, receptors are shown in a ribbon representation, ca of residues located in the orthosteric cavity are shown in blue.

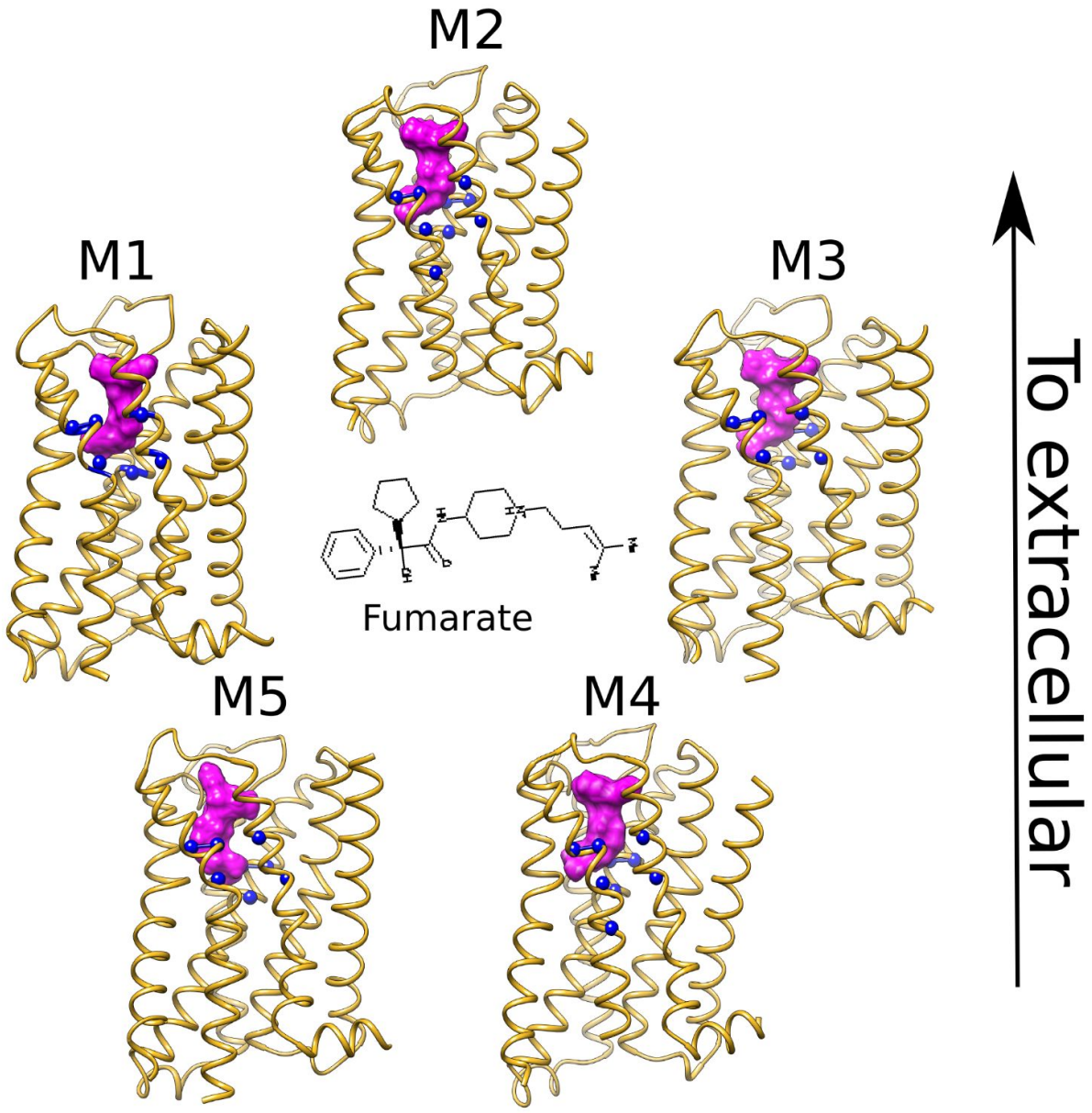

Figure 4.17. J104129 fumarate docking at the binding sites of the M_1-M_5 mouse receptors. The chemical structure of the antagonist, is shown in a 2D representation at the center of the figure, receptors are shown in a ribbon representation, ca of residues located in the orthosteric cavity are shown in blue.

4.5. Discussion and Conclusions

The results obtained in immortalized and primary cell cultures of the mouse brain microvasculature, including capillaries, lead to the conclusion that all muscarinic acetylcholine receptor subtypes are present in mouse brain endothelial cells. To our knowledge, this is the first report in which all mAChRs have been studied in terms of both mRNA expression and protein quantification in these cell types, thereby filling a gap in the existing literature, which focused on specific subsets. In addition, we provide a functional characterization of M_1 and M_3 and argue that the distribution of $M_{1\text{-}5}$ receptors may provide important insight into the endothelial response to cholinergic stimuli.

The analysis of transcripts revealed a gradient of mRNA expression by receptor subtype, with M3 representing the most abundant and M2 the lowest. In a previous study conducted in mouse retinal arterioles (Gericke et al., 2011a), mRNA levels for the M_3 receptor were similar to those reported here, but no other subtypes were detected. The discrepancy may be due to the substantial difference in detection thresholds, since in that study the cut-off was set at 10^{-4} relative to β-actin, which is above the levels we report here for the other 4 subtypes. Low levels of M_2 (mRNA and protein abundance) in our brain microvascular endothelial cells are consistent with data reported recently for the proteome of mouse cerebral arteries (Badhwar et al., 2014).

An important finding in the present work concerns the cellular localization of mAChRs as revealed by immunofluorescence. Aside from the plasma membrane, labeling was found in both the nucleus and the cytoplasm, with a subtype-specific distribution. This result fits within the framework of a novel paradigm that has emerged in the last ten years, indicating that GPCRs (the receptor family which mAChRs belong to) are able to engage in signaling even when positioned inside the cell, including the nucleus (Gobeil et al., 20006). In particular, we found M_1 mostly distributed in nuclear and cytoplasmic compartments, similarly to what has been reported for M_1 in other cell types (Lind and Cavanagh, 1993), where the intracellular localization was explained either on the basis of constitutive internalization through a clathrin-dependent mechanism (Uwada et al., 2014) or via agonist exposure-dependent internalization (Thomas et al., 2009). In another report, the intracellular localization of M_1 in neuroblastoma cells was considered associated with a distinct signalling pathway from the same receptors located in the plasma membrane (Uwada et al., 2011). On the other hand, the demonstration of intracellular mAChRs is not in itself proof of their involvement in specific alternative pathways. For one thing, receptor proteins must be present in the cytoplasm during their folding and maturation process until insertion in the plasmalemma. Additional experiments are necessary to describe the role of these intracellular fractions of mAChRs in brain endothelial cells.

Acetylcholine can trigger cytosolic calcium messenger pathways via both nicotinic and muscarinic receptors. The mechanisms of action of these receptors are very different;

nicotinic receptor activation allows direct calcium ion influx from outside the cells, while the activation of Gq-coupled muscarinic receptors (M_1, M_3 and M_5) triggers the IP_3 calcium pathway. Our results show that nicotine could not elicit any calcium signaling in mouse brain microvascular preparations, which is in accordance with previous reports on rat coronary microvascular endothelial cells (Moccia et al., 2004). We therefore suggest that the measured calcium signals are due exclusively to the contribution of muscarinic acetylcholine receptors, e.g., M_1, M_3, and M_5 receptors coupled to the phosphatidylinositol signaling pathway (Eglen, 2006), and not to nicotinic acetylcholine receptors. As M_2 and M_4 do not contribute to the calcium signaling pathway, we did not include these receptors in the functional study. However, the high M_4 protein expression levels, comparable to those of M_1 (**Fig. 4.5**), prompt further investigations into the role of this receptor in brain endothelial cells function.

In spite of the very recent availability of an M_5-specific antagonist, VU 0488130 (ML381) (Gentry et al. 2014), we opted to exclude M_5 from our functional characterization, due to its very low expression levels compared to M_1 or M_3 (**Fig. 4.3** and **Fig 4.5**). Moreover, an attempt to isolate the M_5 response by saturating M_1 and M_3 with specific antagonists would be most likely unsuccessful because of the very small difference in the affinity of 4-DAMP to M_3 and M_5. In addition, no data are available on the affinity of J104129 fumarate to M_5. According to **Table 4.2**, the affinity of 4-DAMP to M_5 is only twice as high as for M_3 which suggests that the antagonist, at concentrations saturating M_3, will also strongly inhibit the M_5 signal. We also report here that the selective blocking of M_1 receptors does not reduce ACh-induced calcium signals. The functional expression of M_1 receptors in brain microvascular endothelial cells is particularly important, not only because of their high relevance in murine models of neurological diseases (Sheffler et al., 2009; Xiang et al., 2012; Puri et al., 2015), but also because their role is often neglected in favor of their neuronal counterparts.

Our data show a mismatch between M_1 mRNA levels and protein abundance. Previous studies have described that the synthesis, trafficking and localization of muscarinic receptors is influenced by multiple mechanisms (Nathanson, 2008), including chaperone-assisted synthesis and transport (for example, it has been shown that small G-protein ARF6 modulate trafficking of M_2 receptor, Nathanson, 2008). These processes might exert a major influence on how much mRNA is translated into functional proteins. In this context, one of the major findings revealed by the pharmacological characterization of mAChRs in our cells was the very low efficacy of VU 0255035 in inhibiting ACh-triggered signals. Considering the affinities of this antagonist for M_1 and M_3, we speculate that the small amount of inhibition we did observe was due to its binding to M_3 and not to M_1. This argument is supported by the fact that MT-7 (the most specific allosteric M_1 antagonist, with no affinity for any mAChR subtypes other than M_1, Adem and Karlsson, 1997) also did not diminish the ACh signal. In turn, M_3 antagonist J104129 fumarate completely inhibited the ACh signal over a range of concentrations corresponding to its specific affinity value. This strongly suggests that even if the protein expression of M_1 was comparable to that of M_3 (as shown by the MALDI-TOF data) the level of functional, plasma membrane-embedded M_1

receptors is very low. This hypothesis is in accordance with previously reported values from mouse retinal arterioles (Gericke et al., 2011a), where the presence of M_3 was shown based on both mRNA quantification and a functional assay. In addition, the suggestion agrees with the low M_1 levels revealed by immunofluorescence in the plasma membrane, with the majority of the protein being located near the nucleus. These data are further supported by the lack of M_1 receptor activation in the presence of its very specific agonist, AC-42 (Spalding et al., 2002).

Another key result of the present study is that the allosteric binding site of muscarinic receptors, including mouse receptors, is highly variable. Despite the commonly reported blocking specificity of J104129 fumarate, 4-DAMP, and telenzepine for M_3 and M_1, these antagonists can bind to all mAChRs, and the differences between their binding affinities for each receptor subtype are not very prominent (Lazareno et al., 1990; Michel et al., 1989) (**Table 4.4**). From our molecular docking experiments it can be appreciated that these three antagonists interact with highly conserved residues mainly located in the orthosteric binding site. We paid instead particular attention to VU 0255035 and VU 0488130 (a high affinity M5 antagonist) and found that they could both interact with residues located in both the orthosteric and allosteric sites. The variability in the allosteric site could explain the differences in antagonist binding affinities.

Table 4.4. Affinity constants of different antagonists for muscarinic acetylcholine obtained from the literature. The values for the affinity constants that match our experimental data for the effect of each antagonist on the total ACh-induced calcium signal recorded for BMVECs and bEnd.3 cells are shown in bold.

Antagonist	**Binding affinities for mAChR subtypes (nM)**					**M subtype**	**Biologic source**
	M_1	**M_2**	**M_3**	**M_4**	**M_5**		
Telenzepine	2.52	43.8	**20.7**	12.4	49.9	1	membranes from frozen rat brain (Tanda et al. 2007)
						2-5	human receptors in CHO cells (Tanda et al. 2007)
VU 0255035	14.87	661.33	876.93	1177.67	2362.33	1	CHO cells stably expressing rat receptor (Sheffler et al. 2009)
						2,3,5	CHO cells stably expressing human receptors (Sheffler et al. 2009)
						4	rat receptor expressed by stably transfected CHO-K1 cells (Sheffler et al. 2009)
J104129 fumarate	19	490	**4.2**			1-3	membranes from CHO cells expressing cloned human receptors (Mitsuya et al. 2000)
4-DAMP	1.02	7.08	**0.56**			1	rat cortex (Lazareno et al. 1990)
						2	rat heart (Lazareno et al. 1990)

						3	rat submandibular gland (Lazareno et al. 1990)
	0.6	3.8	**0.5**	1.17	1.05	1-5	cloned human cells expressed in CHO cells (Dorje et al, 1991)

Early reports demonstrated the presence of M_1, M_3 and M_5 in the human brain microcirculation (Linville and Hamel, 1995; Elhusseiny et al., 1999), which makes a full characterization of all three subtypes in the mouse very important. We excluded M_5 from our functional investigation because the data indicated low levels of both gene and protein expression, and there is limited knowledge on binding specificity of M_5 antagonists (Gentry et al., 2014) to these receptors. The functional characterization that we performed for M_1 and M_3 receptors is physiologically relevant and in line with recent reports providing evidence on the importance of M_1 and M_3 in controlling blood pressure in various districts (i.e. mouse thoracic aorta and mesenteric artery, Yuan et al., 2016; rat mesenteric artery, Tangsucharit et al., 2016; human umbilical vein, Pujol Lereis et al., 2006). Altogether, the present results provide an encouraging platform for future mouse-to-human translational studies. In particular, further experiments will be needed to fill a gap in our study, i.e. the functional characterization of the M_4 subtype.

In summary, our findings highlight M_3 receptors as major players in mouse brain microvasculature endothelium. On the other hand, the role of M_1 receptors in microvasculature should not be discounted, in spite of its low functional contribution to the ACh-induced calcium signaling, since a high amount of protein was found expressed in the cells. As previously mentioned, the presence of this receptor family in brain microvasculature endothelia holds promise for the identification of novel non-neuronal drug targets. Our data specifically point out the M_1 and M_3 subtypes as interesting targets in translational studies when designing drugs that act on the blood brain barrier. Moreover, the levels of M_4 protein expression found in our study, almost as high as M_1, prompt further investigations that might extend our understanding of the role of muscarinic receptor subtypes in controlling brain endothelial cells.

4.6. Executive summary

Aim

- To assess the expression of all five muscarinic acetylcholine receptors in mouse brain microvascular endothelial cells, with a special focus on the functional expression of M_1 and M_3 receptors.

Results

- The mRNA expression of M_2, M_3, and M_5 correlates with their respective protein abundance, but there is a mismatch for M_1 and M_4 mRNA versus protein levels.
- Although M_1, M_3 and M_4 are the most abundant receptors, only a small fraction of M_1 is present in the plasma membrane and functions in ACh-induced Ca^{2+} signaling.
- Cholinergic activation of calcium signaling pathways in brain microvascular endothelial cells depends on muscarinic, but not on nicotinic, receptors.
- Selective blocking of M_1 receptors does not, while selective blocking of M3 receptors does, reduce ACh-induced calcium signals.
- Bioinformatic analyses performed on eukaryotic muscarinic receptors demonstrate a high degree of conservation of the orthosteric binding site and a great variability of the allosteric site.

Conclusion & future perspective

- Our study indicates muscarinic acetylcholine receptors as potential pharmacological targets in future translational studies.
- We argue that future research on drug development should especially focus on the allosteric binding sites of the M_1 and M_3 receptors.

Chapter 5. Pilocarpine acts on multiple targets of the CNS microvascular endothelium

5.1. Summary

Clinical and experimental epilepsy studies demonstrated the blood brain barrier permeabilization during seizures. Although in epileptogenesis the main focus is on seizures, the aim of study is to understand if blood brain barrier permeabilization is preceding or following neuronal hyperexcitability. We tested the effects of pilocarpine *in vivo* in mice, and *in vitro* on hippocampal slices and brain endothelial cells. We demonstrated that pilocarpine: (1) induces the *in vivo* and *in vitro* cytokines release (e.g. IL-6, KC, MCP-1, and TNF-α), (2) upregulates the expression of adhesion molecules (e.g. VCAM-1, ICAM-1) in brain microvascular endothelial cells, (3) elicits calcium transients in a percentage of brain microvascular endothelial cells but is not inducing epileptic-like discharges in hippocampal pyramidal neurons, (4) downregulates the expression of tight junction proteins (e.g. ZO-1, claudin 5) and permeabilizes the monolayers of brain microvascular endothelial cells, (5) competes with acetylcholine on the same binding site of the muscarinic receptors, (6) downregulates M_1 and M_3 receptors, while upregulates M_2, M_4 and M_5 receptors in brain microvascular endothelial cells. In conclusion, our study indicates that brain endothelium is an important site of action for pilocarpine, and the epileptogenesis mechanisms should be revisited.

5.2. State-of-art

The neuron-centered paradigm that epileptic seizures can be initiated only by epileptic-like neurons has been recently challenged. Although there is an increased interest on elucidating mechanisms of seizure generation and epileptogenesis based on the investigations of cerebral blood flow and permeability of cerebral microvessels, the temporal sequence linking seizures to peripheral inflammation and BBB dysfunction remains to be clarified (Janigro et al., 2012). In the mouse model of pilocarpine-induced epilepsy was previously showed that seizures induce elevated expression of vascular cell adhesion molecules and enhanced leukocyte rolling and arrest in brain vessels (Fabene et al., 2008), and was proposed the emerging role for leukocytes and leukocyte adhesion mechanisms in seizure generation (Fabene et al., 2013).

Muscarinic acetylcholine receptors have been proposed as potential pharmacological targets and/or disease-biomarkers in various CNS pathologies, e.g. schizophrenia (Gibbons et al., 2013; Melancon et al., 2013; Carruthers et al., 2015), Alzheimer's disease (Melancon et al. 2013; Colloby et al. 2015; Waqar et al. 2015; Manuel et al. 2016), Parkinson's disease

(Shen et al., 2015), depression (Witkin et al., 2014; Gibbons et al., 2016; Small et al., 2016), psychosis (Andersen et al. 2015), and epilepsy (Hamilton et al., 1997; Schneider et al., 2013; Capannolo et al., 2014; Yi et al., 2015). In order to delineate the physiological roles of the muscarinic cholinergic system, different muscarinic receptor *knockout* mice have been engineered (Bymaster et al., 2003).

In epilepsy, there are several pieces of evidence pointing out that M_1 receptor plays a key role in mediating seizures. To date, pilocarpine administration caused seizures and lethality in wild-type and M_2-M_5 knockout mice, but had no effect in the M_1 knockout mice (Hamilton et al., 1997) or had reduced effect in the mice knockout for M_1 in the parvalbumin-positive inhibitory neurons (Yi et al., 2015). Intraperitoneal injection of VU0255035 (selective antagonist of M_1 receptor) reduced pilocarpine-induced seizures in mice without severe cognitive deficits, and inhibited the carbachol-induced potentiation of NMDA currents in hippocampal pyramidal cells from rat slices (Sheffler et al., 2009). Despite the importance of these studies in elucidating the seizure-based mechanisms, there is a major limitation in interpreting results by considering only the contribution of neuronal muscarinic receptors (Cataldi et al., 2011), and ignoring how the gene deletion affected other cellular components of the neurovascular unit (e.g. astrocytes, endothelial cells, pericytes, microglia etc.).

Clinical and experimental studies indicated that neurovascular unit activation plays an essential role in ictogenesis (Fabene et al., 2008; Fabene et al., 2013; Bertini et al., 2013; Radu et al., 2013). In particular, brain endothelium alterations and blood brain barrier barrier permeabilization seem to have an important contribution in epileptogenesis (Uva et al., 2008; Fabene et al. 2008; Gorter et al., 2015; Librizzi et al., 2017). Recently, we described the functional expression of all five muscarinic receptors in mouse brain microvascular endothelial cells (Radu et al., 2017a). Therefore, the aim of study is to understand if blood brain barrier permeabilization is preceding or following neuronal hyperexcitability, which a special focus on the possible contribution of muscarinic receptors expressed in the brain endothelium.

5.3. Materials and Methods

5.3.1. Brain endothelial cell cultures

Balb/c mouse primary brain endothelial microvascular cells BMVEC (PELOBiotech, Germany; passages 3 – 6) and the Balb/c mouse cell line bEnd.3 (ATCC, USA; passages 20 – 30), were cultivated as previously described (Radu et al., 2015). Cells were plated at a density of 2 x 10^4 cells/cm^2 onto 24-mm cover glasses for intracellular calcium imaging and immunofluorescence protocols, or onto 25 cm^2 flasks and further harvested for qRT-PCR and protein quantification assays.

5.3.2. In vitro pilocarpine treatment protocol

Brain endothelial cells were treated for 2 hrs, 6 hrs and 24 hrs with 100 µM pilocarpine hydrochloride (#P6503; Sigma) for the qRT-PCR, immunofluorescence staining and protein quantification assays protocols.

Rat slices were treated for 10 min with pilocarpine at 10 µM (Nagao et al., 1996), 100 µM and 200 µM (Marchi et al., 2007), and further whole-cell and local field potential recordings were done.

5.3.3. Gene expression by qRT-PCR

To quantify the expression levels of *chrm1-5* (M_1-M_5 receptor-encoding genes), *Tjp1* (tight junction protein 1 encoding gene) and *Cldn5* (claudin 5 encoding gene) in the mouse brain microvascular endothelial cells, total RNA was extracted using the GenElute Mammalian Total RNA MiniPrep Kit (RTN70, Sigma) according to the manufacturer's instructions. RNA concentrations were determined by spectrophotometric absorption measurements at 260 and 280 nm (Beckman Coulter DU 730). DNase I treatment was used to remove contaminating genomic DNA. In agreement with the manufacturer guidelines (Sigma), in our experiments the A_{260}:A_{280} ratio was 2.03±0.06 (bEnd.3) and 1.93±0.03 (BMVEC). Reverse transcription was performed using the High-Capacity cDNA Archive Kit (Sigma). The following mouse Taqman assays (Life Technologies, USA) were used in accordance to the manufacturer's guidelines: *Chrm1* (Mm00432509_s1), *Chrm2* (Mm01701855_s1), *Chrm3* (Mm01338409_m1), *Chrm4* (Mm00432514_s1), *Chrm5* (Mm01701883_s1), *Tjp1* (Mm00493699_m1), *Cldn5* (Mm00727012_s1), *Gapdh* (Mm999999_g1), *Actb* (Mm00607939_s1). The relative abundance of *Chrm1-5, Tjp1* and *Cldn5* transcripts was assessed by qRT-PCR using TaqMan methodology and the ABI Prism 7300 Sequence Detection System (Applied Biosystems, USA). Reactions were carried out for 50 cycles in triplicate. The β-actin gene (*Actb*) and the glyceraldehyde 3-phosphate dehydrogenase gene (*Gapdh*) were chosen as housekeeping genes, as previously described in other studies of gene quantification in mouse brain endothelial cells (Wang et al., 2006; Navone et al., 2013; Winkler et al., 2015; Radu et al., 2017a).

5.3.4. Immunofluorescence staining of muscarinic receptors and tight junction proteins in brain endothelial cells

The cellular localisation of M_1-M_5 receptors, ZO-1 and claudin-5 was evaluated by immunofluorescence in control and pilocarpine treatment conditions. Brain endothelial cells were treated with blocking and permeabilization solution (0.3% Triton-100, 1% bovine serum albumin, 2% normal goat serum) for 30 min, incubated overnight at room temperature with the primary antibody, incubated for 1h with the secondary antibody followed by TO-PRO®-3 (1:3000, Life Technologies) for 10 min, for nuclear staining, and finally mounted with fluorescent mounting medium. The following polyclonal rabbit primary antibodies from Alomone, Israel were used: anti-M_1 (1:100, #AMR-001), anti-M_2 (1:100, #AMR-002), anti-M_3 (1:100, #AMR-006), anti-M_4 (1:100, #AMR-004), anti-M_5 (1:100, #AMR-005),

anti-PMCA1 (1:200, #ACP-005). Additionally, the polyclonal rabbit primary antibodies from Life Technologies, USA, were used: anti-ZO1 (1:100; #61-7300), anti-claudin5 (1:100; #34-1600). The primary antibody was omitted in negative-control samples. Goat anti-rabbit Alexa 488 (1:1000, Life Technologies) was used as secondary antibody. Normal goat serum and fluorescent mounting medium were purchased from Dako, Milan, Italy.

Specimens were examined using a confocal fluorescence microscope (LSM 710, Carl Zeiss, Germany). The following acquisition parameter settings were used: pinhole corresponding to 1 Airy Unit for each laser, 62 µm for laser 488 nm and 66 µm for laser 633 nm; digital gain was 1.00 for each one; laser intensity was 5% for each one. Acquisition parameter settings were kept fixed for each channel in different image acquisition sessions. Image analysis was carried out using the Zeiss LSM Image Browser software (Carl Zeiss, Germany).

5.3.5. Immunofluorescence staining of adhesion molecules in brain endothelial cells

bEnd.3 cells were seeded at a concentration of 20 x 10^3/mL on a glass coverslip in 24-well plates containing DMEM supplemented with 10% FCS. Cells were stimulated with 15 µM pilocarpine for 18 h in DMEM with 1% FCS. As positive control, cells were treated with 25U/ml of TNF-α for 18 h in DMEM with 1% FCS. bEnd.3 cells were rinsed with PBS and fixed with 4% PFA for 10 min. After washing with PBS, cells were incubated with blocking solution for 1 h at RT and then overnight at 4°C with the primary antibody at the following concentration: anti-VCAM (50 µg/ml) and anti-ICAM (10 µg/ml). Cells were rinsed with PBS, incubated with 7.5 µg/ml biotinylated secondary antibody for 1h at room temperature and with 25 µg/ml Avidin-TexasRed for 1 h at room temperature. Finally, 1 µg/ml DAPI was used for 5 min in the dark. Slides were mounted with Dako and images acquired at Tandem Confocal Scanning-SP5 microscope (Leica, Germany).

5.3.6. Intracellular calcium imaging measurements

Fura-2 AM-based Ca^{2+} imaging experiments based were performed on brain microvascular endothelial cells as previously described (Radu et al., 2015). Measurements were done using a cooled CCD camera (Clara, Andor, Northern Ireland) and a Polychrome V monochromator (Till Photonics, Germany), coupled to a the SliceScope (Scientifica, UK) upright fluorescence microscope with 40x-water immersion objective (Olympus, Japan). Data acquisition was done using Live Acquisition imaging software (Till Photonics, Germany) and calcium changes were determined based on the $R = I_{340nm}/I_{380nm}$ intensity ratio. Ratios were calculated for each cell in the microscope field, based on individually defined regions of interest, after background subtraction. Calcium imaging data were analysed using Offline Analysis software (Till Photonics, Germany) and plotted as mean fluorescence ratio amplitude ($\Delta R = R - R_0$, where R_0 represents the calcium signals recorded in unstimulated cells) ± SEM.

Solutions were delivered over brain endothelial cells through a 100 µm quartz perfusion head using an 8-channel valve pressurized system (ALA Scientific Instruments, USA). Ringer solution contained (in mM): NaCl 140, KCl 5.6, $MgCl_2$ 2, $CaCl_2$ 2, glucose 10, HEPES 10 (pH 7.4 with NaOH). Fura-2 acetoxymethyl ester (Fura-2 AM) and pluronic acid

were purchased from Life Technologies, USA, and all common salts were from Sigma-Aldrich, Milan, Italy. Cytosolic Ca^{2+} transients resulting from the activation of muscarinic acetylcholine receptors were elicited by a 20-s, 1 μM acetylcholine chloride (ACh, Sigma) or by different concentrations of pilocarpine application. The reproducibility of the ACh effect was tested on a double-pulse protocol with a 10-minute between-pulse washing interval with Ringer, as previously described (Radu et al., 2017a). In some experiments, we precede the second ACh pulse with a 2-min application of pilocarpine.

5.3.7. In vitro endothelial cell monolayer permeability assay

Cells were grown on gelatin-coated inserts (0.4 μm pore size plexiglass membrane) of Transwell® Permeable Supports (24-well; Corning, Lowell, MA) to confluence. Cells on the inserts were incubated with 100 μM pilocarpine for 24 h, and incubated with 1 mg/mL 70 kDa FITC-dextran (Sigma) for the last 60 min. The amount of 70kDa FITC-dextran diffused through the endothelial monolayer into the lower chamber was measured by Victor™ X4 2030 multilabel reader (Perkin Elmer, USA) using WorkOut2.5 software and diffusive permeability was calculated as previously described (Li et al., 2010).

5.3.8. Viability testing on mouse brain microvascular endothelial cells

Trypan blue assay was performed on bEnd.3 and BMVECs in control conditions and after pilocarpine treatment, as previously described (Strober et al., 2001; Radu et al., 2015). Cells were detached by trypsin, trypan blue was added (0.2%) and viable cells were counted (at least 150 cells). The viability was calculated relative to controls. Measurements were done in three replicates.

5.3.9. Cytokine level quantification

The cytokines level was quantified in mice plasma (control, methyl-scopolamine, methyl-scopolamine & pilocarpine; see Animals section) and in the supernatant of BMVEC and bEnd.3 cells in control and pilocarpine treatment conditions. The following cytokines were quantified: interleukin 6 (IL-6), interleukin 1 beta (IL-1β), chemokine C-X-C motif ligand 1 (CXCL-1, or KC), monocyte chemoattractant protein-1 (MCP-1 or CCL2), macrophage inflammatory protein 1 alfa (MIP-1α), and tumor necrosis factor alfa (TNF-α) using MAGPIX technology (Mouse Magnetic Cytokines/Chemokines Panel - 5 Plex kit, Millipore).

5.3.10. Flow cytometry analysis of endothelial–leukocyte adhesion molecules

Flow cytometry analysis was performed on bEnd.3 cells for monitoring the following endothelial–leukocyte adhesion molecules: the endothelial expression of intercellular adhesion molecule-1 (ICAM-1), vascular cell adhesion molecule-1 (VCAM-1), and P-selectin (P-sel). We first evaluated the dose-response effect of pilocarpine (ranging from 1 to 15 μM) after 2 and 6 hrs of treatment, on the expression of adhesion molecules (*data not shown*). Then, bEnd.3 cells were stimulated with pilocarpine (15 μM) in DMEM with 1% FCS for 2 hrs and 6 hrs. As positive control, cells were treated with 25U/ml of TNF-α for 18 h in

DMEM with 1% FCS. bEnd.3 were rinsed with PBS and fixed with 4% PFA for 10 min. After washing with PBS, cells were incubated with blocking solution and labeled 40 min at 4°C with the following primary antibodies: anti-VCAM (50 µg/ml), anti-ICAM (10 µg/ml), and anti-P-sel (5 µg/ml). Cells were acquired by flow cytometry with MACSQuant Analyzer (Miltenyi Biotec). Data were analyzed using FlowJo software. The percentage of gated cells and the median channel of fluorescent intensity (MFI) was calculated.

5.3.11. Animals and in vivo pilocarpine treatment

Young Balb/c male mice (30–50 days of age, weight range: 18–24 g) from Harlan-Nossan (Udine, Italy) were adapted to the laboratory and maintained on a 12-h inverted light/dark cycle, at 23 ± 1°C, with access to food and water *ad libitum*. Mice were divided in six groups, n = 5 per group (**Figure 5.1**): Group 1 - saline intraperitoneal injection, Group 2 - methylscopolamine (MS, Sigma, 1 mg/kg i.p., Fabene et al., 2008) followed by blood collection after 2 hrs, Group 3 - MS i.p. followed by blood collection after 6 hrs, Group 4 - MS i.p. followed after 30 min by pilocarpine (P, 300 mg/kg i.p. diluted in 0.01 M PBS, pH 7.4) and blood collection 2 hrs after SE; Group 5 - MS i.p. followed after 30 min by pilocarpine i.p. and blood collection 6 hrs after SE; Group 6 - MS i.p. followed after 30 min by pilocarpine i.p. and blood collection 24 hrs after SE; Group 7 - MS i.p. followed after 30 min by pilocarpine i.p. and blood collection 24 hrs after SE. No group was treated only with pilocarpine due to the peripheral cholinergic effects in the absence of methylscopolamine (Clifford et al., 1987). Blood samples were collected retro-orbital and further processed for the cytokine level quantification.

Adult Wistar rats from Harlan-Nossan (Udine, Italy) were adapted to the laboratory and maintained on a 12-hrs inverted light/dark cycle, at 23 ± 1°C, with access to food and water *ad libitum*. Rats (n = 6) were anaesthetised with isoflurane and transverse hippocampal slices were prepared.

All procedures were carried out in accordance with European Community laws and policies and were approved by the University of Verona and by the University of Rome 'Sapienza' ethical committee, respectively.

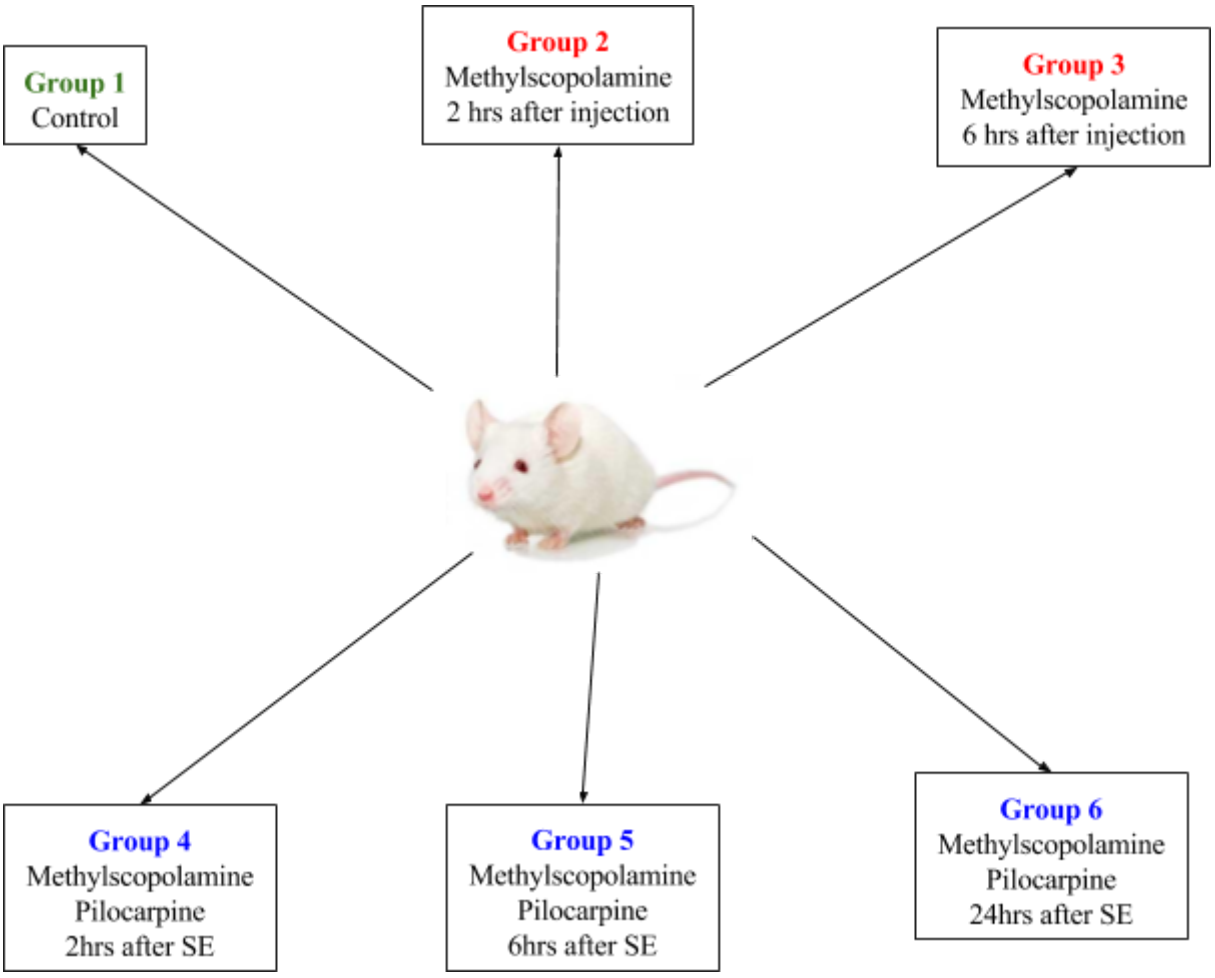

Figure 5.1. Description of the treatment in six mice groups.

5.3.12. Whole-cell recordings on hippocampal pyramidal neurons in rat slices

Rat transverse hippocampal slices (300 μm) were cut in glycerol-based artificial cerebrospinal fluid (ACSF) with a vibratome (Leica VT 1000S) immediately after surgical resection. Slices were placed in a slice incubation chamber at room temperature with oxygenated ACSF and transferred to a recording chamber within 1–2 h after slice preparation. ACSF had the following composition (in mM): NaCl 125; KCl 2.5; $CaCl_2$ 2; NaH_2PO_4 1.25; $MgCl_2$ 1; $NaHCO_3$ 26; glucose 10; Na-pyruvate 0.1; pH 7.35. Glycerol-based ACSF solution contained (in mM): glycerol 250; KCl 2.5; $CaCl_2$ 2.4; $MgCl_2$ 1.2; NaH_2PO_4 1.2; $NaHCO_3$ 26; glucose 11; Na-pyruvate 0.1; pH 7.35. Whole-cell patch clamp recordings were performed on pyramidal neurons at 21–23°C. Patch pipettes were filled with the following solution (in mM): K-gluconate 140; HEPES 10; 1,2-bis(2-aminophenoxy) ethane-N,N,N,N-tetraacetic acid (BAPTA) 5; $MgCl_2$ 2; Mg-ATP 2; pH 7.35. The effect of pilocarpine on the neuronal activity was measured both in voltage- and current-clamp configuration. Membrane currents were recorded in voltage-clamp by using glass electrodes (3–4 MΩ), at a -50 mV holding membrane potential, in order to distinguish between excitatory (inward) and inhibitory

(outward) synaptic activity. Under these experimental conditions cells were stable and healthy for 1–2 hrs. Spontaneous postsynaptic currents (sPSCs) were filtered at 1 kHz, digitized at 2 kHz, and analyzed with pClamp10 programs (Molecular Devices, Sunnyvale, CA). sPSCs were automatically identified by the software as trace deflections crossing area and amplitude thresholds, and then inspected by eye to avoid misclassification. Amplitude and frequency of spontaneous postsynaptic potentials (sPSPs) were recorded in current-clamp mode and analyzed as sPSCs.

5.3.13. Molecular docking

GOMoDo web-server (Sandal et al., 2013) was used to predict the 3D structures of mouse M_1 and M_3 acetylcholine receptors, using the hidden Markov model based-profiles (HMM-profiles) alignments. We use the structure of rat M_3 muscarinic receptor as template (PDB code: 4U15). The sequence alignments between targets and template were checked manually in order to enforce the conserved structural fingerprints of class A (rhodopsin-like) GPCRs (Venkatakrishnan et al., 2013). The models were evaluated on the basis of structural parameters as previously described (Sandal et al., 2013). The models obtained in the homology modeling step were used then to perform virtual docking experiments using the HADDOCK docking program (de Vries et al., 2010) through the GOMoDo web-server. We used the GPCRdb generic number position (Isberg et al., 2014), which generalized the classical Ballesteros-Weinstein numbering. Residues in positions 3.32, 3.33, 3.36, 3.37, 4.57, 5.39, 5.42, 6.48, 6.51, 7.39, 7.43 were considered as 'Active Residues' in order to guide the docking. These residues were already characterized as involved in agonist/antagonist binding (Lu and Hulme, 1999; Goodwin et al., 2007). The structures were downloaded from the ZINC database (Irwin et al., 2012) and the ligands were parametrized with ACPYPE (Sousa da Silva and Vranken, 2012) in terms of topology, including charge, and structural parameters. The charge of both agonist was cross checked using the MarvinSketch program (http://www.chemaxon.com) at pH 7.4. The docking protocol included three stages: (a) a rigid-body energy minimization, (b) a semi-flexible refinement in torsion angle space, and (c) a final refinement in explicit solvent. We chose 1000 structures for the first step and 200 structures for the second and third docking steps with default parameters. We selected the best structure for each docking as the one corresponding to the most populated cluster with the lowest energy value. Docking figures were generated with Chimera (Pettersen et al., 2004).

5.3.14. Data analysis

Quantitative RT-PCR data were obtained by normalizing *chrm1-chrm5, Tjn1, Cldn5* mRNA levels against those of *Gapdh* or *Actb*, using the 2(-Delta C(T)) method as previously described (Livak and Schmittgen, 2001). qRT-PCR results were expressed as $\log_{10}$-fold change, due to their extended scale distribution, and were plotted as mean ± SEM. Statistical

analysis for qRT-PCR data was done by one-way ANOVA followed by Fisher LSD *post hoc* tests. Data of intracellular calcium imaging were expressed as mean fluorescence ratio amplitude ± SEM, and statistical significance was assessed by unpaired t-test. One-way ANOVAs followed by Fisher LSD *post hoc* tests were used to assess BMVEC and bEnd.3 endothelial cell viability, comparing cells treated with different concentrations of pilocarpine to untreated controls. A two-tailed Student's t test was employed for statistical comparison of two flow cytometry samples and multiple comparisons were performed employing analysis of variance (ANOVA) with the Bonferroni correction of P. * $p<0.05$. Patch-clamp data were reported as means ± SEM and statistical significance was assessed by ANOVA tests. Statistical analysis and data plotting were done using OriginPro 8 (OriginLab Corporation, USA) and GraphPad Prism version 6.00 for Mac (GraphPad Software, La Jolla California USA).

5.4. Results

5.4.1. Pilocarpine stimulates the in vivo and vitro release of cytokines

In order to characterize the inflammatory effect induced by pilocarpine in the pilocarpine-based mouse model of epilepsy, we first quantified the cytokines serum levels (e.g. IL-6, KC, MCP-1, MIP-1α, IL-1β, and TNF-α) in 6 mice groups (**Figure 5.2**). The mice groups have been treated as follows: saline, methylscopolamine (MS; 2 hrs and 6 hrs), methylscopolamine followed by pilocarpine (P; 2 hrs and 6 hrs) and pilocarpine (24 hrs) (for details of the protocol see *5.3. Materials and Methods, 5.3.11. Animals*). The treatment scheme followed the protocol of pilocarpine-based mouse model for epilepsy which involves in a first step the treatment with methylscopolamine and afterwards the addition of pilocarpine. Methylscopolamine alone proves being able to induce significant increases in some of the analysed cytokines: IL-6 (6 hrs), MCP-1 (2 and 6 hrs), MIP-1 α (6 hrs) and IL-1β (2 and 6 hrs). For this reason, the comparison of data sets have been done with methylscopolamine treated groups as control instead of saline (the one-way ANOVA test was performed only for MS 2 hrs, MS 6 hrs, MS+P 2 hrs and MS+P 6 hrs data sets).

Among the analyzed cytokines, by far IL-6 is the most affected cytokine being ~100-fold up-regulated at 2 hrs and ~3-fold at 6 hrs, one-way ANOVA $F = 10.57$, $p = 4.46*10^{-4}$, (**Figure 5.2 A**). Similarly, KT is strongly upregulated at 2 hrs (~10-folds) and 6 hrs (~2.5-folds), one-way ANOVA $F = 12.48$, $p = 1.46*10^{-4}$, (**Figure 5.2 B**). MCP-1 is also up-regulated ~3-fold at 2 hrs and ~2-fold at 2 hrs, one-way ANOVA $F = 16.59$, $p = 2.68*10^{-5}$, (**Figure 5.2 C**). TNF-α is significantly up-regulated only at 6 hrs, one-way ANOVA $F = 2.67$, $p = 0.07$, *post hoc* Fisher test $p < 0.05$, but an increasing trend is observed also at 2 hrs (**Figure 5.2 D**). No significant changes was observed for other two cytokines (MIP-1 α and IL-1β) (**Figure 5.2 E, F**). An interesting observation shows that at 24 hrs the MS+P effect is vanished, no significant differences with respect to saline being revealed.

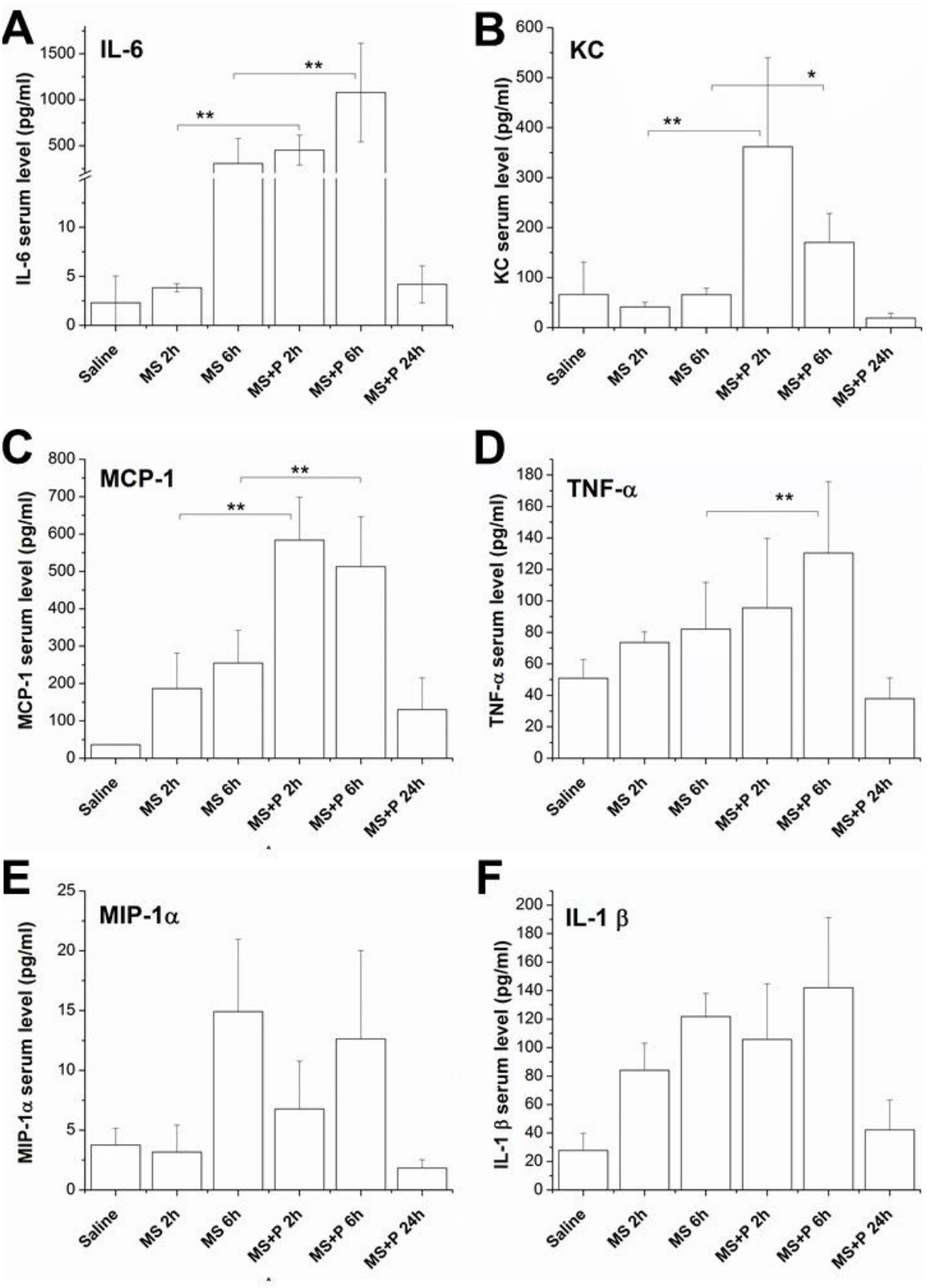

Figure 5.2. ***In vivo*** **cytokine release in mouse serum after status epilepticus.** The serum levels for IL-6 (**A**), KC (**B**), MCP-1 (C), TNF-α (D), MIP-1α (E), and IL-1β (F) (one-way ANOVA followed by *post hoc* Fisher test, *p<0.05,**p<0.01)

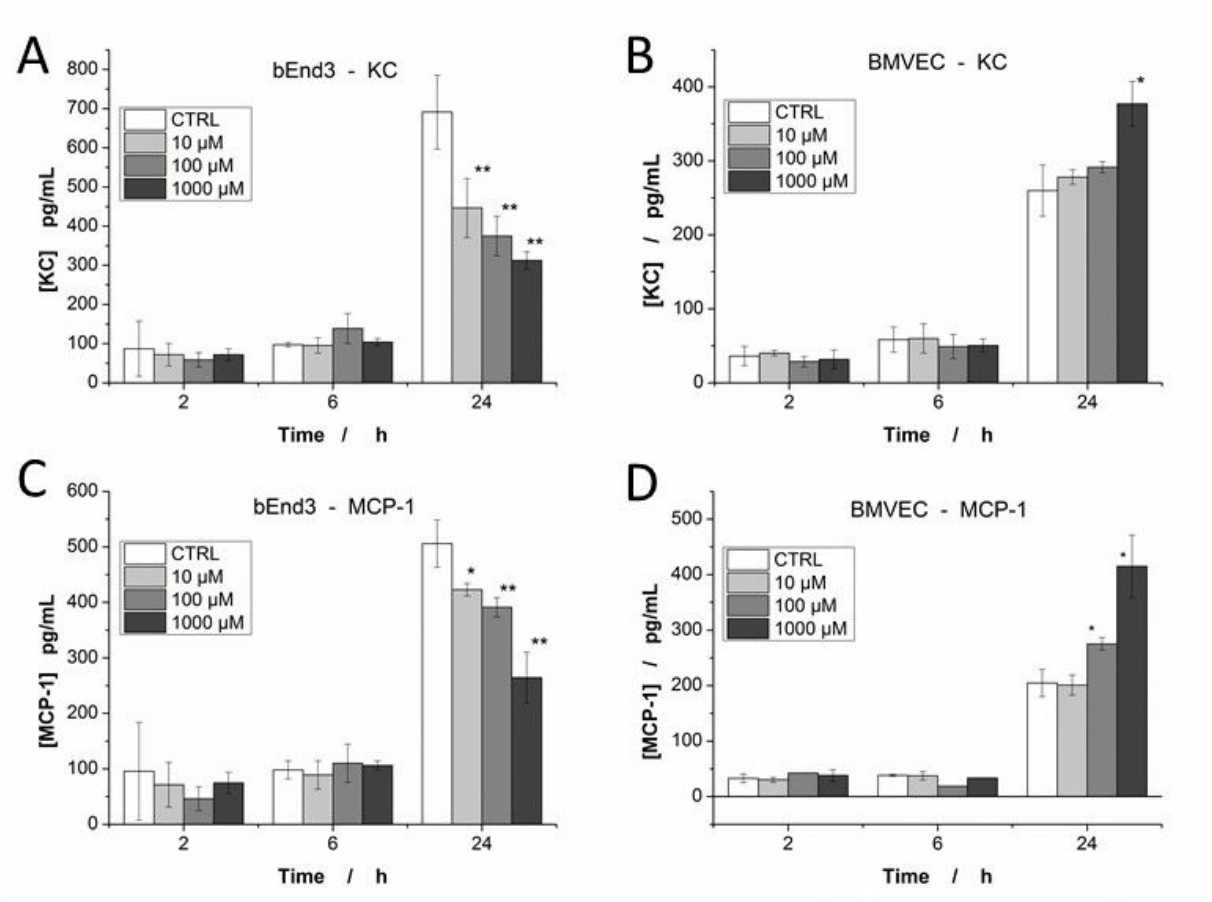

Figure 5.3. *In vitro* cytokines release by brain microvascular endothelial cells. The release of KC (A and B) and MCP-1 (C and D) by brain microvascular endothelial cells (bEnd3 and BMVEC) was evaluated upon pilocarpine treatment (10, 100, 1000 microM; 2, 6 and 24 hrs) by Luminex xMAP Technology. The statistical significance was analyzed by one-way ANOVA followed by *post-hoc* Fisher test (* $p < 0.05$, ** $p < 0.01$)

We also quantified the *in vitro* release of the same cytokines by brain microvascular endothelial cells exposed to pilocarpine (10, 100, 1000 µM) for 2, 6 or 24 hrs. Only KC and MCP-1 had detectable values for all the timepoints and doses of pilocarpine (**Figure 5.3. A-D**). It should be mentioned that in control conditions after 24 hrs, brain endothelial cells (BMVEC and bEnd.3) release in the culture medium KC and MCP-1 at levels significantly higher compared to 2 hrs or 6 hrs cell maintenance (unpaired *t*-test, $p < 0.0.1$). There is significant decrease of the KC production at 24 hrs, after exposure to 10 µM, 100 µM or 1000 µM compared to control (one way ANOVA, $F = 18.73$, $p < 5.63*10^{-4}$), in bEnd.3 (**Figure 5.3 A**). Similarly, there is a significant decrease of the MCP-1 production at 24 hrs, after exposure to 10 µM, 100 µM and 1000 µM compared to control (one way ANOVA. $F = 27.82$, $p = 1.39*10^{-4}$), in bEnd.3 (**Figure 5.3 C**). Oppositely, there is an increase at 24 hrs, after exposure to 10 µM, 100 µM or 1000 µM compared to control (one way ANOVA: $F=28.43$, $p=1.28*10^{-4}$), in BMVEC (**Figure 5.3 D**). Only a slight enhancement of KC in BMVEC at 1000 µM was observed (one way ANOVA: $F = 11.64$, $p = 0.01$). IL-6, IL-1β, TNF-α, did not had detectable values (*data not shown*).

5.4.2. Pilocarpine upregulates the expression of adhesion molecules in brain microvascular endothelial cells

We also tested the *in vitro* effect of pilocarpine on the expression of adhesion molecules on the brain endothelial cell line bEnd.3. Considering the already known ability of TNF-α to up-regulate adhesion molecules expression (Kirchhofer et al., 1994), it was used as positive control. **Figure 5.4 up** shows the flow-cytometry quantification of adhesion molecule expression of bEnd.3 cells stimulated with pilocarpine represented as fold increase compared to basal condition of mean fluorescence intensity (MFI) and % of positive cells among whole cell population (% of gated cells).

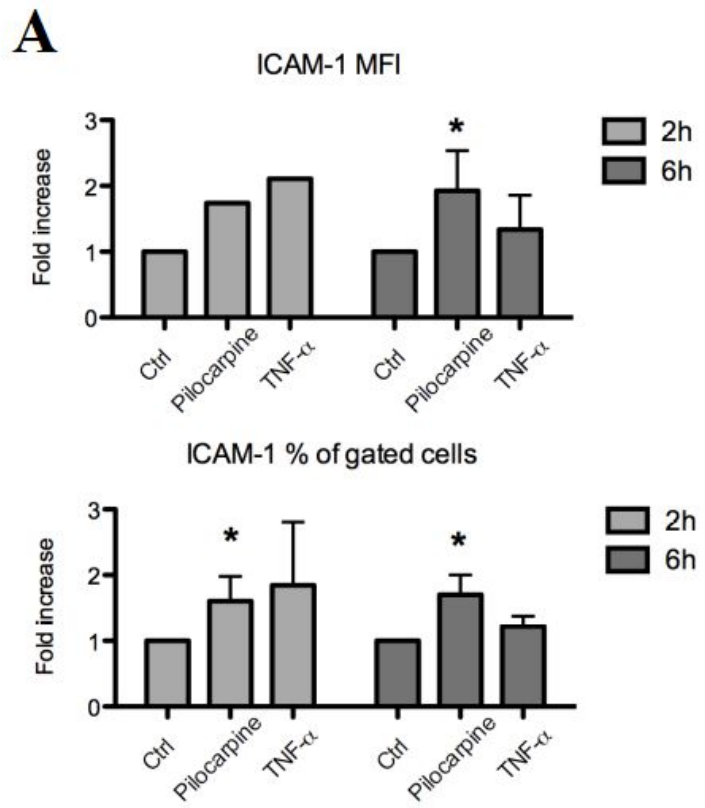

Our data show that the MFI expression of P-selectin was slightly increased on pilocarpine-stimulated cells when compared to unstimulated ones, moreover the percentage of cells expressing P-selectin was significantly increased at 2 hrs and 6 hrs after pilocarpine treatment (**Figure 5.4 A**). We observed no statistically significant differences in % of positive cells for E-selectin after pilocarpine treatment, however MFI expression trend to increase after 6 hrs.

Interestingly, we observed a significant increase of bEnd.3 cells expressing the integrin-ligands ICAM-1 and VCAM-1 after 2 hrs of pilocarpine treatment and the effect was maintained at 6 hrs (**Figure 5.4 B. C**), although the MFI did not reach statistical significance after 2 hrs treatment.

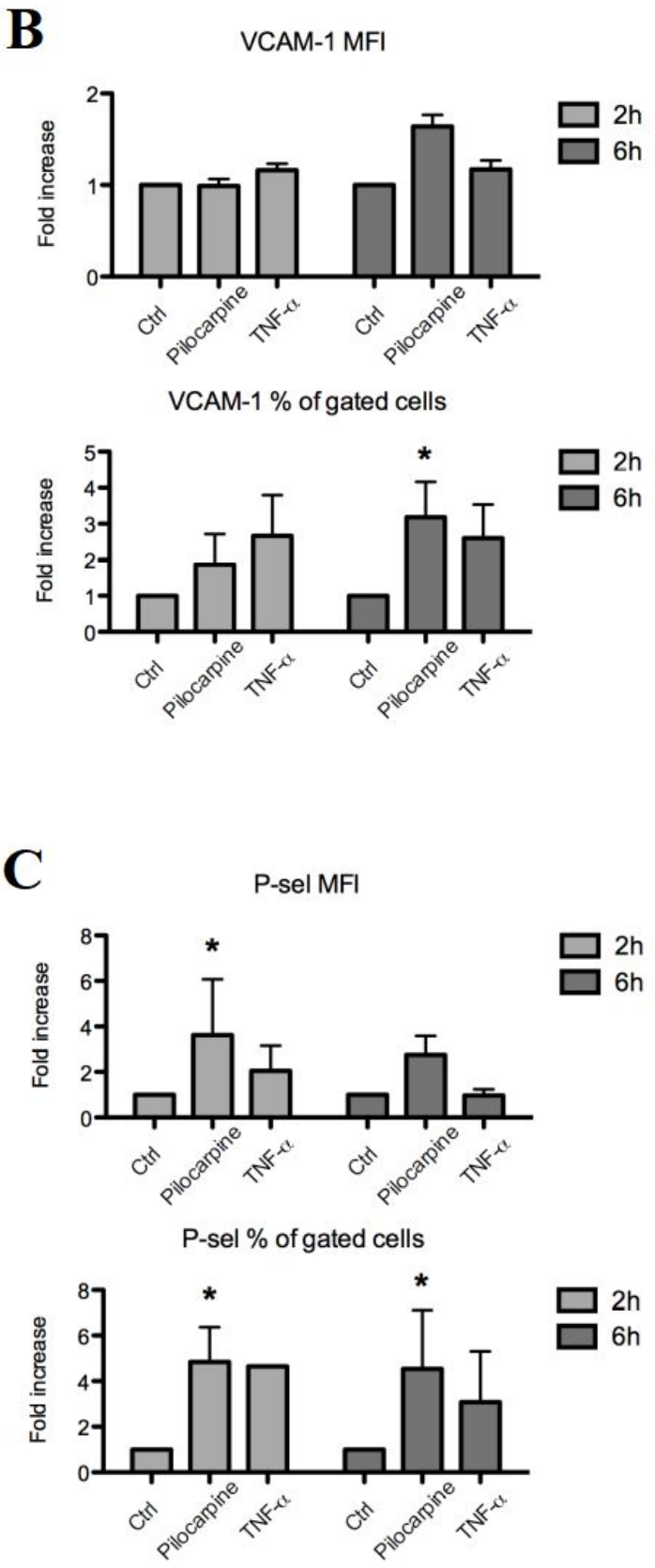
B
VCAM-1 MFI
Fold increase
2h
6h
Ctrl
Pilocarpine
TNF-α
VCAM-1 % of gated cells
*
C
P-sel MFI
P-sel % of gated cells

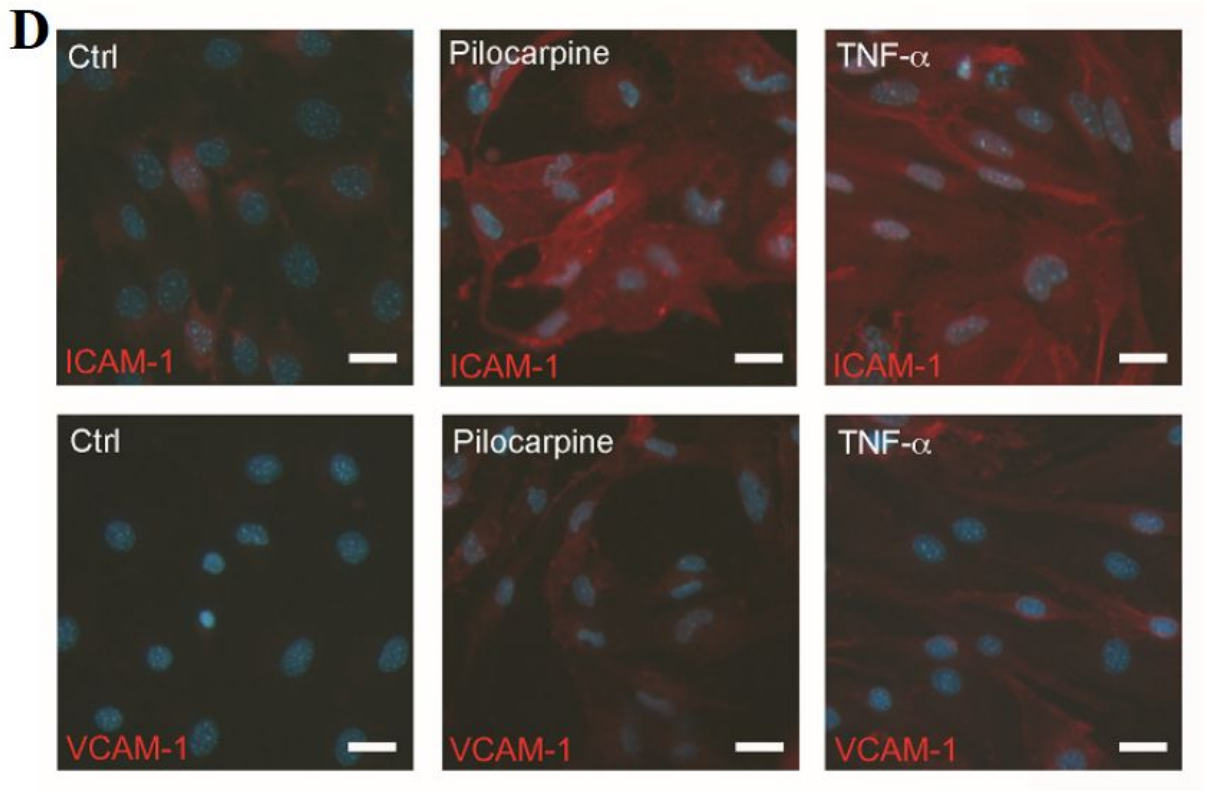

Figure 5.4. Expression of adhesion molecules in brain endothelial bEnd.3 cells upon pilocarpine treatment. Expression of adhesion molecules ICAM-1 (**A**), VCAM-1 (**B**), and P-selectin (**C**) in unstimulated cells and upon 2hrs and 6hrs of cell stimulation with pilocarpine (15 µM) and TNF-alfa, by flow-cytometry; (**D**) Expression of adhesion molecules ICAM-1 and VCAM-1 in control unstimulated conditions and upon stimulation with pilocarpine (15 µM; 18 hrs) and TNF-alfa, by fluorescence microscopy.

By immunofluorescence staining, we evidenced that after 18 hrs treatment with 15 µM pilocarpine, there is a significant up-regulation of VCAM-1 and ICAM-1 compared to unstimulated control cells. ICAM-1 was constitutively expressed at low levels on bEnd.3 cells, however 18 hrs treatment with pilocarpine led to a significant increase of ICAM-1 expression (**Figure 5.4 D**). VCAM-1 was not expressed at basal condition on bEnd.3 cells and pilocarpine treatment highly up-regulated its expression (**Figure 5.4 D**).

5.4.3. Pilocarpine elicits calcium transients in brain microvascular endothelial cells but is not inducing neuronal epileptic-like discharges

The application of pilocarpine (10 min, 10 µM; Nagao et al., 1996) on whole-cell voltage-clamped CA3 hippocampal pyramidal neurons in slices produced a significant enhancement of the mean frequency of spontaneous excitatory postsynaptic currents (sEPSCs), from 0.4 ± 0.2 Hz to 0.9 ± 0.2 Hz (n = 5; $p < 0.05$; **Figure 5.5**). Pilocarpine at a higher concentration, similar to the level found in cerebrospinal fluid of pilocarpine-treated rats (200 µM; Marchi et al., 2007), induced in the same type of neurons a comparable increase of the sPSECs mean frequency, from 0.4 ± 0.1 Hz to 0.7 ± 0.1 Hz (n = 7; $p < 0.05$; **Figure**

5.5). Similarly, the frequency of spontaneous inhibitory postsynaptic currents (sIPSCs) was significantly increased by pilocarpine at both concentration, 10 µM and 200 µM, from 0.18 ± 0.09 Hz to 0.3 ± 0.1 Hz (n = 5; $p < 0.05$, **Figure 5.5**) and from 0.16 ± 0.05 Hz to 0.4 ± 0.1 Hz (n = 8, $p < 0.05$; **Figure 5.5**), respectively. The amplitude of both excitatory and inhibitory spontaneous synaptic events was not significantly affected by pilocarpine (*not shown*). Furthermore, when current-clamped, hippocampal pyramidal neurons exhibited a similar increase of the frequency of spontaneous excitatory postsynaptic potentials (sEPSPs). In these cells the pilocarpine application did not elicit any paroxystical depolarization or other epileptiform activity (n = 10).

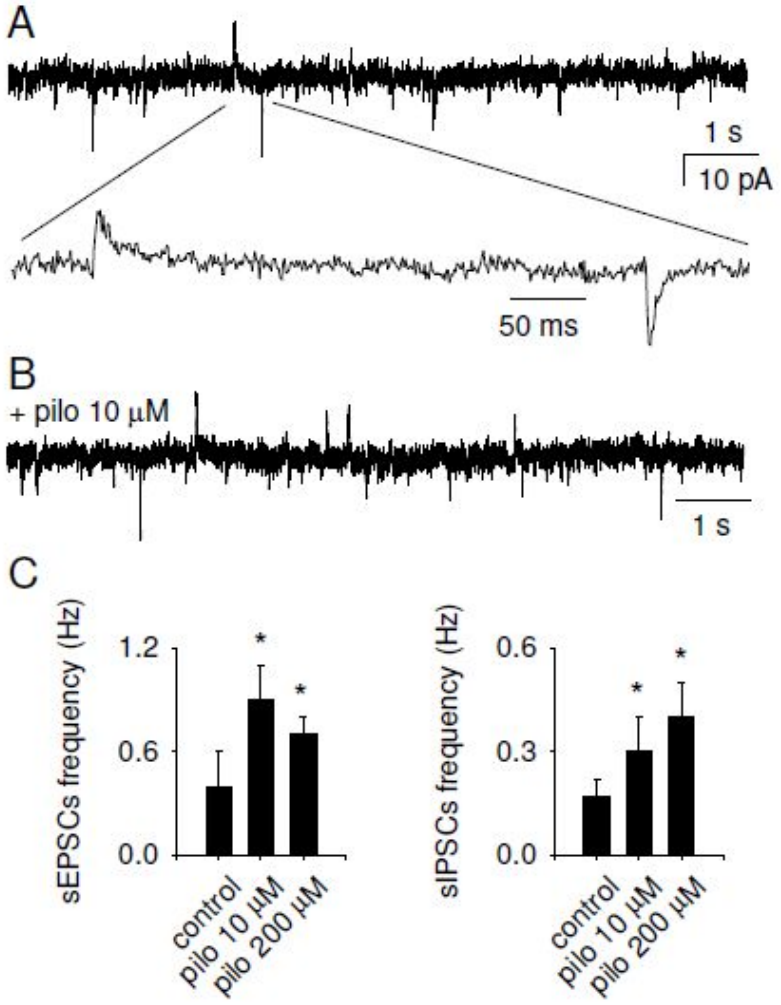

Figure 5.5. Pilocarpine is not producing any epileptic-like discharge in rat hippocampal slices. Pilocarpine modulates the frequency of both excitatory and inhibitory spontaneous synaptic activity. **A.** top, typical trace recorded from a CA3 hippocampal pyramidal neuron in whole-cell voltage-clamp configuration at -50 mV. Note that inward and outward currents represent excitatory and inhibitory events, respectively. Bottom, enlarged trace of the top trace, showing the kinetics of individual events. **B.** trace recorded from the same neuron as A, in the presence of pilocarpine 10 µM. Note the frequency increase of both excitatory and inhibitory events. Mean amplitudes were not affected. **C.** Histograms representing the effect of pilocarpine at 10 µM and 200 µM on the mean frequencies of sEPSCs (left) and of sIPSCs (right). *, significantly different from control, $p<0.05$.

Brief exposure (2 min) of BMVEC and bEnd.3 cells to pilocarpine (10, 100, and 1000 µM; **Figure 5.6**) elicited three types of responses: (type 1) peak-like calcium transients; (type 2) continuous plateau-like calcium increases; (type 3) no response. The maximal amplitude (ΔR) for the type 1 response was obtained at 10 µM pilocarpine (**Figure 5.6 A, B**), where the response amplitude is almost double for BMVEC compared to bEnd.3 cells, representative traces being presented in **Figure 5.6B**, and **Figure 5.6A**, respectively.

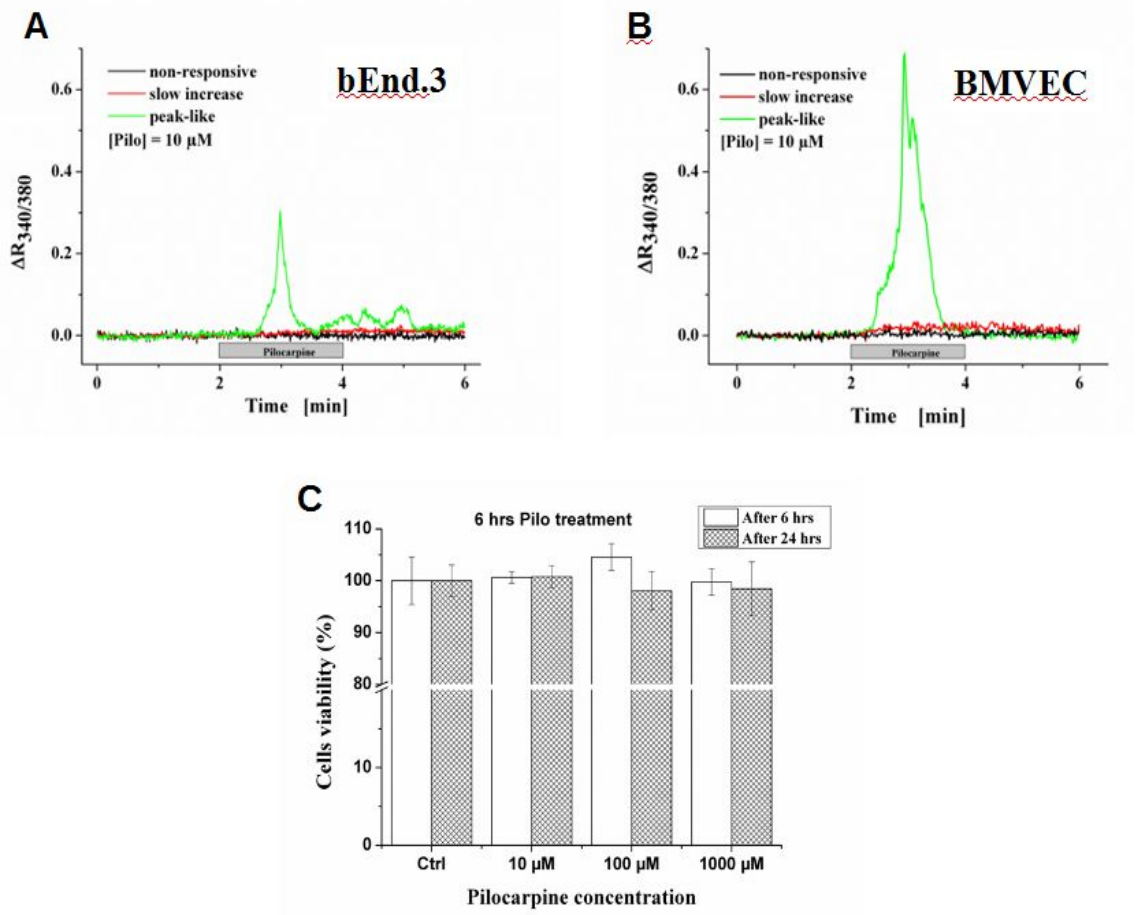

Figure 5.6. Pilocarpine elicits calcium transients in a certain percentage of the brain endothelial cells, without significant changes in cell viability. (A) Pilocarpine elicits three types of responses in bEnd.3 cells (**A**) and BMVEC (**B**), (**C**) bEnd.3 endothelial cells were exposed to pilocarpine (100 µM) for 6 hrs, then recovered for 6 hrs (white bars) or 24 hrs (hatched bars), followed by Trypan blue viability test.

The percentage of type 1 responsive cells is presented in **Table 5.1**, where it is evident that at 10 µM pilocarpine the percentage of responsive BMVEC (13%) is triple compared to the percentage of responsive bEnd.3 cells (4%), the primary microvascular endothelial cells being more sensitive to the exposure of pilocarpine at this dose. However, at 100 µM pilocarpine, the percentage of type 1 responsive cells becomes almost equal for BMVEC and bEnd.3, and at 1000 µM pilocarpine, none of these cells presents the type 1 response. Further, we questioned if the dose-dependent decrease in the maximal amplitude of the type 1 response and the 'absence' of type 1 response at higher concentration could not be the consequence of altered cell viability. We performed the Trypan blue viability test in bEnd.3 cells (**Figure 5.6 C**), and no significant changes were obtained after 6 hrs exposure to

pilocarpine (100 µM). Therefore, we might suppose that brief exposures (<5min) to pilocarpine would not determine any change in cell viability.

Table 5.1. Percentages of type 1 responsive cells at different pilocarpine concentrations

[Pilo] / µM	**10**	**100**	**1000**
Percentage of peak-responding bEnd.3 cells	**4 %** (2/55)	**17 %** (28/164)	0 % (0/71)
Percentage of peak-responding BMVECs	**13 %** (24/183)	**19 %** (11/56)	0 % (0/36)

In the pilocarpine-induced epilepsy model, it should be considered the presence of pilocarpine in the animal's bloodstream, in particular in brain capillaries, and the exposure of of brain endothelium lining to pilocarpine. It is interesting to understanding how brain endothelial cells respond to the repeated exposure to pilocarpine. Therefore, we have tested the effect of a double-pulse pilocarpine application (**Figure 5.7 A**) on the calcium transients in brain microvascular endothelial cells, with a 5 min interval of recovery between drug applications. We obtained several patterns of response that consist in combinations of (i) peak-like response and (ii) very little linear increase of calcium during pilocarpine application. Two of these patterns are presented as examples in **Figure 5.7B** and **Figure 5.7C**.

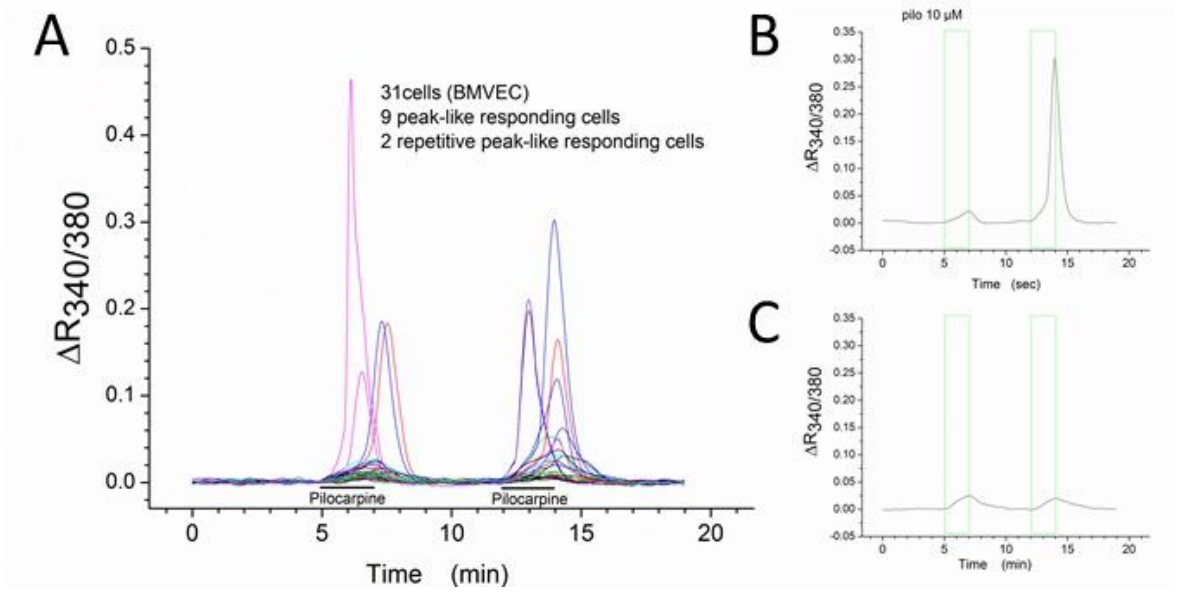

Figure 5.7. Double-pulse pilocarpine application on brain endothelial cells (BMVEC). (A) Pilocarpine elicits three patterns of calcium transients when a double-pulse of drug is applied (2 min application, 5 min Ringer perfusion between pulses). Two examples of individual patterns are presented: (**B**) no peak-like in the first application followed by peak like response, in the second application, and (**C**) no peak-like response in both of pilocarpine applications.

5.4.4. Pilocarpine downregulates the expression of tight junction proteins and permeabilizes the monolayers of brain microvascular endothelial cells

Therefore, we used a simple model of BBB and we have exposed a monolayer of brain microvascular endothelial cells to pilocarpine (100 μM) for 24 hrs and we have measured the monolayer permeability to Dextran 70 kDa by spectrofluorimetric measurements. In control conditions. diffusive permeability was calculated to be 3.04 ± 0.54 x 10^{-6} cm/s (n = 5) for the b.End3 cell monolayer and 2.69 ± 0.98 x 10^{-6} cm/s (n = 5) for the BMVEC cell monolayer (**Figure 5.8**). Upon 24 hrs treatment with pilocarpine (100 μM), the diffusive permeability significantly increases for both types of endothelial cells to 5.55 ± 0.58 x 10^{-6} cm/s (n = 5; $p < 0.01$, unpaired *t* test), and respectively to 6.98 ± 1.12 x 10^{-6} cm/s (n = 5; $p < 0.01$, unpaired *t* test).

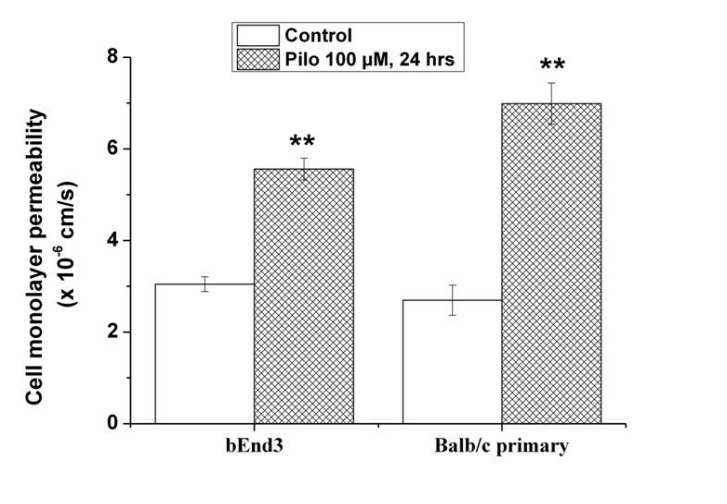

Figure 5.8. Permeability of *in vitro* BBB model to the Dextran 70kDa is increased by pilocarpine treatment (100 μM, 24 hrs).

The immunofluorescence analysis of the ZO-1 and claudin 5 expression in BMVEC, in control conditions and upon exposure to pilocarpine (100 μM) for 2 hrs, 6 hrs and 24 hrs, revealed similar results (**Figure 5.9**). In control conditions, the tight junctions are well delineated, but starting from 2 hrs up to 24 hrs, their expression progressively diminished in the plasma membrane while the protein becomes internalised in the cytoplasm (**Figure 5.9A**). The mean fluorescence intensity was quantified as total pixel green levels in the microscopy images (**Figure 5.9B**), but it is difficult to further interpret these data in the absence of colocalization with fluorescent markers specific for different cellular compartments. To detail, due to the delocalization of the tight junction proteins from the plasma membrane to the cytoplasm, there is difficult to analyze the protein content from the immunofluorescence images (**Figure 5.9A**) only by the total mean fluorescence intensity values (**Figure 5.9B**).

The immunofluorescence analysis of the ZO-1 and claudin 5 expression in bEnd.3 cells (**Figure 5.10A, Figure 5.10B**), in control conditions and upon exposure to pilocarpine (100 μM) for 2 hrs, 6 hrs and 24 hrs, indicated the significant upregulation of ZO-1 after 24 hrs exposure to pilocarpine (one-way ANOVA, F=16.87, p=2.26*10^{-8}, Fisher *post-hoc* test), while the significant downregulation of claudin 5 after 2 hrs and 6 hrs exposure to pilocarpine (one-way ANOVA, F=11.13, p=5.31*10^{-4}, Fisher *post-hoc* test).

We also quantified the mRNA levels for genes encoding tight junctions proteins (e.g. *Tjp1* and *Cldn5*) in control conditions and upon exposure of brain microvascular endothelial cells to pilocarpine (100 μM) for 2 hrs, 6 hrs and 24 hrs (**Figure 5.9C**, and **Figure 5.10C**). In BMVEC, the mRNA for *Tjp1* is significantly downregulated after 6 hrs of exposure to pilocarpine (F=9.04, p=0.004, Fisher *post-hoc* test, with respect to 2 hrs and 24 hrs conditions; **Figure 5.9C**). Oppositely, in bEnd.3 cells, the mRNA for *Tjp1* is significantly upregulated after 6 hrs of exposure to pilocarpine (**Figure 5.10C**). The mRNA for *Cldn5* is significantly downregulated for both endothelial cells tested after 2hrs and 6 hrs exposure to pilocarpine, but the downregulation is more accentuated after 2 hrs in BMVEC (**Figure 5.9C**), while the downregulation is higher after 6 hrs in bEnd.3 cells (**Figure 5.10C**).

It is difficult to make a direct correlation between the permeabilization results obtained on monolayers of endothelial cells (**Figure 5.8**) and the tight junction proteins regulation (**Figure 5.9**, and **5.10**) due to methodological limitations.

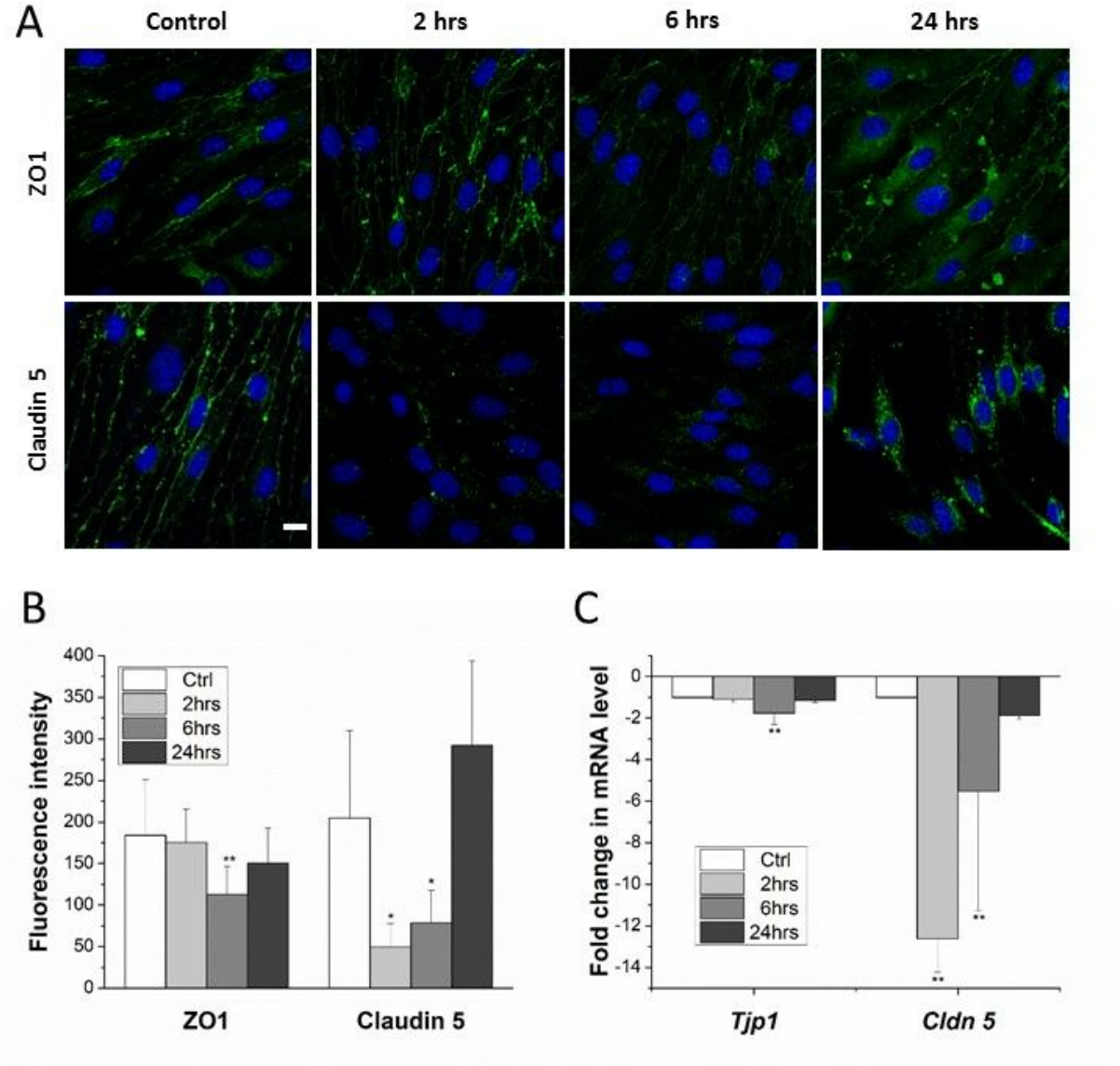

Figure 5.9. **Pilocarpine downregulates tight junctions proteins (ZO-1 and claudin 5) in brain microvascular cells (BMVEC)**. (**A**) Expression of tight junction proteins in control and upon exposure to pilocarpine (100 µM) at 2 hrs, 6 hrs, and 24 hrs by immunofluorescence microscopy; green (Alexa 488), blue (TO-PRO®-3), Scale bar 10 µm. (**B**) Fluorescence intensity expressed pixel grey level. Statistical analysis was done for the ZO-1 expression (one-way ANOVA, F=8.12, p=8.95*10^{-5}, Fisher *post-hoc* test, ** $p < 0.01$), and claudin-5 expression (F=7.96, p=0.0035, Fisher *post-hoc* test, ** $p < 0.01$, * $p < 0.05$). (**C**) Fold change in mRNA level by qRT-PCR. One-way ANOVA test was used, excluding the control, to analyze the statistical significance of *Tjp1* gene expression (F=9.04, p=0.004, Fisher *post-hoc* test, ** $p < 0.01$ with respect to 2 hrs and 24 hrs conditions), and of *Cldn5* expression (F=12.67, p=0.0014, Fisher *post-hoc* test, ** $p < 0.01$ with respect to 24 hrs condition).

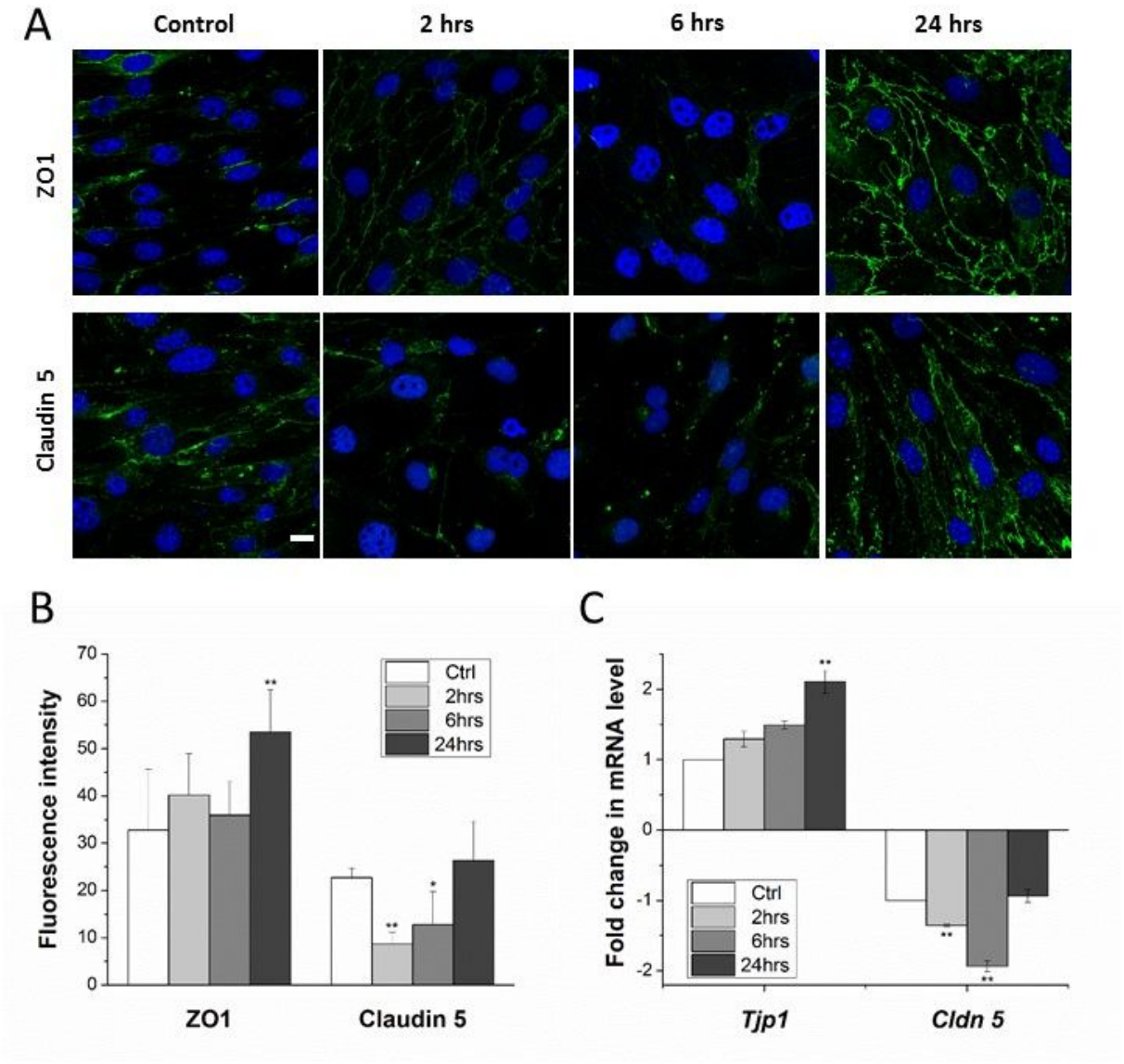

Figure 5.10. **Pilocarpine downregulates tight junctions proteins (ZO-1 and claudin 5) in brain microvascular cells (bEnd3)**. (**A**) Expression of tight junction proteins in control and upon exposure to pilocarpine (100 µM) at 2 hrs, 6 hrs, and 24 hrs by immunofluorescence microscopy; green (Alexa 488), blue (TO-PRO®-3). Scale bar 10 µm. (**B**) Fluorescence intensity expressed pixel grey level. Statistical analysis was done for the ZO-1 expression (one-way ANOVA, F=16.87, $p=2.26*10^{-8}$, Fisher *post-hoc* test, ** $p < 0.01$), and claudin-5 expression (one-way ANOVA, F=11.13, $p=5.31*10^{-4}$, Fisher *post-hoc* test, ** $p < 0.01$, * $p < 0.05$). (**C**) Fold change in mRNA level by qRT-PCR. One-way ANOVA test was used, excluding the control, to analyze the statistical significance of *Tjp1* gene expression (one-way ANOVA, F=40.27, $p=3.33*10^{-4}$, Fisher *post-hoc* test, ** $p < 0.01$ with respect to 2 hrs and 6 hrs conditions), and of *Cldn 5* expression (one-way ANOVA, F=62.21, $p=9.74*10^{-5}$, Fisher *post-hoc* test, ** $p < 0.01$ with respect to 24 hrs condition).

5.4.5. Pilocarpine competes with acetylcholine on the same binding site of the muscarinic receptors and regulates their expression

We evidenced that 10 µM pilocarpine is enough to diminish ~50% of the maximal fluorescence amplitude of the ACh-induced calcium transients, in both endothelial cell preparations (bEnd.3, **Figure 5.11A, B**; and BMVEC, **Figure 5.11C, D**). Moreover, 100 µM pilocarpine almost abolished the ACh-induced calcium transients in bEnd.3 cells, and diminished ~75% of the ACh-induced calcium transients in BMVEC.

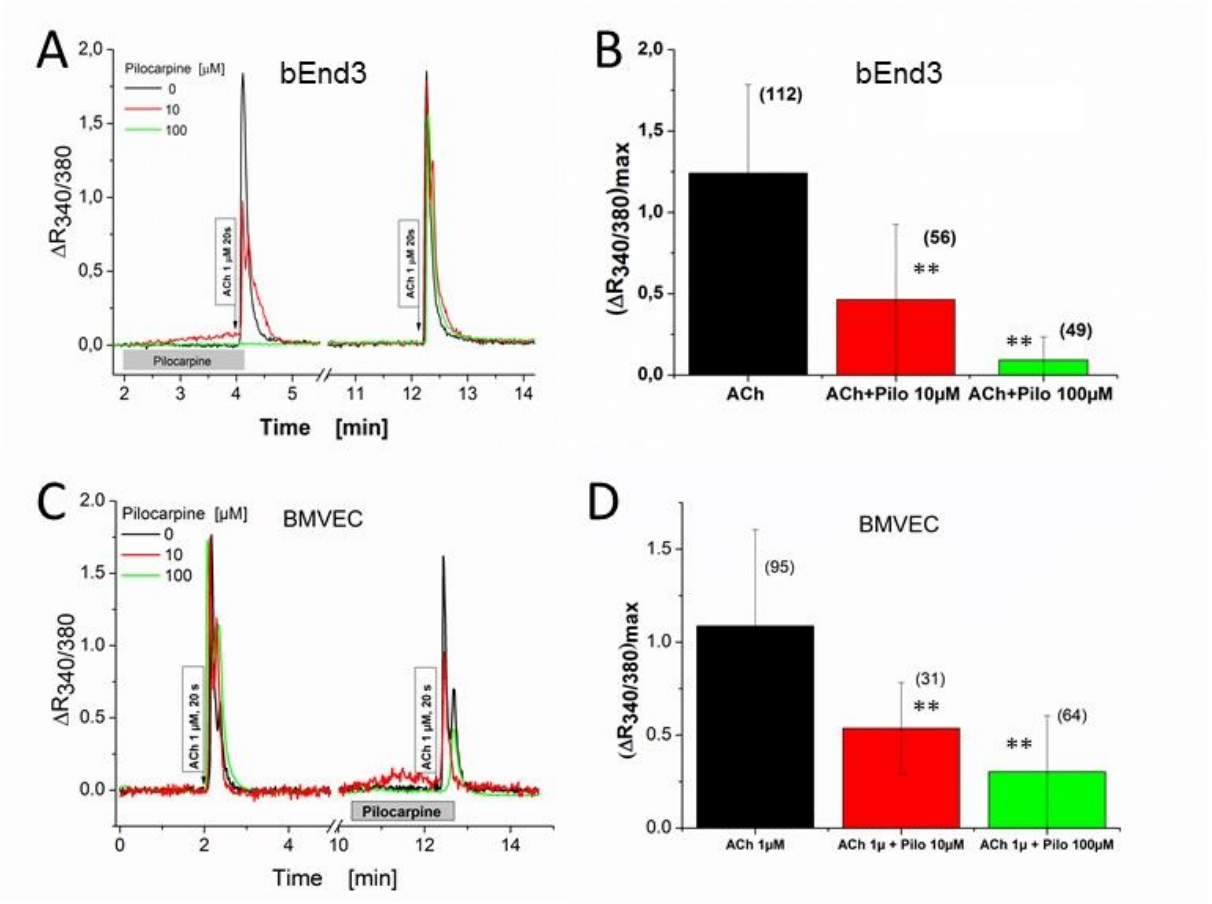

Figure 5.11. Pilocarpine competes with acetylcholine on the binding site of the muscarinic receptors. Pilocarpine (10, 100 µM) significantly diminishes the acetylcholine (1 µM)-induced cytosolic calcium transients in brain microvascular endothelial cells, bEnd.3 (**A, B**) and BMVEC (**C, D**).

As we previously demonstrated that all five muscarinic receptors are expressed in brain microvascular endothelial cells (Radu et al., 2017a), the next step in our study was to analyze if pilocarpine distinctly regulates the expression of these receptors in endothelial cells. We evidenced the mRNA downregulation for *Chrm1* and *Chrm3*, and the upregulation of *Chrm2*, *Chrm4* and *Chrm5* in BMVEC (**Figure 5.12 A**). In bEnd.3 cells was observed the downregulation of *Chrm3* and upregulation of *Chrm2* (**Figure 5.12 B**).

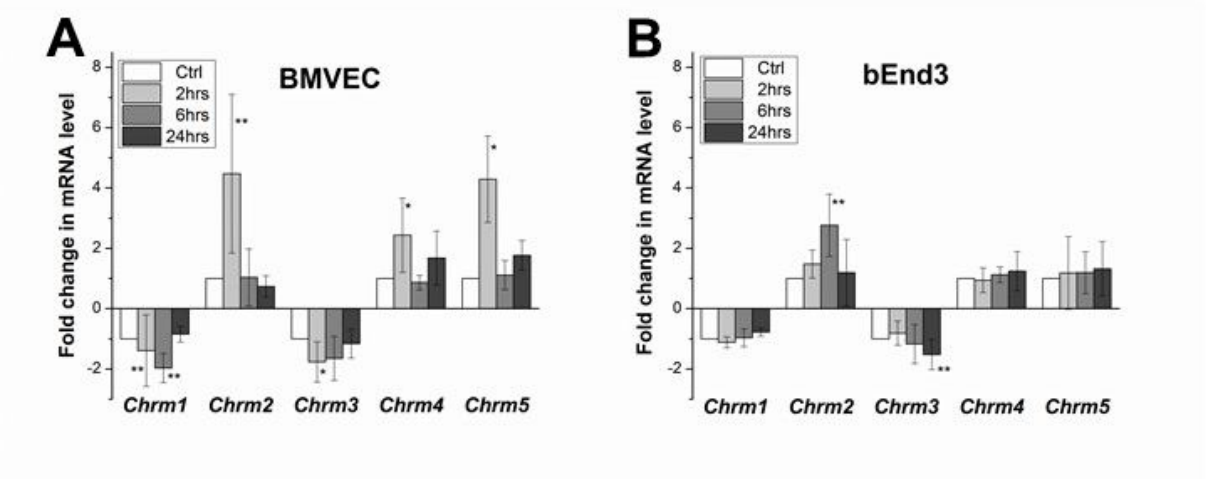

Figure 5.12. Pilocarpine regulates the levels of mRNA encoding muscarinic receptors in brain microvascular endothelial cells. qRT-PCR measurements evidenced that pilocarpine downregulates the mRNA level for M_1 and M_3 receptors, while it upregulates the mRNA level for M_2, M_4 and M_5 receptors in BMVEC (**A**) and bEnd.3 cells (**B**). The mRNA encoding *Chrm1-Chrm5* have been first normalized to the mRNA encoding *Gapdh*, followed by the normalized to the control (cells unstimulated with pilocarpine). Statistical analysis was done using one-way ANOVA (excluding the control), followed by *post-hoc* Fisher test for each receptor subtype in order to evidence the effect of pilocarpine at different timepoints of exposure with respect to 24 hrs, $**p < 0.01$, $*p < 0.05$.

We have also analyzed the changes in protein expression of the muscarinic receptors (M_1-M_5) upon exposure to pilocarpine (2 hrs, 6 hrs and 24 hrs) by immunofluorescence (**Figure 5.13**, **Figure 5.14**) As we previously demonstrated, in control conditions, the M_1 receptor is localized in the plasma membrane, and also nuclear and perinuclear, while the other receptors M_2-M_5 are mostly expressed in the plasma membrane and/or cytoplasm (Radu et al., 2017a). Upon exposure to pilocarpine, M_1 and M_3 are downregulated after 2 hrs and 6 hrs, and recovers after 24 hrs at control levels in BMVEC and in bEnd.3 cells.

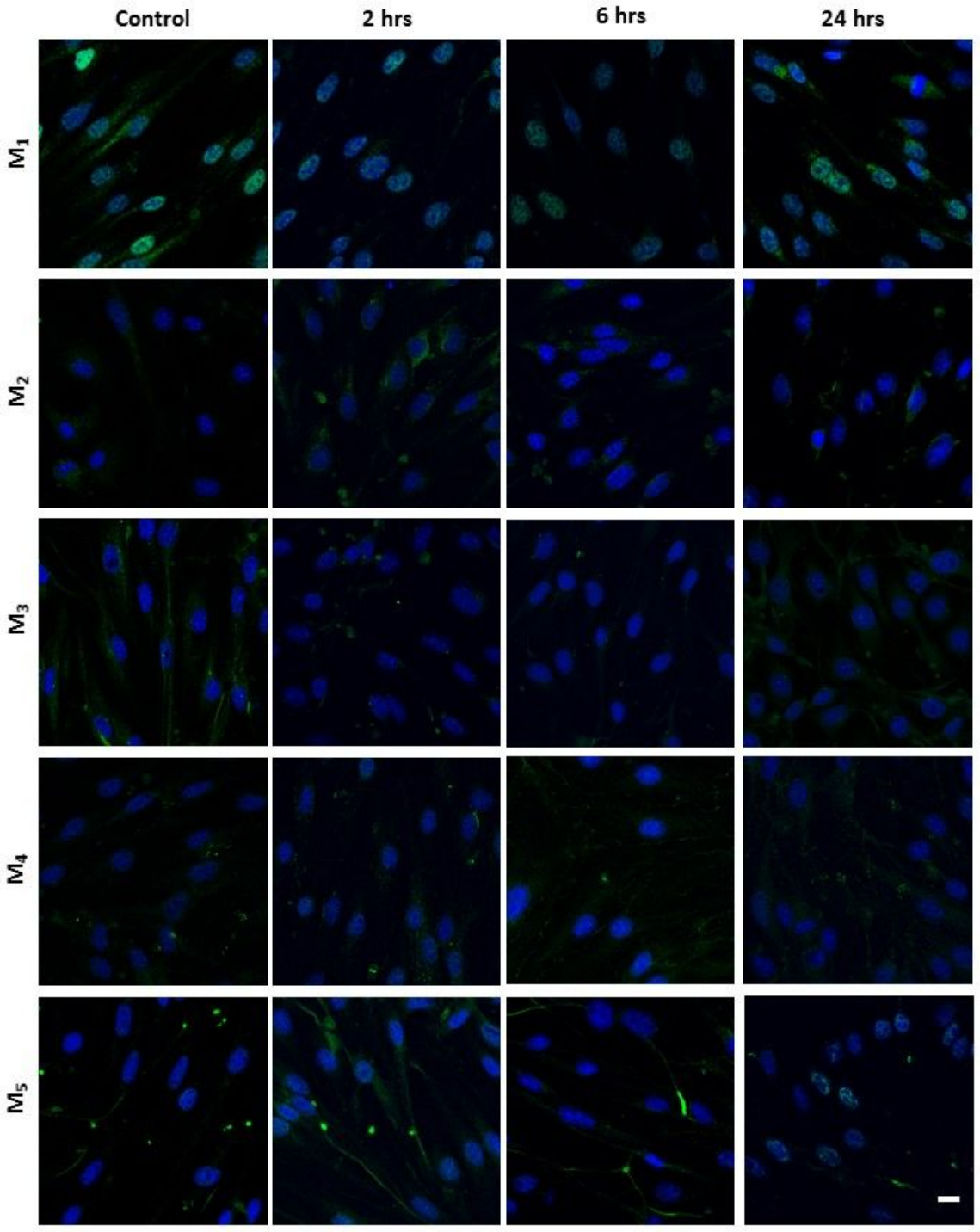

Figure 5.13. Pilocarpine regulates the muscarinic receptor expression in brain microvascular endothelial cells (BMVEC). Immunofluorescence images in control conditions and upon 2hrs, 6 hrs and 24 hrs exposure to pilocarpine evidence the downregulation of M_1 and M_3 receptors, and upregulation of M_2, M_4 and M_5 receptors in BMVEC; (green) Alexa488, (blue) TO-PRO®-3, scale bar 10 μm.

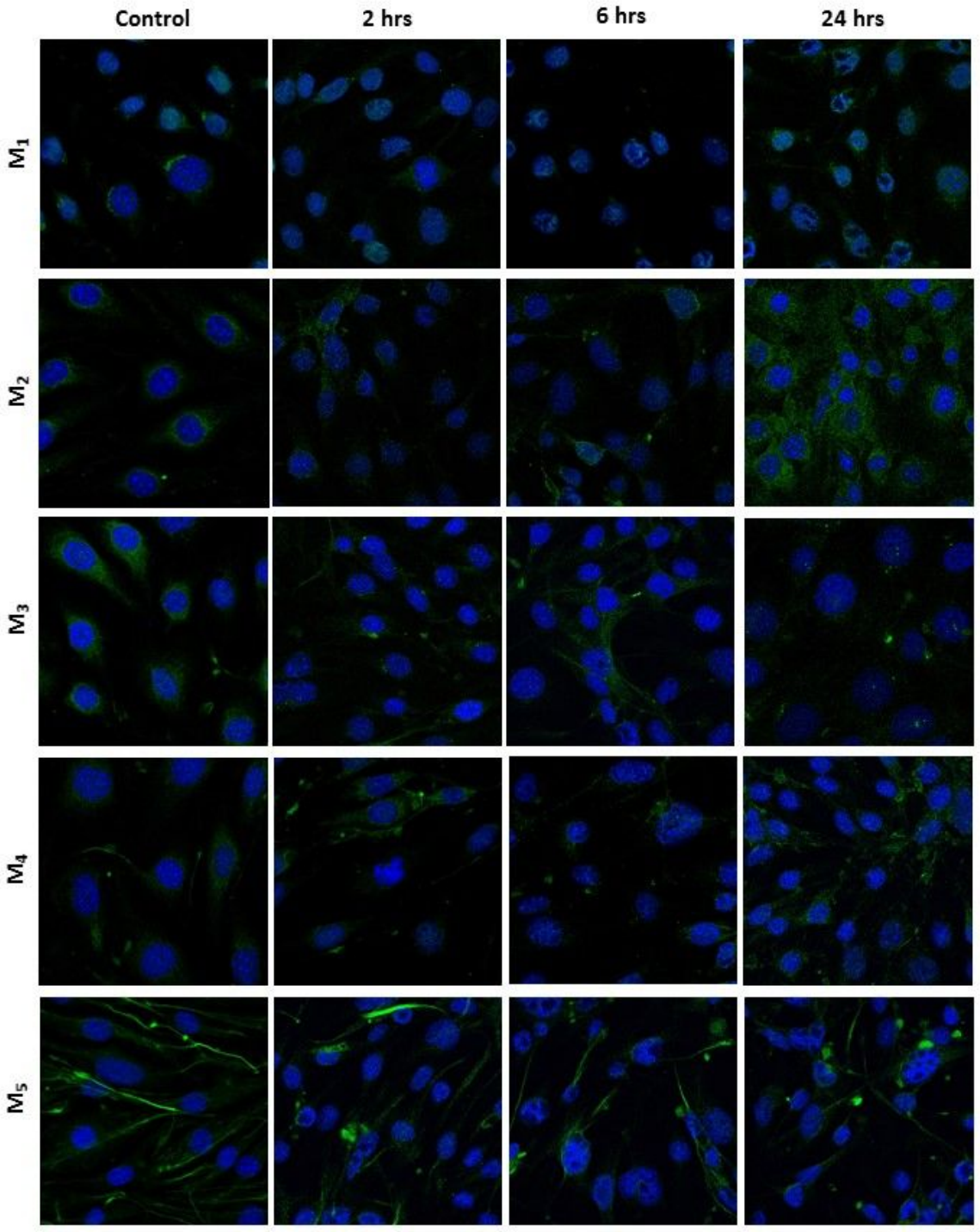

Figure 5.13. Pilocarpine regulates the muscarinic receptor expression in brain microvascular endothelial cells (bEnd.3). Immunofluorescence images in control conditions and upon 2hrs, 6 hrs and 24 hrs exposure to pilocarpine for the M_1, M_2, M_3, M_4 and M_5 receptors in bEnd.3 cells. (green) Alexa488, (blue) TO-PRO®-3, scale bar 10 μm.

As mentioned in the previous paragraph, pilocarpine competes with acetylcholine on the same binding site of M_1-M_5 muscarinic receptors. The binding site of acetylcholine was

demonstrated to be the orthosteric cavity (Karen J Gregory et al., 2007). We thus used this information to drive the docking of both molecules (pilocarpine and acetylcholine) inside the orthosteric binding cavity. We docked the two molecules only with M_1 and M_3 muscarinic receptors since, i) the latter are the most abundant among the five muscarinic receptors in microvascular endothelial cells (Radu et al., 2017a), and ii) pilocarpine was shown to exhibit higher selectivity values for the M_1 and M_3 subtypes (Figueroa et al., 2009). As shown in **Figure 5.14**, both the molecules interact in the same cavity of M_1 and M_3 receptors, but interacting with slightly different aminoacids. While acetylcholine's quaternary amino group (indicated with (+1) in Figure 5.14, panel C and D), interacts with D3.32, in agreement with previous studies (Yinglong et al., 2013); pilocarpine establishes several π-stacking interactions with aromatic residues of the orthosteric binding cavity like Y3.33, W4.57, and Y6.51. In particular, our models are in agreement with the work of Heitz and collaborators (Heitz et al., 1999), that observed that the mutation of W4.57A resulted in a greater than 100-fold decrease in affinity for pilocarpine. Finally, from Figure 5.14 it can be noticed that both molecules interact with polar residues, i.e T5.39 and T5.42, forming h-bonds. We can conclude that, within the limitations of the method, pilocarpine probably binds muscarinic receptors in the orthosteric binding cavity, acting as a competitor of acetylcholine.

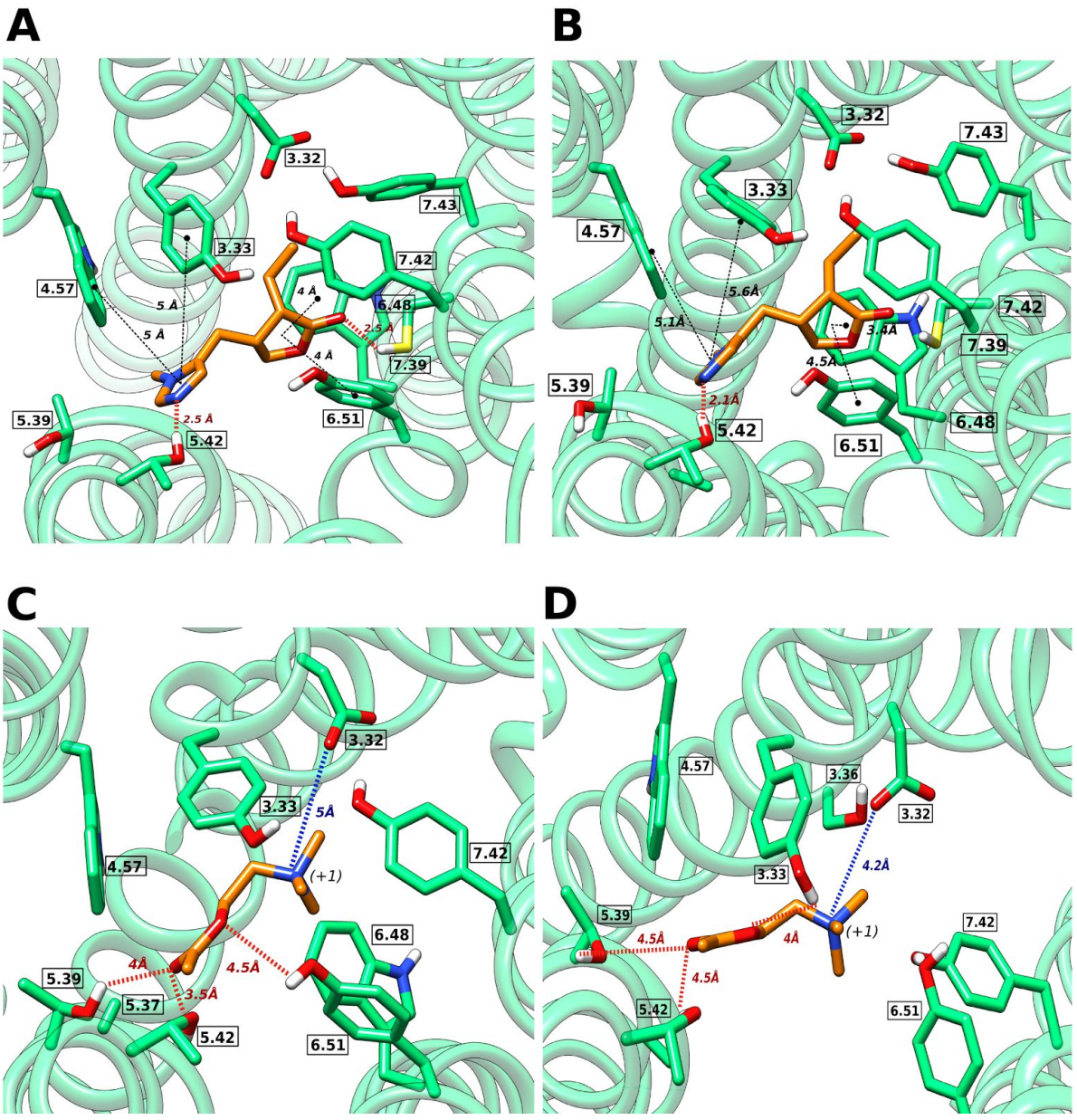

Figure 5.14. *In silico* docking poses of M_1 and M_3 muscarinic receptor with pilocarpine (panel A and B) and acetylcholine (panel C and D) agonists, respectively. Receptors backbone are shown in transparent green, residues side chains allocated in the orthosteric cavity are shown in green. Both agonists are colored in orange with oxygen atoms in red and nitrogen atoms in blue. Π-stacking interactions, salt bridges and hydrogen bonds are highlighted with black, blue and red dashes respectively. The charge of acetylcholine agonist is indicated with (+1).

5.5. Discussion and Conclusions

5.5.1. Pilocarpine triggers the proinflammatory cytokines release and upregulates the adhesion molecules in brain microvascular endothelial cell

Some of the cytokines we analyzed were significantly up-regulated (IL-6, KC, MCP-1, and TNF-α) by pilocarpine following the *in vivo* administration protocol specific to pilocarpine mouse model. According to this administration protocol, firstly the mice are treated with methylscopolamine, and our data show a significant stimulation of some cytokines production triggered by this treatment alone. This result is not in line with a previous report showing that *in vitro* exposure of rat brain microvascular endothelial cells co-cultured with white blood cells, exposed to relevant concentrations (similar to values measured in serum immediately before status epilepticus) as 1.5 mM of pilocarpine and 4 μM of methylscopolamine, elicits the level of IL-1β at similar values independent of the presence of methylscopolamine after 30 min of treatment (Marchi et al., 2007). Contrary, our data show that the methylscopolamine alone stimulate the cytokines release at 2 and 6 hrs time points. This is a relevant result since a subsequent effect of pilocarpine has to be compared with what methylscopolamine already produced. Moreover, the elevation of IL-1β reported in the same paper by Marchi *et al* as being induced *in vivo* by pilocarpine is matching the increase observed in our records as being produced by methylscopolamine, the subsequent pilocarpine treatment did not producing any significant changes. We conclude that methylscopolamine treatment (a mandatory step in pilocarpine mouse model) is triggering by itself an inflammatory response and the pilocarpine may eventually increase or not this effect. TNF-α was reported by Marchi *et al* as being insensitive to the pilocarpine treatment. In our records TNF-α is slightly increasing, the change becoming significant at MS+P 6 hrs condition. The difference with respect to Marchi's report is probably due to the short period of record used in their protocol (30 min after pilocarpine injection). On the other hand, the pilocarpine clearance period in the mouse brain was reported to be of ~3 hrs, with a peak of pilocarpine (~1 mM) at 30 min, and an elevated concentration (above 100 μM) until 3 hrs (Mazzuferi et al., 2012). With respect to this time evolution of pilocarpine concentration in brain, our results show that the inflammatory response is rapidly triggered by methylscopolamine and eventually enhanced by pilocarpine during the clearance period. However, the elevated level of cytokines at 6 hrs after pilocarpine injection, proves an sustained inflammation even after pilocarpine was cleared.

The duration of *status epilepticus* in pilocarpine-induced epilepsy models for different mice strains was reported between 10 min to 4 hrs when stopped with diazepam (Chen et al., 2013), or spontaneously remitted 5–6 hrs after pilocarpine administration (Curia et al., 2008), and this period corresponds with the clearance period for pilocarpine (Mazzuferi et al., 2012). Our data indicate the elevation of IL-6, KC and MCP-1 released in the blood of mice treated

with pilocarpine after 2 to 6 hrs, suggesting a role of local inflammation in triggering the *status epilepticus*.

In the pilocarpine-induced model of epilepsy, it is important to identify if the pilocarpine determines the cytokines release in the serum by stimulating brain microvascular endothelial cells, or only the immune blood circulating cells. Our *in vitro* data indicate that pilocarpine stimulate the release of KC and MCP-1 by BMVEC only after 24 hrs. The stimulation yield monotonically increases with pilocarpine concentration. This result is in line with the *in vivo* recorded data. However, the panel of cytokines stimulated by pilocarpine in *in vivo* tests is larger including also IL-6 and TNF-α. Such result is expected since the immune cells are well-known to have an important contribution to the cytokines release in the blood stream due to a neuroinflammatory insult (Duque and Descoteaux, 2014). IL-6 and TNF-α are included in the panel of cytokines released by macrophages (Duque and Descoteaux, 2014). Surprisingly, the same cytokines are downregulated with respect to control in bEnd.3 cells, also only after 24 hrs of stimulation.

5.5.2. Pilocarpine activates brain microvascular endothelial cells and the neuronal hyperexcitability might be a secondary phenomenon

Pilocarpine, a well-known agonist for muscarinic receptors and chemo-convulsant used in the epilepsy-induced models, when applied on mice hippocampal slices did not elicit seizure-like discharges even at high concentrations (10-500 μM; Marchi et al., 2007). Additional studies reported that arterial perfusion of the *in vitro* isolated guinea-pig brain with pilocarpine (<1 mM) did not cause epileptiform activity, except if co-perfused with compounds that enhance blood brain permeability, such as bradykinin or histamine (Uva et al., 2008). Our results indicated that pilocarpine (10 μM, 200 μM) applied on rat hippocampal slices determines an increased frequency of the excitatory and inhibitory spontaneous synaptic events, but without any paroxystical depolarization or other epileptiform activity. The absence of ictal-like activity in our recordings, when exposing mice brain slice to pilocarpine (at physiological concentrations, Mazzuferi et al., 2012), was in line with previous reports in the same range of pilocarpine concentrations without any further depolarization (Marchi et al., 2007). However, in terms of epileptogenesis mechanisms, we consider relevant to be in the physiological range of pilocarpine concentrations, that was detected in serum (150-320 μg/mL) or brain (150-180 μg/g) after 10 min up to 1 hr upon its injection in mice (Mazzuferi et al., 2012), and not beyond these limits (Poulsen et al., 2002). It is important to point out that the duration of 1 hr of pilocarpine-induced status epilepticus is sufficient to develop chronic epilepsy in mice, and was described to be associated with the mossy fiber sprouting but not neuronal death (Chen et al., 2013), and the majority of our *in vitro* experiments mimicked the exposure of brain endothelium at doses of pilocarpine corresponding to this post-SE period. In conclusion, pilocarpine *per se* is not able to determine seizure-like activity in brain hippocampal slices, without any dose-dependence.

Exposure of mice hippocampal slices to pilocarpine in the presence of 6 mM extracellular K^+ concentration, triggered epileptiform activity, due to neuronal depolarization (Marchi et al., 2007). Moreover, rat hippocampal slices exposed to pilocarpine (0.1-5 mM) induces ictal-like activity in almost 50% of the pyramidal neurons (Poulsen et al., 2002), either due to the slightly increased extracellular K^+ at 5.4 mM or to the high pilocarpine concentrations. In some preliminary tests, we also reproduced the epileptiform activity in hippocampal brain slices (*data not shown*) when pilocarpine was associated with increased extracellular K^+ concentration (4-8 mM). In conclusion, pilocarpine *per se* is not able to produce ictal-like events in brain slices, but in the presence of elevated extracellular K^+ neurons present seizure-like discharges. In this context, it is important to understand if increased extracellular K^+ mimics or not the consequences of *in vivo* opening of the BBB and subsequent loss of brain homeostasis. It is still an opened issue the extent of K^+ increase in the brain parenchyma after BBB opening, as limited information is available regarding the buffering capacity of glial cells.

Interestingly, pilocarpine concentrations were quantified in brain and blood at different timepoints, and have been reported to equalize after 30 min (Römermann et al., 2015) or 1 hr (Mazzuferi et al., 2012). However, the mechanism of pilocarpine entrance into the brain parenchyma remains to be understood.

Considering the paradigm of neurovascular unit activation in ictogenesis (Bertini et al., 2013), we tested if pilocarpine has a direct effect on brain endothelial microvascular cells. Our data clearly show a percentage of brain microvascular endothelial cells that elicit calcium transients. Extending our data to a broader scenario, we could hypothesize that pilocarpine in the bloodstream acts directly on brain endothelium and triggers calcium waves, as described in the literature for acetylcholine (Tallini et al., 2007).

Beside the acute effect of pilocarpine that triggers calcium transients by activating the muscarinic receptors, chronic exposure to pilocarpine modulates the expression of these receptors. Our results indicating the down-regulation of M_1 and M_3 in brain microvascular endothelial cells upon *in vitro* exposure to pilocarpine for 24 hrs prove that pilocarpine not only act as an muscarinic receptors agonist, but also is able to inhibit the expression of these receptors. The results are in line with previous reports showing that exposure of Chinese hamster ovary (CHO) cells to orthosteric agonists (e.g. pilocarpine) determines the M_1 receptor internalization and down-regulation, while exposure to allosteric agonists cause some receptor internalization, but not down-regulation (Thomas et al., 2009).

Previous studies have hypothesized that the ability of pilocarpine to induce *status epilepticus* depends on activation of the M_1 muscarinic receptor, since M_1 receptor knockout mice do not develop seizures in response to pilocarpine (Hamilton et al., 1997), but this knowledge remained confined around the idea that pilocarpine acts on the neuronal M_1 muscarinic receptor (Cataldi et al., 2011). Our study brings new insights showing the

importance of these receptors expressed in the brain endothelium when exposed to pilocarpine.

5.5.3. Pilocarpine activates brain microvascular endothelial cells by multiple mechanisms that contribute to the blood brain barrier permeabilization

Pilocarpine was demonstrated to have partial agonistic effects on Ca^{2+} responses (Schaafsma et al., 2006; Nezu et al., 2015) and it is documented to act on the orthosteric binding site of the muscarinic receptors (Thomas et al., 2009). We tested if these properties of pilocarpine as partial agonist are also present in the muscarinic receptors expressed in the brain microvascular endothelial cells.

It was demonstrated the association between blood brain barrier permeabilization and seizures (Uva et al., 2008; Fabene et al. 2008; Gorter et al., 2015; Librizzi et al., 2017). As brain microvascular endothelial cells are an important component of the neurovascular unit, and pilocarpine was demonstrated to activate calcium transients in these cells, the next step in understanding its mechanism of action was to elucidate if there is any effect of pilocarpine on the blood brain barrier integrity. Considering our results pointing out that pilocarpine permeabilizes the monolayer of brain microvascular endothelial cells for large molecules (i.e. Dextran 70kDa), we focused our attention on understanding the mechanism of permeabilization. Taking into account that tight junction proteins are well-known 'gate-keepers" of the BBB integrity (Luissint et al., 2012), our data are relevant as we proved that pilocarpine downregulates the tight junctions proteins (e.g. ZO-1 and claudin 5, except for the ZO-1 that was upregulated in bEnd3 cells at 24 hrs) in terms of protein and gene expression. Alghouth these preliminary studies are encouriging, further analysis of the pilocarpine´s effect in more complex *in vitro* systems mimicking the blood brain barrier and/or the neurovascular unit are necessary.

We have previously shown that the acute seizure activity following pilocarpine administration leads to enhanced vascular expression of leukocyte adhesion molecules on brain endothelial cells (Fabene et al., 2008). Interestingly, we found that pilocarpine mediates the upregulation of selectins on bEnd.3 cells, these adhesion molecules are of particular importance for the initial binding of neutrophils on vascular endothelium. Above all, the induction of P-selectin expression on brain endothelial cells is fundamental considering its proven involvement in the recruitment of neutrophils in the brain during acute seizures. Moreover, pilocarpine upregulates ICAM-1 and VCAM-1, and this indicates that pilocarpine directly activates brain microvascular endothelial cells by inducing an augmented expression of adhesion molecules and potentially allowing leukocyte adhesion.

To resume, complex events occur at the brain endothelium level when exposed to pilocarpine, including cytokines release, calcium waves triggering, changes leukocyte-endothelium adhesion, activation/down-regulation of M_1 and M_3 muscarinic receptors, tight junctions loosening, blood brain barrier permeabilization etc. In conclusion,

our study indicates that brain endothelium is an important site of action for pilocarpine, and neurons' exposure to pilocarpine is not triggering seizure-like activity, therefore epileptogenesis mechanisms should be revisited.

5.6. Executive summary

Aim

- To assess the action of pilocarpine on brain microvascular endothelium in an *in vitro* model of epileptogenesis

Results

- Pilocarpine induces the *in vivo* and *in vitro* cytokines release (e.g. IL-6, KC, MCP-1, and TNF-α)
- Pilocarpine upregulates the expression of adhesion molecules on brain microvascular endothelial cells, and interferes with leukocyte-endothelium adhesion and neutrophils recruitment
- Pilocarpine elicits calcium transients in a percentage of brain microvascular endothelial cells
- Pilocarpine is not inducing epileptic-like discharges in hippocampal pyramidal neurons in the absence of a depolarization induced by K^+ extracellular increase
- Pilocarpine downregulates the expression of tight junction proteins and permeabilizes the monolayers of brain microvascular endothelial cells
- Pilocarpine competes with acetylcholine on the same binding site of the muscarinic receptors
- Pilocarpine downregulates M_1 and M_3 receptors, while upregulates M_2, M_4 and M_5 receptors in brain microvascular endothelial cells

Conclusion & future perspective

- We demonstrated that endothelium of brain microvasculature is an important site of action for pilocarpine
- The epileptogenesis mechanisms should be revisited by understanding if the blood-barrier barrier permeabilization precedes or follows neuronal hyperexcitability

Chapter 6. General discussions

Multiple studies are dealing with the cholinergic signaling in the neuronal tissue, but limited information is available on the cholinergic signaling in the non-neuronal tissue, in particular in the brain capillaries. Therefore, we have focused our attention on the brain endothelium of the cerebral microvasculature. Moreover, pilocarpine action (as a common chemo-convulsant) agent is frequently analyzed in the neuronal tissue and its effects on the neuronal excitability are extensively studied. However, ***the mechanisms of pilocarpine action directed against the first barrier encountered*** (the blood brain barrier) ***in the bloodstream are largely neglected***.

Cerebral microvasculature is commonly imaged in different animal studies targeting physiological and pathological conditions (including epilepsy) and the deep-tissue bright nanoparticles-based agents are prefered. Generally, ***the direct action of the fluorescent nanoparticles on brain microvascular endothelium is considered negligible***.

In this thesis, we intended to understand the particularities of nanoparticles-based imaging agents action on the cerebral microvasculature and the cholinergic signaling in brain endothelium under physiological and pathological conditions (e.g. epilepsy). For this purpose we brought together *in vitro, in vivo* and *in silico* models, and several **limitations** of our studies have been identified:

L1. Use of in vitro cell culture models

L2. Use of in vivo animal models

L3. Use of in silico models

L1. Use of in vitro cell culture models. An important limitation of the experimental studies described in this thesis was the use of ***in vitro*** **cell cultures models**, e.g. brain microvascular endothelial cells.

In Chapter 3, we used mouse brain microvascular endothelial cells in primary and immortalized cell cultures, and human umbilical vein endothelial cells. Similar *in vitro* studies on brain endothelial cells have been performed on PEG-coated silica nanoparticles (Liu et al., 2014). The main limitation of our *in vitro* tests was the use of brain microvascular endothelial cells that represent only one of the many pieces in the complex puzzle of the neurovascular unit. Considering the diversity of available 2D and 3D models static/dynamic models for the blood brain barrier and the neurovascular unit (Radu and Radu, 2015), future *in vitro* studies should also consider testing the effect of Qtracker®800 on these models. Further *in vivo*

imaging analysis of Qtracker®800 effect at the level of brain microvasculature should provide more insights on the mechanism of action of nanoparticles.

In Chapter 4 and 5, we also used mouse brain microvascular endothelial cells in primary and immortalized cell cultures for the functional expression analysis of the muscarinic receptors in control and pilocarpine treatment conditions. The main limitation of this approach is related to the use of a simplified *in vitro* model (i.e. brain microvascular endothelial cells), where several important actors of the NVU are missing (especially the neuronal component) and the *in vivo* distribution/expression of the receptors might be altered. More complex *in vitro* models, including 2D and 3D models static/dynamic models, should be further used to mimic the cross-talk between cerebral endothelium and brain parenchyma. Moreover, combining *in vivo* patch-clamp recording with two-photon imaging could provide simultaneous information on neuronal excitability and microvasculature activity/dynamics.

In our studies, we proposed the ***in vitro* pilocarpine model**, where brain microvascular endothelial cells are exposed to pilocarpine to mimic the effects of the chemo-convulsant in the bloodstream. Of course, the model has several limitations related to its simplicity and the use of only one type of cells involved in the NVU, but it represents the initial step in understanding the first steps in ictogenesis mechanisms. If more complex *in vitro*/*in vivo* models will confirm our data, this model could be further used as an *in vitro* platform for pharmacological screening.

L2. Use of in vivo animal models. Another limitation of the study is the use of animals models in some experiments presented in Chapter 3 and Chapter 5 of the thesis.

In Chapter 3, we used a **mouse model to test fluorescent imaging dyes** (e.g. Qtracker®800) for biomedical deep-tissue imaging applications. Animal models have been previously used to test Qtracker®800 for *in-vivo* vasculature imaging applications (Mayes et al., 2008; Lo Celso et al., 2011). Limitations of using animal models in testing fluorescent dyes for deep-tissue vasculature imaging should be considered: (1) mouse-to-human *in vivo* differences of the dye biodistribution and kinetics/dynamics in brain microvasculature, (2) mouse-to-human differences between the imaging procedures.

In order to increase the translational value of our data, we have also tested the effect of Qtracker®800 on human umbilical vein endothelial cells in primary culture derived from different donors. Further *in vivo* testing of Qtracker®800 (and other fluorescent engineered-improved nanoparticles) for deep tissue imaging applications should also consider intravital microscopy experiments to monitor the activation of local calcium waves and their eventual propagation in brain microvasculature.

In Chapter 5, we used the **pilocarpine-induced animal model** in order to quantify the changes in cytokines serum levels. This model was already used in previous studies of Fabene's group (Fabene et al., 2008; Paradiso et al. 2009; Marchi et al. 2011) for showing that

that leukocyte trafficking plays a key role in seizure generation; this study has a good translational outcome supported by recent clinical observations suggesting that therapies able to interfere with leukocyte trafficking may have a therapeutic effect in human epilepsy. In our study, we have tried to diminish the possible experimental biases by comparing the methylscopolamine+pilocarpine animal group with the methylscopolamine animal group, as the methylscopolamine administration is a mandatory step in the pilocarpine mouse model for preventing peripheral cholinergic effects.

The advantages/disadvantages of using this animal model of epilepsy have been extensively described in several reviews (Löscher, 2011; Kandratavicius et al., 2014; Radu et al., 2017b). In animal models, pilocarpine administration was demonstrated to: (i) induce neuropathological alterations (i.e. cell loss, reduced arborization or lesions in different areas, including subiculum, hippocampus, neocortex), (ii) cause cognitive and memory deficits and (iii) triggers kindling and chronic spontaneous recurrent seizures (Turski et al., 1983; Cavalheiro et al., 1991; Mudò et al., 1996; Wozny et al., 2003; Knopp et al., 2005; Pauli et al., 2006), thus mimicking human temporal lobe epilepsy. Although chemical-induced epilepsy models (namely, the kainic acid and pilocarpine administration models) are largely used and reproduce some of the neuropathological, behavioral, cognitive, and psychiatric findings of temporal lobe epilepsy, they share significant limitations in translational medicine studies (Kandratavicius et al., 2014) that should not be neglected.

L3. Use of in silico models. The third important limitation of the study is the use of ***in silico*** **models** in some analysis presented in Chapter 4 and Chapter 5 of the thesis.

The *in silico* models for the molecular docking analysis present several limitations: (i) since mouse M_1-M_5 lack structural information (Haga et al., 2012; Kruse et al., 2012), homology modeling was carried out to predict their 3D structures, (ii) the plasma membrane environment is missing in molecular docking studies, (iii) the ligand-specific conformational changes of the receptors in different tissues is lacking in *in silico* models. Despite these limitations, the predictive power of the *in silico* methods should not be neglected and their contributions in the pharmaceutical industry for the design of specific receptor agonists/antagonists.

The guiding idea in all the experiments contained in this thesis was that cerebral microvasculature (e.g. cerebral microvascular endothelium) plays an active role in physiological and pathological conditions. The **main questions** addressed in this thesis were:

> *Q1. Is cerebral microvascular endothelium reactive/non-reactive to fluorescent intravital imaging dyes?*

Q2. Is cerebral microvascular endothelium activity regulated in physiological conditions by acetylcholine by means of the muscarinic receptors?

Q3. How muscarinic receptors expressed in cerebral microvascular endothelium are contributing to epileptogenesis mechanisms?

Q1. Is cerebral microvascular endothelium reactive/non-reactive to fluorescent intravital imaging dyes? In particular, it is important to understand if fluorescent nanoparticles (QDs800) used for deep intravital imaging are just crossing through the bloodstream or if there are active against the cerebral blood vessels walls, and thus introducing a methodological bias. Beside the accumulation of QDs in the endothelium, we have brought an essential contribution by proving the **activation of calcium transients in brain microvascular endothelial cells upon exposure to nanoparticles**. Our result questions the accuracy of the experiments in which QDs800 are used for fluorescent imaging of the cerebral vasculature for small animals. A second contribution of this study that deserves to be emphasized is the **patient-dependent calcium activation in endothelial cells exposed to QDs800**. This result is crucial in terms of translational potential of QDs800 in imaging techniques applied in patients and limits/prevents the use of these nanoparticles for medical applications. In conclusion, we demonstrated a direct action of Qtracker®800 on the vascular endothelium in the first 3 hrs after administration, thus overlapping the time window recommended for vasculature imaging studies with these fluorescent nanoparticles.

In perspective, keeping in mind the enormous potential of Qtracker®800 deep-tissue penetration in biomedical applications, better manufacturing solutions to diminish/eliminate endothelium actions should be found. Several open questions are emerging: (i) how safe are the contrast agents (Qtracker®800) used for deep tissue microvasculature imaging in small animals?, (ii) are they suitable to image microvasculature in different animal models or their long-term presence into the animal body might induce alterations (including seizure-like events)? (iii) do contrast agents interfere with the quality of the recorded data or does the imaging results on brain microvasculature in different physiological/pathological conditions are altered by the presence of nanoparticles *per se*?

Q2. Is cerebral microvascular endothelium activity regulated in physiological conditions by acetylcholine by means of the muscarinic receptors? Our study demonstrated the **expression of all muscarinic acetylcholine receptors in mouse brain microvascular endothelial cells**. Functional calcium testing also demonstrated that acetylcholine acts on muscarinic, but not nicotinic, mouse receptors. It should be also highlighted that our study brings **the first evidence that M_1 receptors**, together with M_3 receptors, **are functionally expressed in mouse brain microvascular endothelium**. Taking into account the extensive use of mouse models in mimicking pathological conditions (e.g. epilepsy), the second result

of this study is very important in explaining the roles of muscarinic acetylcholine receptors in the cerebral mouse microvasculature. In conclusion, our study suggests muscarinic acetylcholine receptors as potential pharmacological targets in future translational studies.

In perspective, we argue that future research on drug development should especially focus on the allosteric binding sites of the M_1 and M_3 receptors. Several issues should be further studied: (i) the functional expression of M_4 and M_5 in mouse brain microvascular endothelium, (ii) the distinct contribution of the muscarinic receptors in cholinergic signaling that controls the dynamics of brain microvasculature in physiological conditions, (iii) the functional expression of muscarinic receptors in human brain microvasculature using appropriate models mimicking the physiological condition (e.g. human iPS cell-derived brain microvascular endothelial cells, or human brain microvascular endothelial cells), (iv) the *in vivo* muscarinic cholinergic receptor imaging of brain microvasculature in animal models.

Q3. How muscarinic receptors expressed in cerebral microvascular endothelium are contributing to epileptogenesis mechanisms? Using a pilocarpine induced model, our study identified multiple mechanisms by which cerebral microvasculature contributes to ictogenesis. We demonstrated that **pilocarpine exerts a synergic action on muscarinic receptors, tight junctions proteins, adhesion molecules, and cytokines release, determining a joint increase of the blood brain barrier permeability**. We propose that the mechanism of action involves the competition of pilocarpine with acetylcholine on the orthosteric site of muscarinic receptors expressed in cerebral microvascular endothelial cells. We also might speculate that pilocarpine interferes with the ”normal” processes of leukocyte-endothelium adhesion and neutrophils recruitment by altering the adhesion molecules on the surface of brain microvascular endothelium. In conclusion, we demonstrated that endothelium of brain microvasculature is an important site of action for pilocarpine.

In perspective, the epileptogenesis mechanisms should be revisited by understanding if the blood-barrier barrier permeabilization precedes or follows neuronal hyperexcitability. Multiple aspects remain to be further deciphered: (i) to test the alteration of leukocyte-endothelium adhesion in the presence of pilocarpine by employing 3D artificial capillary models and/or 3D dynamic NVU model, (ii) to evidence the changes underwent by the glycocalyx of the brain microvascular endothelium upon exposure to pilocarpine and how is affected the leukocyte-endothelium adhesion, (iii) to understand the mouse-to-human translational potential of our data, and (iv) to evaluate the utility and limitations of using the *in vitro* pilocarpine model for pharmacological screening.

As a **general conclusion**, this thesis revealed some pieces in the complex puzzle of mouse brain microvascular endothelium activation in the presence fluorescent vasculature imaging agents and its role in the pilocarpine-induced ictogenesis model.

References

Abbott NJ. (2002) Astrocyte-endothelial interactions and blood-brain barrier permeability. J Anat. 200(6):629-38.

Abbott NJ, Rçnnbck L, Hansson E. (2006) Astrocyte–endothelial interactions at the blood–brain barrier, Nat. Rev. Neurosci 7:41–53.

Abbott NJ, Yusof SR. (2010). Structure and function of the blood-brain barrier. Front. Pharmacol. Conference Abstract: Pharmacology and Toxicology of the Blood-Brain Barrier: State of the Art, Needs for Future Research and Expected Benefits for the EU. doi: 10.3389/conf.fphar.2010.02.00002

Adem A, Karlsson E. (1997) Muscarinic receptor subtype selective toxins. Life Sci. 60(13-14): 1069-1076.

Akdis CA, Simons FER. (2006) Histamine receptors are hot in immunopharmacology. Eur J Pharmacol. 533(1–3):69–76.

Al Ahmad A, Taboada CB, Gassmann M, Ogunshola OO. (2011) Astrocytes and pericytes differentially modulate blood-brain barrier characteristics during development and hypoxic insult. J Cereb Blood Flow Metab. 31(2):693-705.

Andjelkovic AV, Pachter JS. (2000) Characterization of binding sites for chemokines MCP-1 and MIP-1alpha on human brain microvessels. J Neurochem. 75(5):1898-906.

Ando J, Yamamoto K. (2013) Flow detection and calcium signalling in vascular endothelial cells. Cardiovasc Res. 99(2):260–268.

Andreone BJ, Lacoste B, Gu C. (2015) Neuronal and vascular interactions. Annu Rev Neurosci. 38:25-46.

Araque A, Sanzgiri RP, Parpura V, Haydon PG. (1999) Astrocyte-induced modulation of synaptic transmission. Can J Physiol Pharmacol. 77(9):699-706.

Armulik A, Abramsson A, Betsholtz C. (2005) Endothelial/pericyte interactions. Circ. Res. 97:512–23

Armulik A, Genové G, Mae M, Nisancioglu MH, Wallgard E, Niaudet C, He L, Norlin J, Lindblom P, Strittmatter K, Johansson BR, Betsholtz C. (2010) Pericytes regulate the blood–brain barrier. Nature, 468:557–561.

Armulik A, Genové G, Betsholtz C. (2011) Pericytes: developmental, physiological, and pathological perspectives, problems, and promises, Dev Cell, 21:193–215.

Attwell D, Buchan AM, Charpak S, Lauritzen M, Macvicar BA, Newman EA. (2010) Glial and neuronal control of brain blood flow. Nature 468:232–43.

Badaut J, Moro V, Seylaz J, Lasbennes F. (1997) Distribution of muscarinic receptors on the endothelium of cortical vessels in the rat brain. Brain Res. 778(1): 25-33.

Badhwar A, Stanimirovic D B, Hamel E, Haqqani A S. (2014) The proteome of mouse cerebral arteries. J Cereb Blood Flow Metab. 34(6): 1033-1046.

Bagher P, Davis M J, Segal S S. (2011) Visualizing calcium responses to acetylcholine convection along endothelium of arteriolar networks in Cx40(BAC)-GCaMP2 transgenic mice. Am J Physiol Heart Circ Physiol. 301(3): H794-H802.

Balenci L, Saoudi Y, Grunwald D, Deloulme JC, Bouron A, Bernards A, Baudier J. (2007) IQGAP1 regulates adult neural progenitors in vivo and vascular endothelial growth factor-triggered neural progenitor migration in vitro. J. Neurosci. 27:4716–4724.

Balog S, Rodriguez-Lorenzo L, Monnier CA, Obiols-Rabasa M, Rothen-Rutishauser B, Schurtenberger P, Petri-Fink A. (2015) Characterizing nanoparticles in complex biological media and physiological fluids with depolarized dynamic light scattering. Nanoscale. 7(14):5991-7.

Bandopadhyay R, Orte C, Lawrenson JG, Reid AR, De Silva S, Allt G. (2001) Contractile proteins in pericytes at the blood–brain and blood–retinal barriers, J Neurocytol. 30:35–44.

Bateman A, Martin MJ, O'Donovan C, Magrane M, Apweiler R, Alpi E, Antunes R, Ar-Ganiska J, Bely B, Bingley M, Bonilla C, Britto R, Bursteinas B, Chavali G, Cibrian-Uhalte E, Da Silva A, De Giorgi M, Dogan T, Fazzini F, Gane P, Cas-Tro L G, Garmiri P, Hatton-Ellis E, Hieta R, Huntley R, Legge D, Liu WD, Luo J, MacDougall A, Mutowo P, Nightin-Gale A, Orchard S, Pichler K, Poggioli D, Pundir S, Pureza L, Qi GY, Rosanoff S, Saidi R, Sawford T, Shypitsyna A, Turner E, Volynkin V, Wardell T, Watkins X, Watkins, Cowley A, Figueira L, Li WZ, McWilliam H, Lopez R, Xenarios I, Bougueleret L, Bridge A, Poux S, Redaschi N, Aimo L, Argoud-Puy G, Auchincloss A, Axelsen K, Bansal P, Baratin D, Blatter M C, Boeckmann B, Bolleman J, Boutet E, Breuza L, Casal-Casas C, De Castro E, Coudert E, Cuche B, Doche M, Dornevil D, Duvaud S, Estreicher A, Famiglietti L, Feuermann M, Gasteiger E, Gehant S, Gerritsen V, Gos A, Gruaz-Gumowski N, Hinz U, Hulo C, Jungo F, Keller G, Lara V, Lemercier P, Lieberherr D, Lombardot T, Martin X, Masson P, Morgat A, Neto T, Nouspikel N, Paesano S, Pedruzzi I, Pilbout S, Pozzato M, Pruess M, Rivoire C, Roechert B, Schneider M, Sigrist C, Sonesson K, Staehli S, Stutz A, Sundaram S, Tognolli M, Verbregue L, Veuthey A L, Wu C H, Arighi C N, Arminski L, Chen C M, Chen Y X, Garavelli J S, Huang H Z, Laiho K T, McGarvey P, Natale D A, Suzek B E, Vinayaka C R, Wang Q H, Wang Y Q, Yeh L S, Yerramalla M S, Zhang J. (2015) UniProt: a hub for protein information. Nucleic Acids Research. 43(D1): D204-D212.

Bell MD, Perry VH. (1995) Adhesion molecule expression on murine cerebral endothelium following the injection of a proinflammagen or during acute neuronal degeneration. J Neurocytol. 24(9):695-710.

Benezra M, Penate-Medina O, Zanzonico PB, Schaer D, Ow H, Burns A, DeStanchina E, Longo V, Herz E, Iyer S, Wolchok J, Larson SM, Wiesner U, Bradbury MS. (2011) Multimodal silica nanoparticles are effective cancer-targeted probes in a model of human melanoma. J Clin Invest. 121(7):2768-80.

Bentzen EL, Tomlinson ID, Mason J, Gresch P, Warnement MR, Wright D, Sanders-Bush E, Blakely R, Rosenthal SJ. (2005) Surface modification to reduce nonspecific binding of quantum dots in live cell assays. Bioconjug Chem. 16(6):1488-94.

Beny JL, Nguyen MN, Marino M, Matsui M. (2008) Muscarinic receptor knockout mice confirm involvement of M3 receptor in endothelium-dependent vasodilatation in mouse arteries. J Cardiovasc Pharmacol. 51(5): 505-512.

Bertini G, Bramanti P, Constantin G, Pellitteri M, Radu BM, Radu M, Fabene PF. (2013) New players in the neurovascular unit: insights from experimental and clinical epilepsy. Neurochem Int. 63(7):652-9.

Bland C, Bellanger L, Arrnengaud J. (2014) Magnetic immunoaffinity enrichment for selective capture and MS/MS analysis of N-Terminal-TMPP-labeled peptides. Journal of Proteome Res. 13(2): 668-680.

Boittin FX, Alonso F, Le Gal L, Allagnat F, Beny JL, Haefliger JA. (2013) Connexins and M3 Muscarinic Receptors Contribute to Heterogeneous Ca2+ Signaling in Mouse Aortic Endothelium. Cell Physiol Biochem. 31(1): 166-178.

Bor-Seng-Shu E, Kitam WS, Figueiredo EG, Paiva WS, Fonoff ET, Teixeira MJ, Panerai RB. (2012) Cerebral hemodynamics: concepts of clinical importance. Arq Neuropsiquiatr. 70: 352-6.

Bradbury MS, Phillips E, Montero PH, Cheal SM, Stambuk H, Durack JC, Sofocleous CT, Meester RJ, Wiesner U, Patel S. (2013) Clinically-translated silica nanoparticles as dual-modality cancer-targeted probes for image-guided surgery and interventions. Integr Biol (Camb). 5(1):74-86.

Braet K, Paemeleire K, D'Herde K, Sanderson MJ, Leybaert L. (2001) Astrocyte-endothelial cell calcium signals conveyed by two signalling pathways. Eur J Neurosci. 13(1):79-91.

Braet K, Cabooter L, Paemeleire K, Leybaert L. (2004) Calcium signal communication in the central nervous system. Biol Cell. 96(1):79-91.

Brix B, Mesters JR, Pellerin L, Jöhren O. (2012) Endothelial cell-derived nitric oxide enhances aerobic glycolysis in astrocytes via HIF-1α-mediated target gene activation. J Neurosci. 32(28):9727-35.

Burns AA, Vider J, Ow H, Herz E, Penate-Medina O, Baumgart M, Larson SM, Wiesner U, Bradbury M. (2009) Fluorescent silica nanoparticles with efficient urinary excretion for nanomedicine. Nano Lett. 9(1):442-8.

Burrell K, Agnihotri S, Leung M, Dacosta R, Hill R, Zadeh G. (2013) A novel high-resolution in vivo imaging technique to study the dynamic response of intracranial structures to tumor growth and therapeutics. J. Vis. Exp. 76: e50363.

Bymaster FP, McKinzie DL, Felder CC, Wess J. (2003) Use of M1-M5 muscarinic receptor knockout mice as novel tools to delineate the physiological roles of the muscarinic cholinergic system. Neurochem Res. 28(3-4):437-42.

Cambier S, Gline S, Mu D, Collins R, Araya J, Dolganov G, Einheber S, Boudreau N, Nishimura SL. (2005) Integrin alpha(v)beta8-mediated activation of transforming growth factor-beta by perivascular astrocytes: an angiogenic control switch. Am J Pathol. 166(6):1883-94.

Cardona AE, Li M, Liu L, Savarin C, Ransohoff RM. (2008) Chemokines in and out of the central nervous system: much more than chemotaxis and inflammation. J Leukoc Biol. 84(3):587-94.

Cassé F, Bardou I, Danglot L, Briens A, Montagne A, Parcq J, Alahari A, Galli T, Vivien D, Docagne F. (2012) Glutamate controls tPA recycling by astrocytes, which in turn influences glutamatergic signals. J Neurosci. 32(15):5186-99.

Cataldi M, Panuccio G, Cavaccini A, D'Antuono M, Taglialatela M, Avoli M. (2011) Involvement of inward rectifier and M-type currents in carbachol-induced epileptiform synchronization. Neuropharmacology. 60(4):653-61.

Cauli B, Tong XK, Rancillac A, Serluca N, Lambolez B, Rossier J, Hamel E. (2004) Cortical GABA interneurons in neurovascular coupling: relays for subcortical vasoactive pathways. J. Neurosci. 24:8940–49.

Cauli B, Hamel E. (2010) Revisiting the role of neurons in neurovascular coupling. Front. Neuroenergetics 2:9.

Cavalheiro E.A., Leite J.P., Bortolotto Z.A., Turski W.A., Ikonomidou C., Turski L. (1991) Long-term effects of pilocarpine in rats: structural damage of the brain triggers kindling and spontaneous recurrent seizures. Epilepsia, 32(6):778-782.

Ceccon A, D'Onofrio M, Zanzoni S, Longo DL, Aime S, Molinari H, Assfalg M. (2013) NMR investigation of the equilibrium partitioning of a water-soluble bile salt protein carrier to phospholipid vesicles. Proteins. 81(10):1776-91.

Chedotal A, Cozzari C, Faure MP, Hartman BK, Hamel E. (1994) Distinct choline-acetyltransferase (Chat) and vasoactive intestinal polypeptide (Vip) bipolar neurons project to local blood-vessels in the rat cerebral-cortex. Brain Res. 646(2): 181-193.

Chen Y, Molnár M, Li L, Friberg P, Gan LM, Brismar H, Fu Y. (2013) Characterization of VCAM-1-binding peptide-functionalized quantum dots for molecular imaging of inflamed endothelium. PLoS One. 8(12):e83805.

Chen LL, Feng HF, Mao XX, Ye Q, Zeng LH. (2013) One hour of pilocarpine-induced status epilepticus is sufficient to develop chronic epilepsy in mice, and is associated with mossy fiber sprouting but not neuronal death. Neurosci Bull. 29(3):295-302.

Chiamulera C, Di Chio M, Tedesco V, Cantu C, Formaggio E, Fumagalli G. (2008) Nicotine-induced phosphorylation of phosphorylated cyclic AMP response element-binding protein (pCREB) in hippocampal neurons is potentiated by agrin. Neurosci Letters 442(3): 234-238.

Chin SP, Buckle MJC, Chalmers DK, Yuriev E, Doughty SW. (2014) Toward activated homology models of the human M-1 muscarinic acetylcholine receptor. J Mol Graph Model 49: 91-98.

Christopherson KS, Ullian EM, Stokes CC, Mullowney CE, Hell JW, Agah A, Lawler J, Mosher DF, Bornstein P, Barres BA. (2005) Thrombospondins are astrocyte-secreted proteins that promote CNS synaptogenesis. Cell, 120:421–433.

Cines DB, Pollak ES, Buck CA, Loscalzo J, Zimmerman GA, Mcever RP, Pober JS, Wick TM, Konkle BA, Schwartz BS, Barnathan ES, Mccrae KR, Hug BA, Schmidt AM, Stern DM. (1998) Endothelial cells in physiology and in the pathophysiology of vascular disorders. Blood 91(10): 3527-3561.

Clader JW, Wang YG. (2005) Muscarinic receptor agonists and antagonists in the treatment of Alzheimer's Disease. Curr Pharmac Design 11(26): 3353-3361.

Clift MJ, Boyles MS, Brown DM, Stone V. (2010) An investigation into the potential for different surface-coated quantum dots to cause oxidative stress and affect macrophage cell signalling in vitro. Nanotoxicology 4(2):139–149.

Clift MJ, Stone V. (2012) Quantum dots: an insight and perspective of their biological interaction and how this relates to their relevance for clinical use. Theranostics 2(7):668–680.

Clifford DB, Olney JW, Maniotis A, Collins RC, Zorumski CF. (1987) The functional anatomy and pathology of lithium-pilocarpine and high-dose pilocarpine seizures. Neuroscience. 23(3):953-68.

Collison DJ, Coleman RA, James RS, Carey J, Duncan G. (2000) Characterization of muscarinic receptors in human lens cells by pharmacologic and molecular techniques. Invest Ophthalmol Vis Sci 41(9): 2633-2641.

Colognato H, Yurchenco PD. (2000) Form and function: the laminin family of heterotrimers. Dev Dyn. 218(2):213-34.

Conn PJ, Christopoulos A, Lindsley CW. (2009) Allosteric modulators of GPCRs: a novel approach for the treatment of CNS disorders. Nat Rev Drug Discov. 8(1): 41-54.

Cooke J P. (2000) The endothelium: a new target for therapy. Vasc Med 5(1): 49-53.

Croll SD, Goodman JH, Scharfman HE (2004a) Vascular Endothelial Growth Factor (VEGF) in Seizures: A Double-Edged Sword, Adv Exp Med Biol. 548:57–68

Croll SD, Ransohoff RM, Cai N, Zhang Q, Martin FJ, Wei T, Kasselman LJ, Kintner J, Murphy AJ, Yancopoulos GD, Wiegand SJ (2004b) VEGF-Mediated Inflammation Precedes Angiogenesis in Adult Brain. Exp Neurol. 187:388–402

Curia G, Longo D, Biagini G, Jones RSG, Avoli M. (2008) The pilocarpine model of temporal lobe epilepsy. J Neurosci Methods. 172(2-4): 143–157.

Damalakiene L, Karabanovas V, Bagdonas S, Valius M, Rotomskis R. (2013) Intracellular distribution of nontargeted quantum dots after natural uptake and microinjection. Int J Nanomedicine 8:555–568.

Davalos D, Grutzendler J, Yang G, Kim JV, Zuo Y, Jung S, Littman DR, Dustin ML, Gan WB. (2005) ATP mediates rapid microglial response to local brain injury in vivo. Nat Neurosci. 8:752–758.

del Zoppo GJ, Milner R. (2006) Integrin-matrix interactions in the cerebral microvasculature. Arterioscler Thromb Vasc Biol. 26(9):1966-75.

De Vries S J, van Dijk M, Bonvin AMJJ. (2010) The HADDOCK web server for data-driven biomolecular docking. Nat Protoc. 5(5): 883-897.

Ding D, Goh CC, Feng G, Zhao Z, Liu J, Liu R, Tomczak N, Geng J, Tang BZ, Ng LG, Liu B. (2013) Ultrabright organic dots with aggregation-induced emission characteristics for real-time two-photon intravital vasculature imaging. Adv Mater. 25(42):6083-8.

Dorje F, Wess J, Lambrecht G, Tacke R, Mutschler E, Brann MR. (1991) Antagonist binding profiles of 5 cloned human muscarinic receptor subtypes. J Pharmacol Exp Ther 256(2): 727-733.

Duque GA, Descoteaux A. (2014) Macrophage cytokines: Involvement in immunity and infectious diseases. Front Immunol. 5: 491.

Eglen RM. (2006) Muscarinic receptor subtypes in neuronal and non-neuronal cholinergic function. Auton Autacoid Pharmacol 26(3): 219-233.

Eichhoff G, Brawek B, Garaschuk O. (2011) Microglial calcium signal acts as a rapid sensor of single neuron damage in vivo. Biochim Biophys Acta. 14-1813(5):1014-24.

Elhusseiny A, Cohen Z, Olivier A, Stanimirovic D B, Hamel E. (1999) Functional acetylcholine muscarinic receptor subtypes in human brain microcirculation: Identification and cellular localization. J Cereb Blood Flow Metab. 19(7): 794-802.

Elhusseiny A, Hamel E. (2000) Muscarinic—but not nicotinic—acetylcholine receptors mediate a nitric oxide-dependent dilation in brain cortical arterioles: a possible role for the M5 receptor subtype. J. Cereb. Blood Flow Metab. 20:298–305

Endo K, Kito N, Fukushima Y, Weng H, Iwai N. (2014) A novel biomarker for acute kidney injury using TaqMan-based unmethylated DNA-specific polymerase chain reaction. Biomed Res. 35(3):207–213.

Fabene PF, Navarro Mora G, Martinello M, Rossi B, Merigo F, Ottoboni L, Bach S, Angiari S, Benati D, Chakir A, Zanetti L, Schio F, Osculati A, Marzola P, Nicolato E, Homeister JW, Xia L, Lowe JB, McEver RP, Osculati F, Sbarbati A, Butcher EC, Constantin G. (2008) A role for leukocyte-endothelial adhesion mechanisms in epilepsy. Nat Med. 14(12):1377-83.

Fabene PF, Bramanti P, Constantin G. (2010) The emerging role for chemokines in epilepsy. J Neuroimmunol. 224(1-2):22-7.

Fabene PF, Laudanna C, Constantin G. (2013) Leukocyte trafficking mechanisms in epilepsy. Mol Immunol. 55(1):100-4.

Fabene PF, Salvetti B, Merigo F, Benati D, Tognoli C, Radu BM, Radu M, Bertini G, Osculati F. (2015) Quantum dots as new guests in the body: structural and functional data. Ital J Anat Embryol. 119(1):77.

Feairheller DL, Park JY, Rizzo V, Kim B, Brown MD. (2011) Racial differences in the responses to shear stress in human umbilical vein endothelial cells. Vasc Health Risk Manag. 7:425–431.

Felder CC, Bymaster FP, Ward J, DeLapp N. (2000) Therapeutic opportunities for muscarinic receptors in the central nervous system. J Med Chem. 43(23): 4333-4353.

Fernandez-Klett F, Offenhauser N, Dirnagl U, Priller J, Lindauer U. (2010) Pericytes in capillaries are contractile in vivo, but arterioles mediate functional hyperemia in the mouse brain. PNAS 107:22290–95.

Figueroa KW, Griffin MT, Ehlert FJ. (2009) Selectivity of agonists for the active state of M1 to M4 muscarinic receptor subtypes. J Pharmacol Exp Ther. 328(1):331-42.

Foresti ML, Arisi GM, Katki K, Montañez A, Sanchez RM, Shapiro LA. (2009) Chemokine CCL2 and its receptor CCR2 are increased in the hippocampus following pilocarpine-induced status epilepticus. J Neuroinflammation. 6:40.

Fratta Pasini A, Albiero A, Stranieri C, Cominacini M, Pasini A, Mozzini C, Vallerio P, Cominacini L, Garbin U. (2012) Serum oxidative stress-induced repression of Nrf2 and GSH depletion: a mechanism potentially involved in endothelial dysfunction of young smokers. PLoS One. 7(1):e30291.

Fruchart-Gaillard C, Mourier G, Marquer C, Stura E, Birdsall N J M, Servent D. (2008) Different Interactions between MT7 Toxin and the Human Muscarinic M-1 Receptor in Its Free and N-Methylscopolamine-Occupied States. Mol Pharmacol. 74(6): 1554-1563.

Fujii T, Takada-Takatori Y, Horiguchi K, Kawashima K. (2012) Mediatophore regulates acetylcholine release from T cells. J Neuroimmunol. 244(1-2):16-22.

Galea I, Bechmann I, Perry VH. (2007) What is immune privilege (not)? Trends Immunol. 28:12–18.

Gericke A, Sniatecki JJ, Goloborodko E, Steege A, Zavaritskaya O, Vetter JM, Grus FH, Patzak A, Wess J, Pfeiffer N. (2011) Identification of the muscarinic acetylcholine receptor subtype mediating cholinergic vasodilation in murine retinal arterioles. Invest Ophthalmol Vis Sci. 52(10): 7479-7484.

Gericke A, Steege A, Manicam C, Bohmer T, Wess J, Pfeiffer N. (2014) Role of the M-3 Muscarinic Acetylcholine Receptor Subtype in Murine Ophthalmic Arteries After Endothelial Removal. Investigative Ophthalmology & Visual Science. 55(1): 625-631.

Gobeil F, Fortier A, Zhu T, Bossolasco M, Leduc M, Grandbois M, Heveker N, Bkaily G, Chemtob S, Barbaz D. (2006) G-protein-coupled receptors signalling at the cell nucleus: an emerging paradigm. Can J Physiol Pharmacol. 84(3-4): 287-297.

Goodwin J A, Hulme E C, Langmead C J, Tehan B G. (2007) Roof and floor of the muscarinic binding pocket: Variations in the binding modes of orthosteric ligands. Mol Pharmacol. 72(6): 1484-1496.

Gorter JA, van Vliet EA, Aronica E. (2015) Status epilepticus, blood-brain barrier disruption, inflammation, and epileptogenesis. Epilepsy Behav. 49:13-6.

Graham E S, Woo KK, Aalderink M, Fry S, Greenwood JM, Glass M, Dragunow M. (2013) M1 muscarinic receptor activation mediates cell death in M1-HEK293 cells. PlosOne 8(9).

Haberberger RV, Bodenbenner M, Kummer W. (2000) Expression of the cholinergic gene locus in pulmonary arterial endothelial cells. Histochem Cell Biol 113(5): 379-387.

Haga K, Kruse A C, Asada H, Yurugi-Kobayashi T, Shiroishi M, Zhang C, Weis W I, Okada T, Kobilka B K, Haga T, Kobayashi T. (2012) Structure of the human M2 muscarinic acetylcholine receptor bound to an antagonist. Nature 482(7386): 547-U147.

Halassa MM, Haydon PG. (2010) Integrated brain circuits: astrocytic networks modulate neuronal activity and behavior, Annu. Rev. Physiol., 72 (2010), pp. 335–355.

Hall CN, Reynell C, Gesslein B, Hamilton NB, Mishra A, Sutherland BA, O'Farrell FM, Buchan AM, Lauritzen M, Attwell D. (2014) Capillary pericytes regulate cerebral blood flow in health and disease. Nature 508:55–60.

Hamel E. (2006) Perivascular nerves and the regulation of cerebrovascular tone. J. Appl. Physiol. 100:1059–64

Hamilton SE, Loose MD, Qi M, Levey AI, Hille B, McKnight GS, Idzerda RL, Nathanson NM. (1997) Disruption of the m1 receptor gene ablates muscarinic receptor-dependent M current regulation and seizure activity in mice. Proceedings of the National Academy of Sciences of the United States of America 94(24): 13311-13316.

Hamilton NB, Attwell D, Hall CN. (2010) Pericyte-mediated regulation of capillary diameter: a component of neurovascular coupling in health and disease. Front. Neuroenergetics 2:5

Hansson E, Johansson BB, Westergren I, Rönnbäck L. (1994) Glutamate-induced swelling of single astroglial cells in primary culture, Neuroscience, 63:1057–1066.

Harada K, Matsumoto Y, Umemura K. (2012) M1 and M5 muscarinic acetylcholine receptor-mediated leukocyte migration. J Pharmacol Sci. 118:173P.

Hartmann C, Zozulya A, Wegener J, Galla HJ. (2007) The impact of glia-derived extracellular matrices on the barrier function of cerebral endothelial cells: an in vitro study. Exp Cell Res. 313(7):1318-25.

Hasuo H, Akasu T, Gallagher JP. (1996) Muscarine activates a nonselective cation current through a M(3) muscarinic receptor subtype in rat dorsolateral septal nucleus neurons. J Neurophysiol 76(4): 2221-2230.

Hawkins BT, Davis TP. (2005), The blood-brain barrier/neurovascular unit in health and disease, Pharmacological Reviews, 57(2):173–185.

Helms HC, Madelung R, Waagepetersen HS, Nielsen CU, Brodin B. (2012) In vitro evidence for the brain glutamate efflux hypothesis: brain endothelial cells cocultured with astrocytes display a polarized brain-to-blood transport of glutamate. Glia. 60(6):882-93.

Henneberger C, Papouin T, Oliet SH, Rusakov DA. (2010) Long-term potentiation depends on release of d-serine from astrocytes Nature, 463:232–236.

Hildebrandt M, Amann K, Schröder R, Pieper T, Kolodziejczyk D, Holthausen H, Buchfelder M, Stefan H, Blümcke I. (2008) White matter angiopathy is common in pediatric patients with intractable focal epilepsies. Epilepsia. 49(5):804-15.

Hillman EM. (2014) Coupling mechanism and significance of the BOLD signal: a status report. Annu. Rev. Neurosci. 37:161–81

Ho CC, Chang H, Tsai HT, Tsai MH, Yang CS, Ling YC, Lin P. (2013) Quantum dot 705, a cadmium-based nanoparticle, induces persistent inflammation and granuloma formation in the mouse lung. Nanotoxicology. 7(1):105-15.

Hoheisel D, Nitz T, Franke H, Wegener J, Hakvoort A, Tilling T, Galla HJ. (1998) Hydrocortisone reinforces the blood-brain properties in a serum free cell culture system. Biochem Biophys Res Commun. 247(2):312-5.

Hori S, Ohtsuki S, Hosoya K, Nakashima E, Terasaki T. (2004) A pericyte-derived angiopoietin-1 multimeric complex induces occludin gene expression in brain capillary endothelial cells through Tie-2 activation in vitro. J Neurochem. 89(2):503-13.

Howarth C. (2014) The contribution of astrocytes to the regulation of cerebral blood flow. Front. Neurosci. 8:103

Hyun H, Lee K, Min KH, Jeon P, Kim K, Jeong SY, Kwon IC, Park TG, Lee M. (2013) Ischemic brain imaging using fluorescent gold nanoprobes sensitive to reactive oxygen species. J Control Release. 170(3):352-7.

Ionov ID. (2007) Specific mechanism for blood inflow stimulation in brain area prone to Alzheimer's disease lesions. Int J Neurosci 117(10):1425-1442.

Irwin JJ, Sterling T, Mysinger MM, Bolstad ES, Coleman RG. (2012) ZINC: A Free Tool to Discover Chemistry for Biology. J Chem Inf Model. 52(7):1757-1768.

Isberg V, Vroling B, van der Kant R, Li K, Vriend G, Gloriam D. (2014) GPCRDB: an information system for G protein-coupled receptors. Nucleic Acids Res 42(D1): D422-D425.

Itoh Y, Suzuki N. (2012) Control of brain capillary blood flow. J Cereb Blood Flow Metab. 32(7):1167–1176.

Ivens S, Kaufer D, Flores LP, Bechmann I, Zumsteg D, Tomkins O, Seiffert E, Heinemann U, Friedman A. (2007) TGF-beta receptor-mediated albumin uptake into astrocytes is involved in neocortical epileptogenesis. Brain. 130(Pt 2):535-47.

Jacobson M A, Kreatsoulas C, Pascarella D M, O'Brien J A, Sur C. (2010) The M1 muscarinic receptor allosteric agonists AC-42 and 1-[1 '-(2-Methylbenzyl)-1,4 '-bipiperidin-4-yl]-1,3-dihydro-2H-benzimidazol-2-one bind to a unique site distinct from the acetylcholine orthosteric site. Mol Pharmacol. 78(4):648-657.

Janzer RC, Raff MC. (1987) Astrocytes induce blood-brain barrier properties in endothelial cells. Nature. 325(6101):253-7.

Jaruszewski KM, Curran GL, Swaminathan SK, Rosenberg JT, Grant SC, Ramakrishnan S, Lowe VJ, Poduslo JF, Kandimalla KK. (2014) Multimodal nanoprobes to target cerebrovascular amyloid in Alzheimer's disease brain. Biomaterials. 35(6):1967-76.

Ji K, Akgul G, Wollmuth LP, Tsirka SE. (2013) Microglia actively regulate the number of functional synapses, PLoS ONE, 8:e56293.

Jones CK, Byun N, Bubser M. (2012) Muscarinic and Nicotinic Acetylcholine Receptor Agonists and Allosteric Modulators for the Treatment of Schizophrenia. Neuropsychopharmacology 37(1):16-42.

Kacem K, Lacombe P, Seylaz J, Bonvento G. (1998) Structural organization of the perivascular astrocyte endfeet and their relationship with the endothelial glucose transporter: a confocal microscopy study. Glia. 23(1):1-10.

Kandratavicius L., Balista P.A., Lopes-Aguiar C., Ruggiero R.N., Umeoka E.H., Garcia-Cairasco N., Bueno-Junior L.S., Leite J.P. (2014) Animal models of epilepsy: use and limitations. Neuropsychiatr. Dis. Treat. 10:1693-1705.

Kanemoto Y, Ishibashi H, Doi A, Akaike N, Ito Y. (2002) An electrophysiological study of muscarinic and nicotinic receptors of rat paratracheal ganglion neurons and their inhibition by Z-338. British Journal of Pharmacology 135(6): 1403-1414.

Karpus WJ, Ransohoff RM. (1998) Chemokine regulation of experimental autoimmune encephalomyelitis: temporal and spatial expression patterns govern disease pathogenesis. J Immunol. 161(6):2667-71.

Kastritis PL, Rodrigues JPGL, Bonvin AMJJ. (2014) HADDOCK(2P2I): A Biophysical Model for Predicting the Binding Affinity of Protein-Protein Interaction Inhibitors. J Chem Inf Model 54(3):826-836.

Kawashima K, Fujii T. (2004) Expression of non-neuronal acetylcholine in lymphocytes and its contribution to the regulation of immune function. Frontiers in Bioscience 9:2063-2085.

Kawashima K, Fujii T, Watanabe Y, Misawa H. (1998) Acetylcholine synthesis and muscarinic receptor subtype mRNA expression in T-lymphocytes. Life Sci 62(17-18): 1701-1705.

Kelf TA, Sreenivasan VK, Sun J, Kim EJ, Goldys EM, Zvyagin AV. (2010) Non-specific cellular uptake of surface-functionalized quantum dots. Nanotechnology 21(28):285105.

Keov P, Lopez L, Devine SM, Valant C, Lane JR, Scammells PJ, Sexton PM, Christopoulos A. (2014) Molecular Mechanisms of Bitopic Ligand Engagement with the M-1 Muscarinic Acetylcholine Receptor. J Biol Chem 289(34): 23817-23837.

Keunen O, Taxt T, Grüner R, Lund-Johansen M, Tonn JC, Pavlin T, Bjerkvig R, Niclou SP, Thorsen F. (2014) Multimodal imaging of gliomas in the context of evolving cellular and molecular therapies. Adv Drug Deliv Rev. 76:98-115.

Kim JV, Kang SS, Dustin ML, McGavern DB. (2009) Myelomonocytic cell recruitment causes fatal CNS vascular injury during acute viral meningitis. Nature. 457(7226):191-5.

Kim BY, Rutka JT, Chan WC. (2010) Nanomedicine. N. Engl. J. Med. 363(25):2434–2443.

Kim JW, Lee SH, Ko HM, Kwon KJ, Cho KS, Choi CS, Park JH, Kim HY, Lee J, Han SH, Ignarro LJ, Cheong JH, Kim WK, Shin CY. (2011) Biphasic regulation of tissue plasminogen activator activity in ischemic rat brain and in cultured neural cells: essential role of astrocyte-derived plasminogen activator inhibitor-1. Neurochem Int. 58(3):423-33.

Kirchhofer D, Tschopp TB, Hadváry P, Baumgartner HR. (1994) Endothelial cells stimulated with tumor necrosis factor-alpha express varying amounts of tissue factor resulting in inhomogenous fibrin deposition in a native blood flow system. Effects of thrombin inhibitors. J Clin Invest. 93(5):2073-83.

Knopp A., Kivi A., Wozny C., Heinemann U., Behr J.J. (2005) Cellular and network properties of the subiculum in the pilocarpine model of temporal lobe epilepsy. Comp Neurol. 483:476-488.

Kofuji P, Newman EA. (2004) Potassium buffering in the central nervous system. Neuroscience. 129(4):1045-56.

Konopka A, Grajkowska W, Ziemiańska K, Roszkowski M, Daszkiewicz P, Rysz A, Marchel A, Koperski L, Wilczyński GM, Dzwonek J. (2013) Matrix metalloproteinase-9 (MMP-9) in human intractable epilepsy caused by focal cortical dysplasia. Epilepsy Res. 104(1–2): 45–58.

Koole R, van Schooneveld MM, Hilhorst J, Castermans K, Cormode DP, Strijkers GJ, de Mello Donegá C, Vanmaekelbergh D, Griffioen AW, Nicolay K, Fayad ZA, Meijerink A, Mulder WJ. (2008) Paramagnetic lipid-coated silica nanoparticles with a fluorescent quantum dot core: a new contrast agent platform for multimodality imaging. Bioconjug Chem. 19(12):2471-9.

Kou L, Sun J, Zhai Y, He Z. (2013) The endocytosis and intracellular fate of nanomedicines: implication for rational design. Asian J Pharmac Sci. 8(1):1–10.

Kovács R, Heinemann U, Steinhäuser C. (2012) Mechanisms underlying blood-brain barrier dysfunction in brain pathology and epileptogenesis: role of astroglia. Epilepsia. 53 Suppl 6:53-9.

Krueger JM, Fang J, Hansen MK, Zhang J, Obál Jr. F. (1998a) Humoral regulation of sleep. News Physiol. Sci. 13:189–194.

Krueger JM, Fang J, Taishi P, Chen Z, Kushikata T, Gardi J. (1998b) Sleep. A physiologic role for IL-1 beta and TNF-alpha. Ann. NY Acad. Sci. 856:148–159.

Kruse AC, Hu JX, Pan AC, Arlow DH, Rosenbaum DM, Rosemond E, Green HF, Liu T, Chae PS, Dror RO, Shaw DE, Weis WI, Wess J, Kobilka BK. (2012) Structure and dynamics of the M3 muscarinic acetylcholine receptor. Nature 482(7386): 552-556.

Kruse AC, Kobilka BK, Gautam D, Sexton PM, Christopoulos A, Wess J. (2014) Muscarinic acetylcholine receptors: novel opportunities for drug development. Nature Reviews Drug Discovery 13(7): 549-560.

Kruse AC, Ring AM, Manglik A, Hu JX, Hu K, Eitel K, Hubner H, Pardon E, Valant C, Sexton PM, Christopoulos A, Felder CC, Gmeiner P, Steyaert J, Weis WI, Garcia KC, Wess J, Kobilka BK. (2013) Activation and allosteric modulation of a muscarinic acetylcholine receptor. Nature 504(7478): 101-106.

Kuznetsova E, Schliebs R. (2013) beta-Amyloid, cholinergic transmission, and cerebrovascular system -- a developmental study in a mouse model of Alzheimer's disease. Curr Pharm Des 19(38): 6749-6765.

Kwon KJ, Cho KS, Lee SH, Kim JN, Joo SH, Ryu JH, Ignarro LJ, Han SH, Shin CY. (2011) Regulation of tissue plasminogen activator/plasminogen activator inhibitor-1 by hydrocortisone in rat primary astrocytes. J Neurosci Res. 89(7):1059-69.

Lange C, Storkebaum E, de Almodóvar CR, Dewerchin M, Carmeliet P. (2016) Vascular endothelial growth factor: a neurovascular target in neurological diseases. Nat Rev Neurol. 12(8):439-54.

Langmead C J, Watson J, Reavill C. (2008) Muscarinic acetylcholine receptors as CNS drug targets. Pharmacol Ther. 117(2): 232-243.

Laranjinha J, Santos RM, Lourenso CF, Ledo A, Barbosa RM. (2012) Nitric oxide signaling in the brain: translation of dynamics into respiration control and neurovascular coupling. Ann N Y Acad Sci. 1259: 10-8.

Lazareno S, Buckley N J, Roberts FF. (1990) Characterization of muscarinic M4 binding-sites in rabbit lung, chicken heart, and Ng108-15 cells. Mol Pharmacol 38(6): 805-815.

Leal-Campanario R, Alarcon-Martinez L, Rieiro H, Martinez-Conde S, Alarcon-Martinez T, Zhao X, LaMee J, Popp PJ, Calhoun ME, Arribas JI, Schlegel AA, Stasi LL, Rho JM, Inge L, Otero-Millan J, Treiman DM, Macknik SL. (2017) Abnormal Capillary Vasodynamics Contribute to Ictal Neurodegeneration in Epilepsy. Sci Rep. 7:43276.

Lecrux C, Hamel E. (2011) The neurovascular unit in brain function and disease. Acta Physiol. 203:47–59

Lee SW, Kim WJ, Choi YK, Song HS, Son MJ, Gelman IH, Kim YJ, Kim KW. (2003) SSeCKS regulates angiogenesis and tight junction formation in blood-brain barrier. Nat Med. 9(7):900-6.

Lee TS, Mane S, Eid T, Zhao H, Lin A, Guan Z, Kim JH, Schweitzer J, King-Stevens D, Weber P, Spencer SS, Spencer DD, de Lanerolle NC. (2007) Gene expression in temporal lobe epilepsy is consistent with increased release of glutamate by astrocytes. Mol Med. 13(1-2):1-13.

Li Q, Ford MC, Lavik EB, Madri JA. (2006) Modeling the neurovascular niche: VEGF- and BDNF-mediated cross-talk between neural stem cells and endothelial cells: an in vitro study. J Neurosci Res. 84(8):1656-68.

Li C, Zhang Y, Wang M, Zhang Y, Chen G, Li L, Wu D, Wang Q. (2014) In vivo real-time visualization of tissue blood flow and angiogenesis using Ag2S quantum dots in the NIR-II window. Biomaterials. 35(1):393-400.

Librizzi L, Regondi MC, Pastori C, Frigerio S, Frassoni C, de Curtis M. (2007) Expression of adhesion factors induced by epileptiform activity in the endothelium of the isolated guinea pig brain in vitro. Epilepsia. 48(4):743-51.

Librizzi L, Curtis M, Janigro D, Runtz L, deBock F, Barbier EL, Marchi N. (2017) Cerebrovascular heterogeneity and neuronal excitability. Neurosci Lett. 2017 Jan 10. pii: S0304-3940(17)30023-X. doi: 10.1016/j.neulet.2017.01.013.

Lind G J, Cavanagh HD. (1993) Nuclear muscarinic acetylcholine-receptors in corneal cells from rabbit. Invest Ophthalmol Vis Sci. 34(10): 2943-2952.

Linville DG, Hamel E. (1995) Pharmacological characterization of muscarinic acetylcholine binding sites in human and bovine cerebral microvessels. Naunyn Schmiedebergs Arch Pharmacol. 352(2): 179-186.

Liu J, Jin X, Liu KJ, Liu W. (2012) Matrix metalloproteinase-2-mediated occludin degradation and caveolin-1-mediated claudin-5 redistribution contribute to blood-brain barrier damage in early ischemic stroke stage. J Neurosci. 32(9):3044-57.

Liu D, Lin B, Shao W, Zhu Z, Ji T, Yang C. (2014) In vitro and in vivo studies on the transport of PEGylated silica nanoparticles across the blood-brain barrier. ACS Appl. Mater. Interfaces 6(3):2131–2136.

Livak KJ, Schmittgen TD. (2001) Analysis of relative gene expression data using real-time quantitative PCR and the 2(T)(-Delta Delta C) method. Methods 25(4): 402-408.

Lo Celso C, Lin CP, Scadden DT. (2011) In vivo imaging of transplanted hematopoietic stem and progenitor cells in mouse calvarium bone marrow. Nat Protoc. 6(1):1–14.

Löscher W. (2011) Critical review of current animal models of seizures and epilepsy used in the discovery and development of new antiepileptic drugs. Seizure. 20(5):359-368.

Long J, Junkin M, Wong PK, Hoying J, Deymier P. (2012) Calcium wave propagation in networks of endothelial cells: model-based theoretical and experimental study. PLoS Comput. Biol. 8(12):e1002847.

Lu ZL, Hulme EC. (1999) The functional topography of transmembrane domain 3 of the M1 muscarinic acetylcholine receptor, revealed by scanning mutagenesis. J Biol Chem. 274(11): 7309-7315.

Luissint AC, Artus C, Glacial F, Ganeshamoorthy K, Couraud PO. (2012) Tight junctions at the blood brain barrier: physiological architecture and disease-associated dysregulation. Fluids Barriers CNS. 9(1):23.

Luiten PGM, deJong GI, VanderZee EA, van Dijken H. (1996) Ultrastructural localization of cholinergic muscarinic receptors in rat brain cortical capillaries. Brain Res. 720(1-2): 225-229.

Macdonald JA, Murugesan N, Pachter JS. (2010) Endothelial cell heterogeneity of blood-brain barrier gene expression along the cerebral microvasculature. J Neurosci Res. 88(7):1457-74.

Maier T, Guell M, Serrano L. (2009) Correlation of mRNA and protein in complex biological samples. Febs Lett. 583(24): 3966-3973.

Manley NC, Bertrand AA, Kinney KS, Hing TC, Sapolsky RM. (2007) Characterization of monocyte chemoattractant protein-1 expression following a kainate model of status epilepticus. Brain Res. 1182:138-43.

Marchi N, Oby E, Batra A, Uva L, De Curtis M, Hernandez N, Van Boxel-Dezaire A, Najm I, Janigro D. (2007) In vivo and in vitro effects of pilocarpine: Relevance to ictogenesis. Epilepsia 48(10): 1934-1946.

Marchi N, Johnson AJ, Puvenna V, Johnson HL, Tierney W, Ghosh C, Cucullo L, Fabene PF, Janigro D. (2011) Modulation of peripheral cytotoxic cells and ictogenesis in a model of seizures. Epilepsia. 52(9):1627-34.

Marchi N, Lerner-Natoli M. (2013) Cerebrovascular remodeling and epilepsy. Neuroscientist. 19(3):304-12.

Mazzuferi M, Kumar G, Rospo C, Kaminski RM. (2012) Rapid epileptogenesis in the mouse pilocarpine model: video-EEG, pharmacokinetic and histopathological characterization. Exp Neurol. 238(2):156-67

Mayes P, Dicker D, Liu Y, El-Deiry W. (2008) Noninvasive vascular imaging in fluorescent tumors using multispectral unmixing. Biotechniques 45(4):459–464.

Maysinger D, Behrendt M, Lalancette-Hébert M, Kriz J. (2007) Real-time imaging of astrocyte response to quantum dots: in vivo screening model system for biocompatibility of nanoparticles. Nano Lett. 7(8):2513–2520.

McCarty JH, Monahan-Earley RA, Brown LF, Keller M, Gerhardt H, Rubin K, Shani M, Dvorak HF, Wolburg H, Bader BL, Dvorak AM, Hynes RO. (2002) Defective associations between blood vessels and brain parenchyma lead to cerebral hemorrhage in mice lacking alphav integrins. Mol Cell Biol. 22(21):7667-77.

Medintz IL, Uyeda HT, Goldman ER, Mattoussi H. (2005) Quantum dot bioconjugates for imaging, labelling and sensing. Nat Mater. 4(6):435–446.

Michalet X, Pinaud FF, Bentolila LA, Tsay JM, Doose S, Li JJ, Sundaresan G, Wu AM, Gambhir SS, Weiss S. (2005) Quantum dots for live cells, in vivo imaging, and diagnostics. Science. 307(5709):538-44.

Michel AD, Stefanich E, Whiting R L. (1989) Direct Labeling of Rat M3-Muscarinic Receptors by [H-3] 4Damp. Eur J Pharmacol. 166(3): 459-466.

Milner R, Campbell IL. (2002) The integrin family of cell adhesion molecules has multiple functions within the CNS. J Neurosci Res. 69(3):286-91.

Miragoli M, Novak P, Ruenraroengsak P, Shevchuk AI, Korchev YE, Lab MJ, Tetley TD, Gorelik J. (2013) Functional interaction between charged nanoparticles and cardiac

tissue: a new paradigm for cardiac arrhythmia? Nanomedicine (Lond). 2013 May;8(5):725-37. doi: 10.2217/nnm.12.125. Epub 2012 Nov 12.

Mitsuya M, Mase T, Tsuchiya Y, Kawakami K, Hattori H, Kobayashi K, Ogino Y, Fujikawa T, Satoh A, Fujikawa T, Satoh A, Kimura T, Noguchi K, Ohtake N, Tomimoto K. (1999) J-104129, a novel muscarinic M-3 receptor antagonist with high selectivity for M-3 over M-2 receptors. Bioorg Med Chem. 7(11): 2555-2567.

Mitsuya M, Ogino Y, Kawakami K, Uchiyama M, Kimura T, Numazawa T, Hasegawa T, Ohtake N, Noguchi K, Mase T. (2000) Discovery of a muscarinic M-3 receptor antagonist with high selectivity for M-3 over M-2 receptors among 2-[(1S, 3S)-3-sulfonylaminocyclopentyl]phenylacetamide derivatives. Bioorg Med Chem. 8(4):825-832.

Miyamoto N, Pham LD, Seo JH, Kim KW, Lo EH, Arai K. (2014) Crosstalk between cerebral endothelium and oligodendrocyte. Cell Mol Life Sci. 71(6):1055-66.

Mizoguchi H, Nakade J, Tachibana M, Ibi D, Someya E, Koike H, Kamei H, Nabeshima T, Itohara S, Takuma K, Sawada M, Sato J, Yamada K. (2011) Matrix metalloproteinase-9 contributes to kindled seizure development in pentylenetetrazole-treated mice by converting pro-BDNF to mature BDNF in the hippocampus. J. Neurosci. 31:12963–12971.

Moccia F, Dragoni S, Lodola F, Bonetti E, Bottino C, Guerra G, Laforenza U, Rosti V, Tanzi F. (2012) Store-Dependent Ca2+ Entry in Endothelial Progenitor Cells As a Perspective Tool to Enhance Cell-Based Therapy and Adverse Tumour Vascularization. Curr Med Chem. 19(34): 5802-5818.

Moccia F, Tanzi F, Munaron L. (2014) Endothelial remodelling and intracellular calcium machinery. Curr. Mol. Med. 14(4):457–480.

Moquin A, Neibert KD, Maysinger D, Winnik FM. (2015) Quantum dot agglomerates in biological media and their characterization by asymmetrical flow field-flow fractionation. Eur J Pharm Biopharm. 89:290-9.

Morin-Brureau M, Lebrun A, Rousset M-C, Fagni L, Bockaert J, de Bock F, Lerner-Natoli M. (2011) J Neurosci. 31(29):10677–10688.

Morita S, Miyata S. (2012) Different vascular permeability between the sensory and secretory circumventricular organs of adult mouse brain, Cell and Tissue Research, 349(2):589–603.

Mudò G., Jiang X.H., Timmusk T., Bindoni M., Belluardo N. (1996) Change in neurotrophins and their receptor mRNAs in the rat forebrain after status epilepticus induced by pilocarpine. Epilepsia. 37(2):198-207.

Mufti RE, Brett SE, Tran CH, Abd El-Rahman R, Anfinogenova Y, El-Yazbi A, Cole WC, Jones PP, Chen SR, Welsh DG. (2010) Intravascular pressure augments cerebral arterial constriction by inducing voltage-insensitive Ca2+ waves. J Physiol. 588(Pt 20):3983-4005.

Nagao T, Alonso A, Avoli M. (1996) Epileptiform activity induced by pilocarpine in the rat hippocampal-entorhinal slice preparation. Neuroscience. 72(2):399-408.

Nathanson NM. (2008) Synthesis, trafficking, and localization of muscarinic acetylcholine receptors. Pharmacol Ther. 119(1): 33-43.

Navarro Mora G, Bramanti P, Osculati F, Chakir A, Nicolato E, Marzola P, Sbarbati A, Fabene PF. (2009) Does pilocarpine-induced epilepsy in adult rats require status epilepticus? PLoS One. 4(6):e5759.

Navone SE, Marfia G, Nava S, Invernici G, Cristini S, Balbi S, Sangiorgi S, Ciusani E, Bosutti A, Alessandri G, Slevin M, Parati EA. (2013) Human and mouse brain-derived endothelial cells require high levels of growth factors medium for their isolation, in vitro maintenance and survival. Vasc Cell 5(1):10.

Nezu A, Morita T, Tojyo Y, Nagai T, Tanimura A. (2015) Partial agonistic effects of pilocarpine on Ca(2+) responses and salivary secretion in the submandibular glands of live animals. Exp Physiol. 100(6):640-51.

Nguyen MD, Julien JP, Rivest S. (2002) Innate immunity: the missing link in neuroprotection and neurodegeneration? Nat Rev Neurosci. 3:216–227.

Nicoletti JN, Shah SK, McCloskey DP, Goodman JH, Elkady A, Atassi H, Hylton D, Rudge JS, Scharfman HE, Croll SD. (2008) Vascular endothelial growth factor is up-regulated after status epilepticus and protects against seizure-induced neuronal loss in hippocampus. Neuroscience. 151(1):232-41.

Nicoletti JN, Lenzer J, Salerni EA, Shah SK, Elkady A, Khalid S, Quinteros D, Rotella F, Betancourth D, Croll SD. (2010) Vascular endothelial growth factor attenuates status epilepticus-induced behavioral impairments in rats. Epilepsy Behav. 19(3):272-7.

Nimmerjahn A, Kirchhoff F, Helmchen F. (2005) Resting microglial cells are highly dynamic surveillants of brain parenchyma in vivo. Science, 308:1314–1318.

Opp MR. (2005) Cytokines and sleep. Sleep Med Rev. 9:355–364.

Osaki F, Kanamori T, Sando S, Sera T, Aoyama Y. (2004) A quantum dot conjugated sugar ball and its cellular uptake. On the size effects of endocytosis in the subviral region. J Am Chem Soc. 126(21):6520–6521.

Paemeleire K. (2002) Calcium signaling in and between brain astrocytes and endothelial cells. Acta Neurol Belg. 102(3):137-40.

Paganetti P, Antoniello K, Devraj K, Toni N, Kieran D, Madani R, Pihlgren M, Adolfsson O, Froestl W, Schrattenholz A, Liebner S, Havas D, Windisch M, Cirrito J R, Pfeifer A, Muhs A. (2014) Increased efflux of amyloid-beta peptides through the blood-brain barrier by muscarinic acetylcholine receptor inhibition reduces pathological phenotypes in mouse models of brain amyloidosis. J Alzheimers Dis. 38(4):767-786.

Pannell M, Szulzewsky F, Matyash V, Endres M, Heppner F L, Kronenberg G, Prinz V, Prokop S, Waiczies S, Wolf S A, Kettenmann H. (2013) The subpopulation of microglia expressing functional muscarinic acetylcholine receptors expands in stroke and Alzheimer's disease. Glia 61: S207.

Paolicelli RC, Bolasco G, Pagani F, Maggi L, Scianni M, Panzanelli P, Giustetto M, Ferreira TA, Guiducci E, Dumas L, Ragozzino D, Gross CT. (2011) Synaptic pruning by microglia is necessary for normal brain development. Science, 333:1456–1458.

Paradiso B, Zucchini S, Su T, Bovolenta R, Berto E, Marconi P, Marzola A, Navarro Mora G, Fabene PF, Simonato M. (2011) Localized overexpression of FGF-2 and BDNF in hippocampus reduces mossy fiber sprouting and spontaneous seizures up to 4 weeks after pilocarpine-induced status epilepticus. Epilepsia. 52(3):572-8.

Pauli E., Hildebrandt M., Romstöck J., Stefan H., Blümcke I. (2006) Deficient memory acquisition in temporal lobe epilepsy is predicted by hippocampal granule cell loss. Neurology. 67(8):1383-1389.

Peppiatt CM, Howarth C, Mobbs P, Attwell D. (2006) Bidirectional control of CNS capillary diameter by pericytes. Nature 443:700–4.

Pettersen E F, Goddard T D, Huang C C, Couch G S, Greenblatt D M, Meng E C, Ferrin T E. (2004) UCSF chimera - A visualization system for exploratory research and analysis. J Comput Chem. 25(13): 1605-1612.

Peyter AC, Muehlethaler V, Liaudet L, Marino M, Di Bernardo S, Diaceri G, Tolsa JF. (2008) Muscarinic receptor M(1) and phosphodiesterase 1 are key determinants in pulmonary vascular dysfunction following perinatal hypoxia in mice. Am J Physiol Lung Cell Mol Physiol 295(1): L201-L213.

Pham LD, Hayakawa K, Seo JH, Nguyen MN, Som AT, Lee BJ, Guo S, Kim KW, Lo EH, Arai K. (2012) Crosstalk between oligodendrocytes and cerebral endothelium contributes to vascular remodeling after white matter injury. Glia. 60(6):875-81.

Pickering M, O'Connor JJ. (2007) Pro-inflammatory cytokines and their effects in the dentate gyrus, Prog Brain Res. 163:339–354.

Pollinger K, Hennig R, Ohlmann A, Fuchshofer R, Wenzel R, Breunig M, Tessmar J, Tamm ER, Goepferich A. (2013) Ligand-functionalized nanoparticles target endothelial cells in retinal capillaries after systemic application. Proc Natl Acad Sci U S A. 110(15):6115-20.

Poulsen FR, Jahnsen H, Blaabjerg M, Zimmer J. (2002) Pilocarpine-induced seizure-like activity with increased BNDF and neuropeptide Y expression in organotypic hippocampal slice cultures. Brain Res. 950(1-2):103-18.

Pozzi-Mucelli S, Boschi F, Calderan L, Sbarbati A, Osculati F. (2009) Quantum Dots: Proteomics characterization of the impact on biological systems. J Phys Conference Series 170:012021.

Puri V, Wang X H, Vardigan J D, Kuduk S D, Uslaner J M. (2015) The selective positive allosteric M1 muscarinic receptor modulator PQCA attenuates learning and memory deficits in the Tg2576 Alzheimer's disease mouse model. Behav Brain Res. 287: 96-99.

Radu BM, Dumitrescu DI, Mustaciosu CC, Radu M. (2012) Dual effect of methylglyoxal on the intracellular Ca2+ signaling and neurite outgrowth in mouse sensory neurons. Cell Mol Neurobiol. 32(6):1047–1057.

Radu BM, Bramanti P, Osculati F, Flonta ML, Radu M, Bertini G, Fabene PF. (2013) Neurovascular unit in chronic pain. Mediators Inflamm. 2013:648268.

Radu BM, Radu M, Tognoli C, Benati D, Merigo F, Assfalg M, Solani E, Stranieri C, Ceccon A, Pasini A M F, Cominacini L, Bramanti P, Osculati F, Bertini G, Fabene PF. (2015) Are they in or out? The elusive interaction between Qtracker (R) 800 vascular labels and brain endothelial cells. Nanomedicine (Lond). 10(22): 3329-3342.

Radu BM, Radu M. (2015) Recent preclinical and clinical technological advances suitable to unravel the blood brain barrier characteristics in physiological and pathological neurological states. EC Neurol. 1(2):22–27.

Radu BM, Osculati AMM, Suku E, Banciu A, Tsenov G, Merigo F, Di Chio M, Banciu DD, Tognoli C, Kačer P, Giorgetti A, Radu M, Bertini G, Fabene PF (2017a) Functional expression of murine muscarinic acetylcholine receptors in CNS microvascular endothelium. Sci Rep. 7(1):5083.

Radu BM, Epureanu FB, Radu M, Fabene PF, Bertini G. (2017b) Nonsteroidal anti-inflammatory drugs in clinical and experimental epilepsy. Epilepsy Res. 131:15-27.

Rampazzo E, Boschi F, Bonacchi S, Juris R, Montalti M, Zaccheroni N, Prodi L, Calderan L, Rossi B, Becchi S, Sbarbati A. (2012) Multicolor core/shell silica nanoparticles for in vivo and ex vivo imaging. Nanoscale. 4(3):824-30.

Ramsauer M, Krause D, Dermietzel R. (2002) Angiogenesis of the blood-brain barrier in vitro and the function of cerebral pericytes. FASEB J. 16(10):1274-6.

Rana OR, Schauerte P, Kluttig R, Schroder JW, Koenen RR, Weber C, Nolte KW, Weis J, Hoffmann R, Marx N, Saygili E. (2010) Acetylcholine as an age-dependent non-neuronal source in the heart. Autonomic Neuroscience-Basic & Clinical. 156(1-2): 82-89.

Rist RJ, Romero IA, Chan MW, Couraud PO, Roux F, Abbott NJ. (1997) F-actin cytoskeleton and sucrose permeability of immortalised rat brain microvascular endothelial cell monolayers: effects of cyclic AMP and astrocytic factors. Brain Res. 768(1-2):10-8.

Rivers RJ, Duling BR. (1992) Arteriolar endothelial-cell barrier separates 2 populations of muscarinic receptors. Am J Physiol. 262(4): H1311-H1315.

Römermann K, Bankstahl JP, Löscher W, Bankstahl M. (2015) Pilocarpine-induced convulsive activity is limited by multidrug transporters at the rodent blood-brain barrier. J Pharmacol Exp Ther. 353(2):351-9.

Rostène W, Kitabgi P, Parsadaniantz SM. (2007) Chemokines: a new class of neuromodulator? Nat Rev Neurosci. 8(11):895-903.

Ryman-Rasmussen JP, Riviere JE, Monteiro-Riviere NA. (2007) Surface coatings determine cytotoxicity and irritation potential of quantum dot nanoparticles in epidermal keratinocytes. J Invest Dermatol. 127(1):143–153.

Ruck T, Bittner S, Epping L, Herrmann AM, Meuth SG. (2014) Isolation of primary murine brain microvascular endothelial cells. J. Vis. Exp. 93, e52204.

Salvetti B. (2014) A multidisciplinary and functional approach to neurotoxicity: the case of Quantum Dots, *Doctoral thesis*, retrieved from IRIS, University of Verona

Sandal M, Duy T P, Cona M, Zung H, Carloni P, Musiani F, Giorgetti A. (2013) GOMoDo: A GPCRs Online Modeling and Docking Webserver. PlosOne 8(9).

Schaafsma D, Boterman M, de Jong AM, Hovens I, Penninks JM, Nelemans SA, Meurs H, Zaagsma J. (2006) Differential Rho-kinase dependency of full and partial muscarinic receptor agonists in airway smooth muscle contraction. Br J Pharmacol. 147(7):737-43.

Schinkel AH. (1999) P-Glycoprotein, a gatekeeper in the blood-brain barrier. Adv Drug Deliv Rev. 36(2-3):179-194.

Schlosser G, Kacer P, Kuzma M, Szilagyi Z, Sorrentino A, Manzo C, Pizzano R, Malorni L, Pocsfalvi G. (2007) Coupling immunomagnetic separation on magnetic beads with matrix-assisted laser desorption ionization-time of flight mass spectrometry for detection of staphylococcal enterotoxin B. Appl Environ Microbiol. 73(21): 6945-6952.

Schummers J, Yu H, Sur M. (2008) Tuned responses of astrocytes and their influence on hemodynamic signals in the visual cortex. Science, 320:1638–1643.

Seiffert E, Dreier JP, Ivens S, Bechmann I, Tomkins O, Heinemann U, Friedman A. (2004) Lasting blood-brain barrier disruption induces epileptic focus in the rat somatosensory cortex. 24(36):7829-36.

Seo JH, Guo S, Lok J, Navaratna D, Whalen MJ, Kim KW, Lo EH. (2012) Neurovascular matrix metalloproteinases and the blood-brain barrier. Curr Pharm Des. 18(25):3645-8.

Shang L, Nienhaus K, Nienhaus GU. (2014) Engineered nanoparticles interacting with cells: size matters. J. Nanobiotechnol. 12:5.

Shapiro LA, Korn MJ, Ribak CE. (2005) Newly generated dentate granule cells from epileptic rats exhibit elongated hilar basal dendrites that align along GFAP-immunolabeled processes. Neuroscience, 136:823–831.

Sheffler DJ, Williams R, Bridges TM, Xiang ZX, Kane AS, Byun NE, Jadhav S, Mock M M, Zheng F, Lewis L M, Jones C K, Niswender C M, Weaver CD, Lindsley CW, Conn PJ. (2009) A novel selective muscarinic acetylcholine receptor subtype 1 antagonist reduces seizures without impairing hippocampus-dependent learning. Mol Pharmacol. 76(2): 356-368.

Smalheiser NR. (2009) Do Neural Cells Communicate with Endothelial Cells via Secretory Exosomes and Microvesicles? Cardiovasc Psychiatry Neurol. 2009:383086.

Sobue K, Yamamoto N, Yoneda K, Hodgson ME, Yamashiro K, Tsuruoka N, Tsuda T, Katsuya H, Miura Y, Asai K, Kato T. (1999) Induction of blood-brain barrier properties in immortalized bovine brain endothelial cells by astrocytic factors. Neurosci Res. 35(2):155-64.

Socha MJ, Hakim CH, Jackson WF, Segal SS. (2011) Temperature effects on morphological integrity and Ca2+ signaling in freshly isolated murine feed artery endothelial cell tubes. American Journal of Physiology-Heart and Circulatory Physiology 301(3): H773-H783.

Sousa da Silva AW, Vranken WF (2012) ACPYPE - AnteChamber PYthon Parser interfacE. BMC research notes 5: 367–367.

Sriram K, O'Callaghan JP. (2007) Divergent roles for tumor necrosis factor-alpha in the brain. J Neuroimmune Pharmacol. 2:140–153.

Stellwagen D, Malenka RC. (2006) Synaptic scaling mediated by glial TNF-alpha Nature, 440:1054–1059.

Streit WJ. (2002) Microglia as neuroprotective, immunocompetent cells of the CNS. Glia, 40:133–139.

Stylianou P, Skourides PA. (2009) Imaging morphogenesis, in xenopus with quantum dot nanocrystals. Mech. Dev. 126(10):828–841.

Swift MR, Weinstein BM. (2009) Arterial-venous specification during development. Circ Res. 104(5):576-88.

Takacs E, Nyilas R, Szepesi Z, Baracskay P, Karlsen B, Rosvold T, Bjorkum AA, Czurko A, Kovacs Z, Kekesi AK, Juhasz G. (2010) Matrix metalloproteinase-9 activity increased by two different types of epileptic seizures that do not induce neuronal death: a possible role in homeostatic synaptic plasticity. Neurochem Int. 56:799–809.

Tallini YN, Brekke JF, Shui B, Doran R, Hwang S, Nakai J, Salama G, Segal SS, Kotlikoff MI. (2007) Propagated Endothelial Ca2+ Waves and Arteriolar Dilation In Vivo. Circ Res. 101:1300-1309.

Tanda G, Ebbs AL, Kopajtic TA, Elias LM, Campbell BL, Newman AH, Katz JL. (2007) Effects of muscarinic M-1 receptor blockade on cocaine-induced elevations of brain dopamine levels and locomotor behavior in rats. J Pharmacol Exp Ther. 321(1): 334-344.

Tang M, Wang M, Xing T, Zeng J, Wang H, Ruan DY. (2008) Mechanisms of unmodified CdSe quantum dot-induced elevation of cytoplasmic calcium levels in primary cultures of rat hippocampal neurons. Biomaterials 29(33):4383–4391.

Tang M, Xing T, Zeng J, Wang H, Li C, Yin S, Yan D, Deng H, Liu J, Wang M, Chen J, Ruan DY. (2008) Unmodified CdSe quantum dots induce elevation of cytoplasmic calcium levels and impairment of functional properties of sodium channels in rat primary cultured hippocampal neurons. Environ Health Perspect. 116(7):915-22.

Taylor MS, Francis M. (2014) Decoding dynamic Ca2+ signaling in the vascular endothelium. Front Physiol. 5:447.

Thal DM, Sun BF, Feng D, Nawaratne V, Leach K, Felder CC, Bures MG, Evans DA, Weis WI, Bachhawat P, Kobilka TS, Sexton PM, Kobilka BK, Hristopoulos AC. (2016) Crystal structures of the M1 and M4 muscarinic acetylcholine receptors. Nature 531(7594): 335-340.

Thanabalasundaram G, Schneidewind J, Pieper C, Galla HJ. (2011) The impact of pericytes on the blood–brain barrier integrity depends critically on the pericyte differentiation stage. Int J Biochem Cell Biol. 3:1284–1293.

Thomas RL, Langmead CJ, Wood MD, Challiss RAJ. (2009) Contrasting Effects of Allosteric and Orthosteric Agonists on M-1 Muscarinic Acetylcholine Receptor Internalization and Down-regulation. J Pharmacol Exp Ther 331(3): 1086-1095.

Tracey WR, Peach MJ. (1992) Differential Muscarinic Receptor Messenger-Rna Expression by Freshly Isolated and Cultured Bovine Aortic Endothelial-Cells. Circ Res 70(2): 234-240.

Traish AM, Kim N, Carson MP, Detejada IS. (1994) Characterization of Muscarinic Acetylcholine-Receptors in Cultured Bovine Aortic Endothelial-Cells. J Recept Res 14(3-4): 153-166.

Tran ND, Correale J, Schreiber SS, Fisher M. (1999) Transforming growth factor-beta mediates astrocyte-specific regulation of brain endothelial anticoagulant factors. Stroke. 30(8):1671-8.

Tran QK, Ohashi K, Watanabe H. (2000) Calcium signalling in endothelial cells. Cardiovasc Res. 48(1):13–22.

Tsukahara T, Kassell NF, Hongo K, Vollmer DG, Ogawa H. (1989) Muscarinic Cholinergic Receptors on the Endothelium of Human Cerebral-Arteries. J Cereb Blood Flow Metab 9(6):748-753.

Turski W.A., Cavalheiro E.A., Schwarz M., Czuczwar S.J., Kleinrok Z., Turski L. (1983) Limbic seizures produced by pilocarpine in rats: behavioural, electroencephalographic and neuropathological study. Behav. Brain Res. 9(3):315-335.

Utsumi H, Chiba H, Kamimura Y, Osanai M, Igarashi Y, Tobioka H, Mori M, Sawada N. (2000) Expression of GFRalpha-1, receptor for GDNF, in rat brain capillary during postnatal development of the BBB. Am J Physiol Cell Physiol. 279(2):C361-8.

Uwada J, Anisuzzaman A S M, Nishimune A, Yoshiki H, Muramatsu I. (2011) Intracellular distribution of functional M-1-muscarinic acetylcholine receptors in N1E-115 neuroblastoma cells. J Neurochem 118(6): 958-967.

Uwada J, Yoshiki H, Masuoka T, Nishio M, Muramatsu I. (2014) Intracellular localization of the M1 muscarinic acetylcholine receptor through clathrin-dependent constitutive internalization is mediated by a C-terminal tryptophan-based motif. J Cell Sci 127(14): 3131-3140.

van Vliet EA, da Costa Araújo S, Redeker S, van Schaik R, Aronica E, Gorter JA. (2007) Blood-brain barrier leakage may lead to progression of temporal lobe epilepsy. Brain. 130(Pt 2):521-34.

Vandenhaute E, Dehouck L, Boucau MC, Sevin E, Uzbekov R, Tardivel M, Gosselet F, Fenart L, Cecchelli R, Dehouck MP. (2011) Modelling the neurovascular unit and the blood–brain barrier with the unique function of pericytes. Curr Neurovasc Res. 8:258–269.

Vaucher E, Hamel E. (1995) Cholinergic basal forebrain neurons project to cortical microvessels in the rat - electron-microscopic study with anterogradely transported

phaseolus-vulgaris-leukoagglutinin and choline-acetyltransferase immunocytochemistry. J Neurosci 15(11): 7427-7441.

Veeraragavan S, Bui N, Perkins JR, Yuva-Paylor LA, Carpenter RL, Paylor R. (2011) Modulation of behavioral phenotypes by a muscarinic M1 antagonist in a mouse model of fragile X syndrome. Psychopharmacology 217(1):143-151.

Venkatakrishnan AJ, Deupi X, Lebon G, Tate CG, Schertler GF, Babu MM. (2013) Molecular signatures of G-protein-coupled receptors. Nature 494(7436):185-194.

Verderio C, Matteoli M. (2001) ATP mediates calcium signaling between astrocytes and microglial cells: modulation by IFN-gamma. J Immunol. 166(10):6383-91.

Vezzani A. (2005) VEGF and Seizures: Cross-talk between Endothelial and Neuronal Environments, Epilepsy Curr. 5(2): 72–74.

Viviani B, Gardoni F, Marinovich M. (2007) Cytokines and neuronal ion channels in health and disease. Int Rev Neurobiol. 82:247–263.

Wagner S, Gardner H. (2000) Modes of regulation of laminin-5 production by rat astrocytes. Neurosci Lett. 284(1-2):105-8.

Wake H, Moorhouse AJ, Jinno S, Kohsaka S, Nabekura J. (2009) Resting microglia directly monitor the functional state of synapses in vivo and determine the fate of ischemic terminals. J Neurosci. 29:3974–3980.

Wang L, Zhang ZG, Zhang RL, Gregg SR, Hozeska-Solgot A, LeTourneau Y, Wang Y, Chopp M. (2006) Matrix metalloproteinase 2 (MMP2) and MMP9 secreted by erythropoietin-activated endothelial cells promote neural progenitor cell migration. J Neurosci 26(22):5996-6003.

Wess J, Duttaroy A, Zhang W, Gomeza J, Cui Y, Miyakawa T, Bymaster FP, McKinzie L, Felder CC, Lamping KG, Faraci FM, Deng C, Yamada M. (2003) M-1-M-5 muscarinic receptor knockout mice as novel tools to study the physiological roles of the muscarinic cholinergic system. Recept Channels 9(4):279-290.

Wessler I, Kirkpatrick CJ. (2008) Acetylcholine beyond neurons: the non-neuronal cholinergic system in humans. British J Pharmacol 154(8):1558-1571.

Wessler IK, Kirkpatrick CJ. (2012) Activation of muscarinic receptors by non-neuronal acetylcholine. Handb Exp Pharmacol 208:469-491.

Wilczynski GM, Konopacki FA, Wilczek E, Lasiecka Z, Gorlewicz A, Michaluk P, Wawrzyniak M, Malinowska M, Okulski P, Kolodziej LR, Konopka W, Duniec K, Mioduszewska B, Nikolaev E, Walczak A, Owczarek D, Gorecki DC, Zuschratter W,

Ottersen OP, Kaczmarek L. (2008) Important role of matrix metalloproteinase 9 (MMP-9) in epileptogenesis. J. Cell Biol. 180:1021–1035.

Wilhelm I, Nyúl-Tóth Á, Suciu M, Hermenean A, Krizbai IA. (2016) Heterogeneity of the blood-brain barrier. Tissue Barriers. 28;4(1):e1143544.

Willis CL, Nolan CC, Reith SN, Lister T, Prior MJ, Guerin CJ, Mavroudis G, Ray DE. (2004) Focal astrocyte loss is followed by microvascular damage, with subsequent repair of the blood-brain barrier in the apparent absence of direct astrocytic contact. Glia. 45(4):325-37.

Willis CL, Brooks TA, Davis TP. (2008) Chronic inflammatory pain and the neurovascular unit: a central role for glia in maintaining BBB integrity? Curr Pharm Des. 14:1625–1643.

Willis CL. (2012) Imaging in vivo astrocyte/endothelial cell interactions at the blood-brain barrier. Methods Mol Biol. 2012;814:515-29.

Winkler EA, Bell RD, Zlokovic BV. (2011) Central nervous system pericytes in health and disease. Nat Neurosci. 14:1398–1405.

Winkler EA, Nishida Y, Sagare AP, Rege SV, Bell RD, Perlmutter D, Sengillo JD, Hillman S, Kong P, Nelson AR, Sullivan JS, Zhao Z, Meiselman HJ, Wenby RB, Soto J, Abel ED, Makshanoff J, Zuniga E, De Vivo DC, Zlokovic BV. (2015) GLUT1 reductions exacerbate Alzheimer's disease vasculo-neuronal dysfunction and degeneration. Nat Neurosci. 18(4):521-530.

Wittko IM, Schanzer A, Kuzmichev A, Schneider FT, Shibuya M, Raad S, Plate KH. (2009) VEGFR-1 regulates adult olfactory bulb neurogenesis and migration of neural progenitors in the rostral migratory stream in vivo. J. Neurosci. 29:8704–8714.

Wozny C., Kivi A., Lehmann T.N., Dehnicke C., Heinemann U., Behr J. (2003) Comment on On the origin of interictal activity in human temporal lobe epilepsy in vitro Science. 301(5632):463.

Xiang ZX, Thompson AD, Jones CK, Lindsley CW, Conn PJ. (2012) Roles of the M1 muscarinic acetylcholine receptor subtype in the regulation of basal ganglia function and implications for the treatment of Parkinson's disease. J Pharmacol Exp Ther 340(3):595-603.

Xiao Y, Forry SP, Gao X, Holbrook RD, Telford WG, Tona A. (2010) Dynamics and mechanisms of quantum dot nanoparticle cellular uptake. J Nanobiotechnol. 8:13.

Xu JH, Long L, Tang YC, Zhang JT, Hut HT, Tang FR. (2009) CCR3, CCR2A and macrophage inflammatory protein (MIP)-1a, monocyte chemotactic protein-1 (MCP-1) in the mouse hippocampus during and after pilocarpine-induced status epilepticus (PISE). Neuropathol Appl Neurobiol. 35(5):496-514.

Yamamoto K, Korenaga R, Ohura N, Sokabe T, Kamiya A, Ando J. (2000) Role of P2X4 purinoceptors in endothelial Ca2+ response to shear stress. Ann Biomed Eng. 28(Suppl. 1):S68.

Zhang F, Xu S, Iadecola C. (1995) Role of nitric oxide and acetylcholine in neocortical hyperemia elicited by basal forebrain stimulation: evidence for an involvement of endothelial nitric oxide. Neuroscience 69:1195–204

Zhang L. Cholinergic receptor knockout mice. In: Animal models of cognitive impairment. (Eds. Levin E, Buccafusco J). CRC Press/Taylor & Francis, Boca Raton, London, New York, 2006; 199-222.

Zhang LW, Monteiro-Riviere NA. (2009) Mechanisms of quantum dot nanoparticle cellular uptake. Toxicol Sci. 110(1):138–155.

Zhang JM, Wang HK, Ye CQ, Ge W, Chen Y, Jiang ZL, Wu P, Poo MM, Duan S. (2003) ATP released by astrocytes mediates glutamatergic activity-dependent heterosynaptic suppression. Neuron, 40:971–982.

Zhang YY, Shen W, Zhang LC, Pan ZY, Long CL, Cui WY, Zhang YF, Wang H. (2014) Proteomics reveals potential non-neuronal cholinergic receptor-effectors in endothelial cells. Acta Pharmacol Sin 35(9):1137-1149.

Zhang C, Moeini M, Lesage F. (2017) Spatial landscape of oxygen in and around microvasculature during epileptic events. Neurophotonics. 4(1):010501.

Zhu Y, Hong H, Xu ZP, Li Z, Cai W. (2013) Quantum dot-based nanoprobes for in vivo targeted imaging. Curr Mol Med. 13(10):1549–1567.

Ziv Y, Ron N, Butovsky O, Landa G, Sudai E, Greenberg N, Cohen H, Kipnis J, Schwartz M. (2006) Immune cells contribute to the maintenance of neurogenesis and spatial learning abilities in adulthood. Nat Neurosci. 9(2):268-75. Epub 2006 Jan 15.

Zlokovic BV. (2005) Neurovascular mechanisms of Alzheimer's neurodegeneration. Trends Neurosci. 28:202–208.

Zonta M, Angulo MC, Gobbo S, Rosengarten B, Hossmann KA, Pozzan T, Carmignoto G. (2003) Neuron-to-astrocyte signaling is central to the dynamic control of brain microcirculation. Nat. Neurosci. 6:43–50

Zozulya A, Weidenfeller C, Galla HJ. (2008) Pericyte-endothelial cell interaction increases MMP-9 secretion at the blood-brain barrier in vitro. Brain Res. 1189:1-11.